University of Nottingham
UK | CHINA | MALAYSIA

Using MRI to elucidate the importance of physical activity to brain health and motor function in ageing

Thesis submitted to the University of Nottingham for the degree of **Doctor of Philosophy, June 2023.**

Rosemary Nicholas

14342421

Supervised by

Professor Susan Francis
Professor Paul Greenhaff

Abstract

We live in an increasingly ageing population where people are living longer, but quality of life is not keeping up with increased lifespan. Concerns contributing to poor health in ageing include cognitive impairment and frailty driven by neurodegeneration and declining musculoskeletal health. Inactivity is also a significant driver of poor health in ageing and this may divulge important mechanisms of age-related decline. This thesis aims to differentiate whether activity in ageing impacts on physiological responses by studying trained and untrained individuals.

Lifelong highly active male cyclists (Older Trained, OT), age-matched healthy older untrained (OU) males and young untrained (YU) males participants underwent cognitive and physiological tests, and MRI structural and functional scans of the muscle, heart and brain. Brain and heart functional measures were collected at rest, during supine exercise using a Ergospect Cardio-Step module, and during a recovery period post-exercise. A semi-automatic muscle segmentation method was developed to extract measures of leg muscle volume and fat fraction from wholebody mDIXON MRI scans. In general age was the primary driver of differences found rather than training.

In the muscle, lower muscle strength was associated with older age. Additionally, the older untrained (OU) had greater fat percentages within their calf muscles than the young untrained (YU). The OT group were more similar to the YU group than the OU group in muscle quality during isokinetic contractions.

For cardiac measures, peak heartrate during the VO_2 test, aortic stroke volume and stroke distance were all lower in the OT and OU groups. Aortic stroke volume was higher in the older OT and OU groups than the YU group during supine exercise. Heartrate increased during exercise in all participants, but for the YU group this was the primary driver of their

increase in cardiac output with no increase in stroke volume, whereas the older OT and OU groups compensated for lower increases in heartrate with concurrent increases in stroke volume. Aortic backflow was greater in older groups at rest, without increased aortic stiffening, suggesting greater peripheral vasculature resistance in the older groups.

In the brain measures, gmCBF at baseline and cerebral vessel velocity at both baseline and during supine exercise were lower with age. OEF was higher in the OU group than YU group. As expected, white matter, cortical and subcortical grey matter volume, as well as cortical thickness were lower in the older groups than the young group. Modest correlations existed between cerebral velocity during supine exercise and cortical and sub-cortical grey matter, white matter and cortical thickness. Structural connectivity measured was greater in the young than older groups, along with the cognitive scores from the MOCA and Trail A tests.

Some effects of a long term high physical activity were seen, where the OT group were more similar to the YU group than the OU group. This lifestyle effect was exhibited in maintained muscle quality during isokinetic contractions, higher VO_2peaks, and greater velocity of cerebral blood flow at rest. All of the older volunteers in this thesis were non-frail, non-sedentary and healthy, and therefore differences of activity levels may not have been large enough to reveal significant impacts of a highly active lifestyle in a small sample size. Future work will increase the sample size, examine more differentiated groups or introduce an intervention and improve acquisition techniques for better data quality.

Acknowledgements

Thanks go first and foremost to my incredible supervisors, Sue Francis and Paul Greenhaff, without whom none of this would have been possible. Your guidance and constant support, day and night, through this project have been invaluable.

I owe a great deal of the success of this thesis to Jordan McGing and Ayushman Gupta. Jordan, thank you for paving the way on the development of the Ergospect equipment protocols and guiding me through as I stumbled along. The three of us working together made cajoling the kit into cooperation and trouble shooting a manageable process, and running study days together helped keep the chaos at bay. Thank you to both for being there to bounce ideas off, to share analysis strategies, and as key members of the Ergospect Taxi Service. Additionally, thank you Ayushman for your clinical support.

Thank you to Chris Bradley for running the long, stressful scanning sessions and tolerating my peppering of questions throughout. Everyone in the DGHPU was incredibly helpful, thank you for all of your support throughout. Thank you to Mat Piasecki, Celia Guo and Eleanor Jones for all the iEMG data collection and analysis. I also owe Paul Glover and Stuart Salter my thanks for helping with the Ergospect Cardio-Step diagnostics and repair, keeping the project going when it was in trouble.

Alex Daniel endured my many questions with good cheer and was an invaluable resource. I extend my thanks to him and the rest of the Barn, past and present, who have helped me and been good friends throughout this process.

I of course also owe a huge thanks to the participants who took part in this study, who coped with long study days and travelled far to contribute to this research. They were not only ideal participants, but made the study days something to look forward to with many interesting conversations,

and were good sports about the occasional technical malfunction.

I would also like to thank my parents, who have always supported me and encouraged me to pursue my goals and my brother Joseph Nicholas, without whose coding tutoring over the years I would not have the knowledge I have today. Lastly, thank you to my partner, Luke Humphreys, for keeping me going through the write up process without complaint, you put up with a lot.

Impact of COVID-19

The original thesis was to investigate the impact of life-long exercise on the ageing phenotype using physiology measures and MR imaging, in three groups of participants in an older age range (70-80 years old); sedentary participants, master cyclists and master sprinters. For all participants the study comprised a multi-day, multi-site visit. This involved a screening visit to test for eligibility and safety, one day of exercise, strength and cognitive testing in the David Greenfield Human Physiology Unit (DGHPU) in Queen's Medical Centre (QMC), and one day divided between the MRI facilities of the Sir Peter Mansfield Imaging centre (SPMIC) at University of Nottingham University Park Campus and the School of Life Sciences building at Royal Derby Hospital. In the case of the majority of the cyclists and the one sprinter recruited, the study involved travelling in from another city and staying in a hotel overnight.

COVID-19 restrictions meant no study visits could take place from mid-March 2020 until May 2021, a time period of 13 months without being able to recruit any new participants to this work. At the time of lockdown, two participants were scheduled for the week the University shut down, with one further participant who was scheduled to take part later in the month. When restarting the study as restrictions were being reduced, there were strong ethical concerns about older vulnerable groups taking part and exercise protocols were slower to resume than others due to concerns with aerosol generation. As a result of COVID-19, the majority of one group (endurance cyclists) were recruited before March 2020, but only one participant in the OU group had completed the study at this time. Of the additional comparison group composed of master sprinters, only one participant had already recruited pre-COVID-19, so recruitment of this group was suspended in an effort to focus on completing the master cyclist (older trained) and age-matched control (older untrained) datasets. After COVID-19 restart, a group of younger (18-30 years) untrained (YU)

participants were recruited instead, allowing for a comparison across age and in a group that was easier to recruit and did not require hotel stays. During the time of the COVID-19 lockdown, the thesis was expanded to include analysis of the data (muscle and fat composition) in other participant groups that had been collected pre-lockdown (Irritable Bowel Disease, Chronic Obstructive Pulmonary Disease), or that were priority projects and went ahead earlier (Post-COVID-19), this work is presented in Chapter 4.

Contents

Chapter 1

Introduction

1.1 Ageing and exercise

We live in an increasingly ageing population. In the United Kingdom, The Office for National Statistics show that in 50 years the number of people aged 65 and over will increase by 8.6 million and a quarter of all children born today will live to 100. twenty five% of the population is over 60 years old. People are living longer, but quality of life is not keeping up with increased lifespan. After the age of 65, it is expected that this population will spend half of their remaining lives in poor health, with the proportion increasing with life expectancy [1]. Concerns contributing to poor health in ageing include cognitive impairment and frailty driven by neurodegeneration and declining musculoskeletal health.

At present, it is not clear how much of this perceived age-related poor health is due to a chronological ageing process and how much may be attributed to lifestyle change, in the context of this thesis decreased habitual physical activity levels. The World Health Organisation rank inactivity in the top 5

of leading risk factors for chronic disease and global mortality, and attribute 5.5% of deaths to sedentary behaviour [2]. In the United Kingdom, 47% of men over 70 years old are classified as being inactive, defined less than 150 minutes of activity a week [3].

Muscle mass and neuromuscular function decline with age, yielding deficits in muscle strength, motor control, balance and gait [4]. Fat infiltration within muscle also impacts muscle function, correlated to gait speed, grip strength, and muscle power measured by isokinetic knee extension, and has been found to be accelerated in ageing [5]. However, high levels of habitual physical activity slow muscle volume loss [6] and intermuscular adipose tissue infiltration [7].

Cardiorespiratory fitness as measured by maximum oxygen uptake (VO_2max) is considered one of the best predictors for all-cause mortality [8] and decreases with chronological age [9]. High levels of physical activity mitigate this change, with an exercise training intervention increasing VO_{2peak} [10]. Cardiac function has been shown to change with chronological ageing, with lower cardiac output driven by smaller stroke volumes [11]. With high levels of physical activity, these changes in stroke volume can be mitigated [12].

Changes in brain structure and function thought to be attributable to chronological ageing processes have been associated with decreased habitual physical activity levels by both our [13] and other research groups. Inactivity in ageing has been linked to a decrease in cerebral blood flow (CBF) [14] and the onset of neurodegenerative disease [15]. Structural changes associated with physical inactivity include decreases in grey matter volume [16] and hippocampal volume [17]. Greater plasticity and adaptability of the brain and slowed cognitive decline have been associated

with greater physical activity [18, 19]. Despite the benefits that have been shown to be associated with physical activity and ageing, the mechanisms that may blunt or prevent decline are poorly understood and requires further research.

1.2 Aims of this thesis

The overarching aim of this study is to understand the effects of lifelong high levels of habitual physical activity on age-related differences to the structure and function of the body, to help identify structural and functional organ level physiological characteristics attributable to ageing from those due to inactivity. To achieve this, lifelong highly active male cyclists, termed the 'older trained' (OT) group in this thesis, age-matched healthy older untrained (OU) males and young untrained (YU) males are studied. Participants underwent physiological tests and MR scans at rest, during supine exercise using a Ergospect Cardio-Step module, and during a recovery period post-exercise. MRI provides a powerful tool to investigate many acute and chronic physiological changes and adaptations within the body, including quantification of dynamic and structural changes. To understand the effects of lifelong high levels of physical activity on age-related changes, MRI measures of the brain (segmented volumes, connectivity, lesions, vessel structure, blood flow and oxygenation), heart (including stroke volume, aortic velocity and cardiac output), and muscle (whole body skeletal muscle and fat composition) are collected. Functional measures of cerebral blood flow and cerebral oxygen extraction fraction and cardiac measures are collected at three timepoints: before, during, and immediately after supine exercise. Measuring these changes during acute exercise and recovery allows the investigation of traits not manifested in the low physiological

stress resting state. Additional cardiovascular fitness, strength, motor control and cognitive measures were also taken outside the MR scanner.

Hypothesis: Many factors considered part of the normal chronological ageing process may in reality be as much or more a function of age-related declines in habitual physical activity levels that often accompanies ageing.

We hypothesise people who have maintained high levels of habitual physical activity may exhibit a number of physiological and structural characteristics closer to a younger group of untrained volunteers than an age-matched untrained group of volunteers. These characteristics will manifest across a number of organ systems (brain, cardiac, and muscle investigated in this thesis) at rest and during acute exercise stress.

The mechanism by which decreased brain atrophy in the highly physically active takes place is likely related to blood flow and oxygenation supply to the brain, so we also hypothesise increased cerebral blood flow alongside higher cardiac output will occur in the YU and OT groups. Greater blood flow and oxygenation in the brain may slow neurodegeneration, with greater structural volumes and cognitive scores in the older trained (OT) than older untrained (OU) individuals.

1.3 Thesis overview

Chapter Two of this thesis explains the theoretical principles behind Magnetic Resonance Imaging (MRI), including an explanation of K-space and MR relaxation times. Image acquisition techniques used in this thesis are outlined including 2D echo-planar imaging (EPI), Phase Contrast MRI (PC-MRI), T_2 relaxation-under-spin-tagging (TRUST), multipoint DIXON

(mDIXON), Magnetization Prepared Rapid Acquisition of Gradient Echo (MPRAGE), T_2 weighted FLuid Attenduated Inversion Recovery sequence (T_2-FLAIR) and Diffusion Tensor Imaging (DTI).

Chapter Three describes the methods development to enable use of the Cardio-Step to conduct VO_2peak testing and for performing supine exercise in the MR scanner. It also details the full study protocol and MR scans acquired for work described in the following chapters within this thesis.

In **Chapter Four** a semi-automatic pipeline to segment calf and thigh muscle volumes and muscle fat fraction from an mDIXON scan is implemented. Results are compared to other leg volume measure tools including manually drawing regions of interest (ROIs) and machine learning, as well as being contrasted to the alternative method of Dual X-Ray absorptiometry (DEXA).

In **Chapter Five**, leg muscle volumes and muscle fat fractions are compared in the OT, OU and YU groups. In addition, other measures of physical function are considered, including muscle strength and work done. Motor control measures consisting of motor unit firing and balance are also measured and results are discussed.

Chapter Six explores the cardiorespiratory response of the OT, OU and YU groups to a VO_2peak test. Results of expired gas data, blood gas data and heartrate are described. MR measures of cardiac structure in the groups are compared and cardiac function at baseline, exercise and recovery are discussed.

Chapter Seven investigates the differences between the OT, OU and YU groups in brain structure, as well as studying functional measures of cerebral blood flow and oxygen extraction fraction at baseline, during supine

exercise and recovery.

Chapter Eight concludes this thesis by summarising the findings and provides suggestions for future work.

References

[1] Office for National Statistics. Living longer: how our population is changing and why it matters. *Office for National Statistics*, 2018.

[2] World Health Organization. *Global health risks: mortality and burden of disease attributable to selected major risks.* World Health Organization, 2009.

[3] World Health Organization. *Global status report on physical activity.* World Health Organization, 2022.

[4] Rachael D Seidler, Jessica A Bernard, Taritonye B Burutolu, Brett W Fling, Mark T Gordon, Joseph T Gwin, Youngbin Kwak, and David B Lipps. Motor control and aging: links to age-related brain structural, functional, and biochemical effects. *Neuroscience & Biobehavioral Reviews*, 34(5):721–733, 2010.

[5] Matt Farrow, John Biglands, Steven F Tanner, A Clegg, L Brown, EMA Hensor, P O'Connor, P Emery, and AL Tan. The effect of ageing on skeletal muscle as assessed by quantitative mr imaging: an association with frailty and muscle strength. *Aging clinical and experimental research*, 33:291–301, 2021.

[6] Adeel Safdar, Mazen J Hamadeh, Jan J Kaczor, Sandeep Raha, Justin Debeer, and Mark A Tarnopolsky. Aberrant mitochondrial home-

ostasis in the skeletal muscle of sedentary older adults. *PloS one*, 5(5):e10778, 2010.

[7] Bret H Goodpaster, Peter Chomentowski, Bryan K Ward, Andrea Rossi, Nancy W Glynn, Matthew J Delmonico, Stephen B Kritchevsky, Marco Pahor, and Anne B Newman. Effects of physical activity on strength and skeletal muscle fat infiltration in older adults: a randomized controlled trial. *Journal of applied physiology*, 105(5):1498–1503, 2008.

[8] Taryn Davidson, Baruch Vainshelboim, Peter Kokkinos, Jonathan Myers, and Robert Ross. Cardiorespiratory fitness versus physical activity as predictors of all-cause mortality in men. *American heart journal*, 196:156–162, 2018.

[9] Andrew C Betik and Russell T Hepple. Determinants of v˙ o2 max decline with aging: an integrated perspective. *Applied physiology, nutrition, and metabolism*, 33(1):130–140, 2008.

[10] Erin J Howden, Satyam Sarma, Justin S Lawley, Mildred Opondo, William Cornwell, Douglas Stoller, Marcus A Urey, Beverley Adams-Huet, and Benjamin D Levine. Reversing the cardiac effects of sedentary aging in middle age—a randomized controlled trial: implications for heart failure prevention. *Circulation*, 137(15):1549–1560, 2018.

[11] Marcello Ricardo Paulista Markus, Till Ittermann, Christine Julia Drzyzga, Martin Bahls, Sabine Schipf, Ulrike Siewert-Markus, Sebastian Edgar Baumeister, Paul Schumacher, Ralf Ewert, Henry Völzke, et al. Cardiac mri shows an association of lower cardiorespiratory fitness with decreased myocardial mass and higher cardiac stiffness in the general population–the sedentary's heart. *Progress in Cardiovascular Diseases*, 68:25–35, 2021.

[12] Evrim B Turkbey, Neal W Jorgensen, WC Johnson, Alain G Bertoni, Joseph F Polak, AV Diez Roux, Russell P Tracy, Joao AC Lima, and David A Bluemke. Physical activity and physiological cardiac remodelling in a community setting: the multi-ethnic study of atherosclerosis (mesa). *Heart*, 96(1):42–48, 2010.

[13] Andrew P. Hale. *Application of MR to Identify Metabolic and Physiological Correlates of Human Ageing and Inactivity*. PhD thesis, 2017.

[14] Philip N Ainslie, James D Cotter, Keith P George, Sam Lucas, Carissa Murrell, Rob Shave, Kate N Thomas, Michael JA Williams, and Greg Atkinson. Elevation in cerebral blood flow velocity with aerobic fitness throughout healthy human ageing. *The Journal of physiology*, 586(16):4005–4010, 2008.

[15] Nicola T Lautenschlager, Kay Cox, and Elizabeth V Cyarto. The influence of exercise on brain aging and dementia. *Biochimica et biophysica acta (BBA)-Molecular basis of disease*, 1822(3):474–481, 2012.

[16] Seyed Amir Hossein Batouli and Valiallah Saba. At least eighty percent of brain grey matter is modifiable by physical activity: A review study. *Behavioural brain research*, 332:204–217, 2017.

[17] Amanda N Szabo, Edward McAuley, Kirk I Erickson, Michelle Voss, Ruchika S Prakash, Emily L Mailey, Thomas R Wójcicki, Siobhan M White, Neha Gothe, Erin A Olson, et al. Cardiorespiratory fitness, hippocampal volume, and frequency of forgetting in older adults. *Neuropsychology*, 25(5):545, 2011.

[18] Arthur F Kramer and Stanley Colcombe. Fitness effects on the cognitive function of older adults: a meta-analytic study—revisited. *Perspectives on Psychological Science*, 13(2):213–217, 2018.

[19] Benjamin Y Tseng, Jinsoo Uh, Heidi C Rossetti, C Munro Cullum, Ramon F Diaz-Arrastia, Benjamin D Levine, Hanzhang Lu, and Rong Zhang. Masters athletes exhibit larger regional brain volume and better cognitive performance than sedentary older adults. *Journal of Magnetic Resonance Imaging*, 38(5):1169–1176, 2013.

Chapter 2

Magnetic Resonance Imaging Theory

Magnetic Resonance Imaging (MRI) is a non-invasive technique used to produce images of the body by detecting signal intensities from differing tissue types. In static images, contrast between tissue types can be used for diagnostic purposes by visual inspection or by calculating quantitative measures. MRI also allows for dynamic imaging, where images are captured across time, for example depicting the movement of the heart through the cardiac cycle. Unlike PET or CT that use ionising radiation, MRI is non-invasive using the principle of nuclear magnetic resonance (NMR) from the signals of precessing nuclei within a magnetic field.

2.1 Nuclear Magnetic Resonance

Rabi et al first demonstrated the principle of nuclear magnetic resonance (NMR) in 1938 [1] which was further developed by Bloch [2] and Purcell [3]. Bloch and Purcell observed that select atomic nuclei can absorb radio

frequency (RF) energy when placed in a magnetic field, and will resonate at a frequency specific to the atom for a given magnetic field strength. Only atomic nuclei that have spin have the ability to resonate. Spin is an intrinsic property of the atom, with atoms with an odd number of constituent nucleons (such as hydrogen (^{1}H), carbon (^{13}C), fluorine (^{19}F), sodium (^{23}Na), and phosphorous (^{31}P)) having half integer spin, and integer spin belonging to atoms with an odd number of protons and neutrons (such as deuterium (^{2}H) and nitrogen (^{14}N)). ^{1}H imaging is the most commonly used nuclei, both because of its high natural abundance in the body within water and as it possesses the highest NMR sensitivity due to its high gyromagnetic ratio. This thesis exclusively collects ^{1}H MRI data, so this will be the focus of this chapter.

When an ^{1}H atom is placed in a magnetic field, the spin (I) creates a magnetic source referred to as the magnetic moment ($\boldsymbol{\mu}$) (Figure 2.1) and the unbalanced atomic mass creates angular momentum ($\mathbf{J}$) of the spin. The magnetic moment is calculated from the angular momentum ($\mathbf{J}$) and gyromagnetic ratio: (γ), $\boldsymbol{\mu} = \gamma \boldsymbol{J}$.

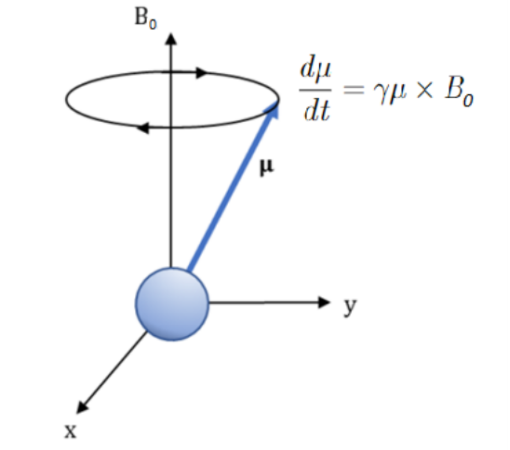

Figure 2.1: Precession of the magnetic moment (μ) around the applied magnetic field (B_0), with the precessional frequency given by the Larmor frequency $\omega_L = \gamma B_0$ which is 127.72 MHz for ^{1}H at 3T as used in this thesis.

A static magnetic field $\boldsymbol{B}_0$, created through a superconducting magnet at a field strength of 3 Tesla (T) is used for all the work in this thesis. The static B_0 aligns the ^{1}H protons' magnetic moment (Figure 2.2) but due to spin angular momentum, the protons also precess in a gyroscopic motion around the static magnetic field. This precession is defined by the equation:

$$\frac{d\boldsymbol{\mu}}{dt} = \gamma\boldsymbol{\mu} \times \boldsymbol{B} \tag{2.1}$$

The frequency of this precession around $\boldsymbol{B}$ is called the Larmor frequency (ω_L) and given by:

$$\omega_L = \gamma B_0 \tag{2.2}$$

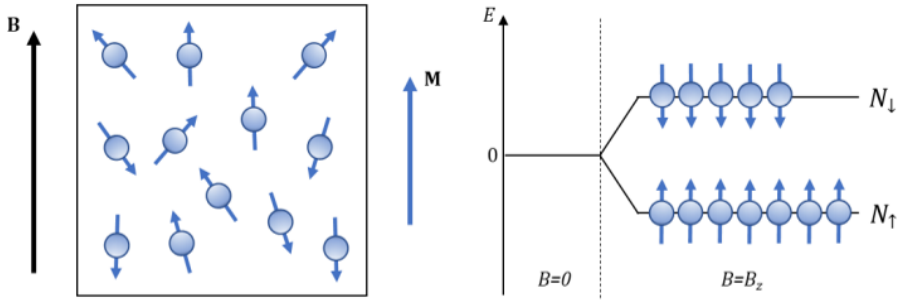

Figure 2.2: Illustration of net magnetisation within an applied magnetic field (B_0). Note that spins can take two possible states, spin up (+1/2) which is the low energy state aligned with B_0 or spin down (-1/2) which is the high energy state opposing B_0.

Each nucleus has a specific gyromagnetic ratio (γ) which for ^1H is 42.56 MHz/T, resulting in the Larmor frequency (ω_L) of protons being 127.72 MHz at 3T. Inside the static field, the spin angular momentum can take two possible values due to being either in the spin up (m_I = +1/2 or N↑) or spin down (m_I = -1/2 or N↓) state given by $\pm\frac{\hbar}{2}$ where $\hbar$ is Plank's constant divided by 2π. This yields two possible energy states of the spins, the high (E_+) and low (E_-) states termed the Zeeman energy levels. The

spins are distributed between the Zeeman energy levels according to the Boltzmann distribution given by:

$$\frac{N\downarrow}{N\uparrow} = e^{\frac{-\Delta E}{k_B T}} = e^{-\frac{\gamma \hbar B_0}{k_B T}} \tag{2.3}$$

where ΔE is the energy difference between the spin states, T is the temperature in Kelvin and k_B is the Boltzmann constant. This leads to a net magnetisation (M_0) of the tissue in the direction of the applied field, B_0. The strength of M_0 is proportional to B_0 strength and inversely proportional to temperature, with greater M_0 yielding greater NMR signal. This is the reason for scanners with a higher static magnetic field being sought. These high static magnetic fields are generated using coils in a superconducting state. By submersion in liquid helium, this keeps them at 4 K, eliminating resistance within the wires to provide a strong magnetic field.

The static (B_0) magnetic field alone cannot create NMR signals, this requires a time varying magnetic field ($B_1(+)$) using radiofrequency waves. Radio-frequency (RF) signals are sent and received by separate RF coils to capture the NMR signals. The RF pulse is sent as an oscillating $B_1(+)$ field at the Larmor frequency. This RF pulse is on resonance with the precession frequency of the magnetic moment and acts to perturb the magnetic moment from the z-axis. The net magnetisation (M_0) can thus be tipped away from B_0 along z into the transverse plane by applying a radiofrequency pulse at a given angle (flip angle) determined by the RF pulse duration (τ) and amplitude (B_1) ($\alpha = \gamma B_1 \tau$) (as shown in Figure 2.3).One specific pulse is an excitation pulse, this often uses a 90° flip angle, this equalises spins in the high and low energy states and brings the spins into phase. This leads to no net magnetisation in the z-plane but a net magnetisation in the xy-plane generating a transverse NMR signal. Another typical RF

pulse is an inversion pulse, this generates a 180° flip angle pulse that inverts the longitudinal magnetisation M_z such that $M_z = -M_0$ (as shown in Figure 2.3). Note 180° pulses can also be used as refocusing pulses to generate an echo for spin echo acquisition as used in diffusion tensor imaging (DTI).

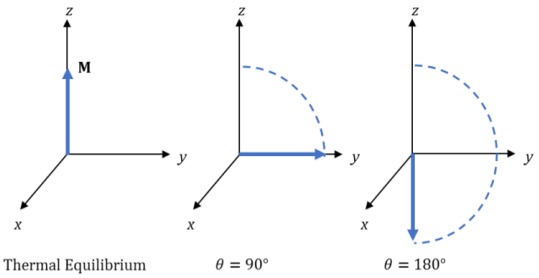

Figure 2.3: Net magnetisation (M) along the z-axis at thermal equilibrium, and the effect of a 90° flip angle (excitation) pulse and a 180° flip angle (inversion) pulse on the magnetisation.

.

The signal generated in the transverse plane (M_{xy}) after the RF pulse induces an electromotive force (emf) in a receive coil, precessing at the Larmor frequency, giving the NMR signal. This signal is called the Free Induction Decay (FID). The longitudinal (M_z) and transverse (M_{xy}) magnetism return to Boltzmann equilibrium through two independent relaxation processes governed by the longitudinal or spin-lattice relaxation (T_1) and transverse or spin-spin relaxation (T_2). This is governed by the Bloch equations:

$$\frac{dM_z}{dt} = -\frac{M_0 - M_z}{T_1} \tag{2.4}$$

$$\frac{dM_x}{dt} = -\frac{M_x}{T_2} + \gamma M_y B_z \tag{2.5}$$

$$\frac{dM_y}{dt} = -\frac{M_y}{T_2} - \gamma M_x B_z \tag{2.6}$$

Longitudinal relaxation is the process of spins returning to their thermal

equilibrium state of M_0 as the longitudinal magnetisation (M_z) recovers and the spins lose their energy to the lattice (T_1 recovery) (Figure 2.5). In transverse relaxation the induced M_{xy} magnetisation decays as spins lose coherence and become out of phase with each other due to spin-spin interactions, leading to an exponential decay in the MR signal governed by the T_2 decay time constant (Figure 2.6). Static field inhomogeneities, spatial encoding gradients, chemical shift and differences in magnetic susceptibility between tissues increase static dephasing and result in a rate of decay of transverse magnetisation above that dictate the T_2 constant, termed T_2^* relaxation ($\frac{1}{T_2*} = \frac{1}{T_2} + \frac{1}{T_2^I}$). The time-scale of T_1 recovery is orders of magnitude greater than that of T_2 decay, with for example the T_1 of brain tissue at 3T of $\sim$ 1600 ms for grey matter compared with a T_2 of $\sim$ 100 ms. Approximate T_1 and T_2 values for tissues at 3 T collected in this study are shown in Figure 2.4. The time chosen to acquire the MR image during relaxation (given by the inversion time (TI) for T_1 and echo time (TE) for T_2) determines the amplitude and thus intensity of the signal in an image and can be used to select different tissue types.

Tissue	T_1 (ms)	T_2 (ms)
CSF	4000	2000
Grey Matter	1600	100
White Matter	800	70
Myocardium	1400	50
Skeletal Muscle	1400	50
Fat	400	130

Figure 2.4: Approximate T_1 and T_2 values at 3 T for tissues investigated in this thesis, [4, 5, 6]

.

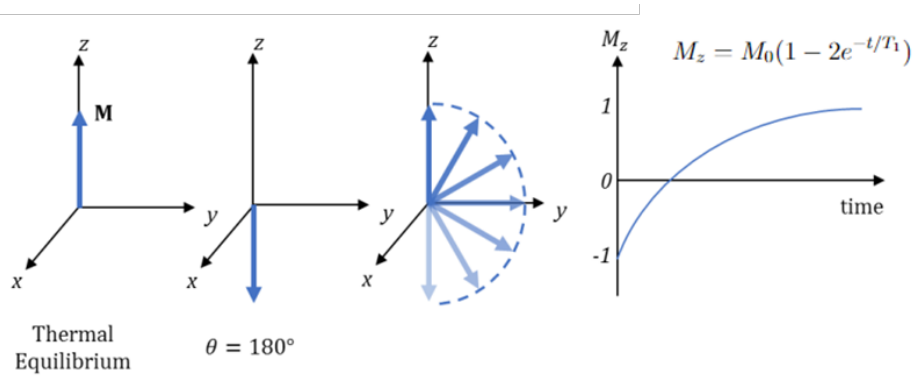

Figure 2.5: Longitudinal relaxation following a 180° pulse showing the magnetisation recovery across time with the T_1 relaxation time constant.

.

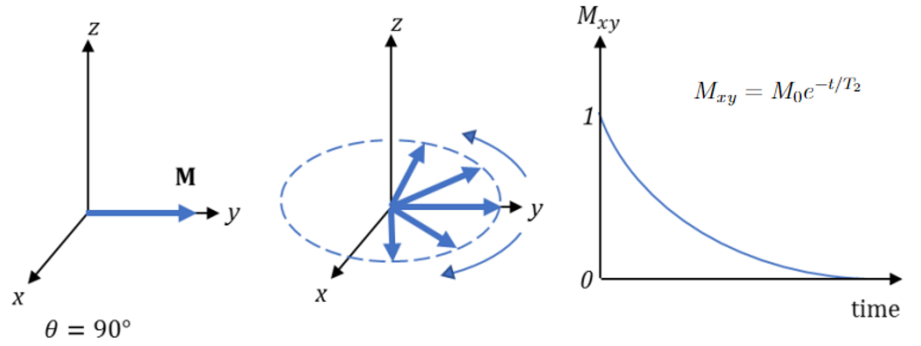

Figure 2.6: Transverse relaxation following a 90° pulse showing exponential decay across time with the T_2 time constant.

.

2.2 Magnetic Resonance Imaging (MRI)

The introduction of spatial gradients to alter the static magnetic field across space allows spatial localisation of protons, and thus the ability to produce MR images. Lauterbur et al [7] reasoned that if the strength of the magnetic field were varied, the resonant frequencies of nuclei would differ based on spatial location within the static magnetic field. By measuring the amount of energy emitted at different frequencies the spatial location of that energy, and thus amount of protons, could be identified. To create

a 2D image, gradient coils arranged along the three orthogonal directions (x,y,z) relative to the static magnetic field (B_0 along z) can be used to resolve spatial information in three dimensions. Data are typically collected in a series of 2D slices, while it is possible to collect 3D images with MR imaging. To select a given single 2D slice, the excitation must be restricted to only the spins within that location. To do this, the frequency range (bandwidth) of the RF pulse must be matched to precessional frequency of the spins in that slice. Frequency is location specific due to the application of a spatially varying magnetic gradient field. This will make only the spins within that slice on-resonance and emit MR signal. The slice thickness (Δz) is determined by the bandwidth of the RF pulse ($\Delta\omega$) and the gradient applied (G_z), as shown in Figure 2.7 and given by:

$$\Delta z = \frac{\Delta\omega}{\gamma G_z} \tag{2.7}$$

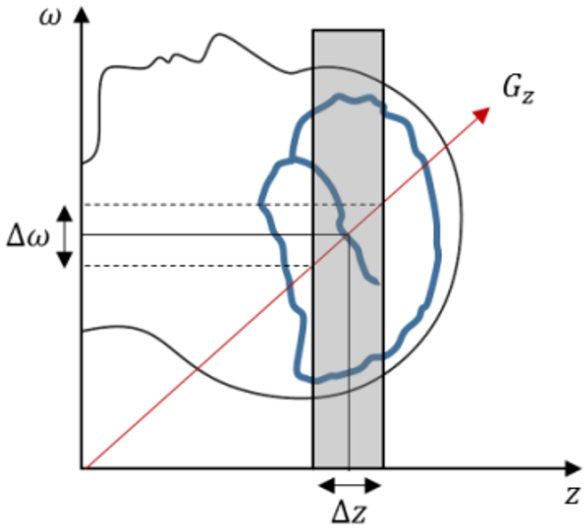

Figure 2.7: Demonstration of slice selection using an RF pulse of bandwidth $\Delta\omega$ and gradient G_z to produce a slice thickness of Δz.

.

Once a slice is selected, it is then followed by a pulse sequence designed to encode the in-plane data in k-space which is then Fourier Transformed to generate an image. To localise the protons within the slice, additional gradient fields in the x and y direction are applied, creating distinct precession frequencies by location. This is called frequency encoding and allows for one-dimensional map of proton density along the direction of the gradient. To achieve a 2D image an additional spatial gradient is needed for phase encoding. Phase encoding gradients are applied sequentially prior to frequency encoding, varying spin phases along the gradient axis (perpendicular to the frequency encoding axis). A Fourier transform (FT) is then used to convert the signal from k-space into image space. Figure 2.8 shows the pulse sequence and k-space for a spin warp readout as used for the structural imaging (MPRAGE and T_2 FLAIR, and cardiac cine data) in this thesis.

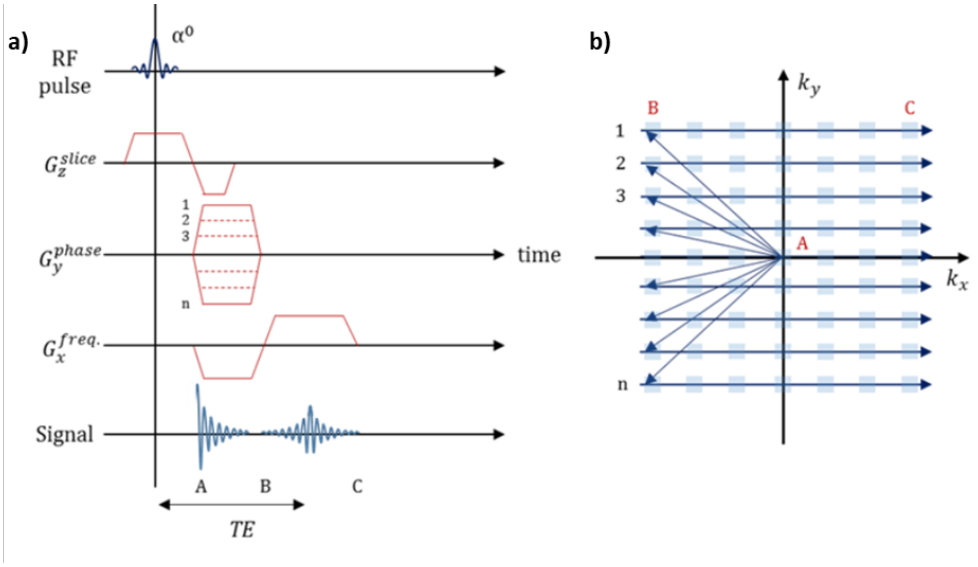

Figure 2.8: a) Spin warp pulse sequence and b) how this is encoded in k-space.

.

In 1977, Sir Peter Mansfield developed a technique for much faster imaging called echo-planar imaging (EPI), this provides a much more efficient

image acquisition by allowing collection of the whole of k-space simultaneously [8]. To achieve this, all phase encoding steps are collected after a single RF excitation pulse by rapidly altering gradients in the read direction to create multiple gradient echoes. Alternating lines are scanned in opposite directions to fill k-space (Figure 2.9). This allows rapid imaging but provides lower resolution than spin warp, in this thesis this acquisition is used for collection of diffusion tensor imaging (DTI) data.

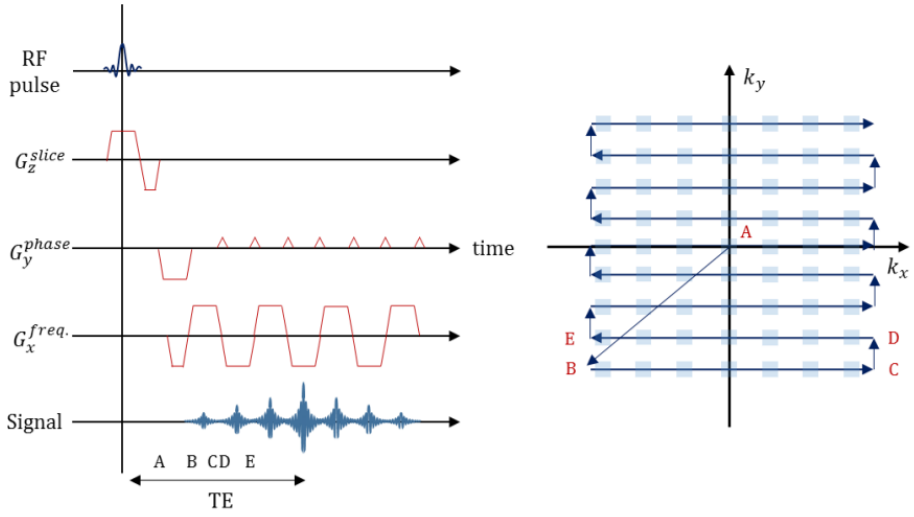

Figure 2.9: Echo Planar pulse sequence demonstrating the alternating direction to fill k-space after a single RF pulse, as used for the collection of diffusion tensor imaging (DTI) data.

.

2.3 Image types and techniques

2.3.1 T_1-weighted and T_2-weighted structural scans

Magnetisation prepared rapid gradient echo (MPRAGE) is a T_1-weighted gradient echo sequence used to produce high spatial resolution images with high contrast between grey, white matter, and cerebral spinal fluid (CSF) (Figure 2.10). The pulse sequence creates a magnetisation preparation

period with an initial 180° pulse to invert the magnetisation followed by an inversion delay to achieve T_1 weighting. A rapid gradient echo sequence follows to sample the prepared magnetisation. A recovery period ends the acquisition. The magnetisation preparation period reduces the acquisition time compared to a steady-state acquisition scheme with the same contrast [9]. An MPRAGE sequence is used in this thesis for the segmentation of grey matter, white matter and CSF to provide cortical volume and cortical thickness metrics (Figure 2.11a). Structural imaging is also used in this thesis to generate cardiac cine scans.

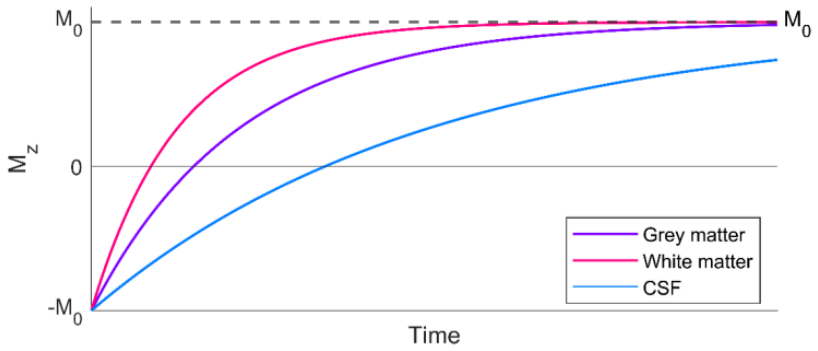

Figure 2.10: Brain tissue (grey matter, white matter and CSF) differentiation using T_1 recovery following a 180° inversion pulse.

.

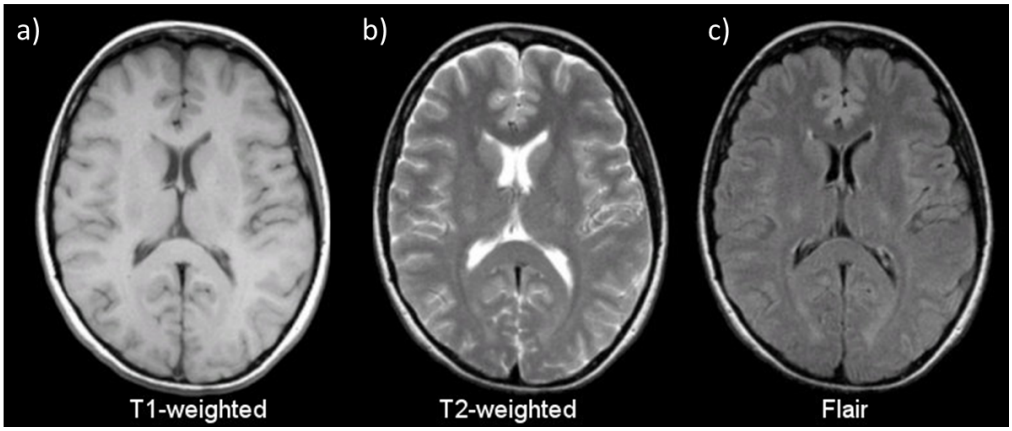

Figure 2.11: T_1 weighted, T_2 weighted and FLAIR images in the brain showing tissue and fluid contrast in grey matter, white matter and CSF, with CSF suppressed in FLAIR.

.

T_2 weighted images provide contrast based on the T_2 relaxation times in Figure 2.4 and shown in Figure 2.11b. In the brain, grey matter and white matter have much shorter T_2 times than CSF (Figure 2.4) due to slower dephasing of water, yielding high signal in CSF. A long TR is used to minimise the T_1 contrast and T_2 contrast levels are dictated by altering the TE, typically a long TE is used to maximise differences in T_2 decay.

FLuid-Attenuated Inversion Recovery (FLAIR) is a T_2 weighted pulse sequence tuned to detect white matter hyperintensities, used primarily in the brain for detecting lesions (Figure 2.11c). The bright contrast of CSF T_2 weighted images make lesion detection difficult because CSF is not sufficiently differentiated from white matter hyperintensities, making lesions that often occur near ventricle borders difficult to identify. FLAIR uses a long TR and TE to create strong T_2-weighting in conjunction with a long inversion time (TI) to suppress signal from CSF.

2.3.2 Diffusion Tensor Imaging (DTI)

Diffusion weighted imaging (DWI) is a technique used to measure diffusion (the random motion of water) within tissue. It can be used in various organs and tissue types. Here diffusion tensor imaging (DTI) is used to measure diffusion within axonal tracts in the brain as shown in Figure 2.12 and is discussed below. Spins diffuse quickly along the length of axonal fibres but slowly across the width, and therefore the structure of axonal bundles throughout the brain can be surmised. In DTI, strong diffusion gradients are applied symmetrically before and after a 180° refocusing pulse. The number of different diffusion gradient directions used can vary, with more gradients allowing for greater specificity of diffusion direction; 64 gradients is a common number used and was the number of directions chosen for this

thesis. The duration of the applied diffusion gradients, the time interval between diffusion gradients and amplitude determine the degree of diffusion weighting (b-value). The primary direction of diffusion determined by the differences in diffusion coefficient between different orientations is termed the fractional anisotropy (FA) and an is indicator of myelination, fibre density and axonal diameter in DTI. The mean of the three eigenvalues of the diffusion tensor is the mean diffusivity (MD) and indicates the mobility of water molecules.

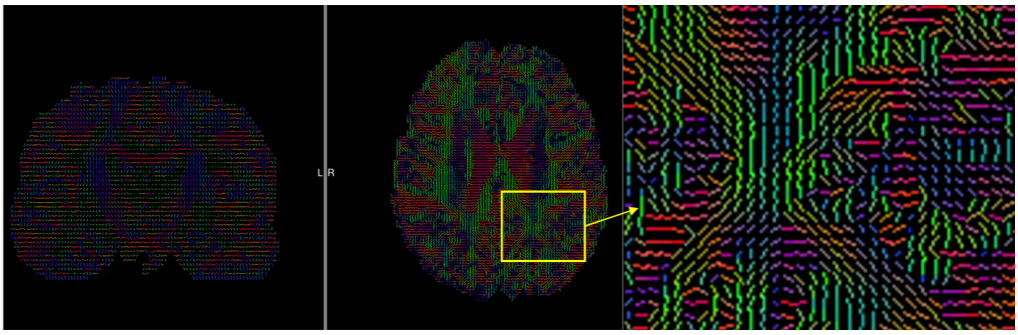

Figure 2.12: Diffusion within the brain with direction indicated by colour and line angle.

.

2.3.3 Phase Contrast MRI (PC-MRI)

Phase contrast MRI (PC-MRI) is a technique used to measure the movement of blood within vessels. A velocity encoding bipolar gradient field is applied in the direction perpendicular to the imaging plane. As spins move through the imaging plane in the blood, the equal and opposite gradient fields of the bipolar gradient induce the spins to de-phase and re-phase (Figure 2.13). A net velocity dependent phase shift (ϕ) is created in the moving blood spins, whilst no net phase shift given for static spins. The net phase of the spins is proportional to the velocity, as given by:

$$\phi = -\gamma v M_1 \tag{2.8}$$

where v is velocity and M_1 is the product of the gradient amplitude and time of application of the gradient field. This is used to quantify the velocity of the blood moving though the imaging plane. Phases can be collected at multiple timepoints throughout the cardiac cycle through cardiac gating. Images are continuously acquired after each heartbeat and selected to distribute images evenly across the cardiac cycle. In this thesis, PC-MRI is used to assess both cardiac output by performing measures across the aorta in Chapter 6 with 30 phases and a velocity encoding (V_{ENC}) of 300 cm/s and for cerebral blood flow by collecting measures across carotid arteries and the basilar artery in Chapter 7 using 30 phases and a V_{ENC} of 140 cm/s.

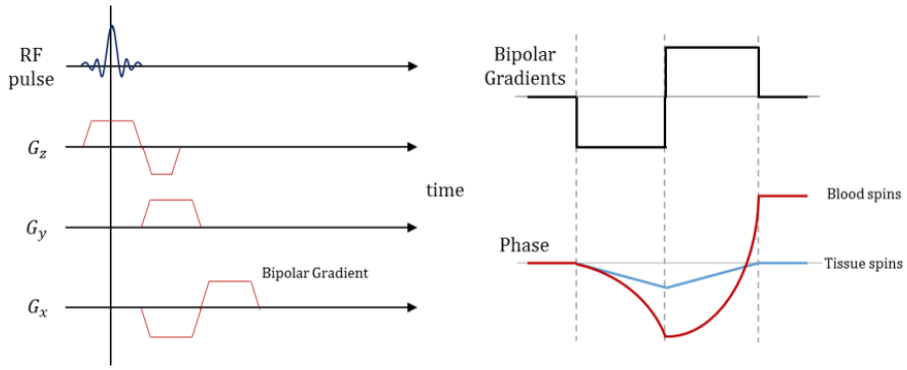

Figure 2.13: Pulse sequence diagram for PC-MRI showing biploar gradients induced phase shift in the blood spins.

.

2.3.4 T_2 Relaxation Under Spin Tagging (TRUST)

T_2 Relaxation Under Spin Tagging (TRUST) is technique used for calculating oxygen extraction fraction (OEF) by measuring venous oxygenation and is most commonly used in the brain for the estimation of venous oxygenation in the sagittal sinus. In this thesis FAIR arterial spin labelling (ASL) images are acquired in pairs of 'label' and 'control' images. Unlike

traditional ASL which focuses on labelling arterial blood, in this case the label image magnetically tags out-flowing blood in a venous vessel (e.g. the sagittal sinus) using an inversion RF pulse in a labelling slab placed above the imaging slice (Figure 2.14a). The control image has no label applied. A series of flow-insensitive T_2-preparation pulses are applied prior to the excitation pulse to modulate T_2-weightings by varying the duration of the T_2 preparation sequence (effective TE), yielding the T_2 relaxation time of the venous blood. Pairwise subtractions between these images across multiple effective TEs will therefore yield difference images that depict the magnetised blood signal (Figure 2.14b). The T_2 relaxation time of this blood is converted into blood oxygenation using a calibration plot [10], further analysis is descried in Chapter 7.

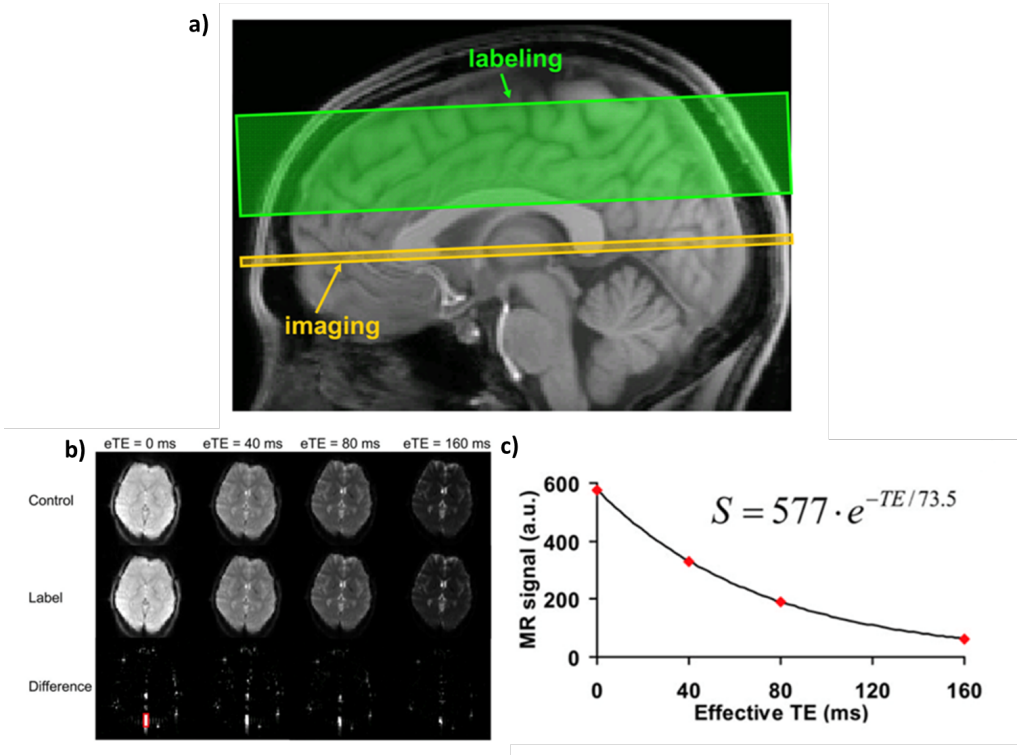

Figure 2.14: TRUST acquisition in the sagittal sinus showing a) image and labelling planes and b) the resultant label, control and difference images (from subtracting the FAIR non-selective and selective images) over 4 effective TEs and c) MR signal decay across effective TEs.

.

2.3.5 DIXON imaging

Fat (F) and water (W) differentiation (to separate fat and muscles and/or organs) can be done using a DIXON imaging technique (Figure 2.15). Water and fat have different resonance frequencies (Δf= 440 Hz at 3 T), resulting in their spins falling in and out-of-phase with each other as a function of time. This phase cycling occurs at $1/\Delta$f or every 1.1 ms at 3 T. Therefore images can be obtained at TEs specified to occur while spins are either in-phase (2.2, 4.4, 6.6 ms, etc) or out-of-phase (1.1, 3.3, 5.5 ms, etc). By collecting images at both in-phase (IP), where the signal can be represent as $W + F$, and out-of-phase (OP), where the signal can be represented as $W - F$, the images can be combined to create fat only and water only images, as given by:

$$\frac{1}{2}[IP + OP] = \frac{1}{2}[(W + F)] + (W - F)] = \frac{1}{2}2W = W \tag{2.9}$$

$$\frac{1}{2}[IP - OP] = \frac{1}{2}[(W + F)] - (W - F)] = \frac{1}{2}2F = F \tag{2.10}$$

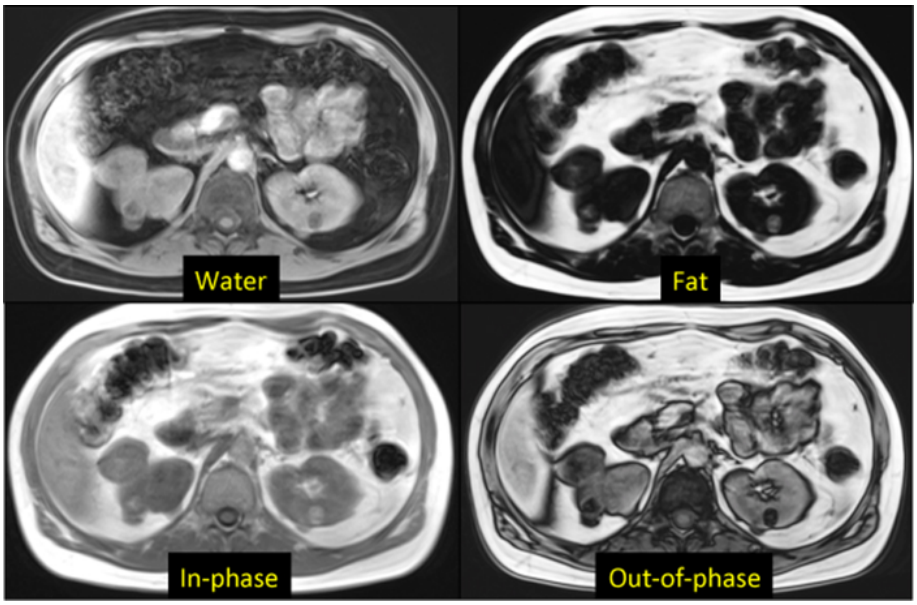

Figure 2.15: Dixon image showing in-phase and out-of-phase images and the resultant water and fat images.

.

More recently, rather than using two echoes, multipoint DIXON (mDIXON) with multiple echoes (six used in this thesis) has been introduced. This provides better image quality and compensates for B_0 heterogeneity to provide estimates of fat fraction and T_2* of tissues.

2.4 Conclusion

This chapter has outlined the core NMR and MRI principles, and introduced the imaging sequences used throughout this thesis.

References

[1] Isidor Isaac Rabi, Jerrold R Zacharias, Sidney Millman, and Polykarp Kusch. A new method of measuring nuclear magnetic moment. *Physical review*, 53(4):318, 1938.

[2] Felix Bloch. Nuclear induction. *Physical review*, 70(7-8):460, 1946.

[3] Edward M Purcell, Henry Cutler Torrey, and Robert V Pound. Resonance absorption by nuclear magnetic moments in a solid. *Physical review*, 69(1-2):37, 1946.

[4] L Chen, M Bernstein, J Huston, and S Fain. Measurements of t1 relaxation times at 3.0 t: implications for clinical mra. In *Proceedings of the 9th Annual Meeting of ISMRM, Glasgow, Scotland*, page 1391, 2001.

[5] Greg J Stanisz, Ewa E Odrobina, Joseph Pun, Michael Escaravage, Simon J Graham, Michael J Bronskill, and R Mark Henkelman. T1, t2 relaxation and magnetization transfer in tissue at 3t. *Magnetic Resonance in Medicine: An Official Journal of the International Society for Magnetic Resonance in Medicine*, 54(3):507–512, 2005.

[6] PJ Wright, OE Mougin, JJ Totman, AM Peters, MJ Brookes, R Coxon, PE Morris, M Clemence, ST Francis, RW Bowtell, et al. Water proton t1 measurements in brain tissue at 7, 3, and 1.5 t using

ir-epi, ir-tse, and mprage: results and optimization. *Magnetic Resonance Materials in Physics, Biology and Medicine*, 21:121–130, 2008.

[7] Paul C Lauterbur. Image formation by induced local interactions: examples employing nuclear magnetic resonance. *nature*, 242(5394):190–191, 1973.

[8] Peter Mansfield. Multi-planar image formation using nmr spin echoes. *Journal of Physics C: Solid State Physics*, 10(3):L55, 1977.

[9] John P Mugler III and James R Brookeman. Three-dimensional magnetization-prepared rapid gradient-echo imaging (3d mp rage). *Magnetic resonance in medicine*, 15(1):152–157, 1990.

[10] Hanzhang Lu and Yulin Ge. Quantitative evaluation of oxygenation in venous vessels using t2-relaxation-under-spin-tagging mri. *Magnetic Resonance in Medicine: An Official Journal of the International Society for Magnetic Resonance in Medicine*, 60(2):357–363, 2008.

Chapter 3

Development of Methods

3.1 Setup of the Cardio-Step and CardioPulmonary Exercise Testing (CPET) equipment

3.1.1 Ergospect Cardio-Step

Research described in this thesis involved in-magnet supine exercise using a Ergospect Cardio-Step unit (Ergospect, Innsbruck, Austria). This work builds upon previous research in this lab by Dr Andrew Hale et al. [1] which used a Lode cycle Ergometer (Lode, Germany) to collect MRI measures during supine exercise. Following Hale's study, the limitations of using the Lode cycle ergometer for exercise studies inside the magnet in terms of participant height and degree of head motion prompted the purchase of an Ergospect Cardio-Step, as seen in Figure 3.1.

Prior to the start of the EXAGE study, some development work was un-

dertaken in this research team by Dr Jordan McGing to assess the validity of using the Cardio-Step during incremental steady-state exercise to assess cardiovascular fitness using expired gas measures and indirect calorimetry for use in the MR environment. A number of challenges with the Cardio-Step equipment were identified in terms of radio-frequency (RF) and noise introduced into the MR scanner. These were resolved with additional shielding and keeping power supply outside of the scanner room, and this work describes the use of the Ergospect Cardio-Step module after this. This and the calibration of the Cardio-Step was outlined in McGing's thesis [2].

Figure 3.1: Ergospect Cardio-Step a) illustration provided by Ergospect b) setup of the Cardio-Step in the David Greenfield Human Physiology Unit with it used on a scanner bed to match in-magnet exercise studies.

The Cardio-Step device allows for physical activity using the legs in the

supine position necessary for MRI, while attempting to have as much of the body inside the magnet as possible and mitigating against movement. Exercise is performed by pushing down against each pedal in an alternating pattern in time with a metronome played to the participant. Air pressure resistance is used to alter the work needed to push the pedals down (as can be seen in the illustration of the MRI setup, Figure 3.2) and can be automatically controlled with pre-assigned timed sequences in the Ergospect software, as well as altered during the exercise session if required. Force transducers within the device measure the force exerted as well as frequency, and these measures are used to maintain the exercise workload throughout the exercise protocol (as shown in the feedback on the Ergospect software in Figure 3.3). Should the participant slow their rate of stepping, the air pressure increases to compensate for this, and the reverse is true if step rate is increased. This therefore allows some deviation from the metronome without large fluctuations in work output (i.e. isokinetic exercise). During studies within this thesis, participants were always verbally encouraged to maintain stepping to the pace of the metronome, if they slowed to 10 bpm below the preset 70 bpm this resulted in the termination of the experiment. These feedback measures also allowed the data to be checked to confirm the desired exercise workload was adhered to.

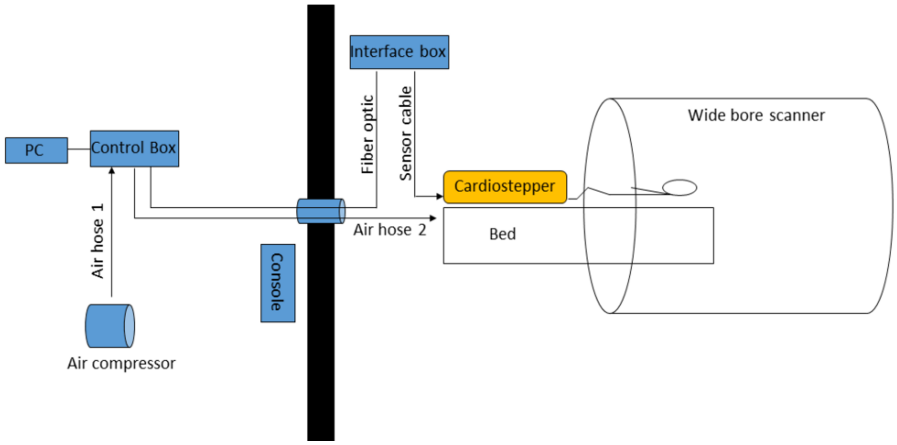

Figure 3.2: Schematic diagram of the Ergospect Cardio-Step in the 3T Ingenia MR scanner. The solid black block indicates the wall between the MR control room and the scanner room.

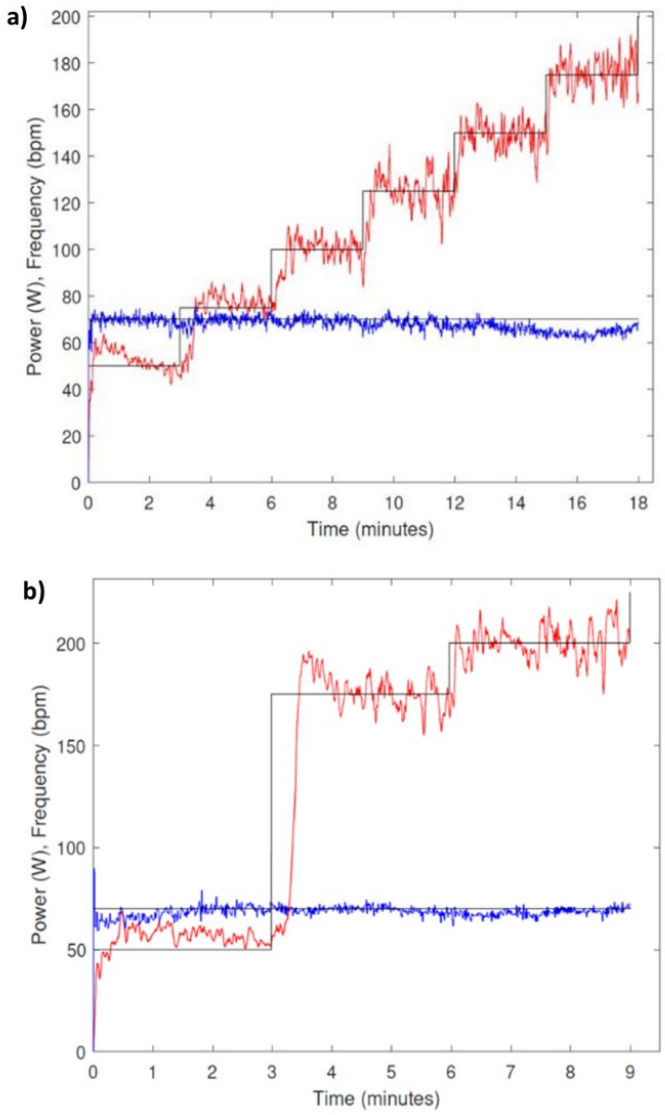

Figure 3.3: Power (red) and frequency (blue) in an a) incremental and b) confirmation exercise test measured on the Cardio-Step extracted from the Ergospect software.

Participants all took part in the screening, consenting and non MRI physiological assessments at the David Greenfield Human Physiology Unit (DGHPU, University of Nottingham) (see Section 3.2), where a custom-made support frame was used to hold a Phillips MR scanner bed onto which the Cardio-Step could be held in place with a vacuum pump, as seen in Figure 3.1. This provided an identical setup to the in-magnet exercise procedure which took place in the Sir Peter Mansfield Imaging Centre (SPMIC). Participants

lay on the bed and had their feet strapped into the pedal boots using Velcro straps, with an optional lumbar support and a pillow for the head. The participant was positioned so their knee angle was 25-30° when the pedal was fully compressed, preventing their knees from hyper-extending when exercising and maintaining a consistent position between exercise sessions. A waistcoat was also worn which was fixed to the Cardio-Step, and straps tightened until secure, preventing the participant from pushing themselves out of position and helping to minimise movement when used in the MRI scanner.

3.1.2 Cardiopulmonary exercise testing (CPET)

Along with the workload measures from the Cardio-Step, expired gases and arterialised-venous blood gases were measured during cardiopulmonary exercise testing (CPET) at the DGHPU. Expired gases were collected and analysed using indirect calorimetry through a 28 mm turbine containing a sampling line connected to a facemask for continuous breath-by-breath online gas analysis (Cosmed, Rome, Italy) (Figure 3.4). A heartrate monitor was worn across the chest, which interfaced with the Cosmed to collect heart rate data throughout each test. Additionally, a 3 lead ECG was used for safety monitoring, and while it does not collect the data, should the heart monitor have failed, heartrates could be manually noted. To collect blood gases during exercise, a retrograde cannula was inserted by a qualified clinician into a vein on the dorsal surface of the participant's hand. The hand was then kept in a hot-box for at least 15 minutes before and for the duration of the exercise session, to allow collection of arterialised-venous blood samples throughout [3, 4]. Blood samples were taken directly from the cannula into 1 ml heparinised syringes during each workload and pro-

cessed on an iStat blood gas analyser (Abbott Laboratories, Abbott Park, IL, USA). The experimental set up depicting the Cardio-Step, CPET and hot-box can be seen in Figure 3.5.

Figure 3.4: Cosmed face mask with turbine, sampling line and head straps.

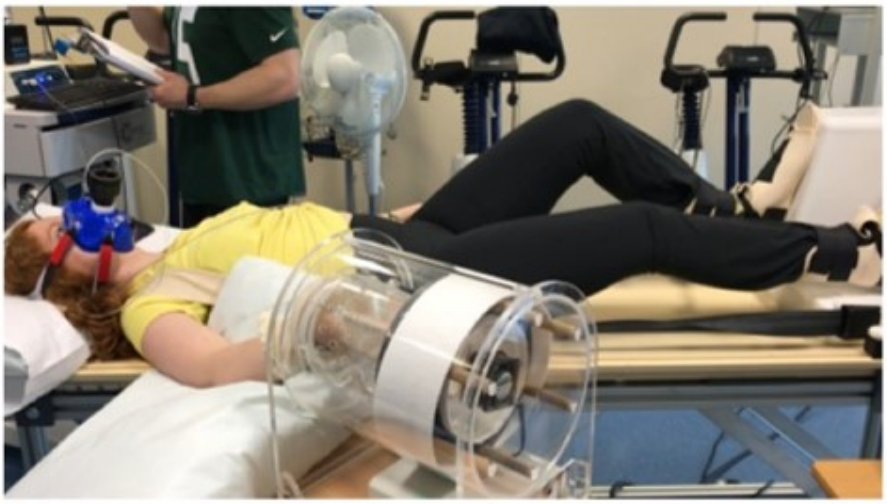

Figure 3.5: Full David Greenfield Human Physiology Unit Cardio-Step setup showing the Cardio-Step, CPET and hot-box

To determine the maximal oxygen consumption for each participant, data was collected at increasing workloads. The metronome was set to 70 bpm, beginning at a workload of 50W. Workloads increased by 20-25W, with each increment lasting three minutes to reach steady-state and proceeding directly onto the next incremental round, with blood samples taken in the last 30 seconds of each workload. Participants were encouraged to exercise until volitional exhaustion, with exercise terminated by the investigator

prior to the participant decision to stop only if there were concerns from the consulting clinician, or if the power and frequency were not met and encouragement failed to get the power back within acceptable bounds.

3.1.3 Assessment of repeatability of Cardio-Step VO_2 measures

The first Cardio-Step device purchased by the University of Nottingham was built to be compatible with a 7T Philips Achieva MR scanner, and was assessed for its validity in quantifying VO_2 and peak measures during incremental intensity supine exercise, as described in McGing's thesis [2]. The protocol is described in Section 3.1. Blood gas measures were not collected in these validation tests. This initial testing found the expected linear response of heartrate and VO_2 to increasing exercise workload, as well as good reliability in a test re-test within participant, yielding a co-efficient of variation of 3.9% for VO_2 peak across four test repetitions. However, subsequent to this testing, a software malfunction caused the device to begin to exhibit power fluctuations that led to random increases and decreases in the intended workload. After discussion with the manufacturer, the Cardio-Step was returned and exchanged for the 3T MR compatible Cardio-Step model which was used in all the work in this thesis. The validity of this 3T Cardio-Step was re-tested within the scope of this thesis alongside McGing and Dr Ayushman Gupta. Figure 3.6 shows the results of testing the 3T Cardio-Step in three participants, while Figure 3.7 shows the results of performing five repeated sessions in a single participant , both minute ventilation and expired CO_2 volumes yielded curvilinear responses to exhaustive incremental exercise, while heartrate and VO_2 exhibited a linear response to increasing exercise workload. The repeatability test indicated

a coefficient variation of 6% for VO_2 peak across the 12-week period, down to 1% when assessing over at a shorter three week period.

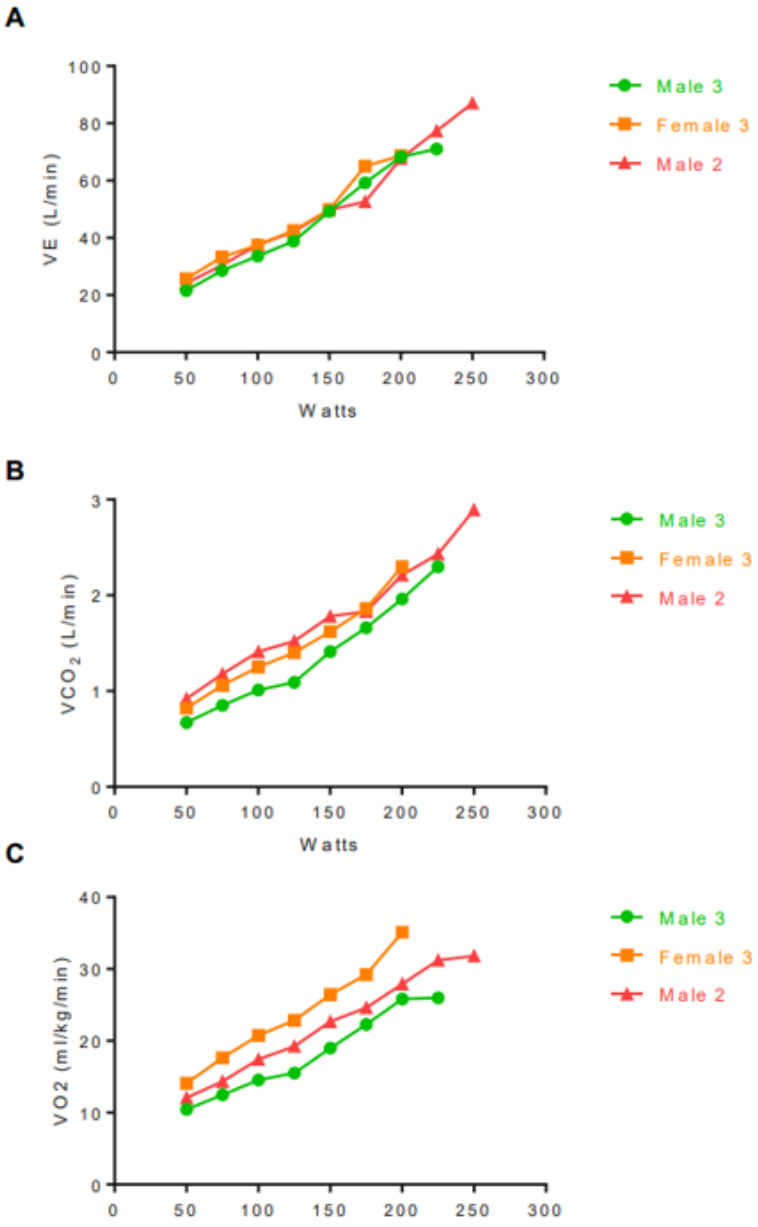

Figure 3.6: 3T Cardio-Step MR system validity testing using expired gas data from three participants [2].

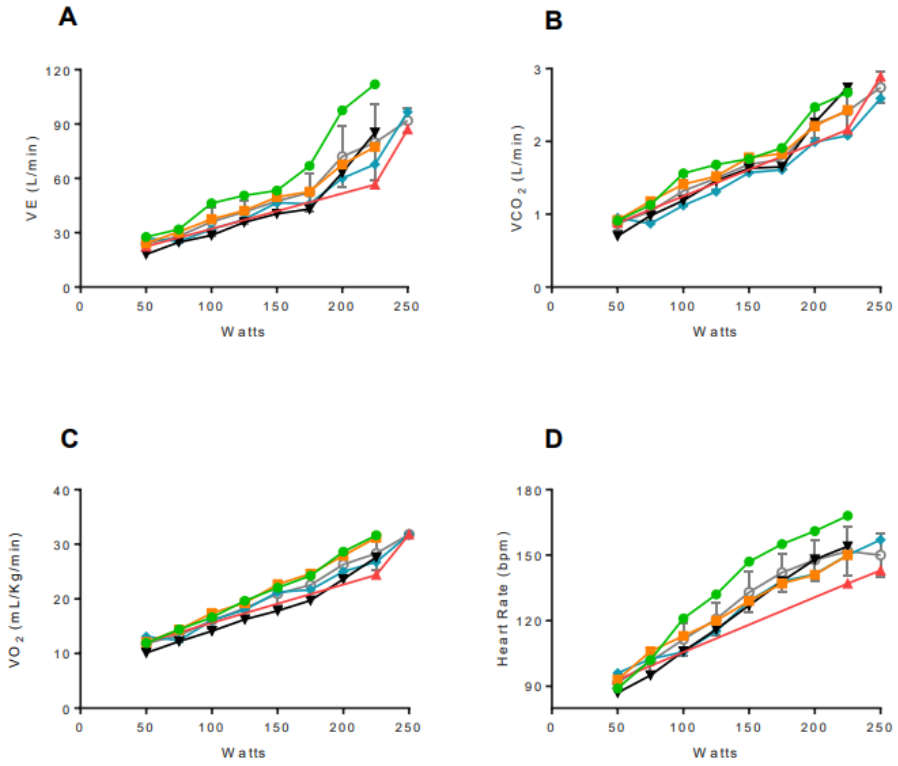

Figure 3.7: 3T Cardio-Step MR system repeatability testing using expired gas data from one participant across five sessions [2]

In 2020, a second Cardio-Step system was purchased from Ergospect in an effort to allow greater flexibility of scheduling multiple studies using the equipment, as well as mitigating the need to transport the Cardio-Step unit and associated equipment between the DGHPU and SPMIC (control box, interface box, air compressor, vacuum pump, vacuum pump hose, compressor-to-control-box hose, control-box-to-Cardio-Step hose, fiberoptic cable, Ethernet cable, sensor cable, waistcoat, calibration module and laptop). Prior to the purchase of a second Cardio-Step unit, duplicates of the majority of the accessory equipment were obtained, leaving only the necessity of transporting the Cardio-Step, waistcoat, calibration module, a hose adaptor and laptop, which continued to be logistically difficult to transport or schedule multiple studies at times. On initial testing of the second Cardio-Step, each workload was perceived to be considerably

more difficult to achieve and maintain than it had on the original stepper. This perceived difference was confirmed by heart rate data generated when comparing measures using the two Cardio-Step systems side by side (Figure 3.8). This initial test was conducted when the lab was beginning to be allowed to return to testing post-COVID, so at this time a VO_2 collection via mask was not allowed, and exercise was required to be submaximal, with participants required to stop exercising at a thresholded heartrate. Data from this submaximal testing was sufficient to decide that the equipment should continue with use of only one Cardio-Step as they were not interchangeable. Once VO_2 collection and exercising to exhaustion was approved, the steppers were compared again, and a difference between the two versions was still notable (Figure 3.9). At the direction of the manufacture, calibration adjustments were attempted without success. The greater resistance found in the second Cardio-Step system was likely due to the tighter fit of the casing into which the pedals are pushed, which have a gap and a rubber seal in the original, but fit snugly and can be felt to generate heat due to the greater friction in the new Cardio-Step, as seen in Figure 3.10.

For the purposes of completing this study without the further delay of sending the equipment to be serviced in Austria (time consuming due to shipment, customs, and potential delays; previously servicing took approximately 8 months due to a part no longer manufactured), a single Cardio-Step device was used within all participants, but as the equipment was not available during the entirety of the study, not all participants used the first Cardio-Step system. Therefore, workloads between participants are not directly comparable, but as each participant only used a single version of the Cardio-Step and the relative workloads are internally consistent. For future studies, the casing could be sanded down and assessed in an attempt

to reach consistency between the two versions.

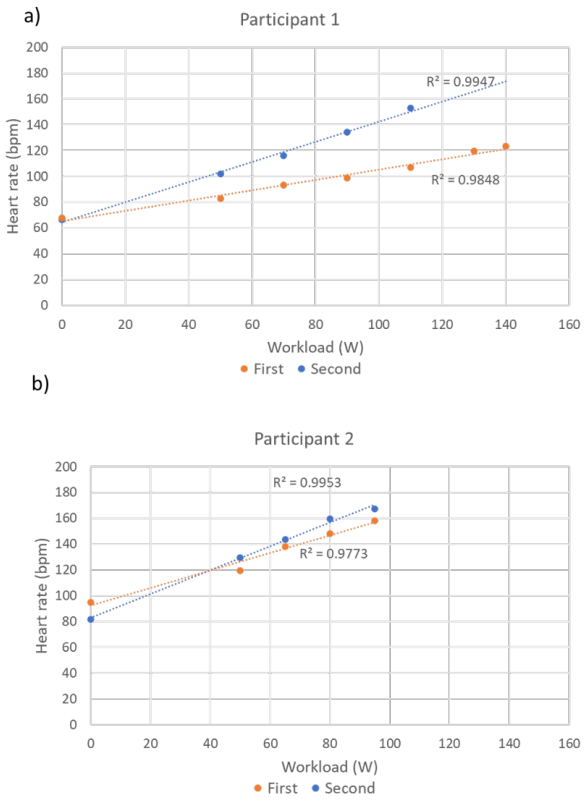

Figure 3.8: Heart rate response to submaximal incremental exercise test comparing the first and second Cardio-Step systems in two participants.

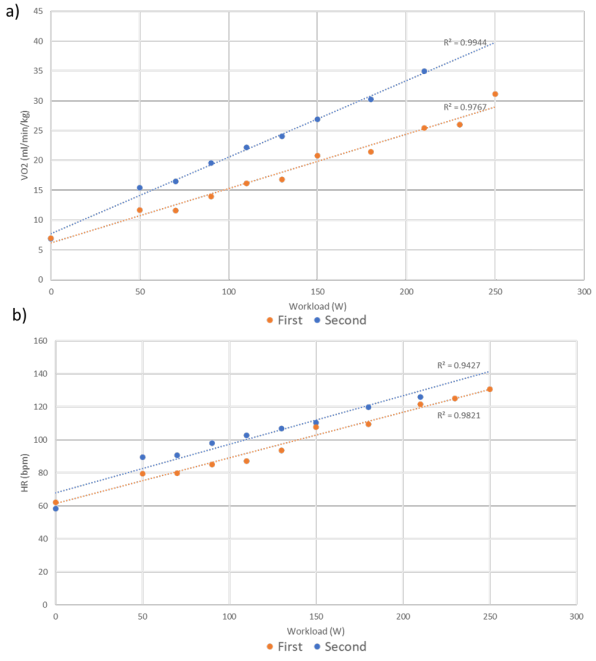

Figure 3.9: a) VO_2 and b) heartrate response to maximal incremental exercise test comparing the fist and second Cardio-Step systems.

Figure 3.10: Pedal casing on the first and second Cardio-Step system

3.2 Full protocol for the EXAGE study

3.2.1 Brief overview

The EXAGE study aimed to investigate the interaction of lifelong EXercise on AGE on the muscles, heart and brain structure and function using MR imaging in the resting state and during acute submaximal exercise and recovery, along with other out of scanner measures of cardiovascular fitness, strength, endurance, motor control and cognitive function.

A group of older (70-76 years old) highly active males who cycled long distances weekly and were capable of cycling 100 km were recruited, referred to in this thesis as the older trained (OT) group. This group had maintained high levels of physical activity throughout their lives with only minimal disruption (e.g a period of 5 years of less activity 15 years prior to the study). To allow investigation of the impact of lifelong habitual exercise, a control group of older males (68-79 years old) who did not take more than 10,000 steps daily and did not take part in any moderate to intense cardiovascular exercise were recruited and referred to as the older

untrained (OU) group. An additional young (21-27 years old) male group was recruited to examine the effect of ageing, who also did not take part in regular intense physical activity and were deemed the young untrained (YU) group.

After a medical screening, participants undergo one day of physiological testing, and one day of MRI and motor unit testing, as outlined in Figure 3.11.

Screening	Study Day 1	Study Day 2
David Greenfield Human Physiology Unit	David Greenfield Human Physiology Unit	Sir Peter Mansfield Imaging Centre
1. Consent 2. Medical/MR safety screening 3. Height/Weight 4. MOCA 5. ECG 6. Blood pressure 7. Blood sample	1. Isometric and Isokinetic strength 2. Familiarisation of Cardio-Step 3. Cannula Insertion 4. Incremental VO_2 peak the Cardio-Step 5. Cognitive tests 6. Confirmation VO_2 peak	1. MR session 1: Anatomical scans 2. MR session 2: Functional scans during: a) rest b) exercise c) recovery
		Royal Derby Hospital
		1. Intramuscular electromyography 2. Timed-up-and-go 3. Jumps 4. Balance

Figure 3.11: Overview of the full study protocol. For the Older Trained participants, the Screening Visit was combined with the Study Day 1 visit.

On the first study day, isometric strength measures were taken with a knee extensor test. Following this, the participants exercised on a supine Cardio-Step (Ergospect), starting at 50 Watts with an increase in workload every 3 minutes, until exhaustion. Respiratory data were collected during exercise through a ventilation mask to measure oxygen uptake, expired CO_2 and minute ventilation, as well as blood sampling during the last 30 s at each workload. A confirmation of peak VO_2 was taken later that same day by having the participants exercise on the Cardio-Step, separated from the incremental test by a minimum of 1.5 hours. Cognitive and motor

skill assessments were carried out in breaks. Time constraints necessitated carrying out the cognitive tests during the break period after the incremental exercise task, which may induce post-exercise effects on cognition, as reviewed in McMorris and Hale's meta-analysis [5].

On the second study day, MRI scans were collected in two sessions. Session one consisted of anatomical measures, after a short break session two consisted of functional MR data collected during rest, exercise and recovery on the Cardio-Step within the MR scanner. On the same day, assessments of physical function were also acquired with measures of peripheral motor unit remodelling using intramuscular electromyography (iEMG) and percutaneous nerve stimulation at the University of Nottingham Royal Derby Hospital site. More specific assessments of muscle control were made using force tracking tasks and standing balance on a force platform.

3.2.2 Recruitment and medical screening

The life-long older trained (OT) exercisers were recruited from a cycling magazine and a curated database of volunteers who had participated in earlier physiological research investigations.

To participate, the OT group had to report a capability of cycling 100 km, and participating in endurance cycles multiple times a week. The OU and YU groups did not take more than 10,000 steps daily and did not regularly take part in aerobic exercise.m Both older untrained (OU) and young untrained (YU) were recruited through posters, local community groups and word of mouth. Participants indicating interest were sent an information sheet to explain the study protocol. An initial medical screening visit took place at the David Greenfield Human Physiology Unit (DGHPU), includ-

ing height, weight, blood pressure, an ECG screening, blood draw, medical history questionnaire, MRI safety screening and exercise history. All participants had to be healthy (not exhibiting any age-related or other diseases and having normal blood count, thyroid function, and kidney function) and have a normal BMI, with a height limitation of 187 cm due to MR scanner bed limits. Cardiac impacting medications were initially all excluded, but difficulties in recruiting participants expanded inclusion criteria to include blood thinners and selective beta-blockers, with non-selective beta-blockers remaining an exclusion criteria. MR safety exclusions also applied, as well as excluding for MR safe metal implants such as hip replacements that would impair image quality. A total of 133 individuals indicated interest, with 9 OT, 7 OU and 8 YU participating. Individuals either withdrew interest or were excluded. Exclusion reasons included MR safety and image quality reasons (pace makers and hip replacements), medications (e.g. non-selective beta-blockers), health conditions, or not meeting either the minimum or maximum exercise levels.

As many of the older trained participants travelled significant distances to participate in this study, it was conducted over the course of two subsequent days with a hotel stay between. Untrained participants' visits were on non-consecutive days. Participants were told to attend the study days having refrained from strenuous exercise in the previous 48 hours, and had abstained from caffeine or alcohol for the previous 24 hours.

Following medical screening and written informed consent, the untrained group participants conducted their first day of testing in the DGHPU, followed by the second day of testing at the SPMIC and Royal Derby Hospital. For the untrained participants, the health screening took place before the first day of testing to allow time for a blood sample to be analysed. Trained participants had this testing done on their first day of testing, with

the blood sample analysed before the second day.

3.2.3 Isometric strength and isokinetic work output assessment

Participants undertook isometric knee extensor strength tests using their dominant leg consisting of a knee extensor isometric strength and isokinetic knee extensor work output measurements using a Cybex dynamometer (Cybex Norm, Rosemont, Illinois, USA). The device was calibrated and then adjusted to the participants' height and proportions, with the knee flexed at 90°. Ten submaxmal isokinetic repetitions were performed at 90° per second as a warmup. The knee was then secured at 60° and 3 maximal voluntary isometric contractions held for 3 seconds were performed, giving 60 seconds recovery between each. Verbal encouragement was used to encourage maximal performance, and participants could view the trace of their effort on the ergometer monitor. The knee was then returned to 90° and the participant performed five isokinetic warm-up repetitions at 90°/s. The participant then performed a set of 20 repeated isokinetic knee extensions at a constant angular velocity of 90°/s to determined muscle torque development, giving maximal effort with each kick, which resulted in fatigue development over time. Each leg extension began at 90° knee flexion and extended to full knee extension, returning passively to 90°. Participants were verbally encouraged to give maximal effort beginning at the first extension and not to 'reserve' energy. Maximal knee extensor isometric strength was taken as the peak torque value (NM) achieved during the three maximum contractions. Total work done during the isokinetic exercise was taken as the sum of the work completed during each of the 20 repetitions.

3.2.4 Cardio-Step VO_2 peak testing

Following the Cybex measurements, participants were familiarised to the Cardio-Step module. Participants were positioned in the Cardio-Step with waistcoat straps and their feet strapped into the boots secured to the pedals. The lowest resistance (50 W) was then applied to the Cardio-Step ergometer and the participant was instructed to push against the steps at 70 bpm, following a metronome. The investigator then either let the full 3 minute baseline finish before introducing a few seconds of the next increment, to familiarise the participant with the sensation of the changing workload, or manually increased the workload earlier if the participant was comfortable with the exercise mechanics. Any adjustments to participant comfort were made at this point, to prevent discomfort and earlier termination in the exercise tests. The length of the waistcoat straps was measured and recorded. The knee angle was also measured bilaterally using a goniometer such that the position could be replicated for the MRI exercise session. The heart rate monitor was placed across the chest. The participant was then prepared for retrograde cannula insertion by a qualified clinician. Their hand was submerged in warm water of approximately 40°C for 10 minutes to dilate superficial veins on the dorsal surface of the hand, whereupon a retrograde cannula was then inserted in a superficial vein. A hot-box maintained at an air temperature of 55°C was then used to maintain arterialisation of the venous drainage of the hand. After another 15 minute rest period with the hand maintained in the hot-box, a baseline blood sample was taken into a 1 ml heparinised syringe and put on ice, and warmed and processed later in an i-STAT CG4+ cartridge and i-STAT blood gas analyser (Abbott Point of Care, USA). Samples were then taken in the last 30 seconds of each incremental exercise round.

Volunteers then performed a continuous, incremental, supine exercise test to determine supine VO_2 peak using an on-line expired gas analysis system (COSMED Quark CPET, Rome, Italy). Minute ventilation (VE), carbon dioxide (CO_2) production and oxygen (O_2) consumption was measured continuously throughout the test. Exercise commenced at a workload of 50W, which was increased at 3-minute intervals. Using the Ergospect software via a PC, the investigators controlled the ergometer exercise resistance via air pressure. Participants received verbal encouragement and feedback throughout the test. The test was terminated when the participant was unable to maintain the required power output or step frequency consistently for 30s, voluntarily stopped due to exhaustion, or it was deemed from a medical safety perspective necessary for them to stop. Following the exercise, the cannula was removed and participants were offered lunch and a drink, and had the option of gently spinning their legs for a few minutes on a cycle ergometer if desired. The rest period was a minimum of 90 minutes and included cognitive tests, discussed below. A confirmation exercise test was then undertaken to assess the reliability of their earlier VO_2 peak test, or see if they were able to continue beyond their initial termination workload. During the confirmation test, participants began with 3 minutes exercise at 50 W, the same initial workload as the incremental test, but then followed with a workload equal to the final exercise workload they completed during the previous incremental test. If they successfully completed that workload, the test continued in the same increments as the incremental test. This protocol is summarised in Figure 3.12.

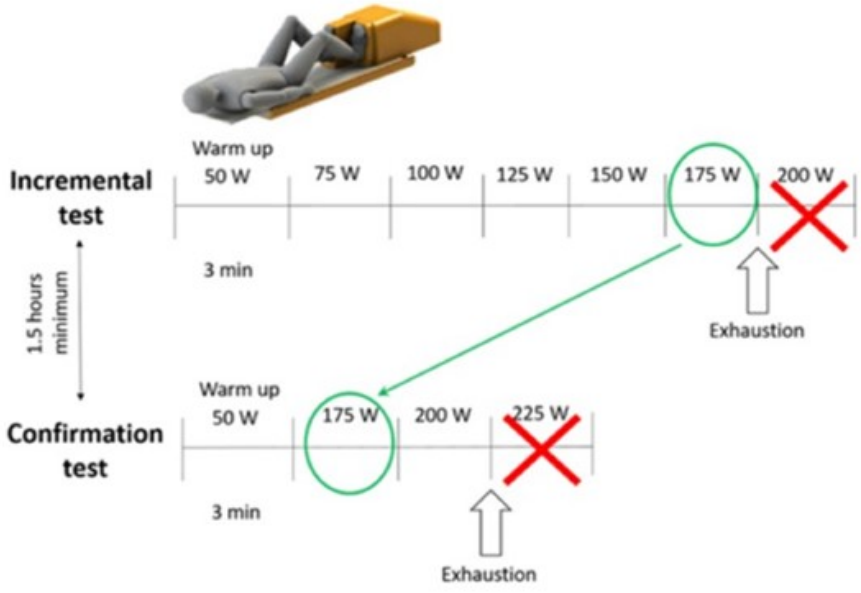

Figure 3.12: Incremental and confirmation VO_2 peak testing protocol.

3.2.5 Motor function measures

Basic functional measures were made with the timed up-and-go (TUG) test, jump tests, and standing balance, assessed with an accelerometer and electronic balance board. These measures are described in more detail in Chapter 5.

3.2.6 iEMG and electrical stimulation

Muscle motor unit size and number of the Vastus Lateralis and Tibialis Anterior was assessed using intramuscular electromyography (iEMG), which involved inserting a small needle (24 gauge) electrode into the target muscle. This was performed by trained specialists led by Dr Matthew Piasecki at the School of Medicine, University of Nottingham Royal Derby Hospital site. The needle was inserted around the belly of the muscle (motor

point), once the area had been cleaned with alcohol adhesive wipes. The investigator then inserted the needle into the muscle until an appropriate depth was reached (0.5 -2.5cm depending on target muscle and muscle size), then slightly retracted the needle during brief rest breaks between contractions, to ensure sampling from different areas of muscle was achieved. Full methods are described by Piasecki et al [6].

Estimates of the amount of excitable tissue within the muscle were made using electrical nerve and muscle stimulation. Electrically evoked percutaneous supramaximal stimulation was applied to the nerve serving the muscle of interest, or directly over the muscle of interest. This ensures all fibres within the muscle are stimulated, known as the compound muscle action potential (CMAP). The intensity of the stimulus was determined by slowly increasing the current with the participant in a relaxed state, starting from 10 mA and increasing until the current was found that elicited a maximum contraction (maximal activity detected via EMG), a further stimulus was then given at 15% higher current, with EMG activity recorded throughout.

3.2.7 Cognitive Measures

Cognitive measures were made with paper and pencil tests consisting of the Montreal Cognitive Assessment (MOCA), Trail making, and letter and category fluency. This measures are discussed in more detail in Chapter 7.

3.3 MRI protocol to study the effects of exercise

MRI scans were collected across two sessions, each of 45-60 minutes, separated by a brief break between. The first session consisted of the collection of images of the whole body, heart and brain obtained at rest. Following this, the participant exited the scanner and the Cardio-Step ergometer was set up on the scanner bed. The second scan session then commenced. In this second scan session a set of cardiac and brain scans were collected three times; at rest, during 15 minutes of supine exercise at 50% VO_2 peak, and during 15 minutes immediately post-exercise recovery. This workload of 50% peak VO_2 was chosen as an intensity to elicit an exercise induced physiological response without reaching the ventilatory threshold, i.e. the exercise intensity at which hyperventilation is induced to maintain blood acid-base status, which in turn would elicit changes in cerebral blood flow. An overview of the scans collected in each scan session are provided in Figure 3.13.

Initial investigations by McGing [2] determined the feasibility of MRI data collection during exercise in the 3T Ingenia while exercising using the Cardio-Step ergometer. The anterior full body coils were used for resting scans in Session One. The body radiofrequency (RF) receive coil (seen in Figure 3.14b) was used to collect the mDIXON data. However, this would not be possible to use when performing exercise as the weight across the chest would cause discomfort and movement of the coil, and thus poor image quality. Instead, for Session Two, a head and neck RF coil (Figure 3.14c) was used to collect both cardiac and brain images, in conjunction with the posterior receive RF coils built into the scanner bed.

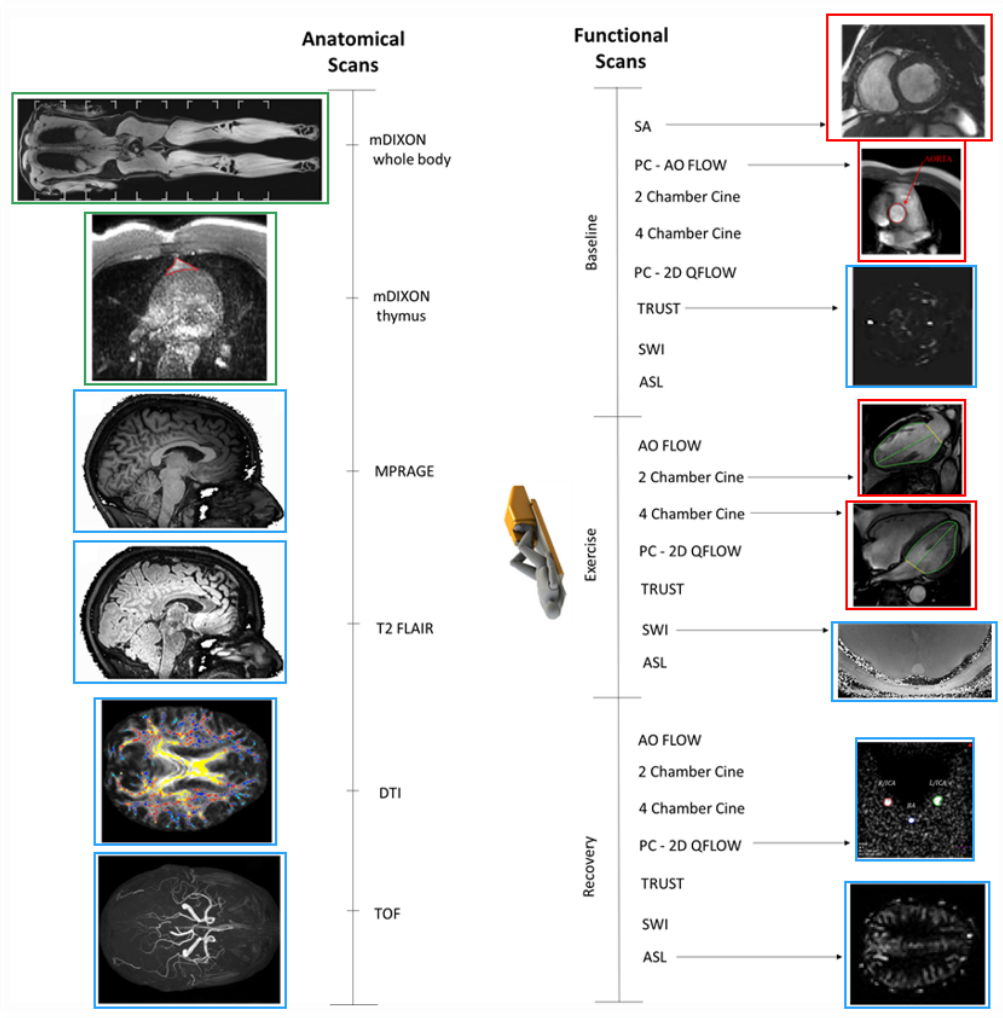

Figure 3.13: Overview of the MRI protocol with scans collected in scan session one at baseline and scan session two at baseline, supine exercise using the Cardio-Step and immediate post-exercise recovery. Those images with a green outline indicate muscle and fat composition scans, in blue brain scans and in red cardiac scans.

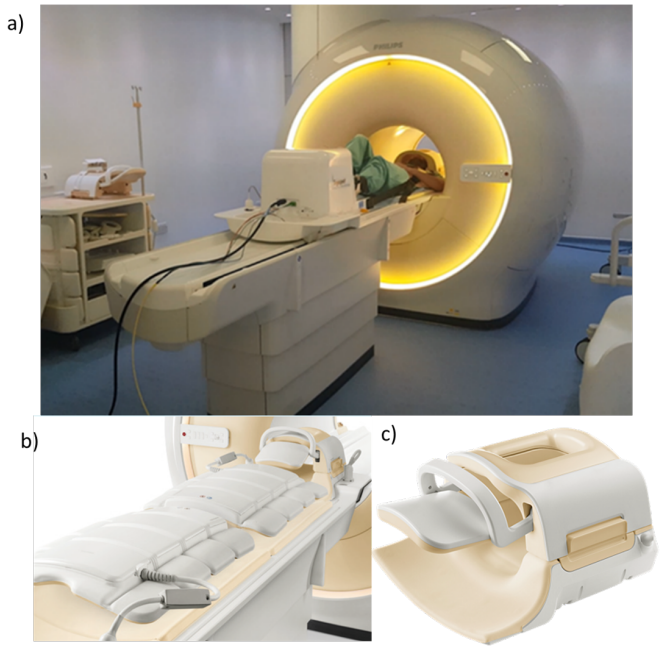

Figure 3.14: a) Cardio-Step ergometer in the 3T Ingenia, b) full set up including two body coils and head coil used in Session One, c) the head and neck coil used in Session Two.

3.4 MRI whole body imaging protocol

A number of anatomical and functional methods were used to assess structure of the brain and body composition. All MR scans were collected on the 3T Ingenia scanner (Philips, Best, The Netherlands).

3.4.1 Brain MRI Measures

3.4.1.1 Grey and White Matter Structure

A whole brain Magnetization-Prepared-Rapid-Acquisition-of-Gradient-Echo (MPRAGE) sequence was collected, as shown in Figure 3.15a. From this, whole brain volume, grey and white matter volume, and cortical thickness

and gyrification index can be calculated. The brain can also be automatically segmented into sub regions, and volume measures can be collected on these substructures. For example, this sequence was used to assess hippocampal volume. The MPRAGE data was collected with a field of view (FOV) of 256 x 256 x 162 mm, 1 mm isometric voxels, slices, and a flip angle of 8.

3.4.1.2 White Matter Hyperintensities

A T_2-weighted-FLuid-Attenduated Inversion Recovery sequence (T_2-FLAIR), as shown in Figure 3.15b, was used to assess white matter hyperintensities or lesions. The T_2 FLAIR was collected with a FOV of 256 x 256 x 162 mm, 1 mm isometric voxels, 162 slices, a TR of 5000 ms and TE of 0.35 ms.

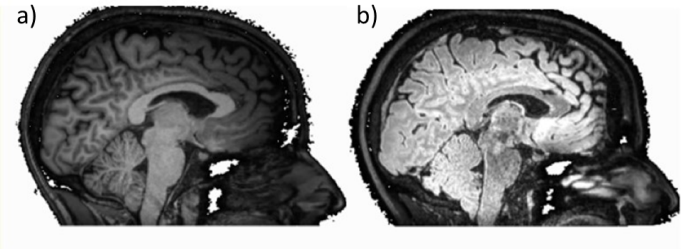

Figure 3.15: Sagittal view of an a) MPRAGE and b) T_2 FLAIR

3.4.1.3 Diffusion Tensor Imaging to study brain myelination

Diffusion tensor imaging (DTI) is a methodology that can measure the diffusion of water through axonal fibres, as shown in Figure 3.16. It allows for the measurement of the degree and directionality of diffusion, indicating the microstructural integrity of brain tissue. This is achieved by applying the diffusion gradients for many different directions, in this study 64 directions

were used. From this, mean diffusivity (MD), which indicates the mean diffusion of water in each measured direction, and fractional anisotropy (FA), which shows the primary direction of water diffusion and is an indicator of myelination, fibre density and axonal diameter, were calculated. DTI data were collected with FOV of 224 x 224 x 105.6 mm, a 2.2 mm^3 isometric voxel size, with 48 slices, a flip angle of 90° TR of 2081 ms, and TE of 88 ms, collecting a b=0 image and 64 directions of a b-value of 1000 s/mm_2 and using a multiband factor of 3.

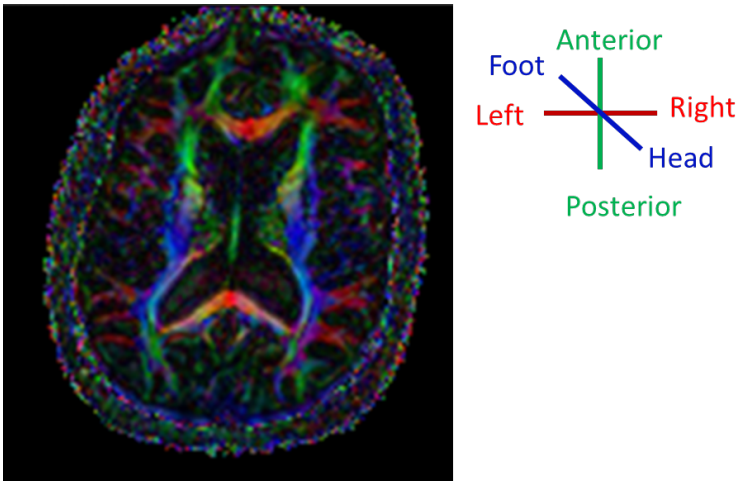

Figure 3.16: Diffusion Tensor Image map, with colour indicating diffusion direction

3.4.1.4 Cerebral Blood Flow through feeding vessels.

A phase contrast MRI (PC-MRI) two-dimensional quantitative flow (2D QFLOW) sequence was used to measure CBF through the carotid and basilar vessels feeding the brain. This measures the phase shifts of moving blood in a single slice, as shown in Figure 3.17. In the analysis, regions of interest (ROIs) were identified in the left and right carotids and basilar artery, and from this the velocity of the blood flow to the brain was obtained. The PC-MRI sequence had a FOV of 150 x 100 mm, voxel resolution of 1.15 x 1.15 mm, and 5 mm slice thickness, and was collected using

a flip angle of 10°.

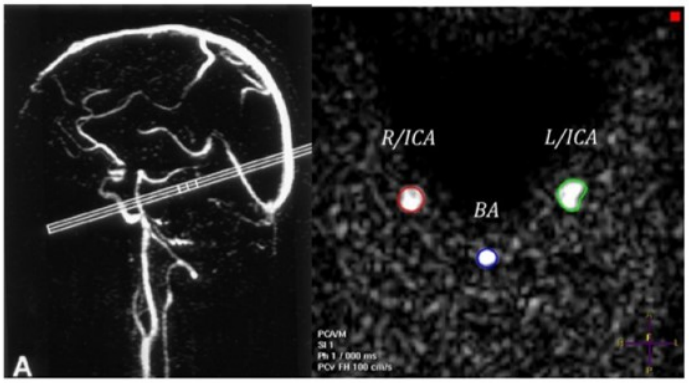

Figure 3.17: Cerebral blood flow phase contrast image over the left internal carotid artery (LICA), right internal carotid artery (RICA) and basilar artery (BA).

3.4.1.5 Cerebral oxygenation trough the assessment of blood oxygenation using TRUST

T2-relaxation-under-spin-tagging (TRUST) imaging quantifies venous oxygenation from measuring the T_2 of venous blood in the sagittal sinus. From this the oxygen extraction faction (OEF can be calculated, as shown in Figure 3.18. A section above the slice of interest is magnetically tagged so that the blood in the imaging slice is outflowing. From this the OEF can be calculated. The TRUST image has an FOV of 220 x 220 x 5 mm,3.4 x 3.4 mm voxels, a slice thickness of 5 mm and a flip angle of 90.

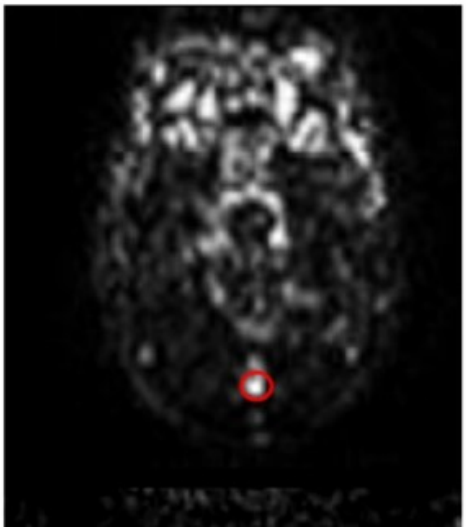

Figure 3.18: TRUST difference image highlighting the sagittal sinus.

3.4.1.6 Time-of Flight angiography to study brain vasculature

A Time of Flight (TOF) angiography was used to obtain an image of blood vessels, from which vessel number and radii can be calculated, as shown in Figure 3.19. The time of flight angiogram was collected with FOV of 200 x 200 x 160 mm, 0.4 x 0.7 x 2 mm voxel size, 160 slices, TR of 21 ms and TE of 4 ms. The results of this data are not shown in this thesis.

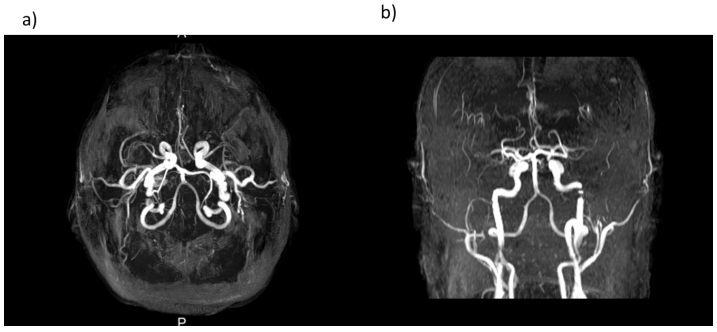

Figure 3.19: Maximal Intensity Projection map of a Time-Of-Flight (TOF) image viewed a) axially and b) coronally

3.4.1.7 Perfusion

In addition, perfusion of blood throughout the brain was measured using a non-contrast based technique called Arterial Spin Labelling (ASL). This sequence magnetically labeled a volume of water in the blood at a given point, which then was able to use that label to measure the perfusion of inflowing blood throughout the brain tissue. The arterial spin labelling sequence used was a FAIR scheme and was acquired with FOV of 240 x 240 x 60 mm, 3.6 x 3.5 mm voxel size, 6 mm slice thickness and 90° flip angle. The results of this data are not shown in this thesis.

3.4.2 Body MRI measures

3.4.2.1 Fat and muscle compartments

An mDIXON - multipoint DIXON scan - uses chemical shift to obtain water and fat images, and in- and out of phase images, from which muscle and fat body compartments can be calculated, as seen in Figure 3.20. This can be used to assess whole body muscle and fat volumes and distribution, as well as the fat fraction of a select tissue. In this study, specifically the fat fraction of leg muscles and the thymus. A full body mDIXON was collected in stacks of 1.5 mm in-plane and a 6 mm slice thickness, reconstructed to 1.92 x 1.92 x 3 mm voxels, flip angle 3, TR 10 ms, TE of 2 ms and 6 echoes. A high resolution mDIXON was also collected of the thymus, this comprised four stacks, with a 1.5 x 1.5 x 2 mm voxel size, across 77 slices. The thymus data is not shown in this thesis.

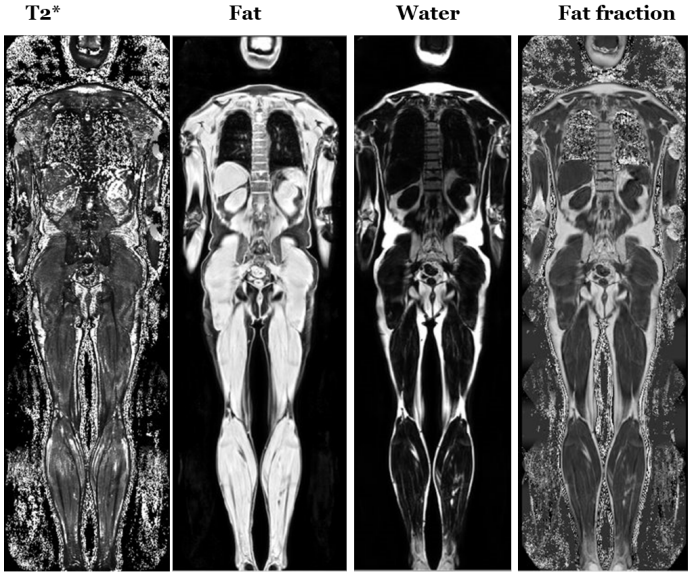

Figure 3.20: Wholebody mDIXON

3.4.3 MR Cardiac measures

Cardiac MR measures were collected using aortic Phase Contrast MRI and cine scans either in the long or short axis. From the cine scans, end systolic volume (ESV) and end diastolic volume (EDV), were measured, from which stroke volume (SV) was calculated by subtracting ESV from EDV. For all scans, stroke volume was then used to calculate ejection fraction (EF), as SV divided by EDV from the cine, or aortic PC-MRI measures allow stroke volume to be calculated. Cardiac output (CO) was calculated as stroke volume multiplied by heartrate, and cardiac index (CI) was cardiac output adjusted for body surface area (BSA).

3.4.3.1 Phase Contrast Cardiovascular MRI

A PC-MRI method was used to measure flow through the aorta (AO) to investigate stroke velocity, stroke distance, SV, EF, CO and CI. The AO PC-MRI cardiac (Figure 3.21) measure was acquired free breathing in 1

min 18 s before without compressed sense and 31 s with compressed sense with FOV of 280 x 264 mm, 2 x 2 mm voxel size, a 10 mm slice thickness, and flip angle of 15°.

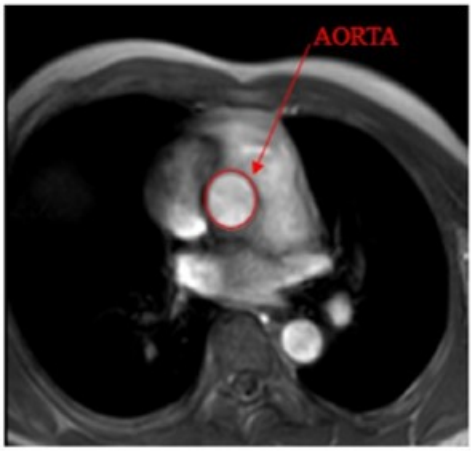

Figure 3.21: Aorta Phase Contrast MR image.

3.4.3.2 Long Axis Cardiac Cine

Long axis scans were taken in single slices across the left ventricle to capture a two chamber (2CH) view and a four chamber (4CH) view across the heart. These scans yielded EDV, ESV, SV, EF and CI. Long axis cine images (Figure 3.22) were acquired using balanced fast-field echo with a typical repetition time of 3.4 ms, echo time of 1.7 ms, flip angle 45° acquisition matrix of 195 x 195, 20-30 phases per cardiac cycle. Scans were taken in a single 10 second breathhold at FOV of 300 x 300 x 118 mm with 2x 1.6 mm voxels in-plane, and a 8 mm slice thickness. Images were collected regardless of the success of the breathholds, with some participants not able to sustain breathholds for the full 10 seconds during exercise.

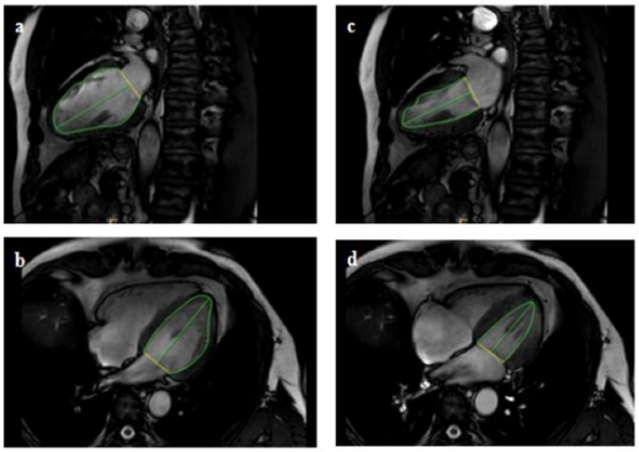

Figure 3.22: Long Axis cardiac two chamber (2CH) and four chamber (4CH) images shown, displaying end diastole in the two chamber (a) and four chamber (b), and end systole in the two chamber (c) and four chamber (d)

3.4.3.3 Short Axis Cardiac Cine

Short axis scans were taken axially across the left ventricle, capturing the entire heart. These scans yielded left ventricle myocardium mass, strain, EDV, ESV, SV, EF and CI. Short axis cine images (Figure 3.23) were acquired using balanced fast-field echo with a typical repetition time of 3.4 ms, echo time of 1.7 ms, flip angle 45° 20-30 phases per cardiac cycle, with one slice per breath hold. Scans were taken at FOV of 300 x 300 x 118 mm with 2 x 1.6 mm voxels, and 8 mm slice thickness. To collect the entire short axis stack required six breathholds.

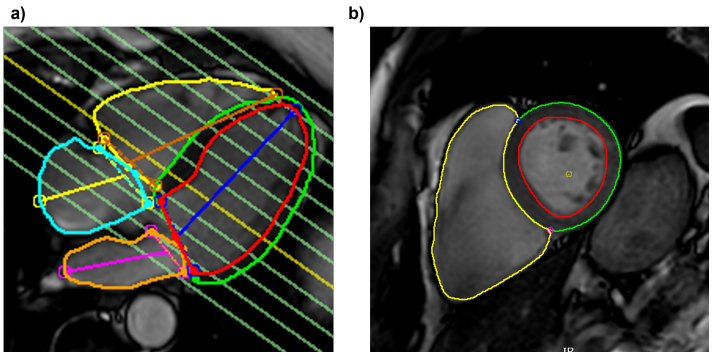

Figure 3.23: a) Four chamber long axis cine showing positioning of the short axis slices and b) Example Short Axis cine slice with epicardium and endocardium contours drawn in the left ventricle. Contours are taken from CVI Circle software.

3.5 Summary

This chapter has provided the details of measures performed for the EXAGE study. The development testing of the Cardio-Step ergometer is explained and its use in the CPET protocol, as well the MR scanner. The full sequence of the study days are outlined, and the MR scan acquisition parameters described.

References

[1] Andrew P. Hale. *Application of MR to Identify Metabolic and Physiological Correlates of Human Ageing and Inactivity.* PhD thesis, 2017.

[2] Jordan J. McGing. *Non-invasice Approaches to Identify the Cause of Premature Fatigue in Inflammatory Bowel Disease Patients.* PhD thesis, 2022.

[3] HV Forster, JA Dempsey, J Thomson, E Vidruk, and GA DoPico. Estimation of arterial po2, pco2, ph, and lactate from arterialized venous blood. *Journal of Applied Physiology*, 32(1):134–137, 1972.

[4] D Liu, E Moberg, M Kollind, P E Lins, U Adamson, and IA Macdonald. Arterial, arterialized venous, venous and capillary blood glucose measurements in normal man during hyperinsulinaemic euglycaemia and hypoglycaemia. *Diabetologia*, 35:287–290, 1992.

[5] Terry McMorris and Beverley J Hale. Differential effects of differing intensities of acute exercise on speed and accuracy of cognition: a meta-analytical investigation. *Brain and cognition*, 80(3):338–351, 2012.

[6] M Piasecki, A Ireland, J Piasecki, H Degens, DW Stashuk, A Swiecicka, MK Rutter, DA Jones, and JS McPhee. Long-term endurance and power training may facilitate motor unit size expansion to compensate

for declining motor unit numbers in older age. *Frontiers in Physiology*, 10:449, 2019.

Chapter 4

Muscle Segmentation of the legs

4.1 Introduction

Skeletal muscle consists of several tissues including muscle fibres, connective tissues, and adipose tissue. Within the leg, the fat is distributed in the subcutaneous adipose tissue (SAT), the intermuscular adipose tissue (IMAT) and intramuscular lipid (IntraMAT), as seen in Figure 4.1 from [1]. These are also referred to as the extramuscular lipid tissue (EMCL) and intramuscular lipid (IMCL) respectively, which will be the terms used in this chapter. The boundary around the muscle is termed the fascia.

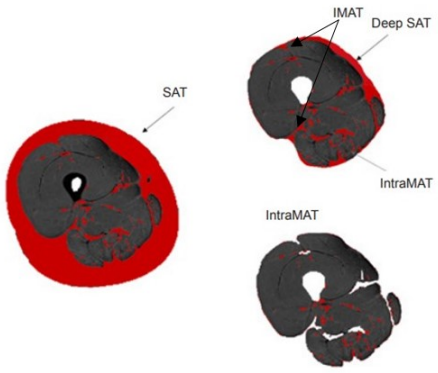

Figure 4.1: Illustration of skeletal muscle showing adipose tissue types in a thigh cross section modified from [1]

Muscle mass and the amount of fat infiltration within the muscle tissues (fat fraction) varies between individuals and pathologies, and can provide a phenotypic marker that reflects the health of the individual or a characteristic of a patient or demographic group. This can be especially important when studying muscle composition and the effect of ageing and lifestyle - where muscle atrophy can have a huge impact on quality of life in the ageing population. In Figure 4.2, taken from [2], an increase in the fat mass can be seen in the lower active older subject (Figure 4.2B) compared to the young (Figure 4.2A) and higher active older subject (4.2C). This can decrease the storage of elastic energy and increase stiffness in the muscle tendon unit, decreasing muscle activation and performance. Muscle insulin resistance and fuel oxidation are also negatively impacted by fat infiltration [3].

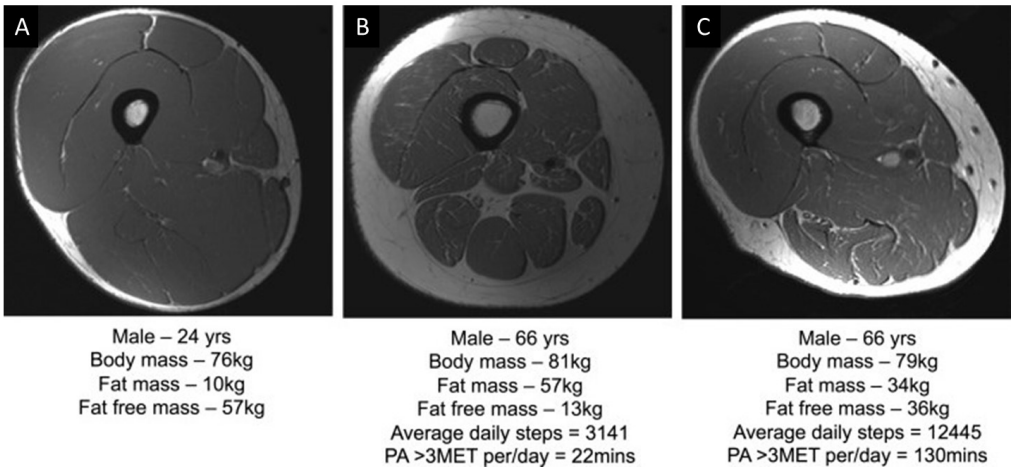

Figure 4.2: Loss of skeletal muscle size and quality during ageing which can be seen to be mediated by exercise, as depicted by McLeod et al. [2]. A) Young subject B) Older low-activity subject C) Older higher activity subject

.

Multiple methods are currently used to asses body composition in patients, including single or multi-slice computerised tomography (CT) scans and dual-energy X-ray absorptomitry (DEXA). DEXA is currently the most commonly used, to measure fat mass, bone mineral content and lean mass, with this including connective tissue, water and organs. However, Magnetic Resonance Imaging (MRI) is increasingly of interest, as it can provide more detailed and higher spatial resolution analysis by producing images of fat (F) and water (W), as well as maps of the transverse relaxation time (T_2*) and quantitative metrics of the fat fraction (FF).

For many years, and until recently, the most effective way of quantifying MRI muscle data has been to perform manual drawing around the areas of interest using a dedicated image analysis programme, such as Horos (www.horosproject.org). This however can be very time consuming and can be susceptible to differing criteria if a universal rubric is not properly established. In more recent years there have been increasing attempts to automate the process to achieve muscle metrics with minimal manual inter-

ference. Artificial Intelligence (AI) has recently been used to analyse both CT data [4], and MRI data [5]. The AMRA™ (Advanced MR Analytics AB, Linköping, Sweden) developed by Thomas et al [5] is a service platform for the automatic segmentation of muscle measures from an mDixon whole body MRI scan which has been shown to have a good correlation between data collected at 1.5T and 3T field strengths [6]. Segmentations using this tool have been shown to provide the ability to detect changes after an exercise training intervention and show a good correlation with segmentations from manual drawings [7]. Another example of the use of this tool is its application to generate muscle segmentation on a patient group of post-menopausal women to detect changes in thigh muscle, lower leg muscles, abdominal muscles, and more specifically changes in the pectoralis, latissimus and rhoboideus following an exercise training program [8].

While there is no doubt that this is a powerful tool, it remains proprietary and requires the images to be sent externally and is a costly process. To develop such AI machine learning tools locally requires AI expertise and the availability of masks for training and validation of the machine learning networks.

To address the limitations of a commercial package such as AMRA, in this thesis chapter a semi-automated pipeline is developed based on an existing brain segmentation tool (The FMRIB Software Library (FSL)'s FMRIB's Automated Segmentation Tool (FAST) [9]) that can be used with relative ease and adapted to other studies without the need for the training required by an AI machine learning tool. The segmentation of the legs in humans, consisting on the calf and thigh, is the focus of this development in this chapter, as these are the muscle groups hypothesised to show the greatest difference with ageing and exercise, in this thesis between cyclists and their

more sedentary peers. The semi-automatic method is compared to manual masking and an AI machine learning convolutional neural network (U-Net) for automatic segmentation which was developed in collaboration with colleagues (Dr Xin Chen and Mr Zhendi Gong) in Computer Science at the University of Nottingham. Measures are computed of muscle volume and intramuscular fat fraction.

4.2 Methods

MRI provides a method of quantifying muscle volume and fat fractions of the leg using images from whole body images, specifically here using a multipoint T_2* corrected DIXON (mDIXON) scan. In 1984, Dixon proposed a chemical shift imaging technique using 2-point in-phase (IP) and out-of-phase (OP) images from a gradient echo imaging acquisition. From this separate water (W) and fat (F) images can be generated [10] from:

$$W = \frac{(IP + OP)}{2} \tag{4.1}$$

$$F = \frac{(IP - OP)}{2} \tag{4.2}$$

The more recent modified Dixon (mDixon) uses Dixon with more flexible echo times rather than collecting images with fixed in-phase and out-of-phase echo times [11]. This allows decreased echo times and lower pixel bandwidth for more efficient acquisition and higher SNR. On a Philips scanner, the mDixon technique uses a 6 echo mDIXON Quant acquisition to yield in-phase and out-of-phase images, water and fat images, and T_2* and quantified fat fraction which can be used to assess intramuscular fat

fraction.

In this thesis, mDIXON Quant images were collected in 6 stacks at 2.5mm x 2.5mm x 6mm. For each stack, 77 coronal slices were acquired, resulting in a whole body acquisition, as detailed in Chapter 3. Example water, fat, fat fraction and T_2* images from this acquisition are shown in Figure 4.3.

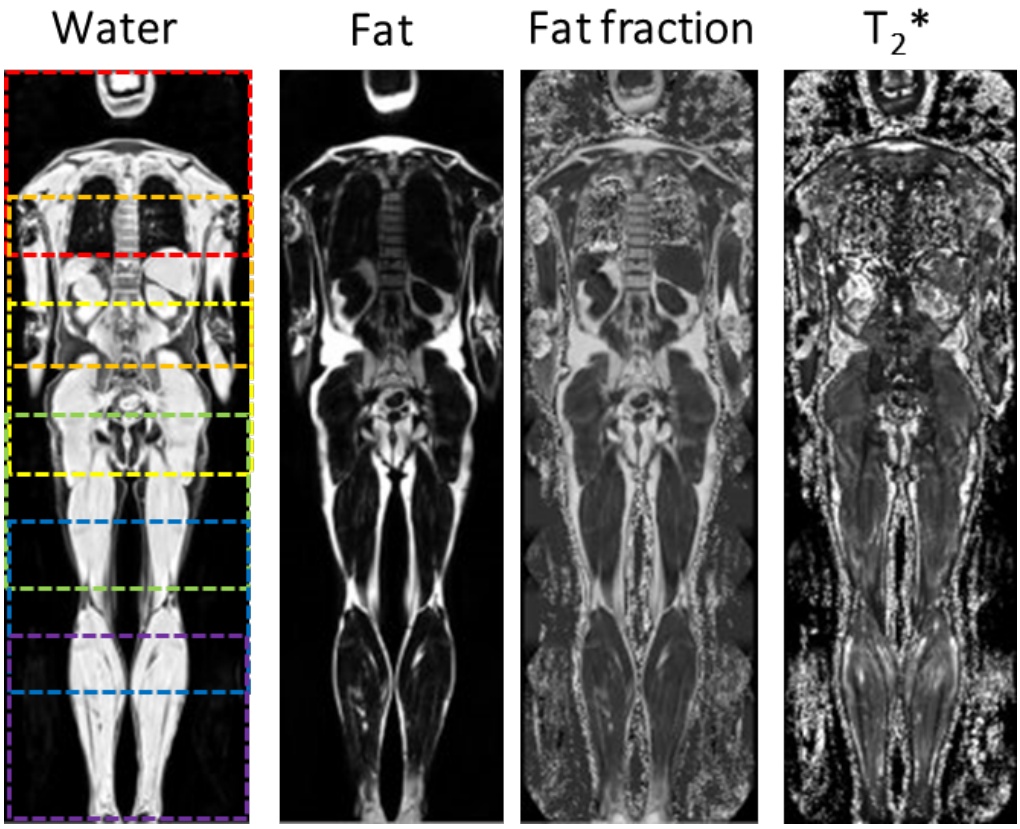

Figure 4.3: Scanner output of mDIXON from combining the six stacks showing the Water (W), Fat (F), Fat Fraction (FF), and T_2* images. The six overlapping stacks of 77 coronal slices are represented on the water image in different colours.

To achieve quantifiable muscle volume measures from the lower leg muscle of these images, a semi-automated analysis segmentation pipeline was developed. Results of this are compared to manually drawn regions of interest and AI methods, as well as results obtained using DEXA. Muscle volume and fat fraction are then compared between subject groups, including older trained (OT), older untrained (OU) and young untrained (YU)

from the EXAGE study (see Chapter 5). Additionally, untrained healthy volunteers (HV) from an Inflammatory Bowel Disease (IBD) study were combined together with the EXAGE YU to form a larger HV group, along with examining Chronic Obstructive Pulmonary Disease (COPD) patients, Inflammatory Bowel Disease (IBD) patients, post-COVID-19 recovery patients and a group of older females deemed Pre-Frail. A breakdown of numbers used per analysis technique (Table 4.17) and group demographics (Table 4.29) can be seen later in this chapter.

4.2.1 Semi-Automatic Pipeline Development for Muscle Segmentation

The following sections outline the steps in the semi-automatic pipeline for leg muscle segmentation.

4.2.1.1 Whole body image stitching and bias correction

The first step in the semi-automatic pipeline is to construct the whole body mDIXON images. Across the length of the whole body, each coronal mDIXON slice has large variations in intensity from head to toe that differ from slice to slice as regions of the body move in and out of the field of view. The scanner automatically stitches the 6 stacks of coronal images together to generate a whole body image. However, when this is performed the online stitching attempts to normalise over these stacks of differing intensity. As a result, this normalises each coronal slice to differing baseline levels, creating a striation effect in the axial and sagittal views of the scanner combined mDIXON stacks, which is visible in Figure 4.4. When manual drawing of regions of interest (ROIs) is performed on the coronal slices

only, the scanner on-line stitched output image with these striations can be used. But this variability in intensity is problematic for any semi-automatic processing. To rectify this, a Matlab script was developed to take the individual stacks that are saved off the scanner and stitch them together following bias correction to remove this intensity variability.

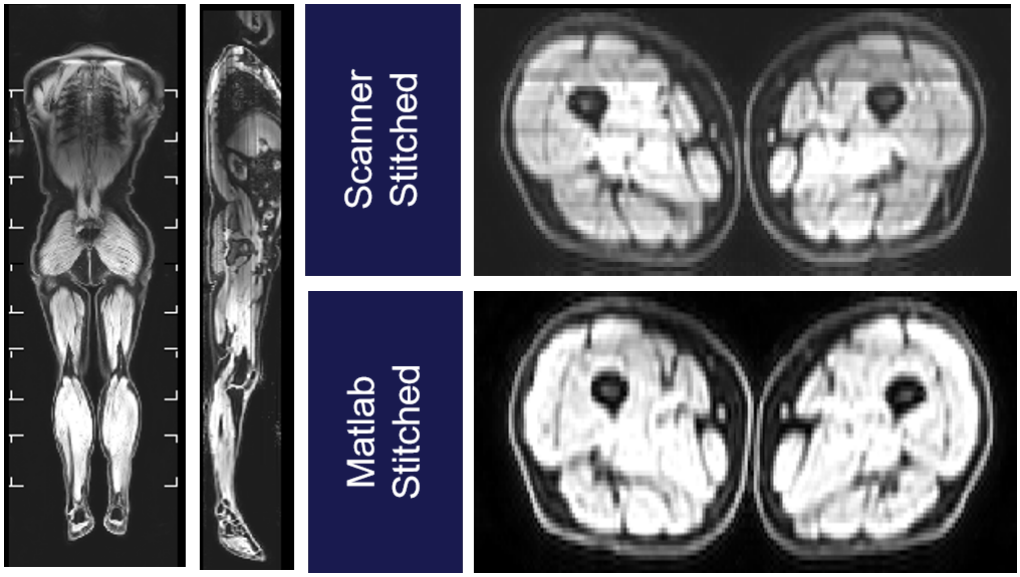

Figure 4.4: Whole body mDIXON water image from the stitched scanner output shown in coronal and sagital views. Note in the sagital view banding can be seen, which is highlighted in the axial view of the leg. This is corrected by offline stitching in Matlab.

To do this, the mDIXON data must be exported from the scanner in the form of enhanced DICOM data. On conversion using 'dcm2nii' this provides separate nifti files for each of the six stacks, for water (*a.nii.gz), fat (*b.nii.gz), fat fraction (*real.nii.gz) and T_2* (*.nii.gz). It was noted that erroneously some files are output from the scanner with both the water and fat as two volumes in the same '*a.nii.gz' image, this is addressed in the next step. First, the semi-automatic Matlab code organises these files into folders by type and checks for whether two volumes exist in a single image. Where two volumes are present, the water and fat are separated out and saved as individual images.

The script then reads in each corrected stack and uses a graduated weighting across the regions of overlap of the stacks to ensure a smooth resultant image, the stacks are then stitched together. The water images are then bias corrected using FSL's FAST tool, as outlined in Figure 4.5. This results in a water image which can now be segmented based on a threshold.

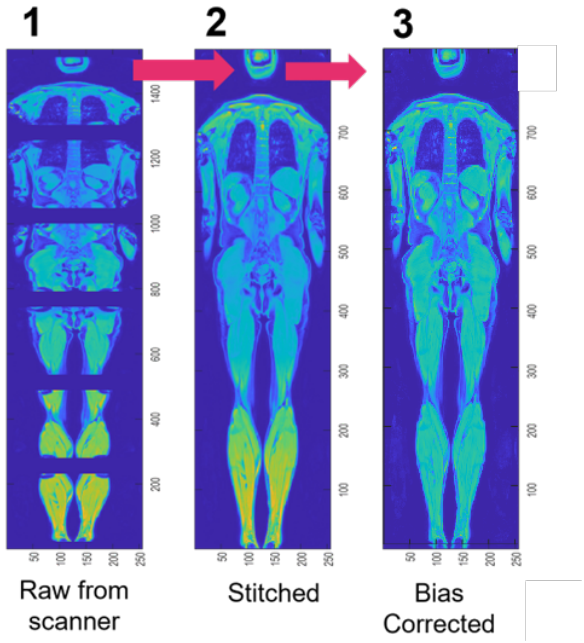

Figure 4.5: The first three pre-processing steps in the semi-automatic segmentation pipeline presented for the water image showing (1) the six stacks of raw data on export from the scanner, (2) the stitched image and (3) the bias corrected image.

4.2.1.2 Normalisation for skin

As the skin is primarily made up of water, like the muscle, it will remain in the FAST segmentation of the water image. Initially, a Euclidian Distance Transform (EDT) method was trialled (as used in Section 4.2.1.4) for removing extraneous non-muscle regions. But this was not successful in most cases, as the areas of skin were too large and too connected to other regions and so could not be separated without also breaking apart the muscle. Therefore an alternative method was introduced to remove the

skin by generating a skin mask (from the perimeter of the image from the whole body fat image) and then applying this to the water image.

This was done by taking the perimeter of the fat image using Matlab's 'bwperim' function, filling it, then taking the perimeter again, first twice sagitally (and dilating the perimeter slightly), then once axially, then coronally, but excluding the dorsal 5 slices; as the calves are pressed up against the scanner bed the skin and fat layer appear thinner here and removing the perimeter in these slices would also remove muscle. The perimeter mask achieved from all three axes was then labelled as the skin, as shown in Figure 4.6. This skin layer was removed from the whole body water image before it was pushed through any segmentations. This skin removal can be thought to be perform a similar step to scalp removal using the brain extraction tool (BET) for brain segmentation.

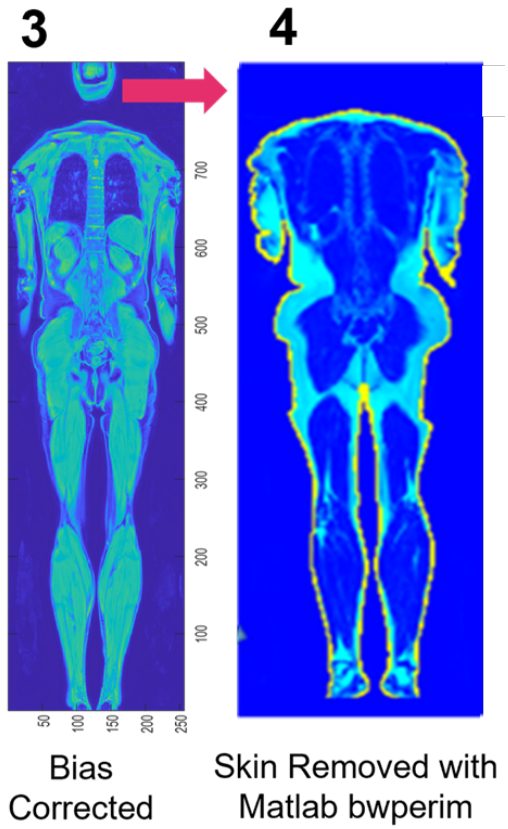

Figure 4.6: Bias corrected water images shown in 3. Removal of the perimeter of the fat image which represents the skin is shown in 4, with the skin to be removed shown in yellow.

4.2.1.3 Calf and Thigh segmentation

FAST in FSL has been developed to separate the brain into white matter, grey matter, and cerebrospinal fluid (CSF) [9], but can be applied to tissue types in other body areas to generate partial volume estimate (PVE) images. FAST uses multiple parameters, such as the number of PVE images to be exported. Initial testing of pushing the whole body image water (W) or fat (F) images through FAST (FSL) did not produce satisfactory results, as the greater variation of intensities found across whole body from the legs and the torso comprising multiple internal organs yielded more differentiation of segmentation. Therefore, since the goal of this chapter is

to segment the leg muscles, to aid FAST segmentation of the leg muscles the decision was made to introduce an initial step of performing a rough crop around the general area of interest, divided into the right thigh, left thigh, right thigh and right calf, as shown in Figure 4.7.

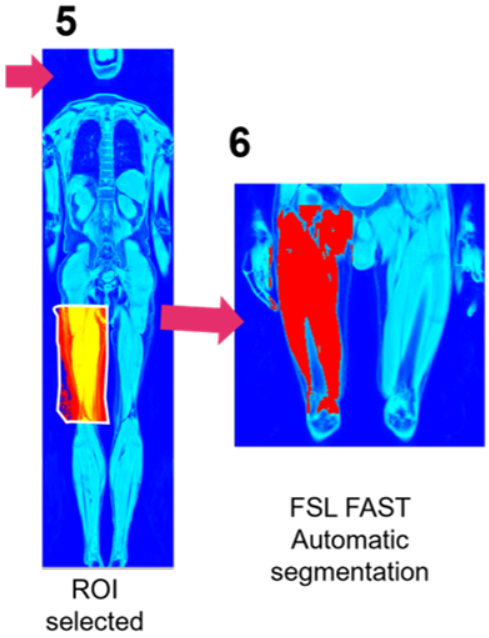

Figure 4.7: Polygonal manual crop (white outline) made roughly around the region of interest within the leg, in this example this is shown for the thigh.

For the calf rough ROIs, the whole body water image was first visually inspected coronally to find a slice where the calf is relatively wide, then a simple polygon was drawn around the region, including space around the muscle to ensure coverage in all slices, but not extending into the contralateral calf. This polygon was then extended to the rest of the image and then applied to the fat and fat fraction images to extract the same rough ROI from all.

For the thighs, the desired ROI excluded the gluteus maximus, rendering a single ROI crop unsuitable coronally, as once extended through all the slices it would include sections of the gluteus maximus if drawing from the

ventral side, or exclude upper sections of the quadriceps if drawn dorsally. Instead, rough polygons were drawn on the water image, first on every slice where tissue is visible and contained under 2000 voxels, then every 10 slices once the slice contained above 2000 voxels, with interpolation applied to the intervening slices. These regions were then applied to the fat and fat fraction images, as seen in Figure 4.8.

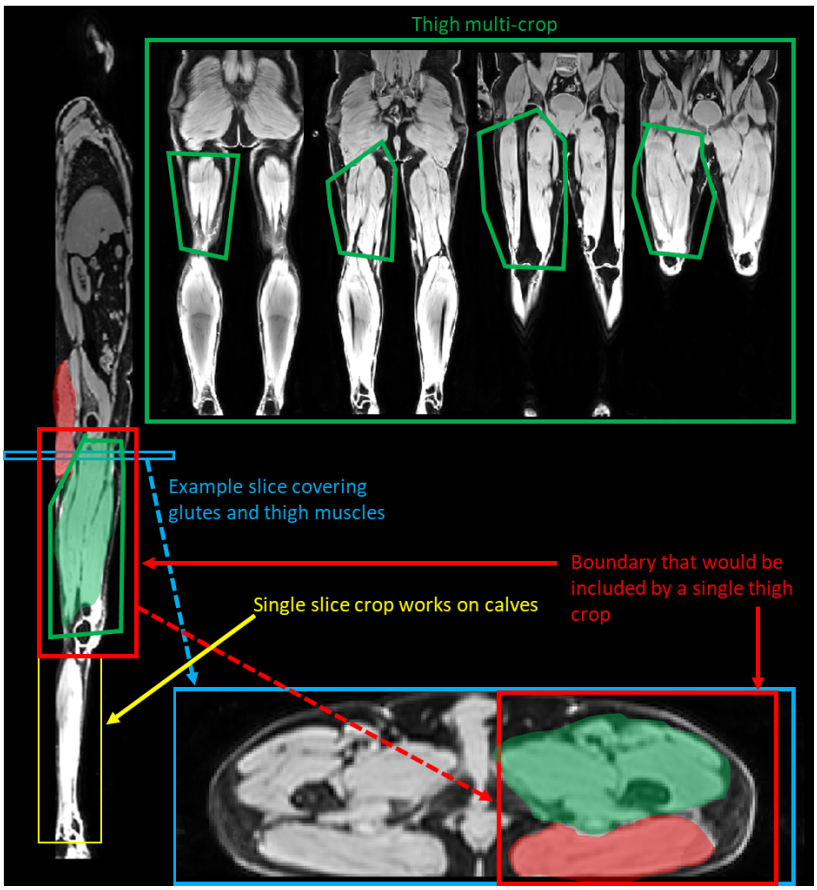

Figure 4.8: Outline of the single crop suitable for the calves (yellow) and illustration of why this method cannot be applied to the thigh (red box and undesired tissue in red). Also shown is an illustration of the multi-crop to yield the thigh volume excluding the glutious maximus (green).

The rough cropped ROI (either single or multi-slice crop) is then pushed through FSL's FAST function to segment the image into three PVE components (Figure 4.9). Dividing the image into four PVE components was also tested. While on visual inspection this seemed to better isolate the

muscles in a few subjects, in many others it over-parcelated the images, excluding muscle. Thus three PVE segmentations were chosen as the best muscle representation, with a comparison shown in Figure 4.10 to illustrate this.

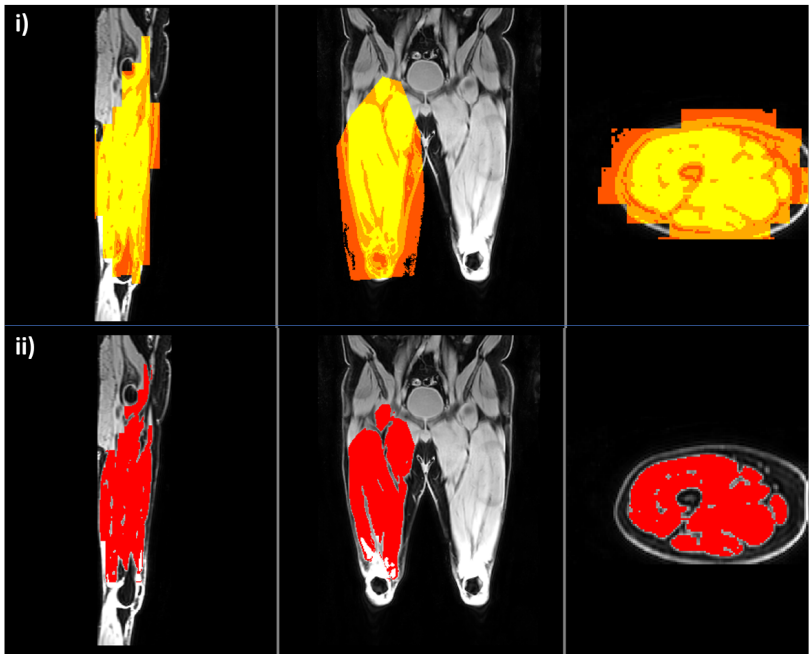

Figure 4.9: PVE map using the FAST command showing in i) the 3 PVE components in yellow (muscle), light orange (subcutaneous and extramuscular lipid (SAT and EMCL) and dark orange (noise). ii) The resultant final muscle mask on pipeline completion (bottom, red).

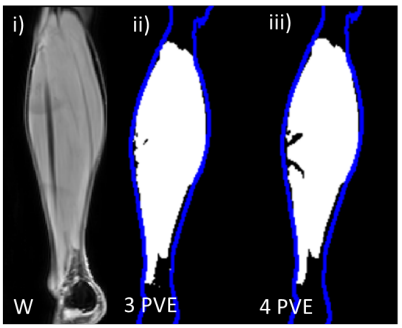

Figure 4.10: Results of the segmentation of the (i) Water (W) image showing the muscle segmentation image that results using (ii) 3 PVE and (iii) 4 PVE components in FAST (FSL).

The use of the fat image instead of, or in conjunction with, the water image was also tested with 3 PVE images, but this performed worse at muscle

segmentation and did not add any additional useful information, as shown in Figure 4.11, and so was not used.

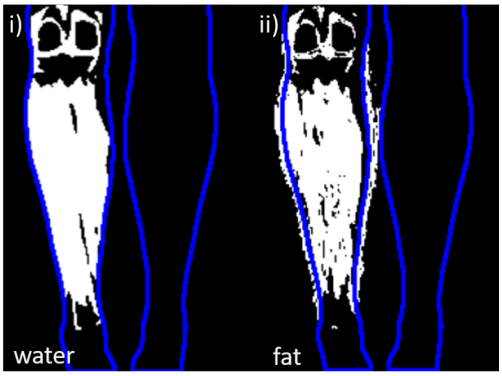

Figure 4.11: Resultant muscle images applying FAST with 3 PVE to the i) water and ii) fat image. Note the fat image removes some muscle and so this was not used.

The final segmentation loop was iterated 4 times (I). It was found that greater than 4 iterations added time but did not improve results, along with a bias smoothing of full width half maximum (FWHM) of 20 mm (l) using the FSL command:

$$fast\ -n\ 3\ -H\ 0.1\ -I\ 4\ -l\ 20.0\ -g\ -B\ -o\ <inputname><outputname> \tag{4.3}$$

4.2.1.4 Final cleaning of the muscle mask

Using the results of FAST with 3 PVE components applied to the water image, the resultant segmentation consisted primarily of the desired muscle tissue (as shown in Figure 4.10 and Figure 4.11), but often included small regions of noise, skin, or muscle of a different muscle group. To discard erroneous regions in these segments, the script was further developed to isolate and remove these areas, as shown in Figure 4.12. First a Euclidean distance transform (EDT) was applied to the binary mask, giving a map of

the distance between each voxel and its nearest non-zero voxel. Through testing, a value of 2 was determined as the best distance to separate out disparate objects, and any values under that value were removed from the EDT map. A connectivity function (Matlab using the 'bwconncomp' function) was then applied to this map, with the newly created gaps between areas that had previously been adjacent, allowing for greater object separation. The objects to be removed were then determined based on size, creating a mask of only the large, highly connected objects. This mask was then dilated outwards 5 times to account for the EDT shrinkage. The segmentation mask was then applied to this dilated EDT mask to remove any areas where the dilation expanded the mask beyond the initial segmentation mask and a final connectivity test was applied to ensure no new small extraneous regions were introduced in the process.

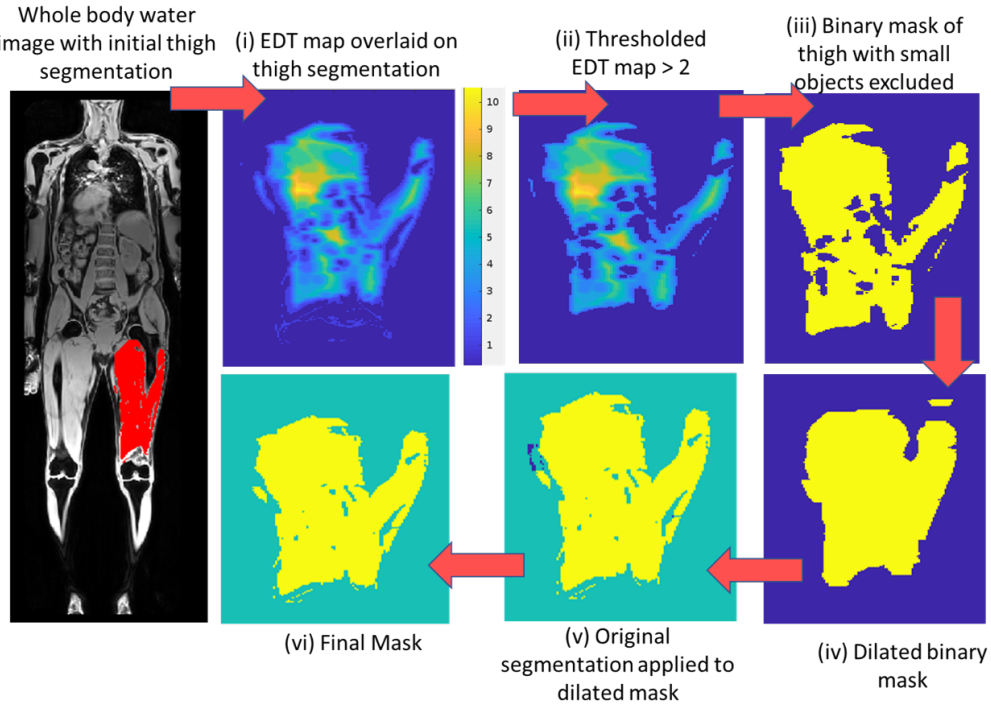

Figure 4.12: Euclidean Distance Transform (EDT) and connectivity cleaning shown for an example thigh segmentation.

The final processing step was to ensure areas of erroneous fat were removed

from tissue. A threshold of greater than 60 % was applied to the fat fraction image to generate a fat mask, this was then applied to the water mask. This acted to threshold out any areas of very high fat fraction that were subcutaneous adipose tissue or physiologically implausible for extramuscular lipid, Figure 4.13.

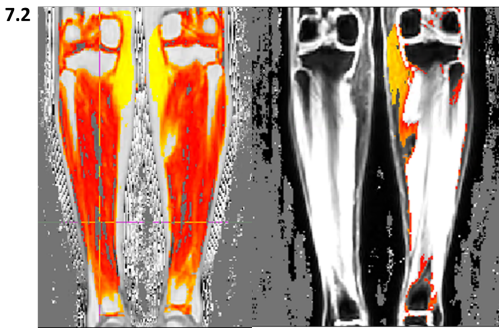

Figure 4.13: High fat fraction threshold removal shown in an example on the right calf.

4.2.1.5 Summary of the semi-automatic pipeline

The final leg muscle segmentation pipeline is shown in Figure 4.14. This shows the stitched (2) and bias corrected (3) water image, removal of the outer perimeter assumed to be skin (4), a rough ROI crop (5), which was applied prior to FSL's FAST into 3 segmentations (6), followed by removal of extraneous regions using a Euclidean Distance Transform and removal of any regions of implausibly very high fat fraction (7). The final mask (8) was then used to calculate the muscle volume and was applied to the intramuscular fat fraction image to compute the fat fraction within the muscle of that volume. The manual selection of the rough ROIs could be drawn in approximately 5-10 minutes per participant for all four regions. All other steps can be batched and run as a group, without supervision, overnight. Final visual inspections check the pipeline's performance.

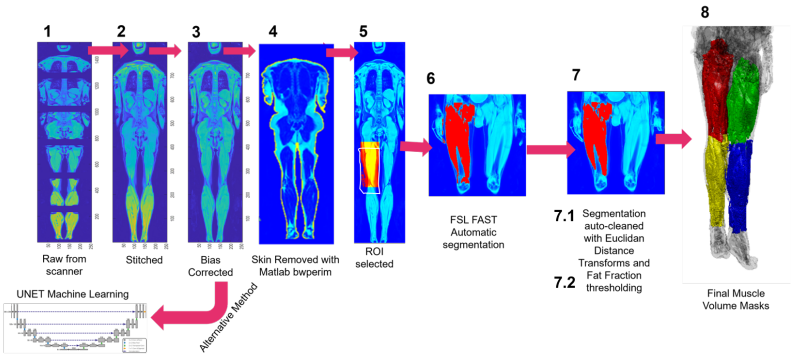

Figure 4.14: Steps of the semi-automatic pipeline to generate the final muscle segmentation of the legs.

4.2.2 Manual ROI for muscle segmentation

Manual ROIs were drawn on the mDIXON images using Horos software to outline separately the calf and thigh. This was performed by two raters, Ms Rosemary Nicholas on n=34 datasets and Dr Ayushman Gupta on n=14 datasets, 11 of which were within that same subset. Raters drew around the muscle tissue on every fifth coronal slice, beginning on the first slice of visible muscle, with an example slice show in Figure 4.15.

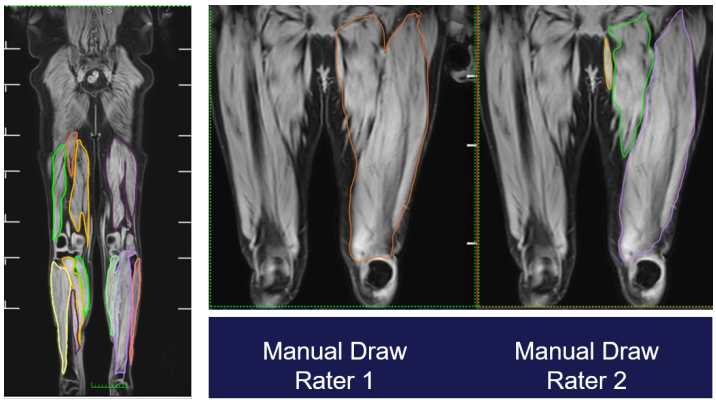

Figure 4.15: Manual Raters drawing ROIs on water mDIXON images in Horos with each coloured outline representing one drawn ROI but not corresponding to specific muscle groups. Where multiple ROIs were drawn per region (eg. left thigh) these were summed together to form one regional ROI.

Areas of non-selected slices are estimated by averaging the bookending slices and applying this to the missing slices. Total muscle volume was then calculated by multiplying the in-plane volume from the ROI of the water image by the slice thickness. Each participant took approximately one hour to complete the drawing of the four regions of interest.

4.2.3 DEXA for regional lean masses

Participants from the IBD and COVID-19 studies underwent DEXA (Lunar prodigy, GE healthcare, Chicago, Illinois) by an IRMER (Ionising Radiation (medical exposure) regulations) trained operator to determine bone mineral density (BMD), lean mass (%) and total body fat mass (%), divided into appendicular masses (arm and leg separately) and trunk, as shown in Figure 4.16.

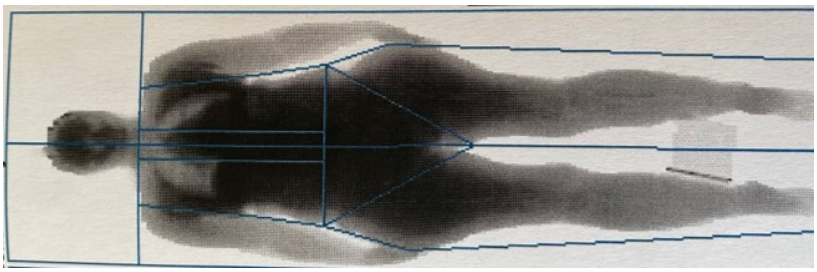

Figure 4.16: DEXA showing lean body mass divided into regions, with leg regions extending up to the hip

4.2.4 UNET for muscle segmentation

In parallel with this work on a semi-automatic segmentation, with collaborators in Computer Science (Dr Xin Chen and Mr Zhendi Gong) a UNET machine learning model to run independently to segment the whole body mDIXON images was also developed as an alternative method. The UNET method is outlined fully in the paper 'Thigh and Calf Muscles Segmenta-

tion Using Ensemble of Patch-Based Deep Convolutional Neural Network on Whole-Body Water-Fat MRI' [12] and is summarised below.

The UNET methodology was performed on the stitched and bias corrected whole body mDIXON images outlined in Section 4.2.1.1. As the thigh and calf muscles are located in the bottom half of the body, firstly a reference plane that is defined by the proximal end of the two femoral bones was used to crop the bottom half of the body from the whole-body MRI. This process was simple and quick and is currently performed manually. Then the thigh and calf muscle regions were identified by applying a fixed ratio (lower l1/L for the calf region and upper l2/L for thigh region, where L is the height of the cropped volume) to split the volume into two overlapping sub-volumes. Next, two patch-based binary-class 3D U-Net models with the same network architecture were trained for thigh and calf muscle segmentation separately, called 'CalfModel' and 'ThighModel'. The UNET was trained on semi-automatic masks (these were chosen as these remove extramuscular fat and connective tissue). During model training, the input volumes for each model were randomly cropped into many overlapping regions and used as the input to train the models. In the model inference process, the input cropped whole-body MRI was pre-processed using the same procedure as for the training. The input volume was then divided into non-overlapping 3D patches and input to the corresponding calf or thigh model for muscle segmentation. Finally, a bespoke post-processing method was used to combine the predicted outputs of the patches from both models to form a whole-leg output and correct any mislabeled areas. From these resulting segmentations muscle volume was then computed for the calf and thigh.

4.3 Statistical Analysis

Muscle masses and fat fractions values were compared between methodologies using linear regression and Bland Altman plot. When comparing MRI derived values to DEXA, the MRI muscle volumes were converted to mass by assuming a density of 1.04 g/cm^3, and calf and thigh values were summed to determine a leg mass to reflect the coarser granularity of the DEXA scan. When comparing between patient groups Bonferoni corrected ANOVA tests were used.

The ROI masks used in each methodology were additionally compared using the DICE similarity coefficient, $\frac{2 \times |X \cap Y|}{|X| + |Y|}$. In the manual drawings, the slice chosen as the first slice with visible muscle varied between raters and therefore offset all subsequent ROI slices. These masks were therefore not comparable, and so a subset of n=7 subjects was used for the inter-rater DICE comparison. All slices were used for the UNET and semi-automatic comparisons.

4.4 Results

Beyond the data collected for the main study group of this thesis (the EXAGE group), in this chapter mDIXON MRI scans were also assessed from healthy volunteers (HV), Chronic Obstructive Pulmonary Disease (COPD) patients, Inflammatory Bowel Disease (IBD) patients, post-COVID-19 recovery patients and those deemed as Pre-Frail. mDIXONs were used from all these studies to develop and test the semi-automatic pipeline across a range of muscle sizes for comparison to other methodologies. Due to study limitations or time constraints, not all methods were assessed on all sub-

jects. Figure 4.17 below details the distribution of datasets tested across methodologies.

	Manual Rater One	Manual Rater Two	Semi-Automatic Pipeline	UNET	DXA
OU (EXAGE)	1	0	7	0	0
OT (EXAGE)	8	0	9	6	0
HV (IBDF+EXAGE)	5	0	20	0	0
COPD	7	7	7	7	0
IBD	10	0	12	16	15
COVID-19	3	7	27	9	28
Pre-Frail	0	0	3	0	0
Total	**34**	**14**	**85**	**38**	**43**

Figure 4.17: Distribution of datasets included from across studies and the analysis methods performed on each.

4.4.1 Comparisons between segmentation methods to estimate volume measures of the legs

4.4.1.1 Volume differences and Bland Altman plots for MRI segmentations

Figure 4.18 compares the calf and thigh volume measures combined across each leg obtained from the semi-automatic and manual segmentations. It can be seen that when considering the data together the calf and thigh muscle volumes correlate strongly overall, r(131) =0.973, p=0.001. Due to a wider range of volumes for the thigh, thigh volumes are more highly correlated between methods than calf volumes (calf r=0.69, thigh r=0.97). The Bland-Altman of the volumes obtained with the semi-automatic and manual method (Figure 4.18b) reveals that the calf volumes are similar for the semi-automatic and manual with a bias of 114 grams (95% confidence interval: -346 to 584 grams). In comparison, the semi-automatic-segmentation-computed thigh volumes resulted in lower volumes than those

computed from manual segmentation, with a bias of -540 grams (95% confidence interval: -1000 to -80 grams). This difference is not due solely to the larger size of the thigh, as seen in Figure 4.18c, where percent differences still show a greater difference in thigh (-18.4%) than calf (6.9%).

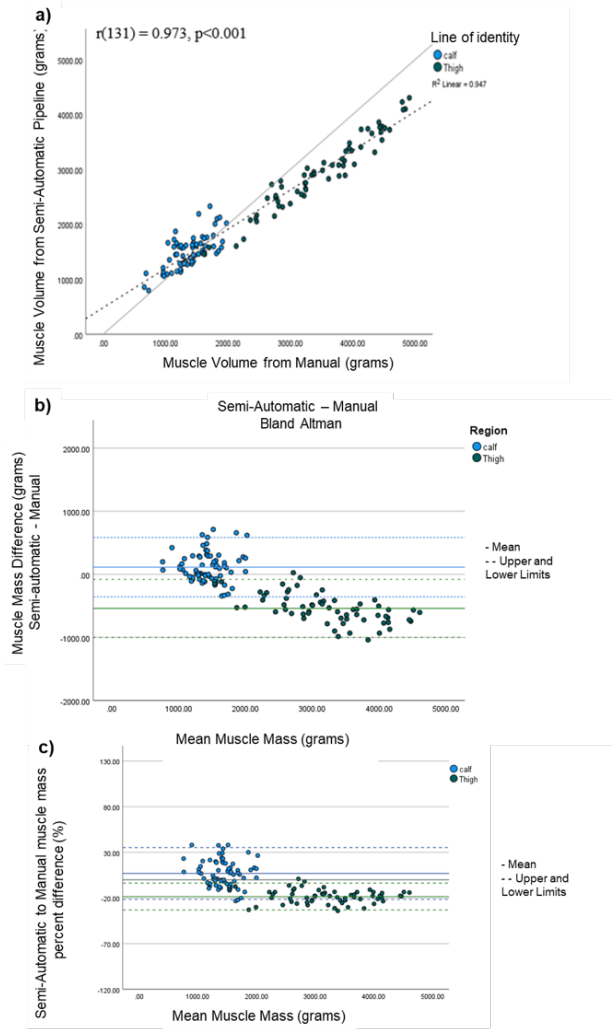

Figure 4.18: a) Semi-automatic generated volumes versus manually drawn volumes for the calf and thigh combined across legs. The linear regression across calf and thigh volumes (dotted line) and the line of identity (solid line). b-c) Bland Altman plot of the semi-automatic versus manual generated volumes differences (b) and percent differences (c) with mean (solid line) and Upper and Lower limits (dashed line) are shown for the calf and thigh.

This difference in absolute thigh volume between the two methods is thought to arise from the exclusion of non-muscle tissue (extramuscular fat and con-

nective tissue) in the semi-automatic segmentation, whilst this is included for the manual method when drawing around large muscle groups without delineating between them. This difference is discussed further below and illustrated in Figure 4.22 when showing DICE similarity scores.

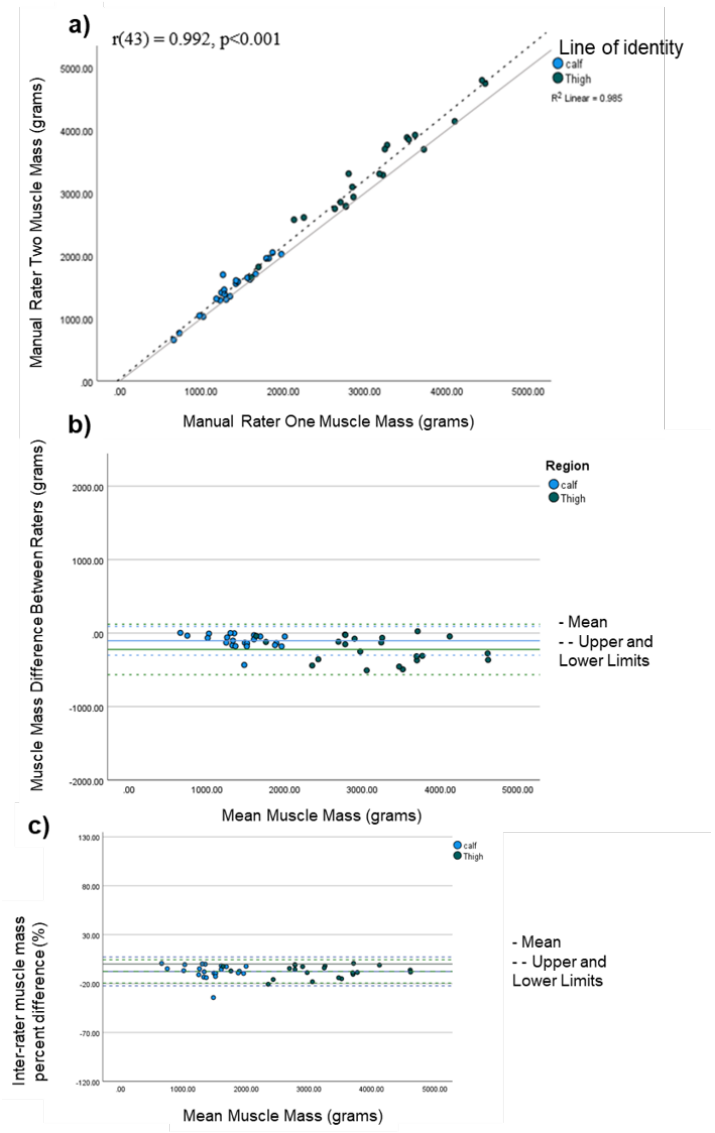

Figure 4.19: a) Inter-rater reliability of manually drawn ROIs for the calf and thigh with linear regression of the group as a whole (dotted line) along with the line of identity (solid line). b-c) Bland Altman plot of inter-rater reliability of differences (b) and percent differences (c) with mean (solid line) and Upper and Lower limits (dashed line) for the calf and thigh separately.

A smaller subset of data was manually drawn by the two raters. The two

raters had extremely high inter-rater reliability overall for segmentation of the calf and thigh when considered together (n=11, ROIs=43), r(43) = 0.992, p=0.001 as well as when divided by region, (calf: r(21) = 0.967, p<0.001, thigh: r(21) = 0.977, p<0.001). However, the volume results for one rater were consistently slightly lower than the other rater with a bias in the calf of -104 grams (95% confidence interval: -296 to 88 grams) and a bias in the thigh of -222 grams (95% confidence interval: -559 to 115 grams), as shown in Figure 4.19b. The rater generating the lower volumes was more experienced at quantifying MR images than the other rater, who was a clinician. Percent differences between regions are consistent (-7.6% for calf and -7.5% for thigh), as seen in Figure 4.19c. While it appears from these initial findings that the manual method shows high reliability, it should be noted that both of the manual drawing was only performed on every 5th slice and thus largely interpolated, therefore it is difficult to establish a true 'gold standard'.

Figure 4.20 compares the muscle volumes generated from the semi-automatic and UNET segmentations and shows a correlation of r(141) =0.865, p<0.001 between muscle volumes, but with variability especially for the thigh (Figure 4.20a). A Bland-Altman plot, Figure 4.20b, reveals that the calf volumes differences between the UNET and semi-automatic segmentation has a bias of -228 grams (95% confidence interval: -903 to 449 grams) broader than those found between the manual drawing and semi-automatic a bias of -540 grams (95% confidence interval: -1000 to -80 grams). The thigh volume segmentation had a bias of -402 grams between the UNET and semi-automatic segmentation (95% confidence interval: -1507 to 703 grams), a larger confidence interval than between the manual and semi-automatic segmentation volumes (-559 to 115 grams). By accounting for the difference in size between the calf and the thigh, the semi-automatic

and UNET are consistent in their percent difference in calf (-19.7%) and thigh (-19.9%), as shown in Figure 4.20c. The percent differences are similar to the difference found between manual and semi-automatic in the thigh (18.4%), but higher than the calf (6.9%). UNET yields predominately lower volumes with a few highly variable exceptions, which will be discussed further when examining the DICE correlations in Section 4.4.1.2. Two UNET masks were removed from analysis due to improper cropping.

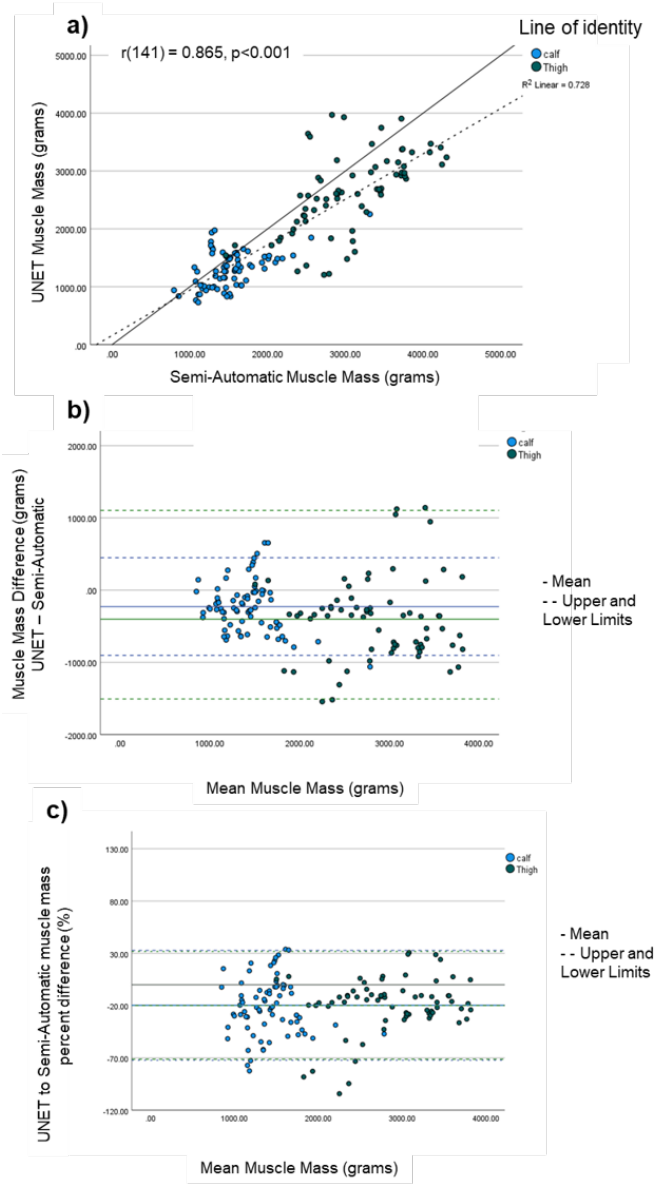

Figure 4.20: a) Semi-automatic vs UNET generated volumes for the calf and thigh with the linear regression of the group as a whole (dotted line) b-c) Bland Altman plot of semi-automatic vs UNET volume differences (b) and percent differences (c) with mean (solid line) and Upper and Lower limits (dashed line) for the calf and thigh.

4.4.1.2 Dice similarity measures for the calf and thigh for MRI measures

Dice similarity coefficients were used to investigate the overlap of the masks generated from the manual, semi-automatic and UNET segmentation meth-

ods. The overlay of the semi-automatic with manual segmentations gave a mean DICE score of 0.828 +/- 0.037 for calf and thigh combined. Between the two manual raters the DICE score was 0.924 +/- .037. Comparing the machine learning UNET with the semi-automatic segmentation gave a DICE of 0.908 +/- .049. See Figure 4.21 for a detailed breakdown the DICE scores for the calf and thigh masks for each of the segmentation methods.

	Manual vs Semi-Automatic			Interrater			UNET vs Semi-Automatic		
	Mean	N	Std Dev	Mean	N	Std Dev	Mean	N	Std Dev
Left Calf	.809	37	.030	.927	7	.040	.922	39	.028
Right Calf	.813	33	.034	.920	7	.043	.922	39	.028
Left Thigh	.848	32	.033	.929	7	.033	.890	39	.060
Right Thigh	.846	34	.035	.920	7	.039	.895	37	.062
Mean	**.828**	**136**	**.037**	**.924**	**28**	**.037**	**.908**	**154**	**.049**

Figure 4.21: Mean DICE scores for the thigh and calf compared across the segmentation methodologies.

Figure 4.22 shows the mean DICE values for the calf and thigh along with an example overlay of the manual and semi-automatic masks. The region in white shows where the masks are in agreement, voxels in pink are those which appear in the manual mask only, and those voxels in green are in the semi-automatic mask only. The manual mask can be seen to include areas between the muscle which are not included in the semi-automatic mask. Much of the reduction in volume from the semi-automatic method arises from the semi-automatic mask excluding areas of connective tissue and high fat that are included in manual segmentations, however the semi-automatic seems to overextend in some areas, and include knee cartilage as seen in green the right calf in Figure 4.22. The overlap of the two manual raters, Figure 4.23, shows only some differences at the borders as well as between the muscles, but overall is closely matched. However, no attempt was made by the manual raters to remove connective tissue and areas of

high fat within the muscle.

When comparing the UNET and semi-automatic masks, DICE scores for the calf overlay were very high (0.922), however, the UNET struggled on some thigh masks. There were two sources of the UNET under-performance. The first, when some bias remained in the water image post-correction which the semi-automatic was able to identify as muscle, but the UNET did not, as shown in the gaps within the masks seen in Figure 4.25. The second source appears to be the initial crop done for the UNET masks, which on occasion seems to cut off the tops on the thigh much more than the semi-automatic crop did, also seen in Figure 4.25. On UNET masks where the crop more closely matches the semi-automatic crop, the UNET masks extends beyond what the semi-automatic mask does at the top and bottom of the mask, with some minor areas also included between muscles that are not included in the semi-automatic mask, as shown in Figure 4.24. These images were chosen as representative of typical datasets.

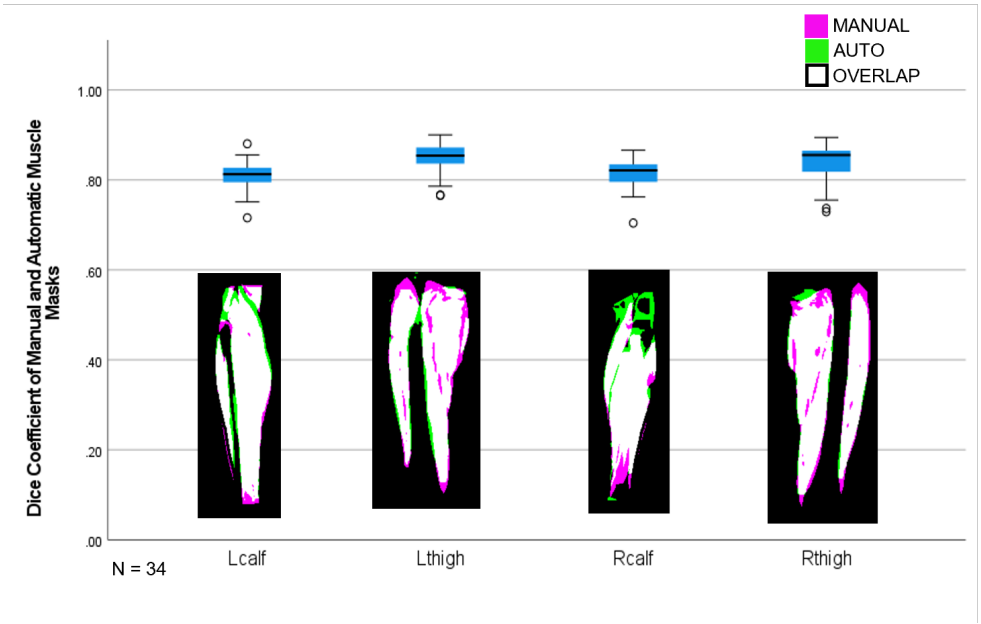

Figure 4.22: Mean DICE score of overlay values of manual and semi-automatic segmentations in each calf and thigh and an example dataset showing the manual in pink, the semi-automatic in green and the area of agreement in white

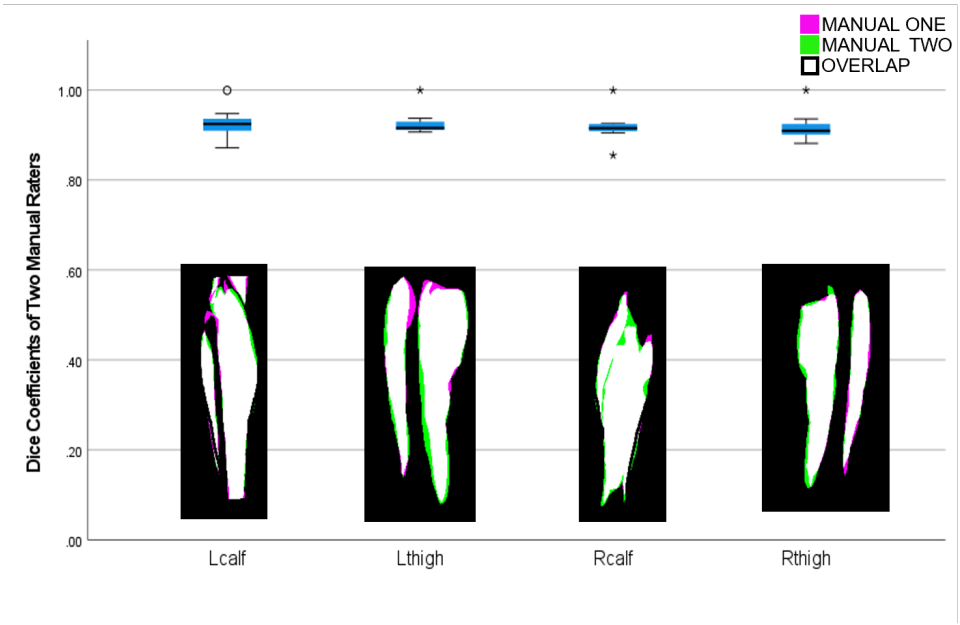

Figure 4.23: Mean DICE score of overlay values of the interrater reliability in each calf and thigh. Also shown is an example dataset showing the rater one in pink, rater two in green and the area of agreement in white

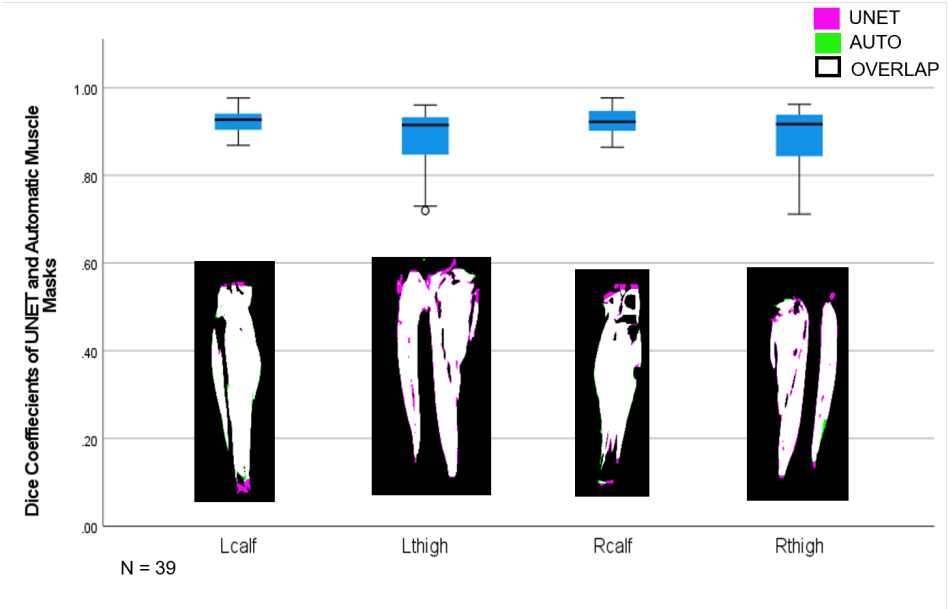

Figure 4.24: Mean DICE score of overlay values of UNET and semi-automatic segmentations in each calf and thigh. Also shown is an example dataset showing the UNET in pink, the semi-automatic in green and the area of agreement in white

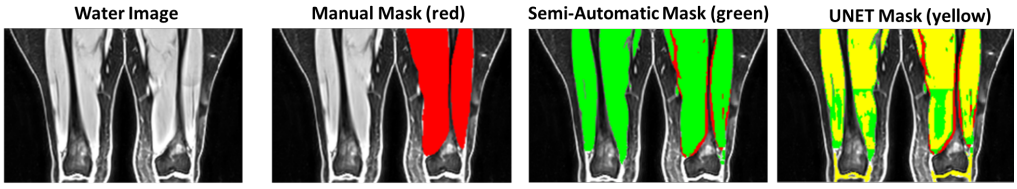

Figure 4.25: Mask overlays of different methodologies on an example water image in the thigh, showing a manual segmentation (red), semi-automatic segmentation (green) and UNET segmentation (yellow). This example demonstrates faults found in some UNET masks, an example of a more successful map can also be seen in Figure 4.24.

4.4.1.3 Comparison of MRI and DEXA measures

The differing regions covered must be kept in mind when comparing MRI measures and DEXA measures, with DEXA extending higher than the crops used for the MRI thigh measures. Figures 4.26 and 4.27 show DEXA gives greater volume with a bias of 3500 g. Comparison of the volume of the muscle from each leg from the semi-automatic segmentation to a subset of n=42 volunteers that also received DEXA scans are shown in Figure 4.26, correlations were good. There was a correlation of r(83) = 0.885, p=0.001 of the semi-automatic leg volumes with DEXA, and the comparison to the manually drawn measures was excellent, Figure 4.27, with a correlation of r(39) = 0.97, p=0.001. To more accurately compare how muscle volumes from the manual and semi-automatic segmentations of MR images compared to the DEXA, only data that is present in both subsets is plot in Figure 4.28. It can be seen that the manual segmentation results have a slightly higher (r=0.969) correlation to the DEXA volume than the semi-automatic derived volumes (r=0.908). While the correlations are strong, the absolute values of the results differ greatly with DEXA yielding high volume measures likely due to resolution, see Figure 4.16, and inclusion of connective tissue and water, see Discussion.

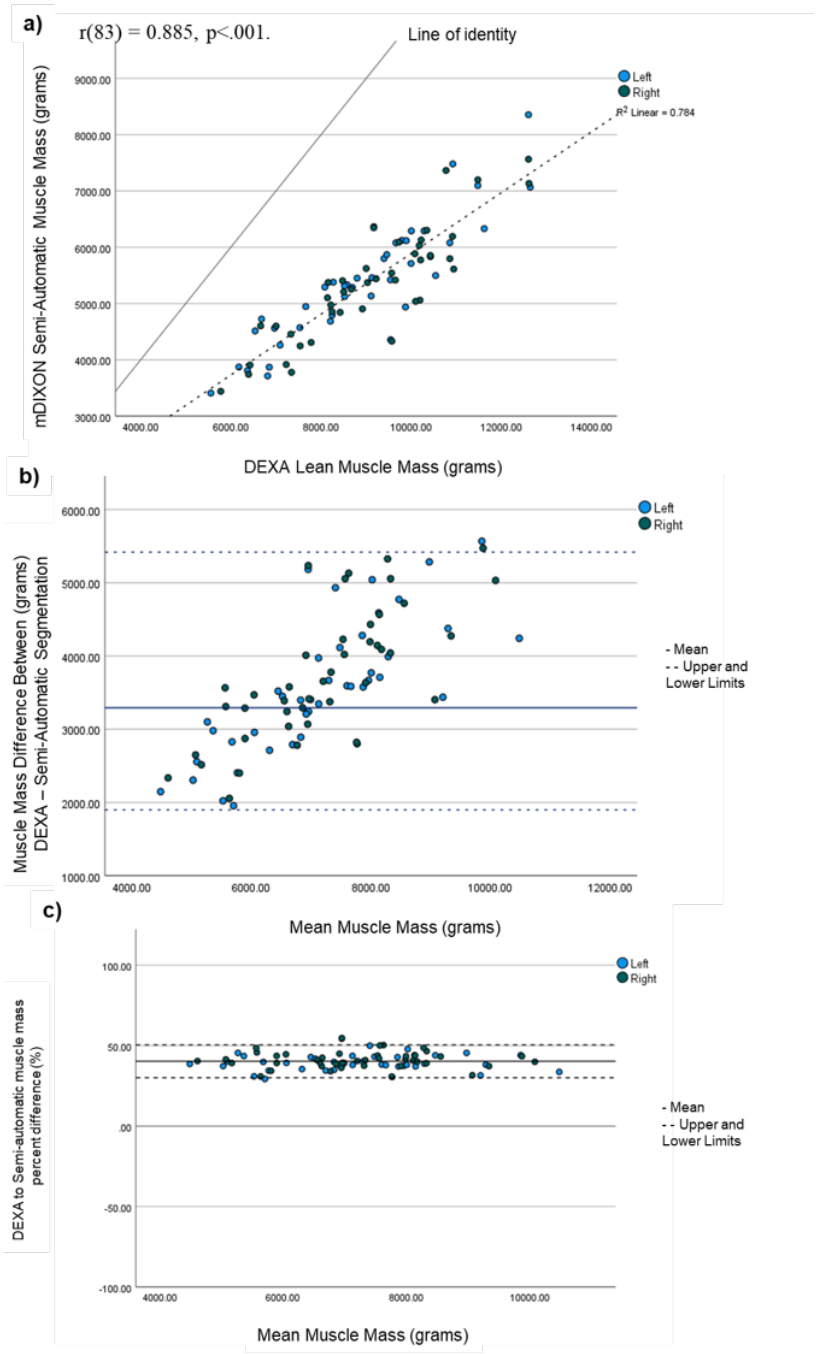

Figure 4.26: Muscle volumes computed with DEXA versus semi-automatic ROIs from mDIXON. The linear regression across left and right volumes (dotted line). b) Bland Altman plot of the DEXA versus semi-automatic volumes differences (b) and percent difference (c) with mean (solid line) and Upper and Lower limits (dashed line) shown.

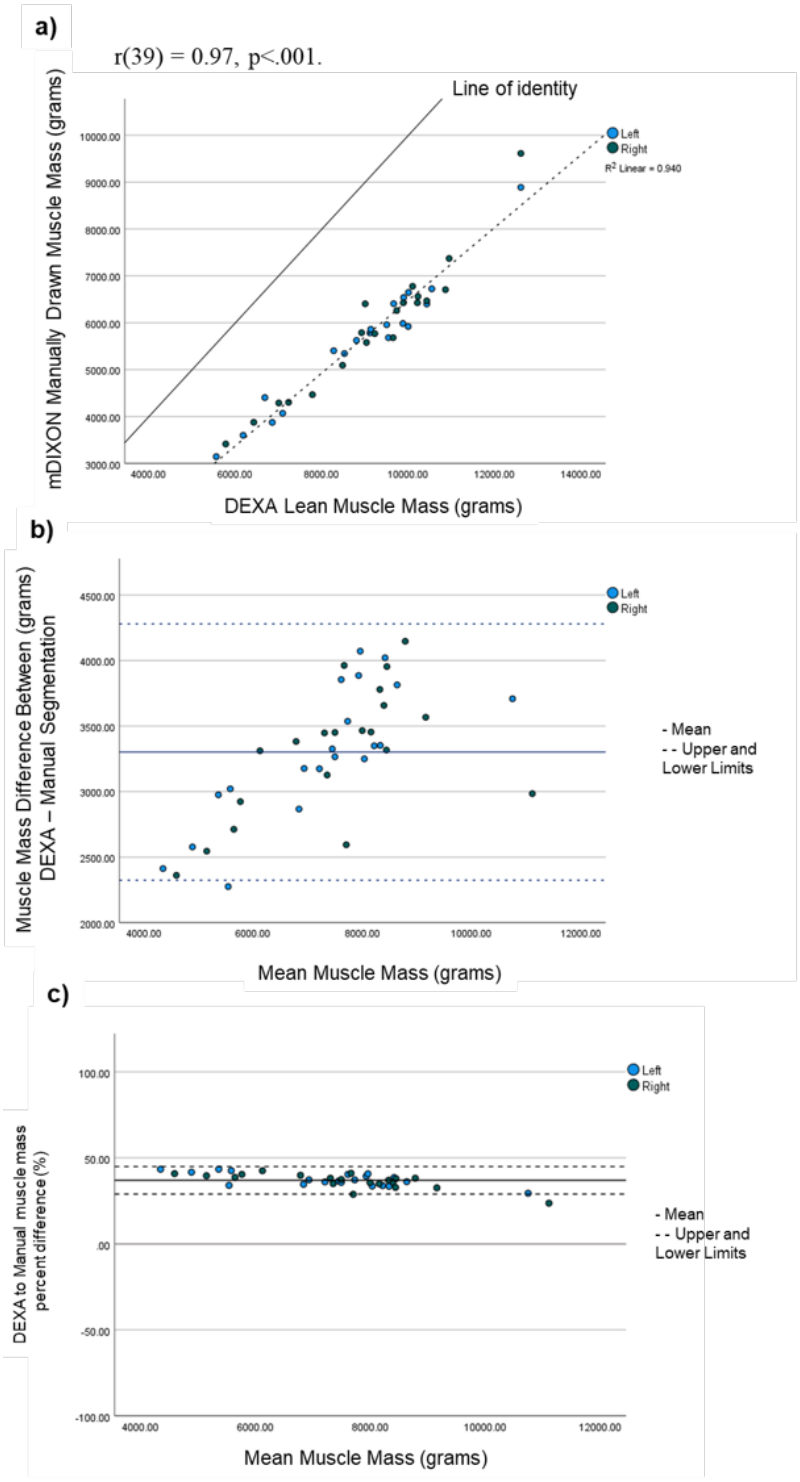

Figure 4.27: Muscle volumes computed with DEXA versus manually drawn ROIs from mDIXON. The linear regression across left and right volumes (dotted line). b-c) Bland Altman plots of the DEXA versus manual generated differences (b) and percent difference (c) with mean (solid line) and Upper and Lower limits (dashed line) shown.

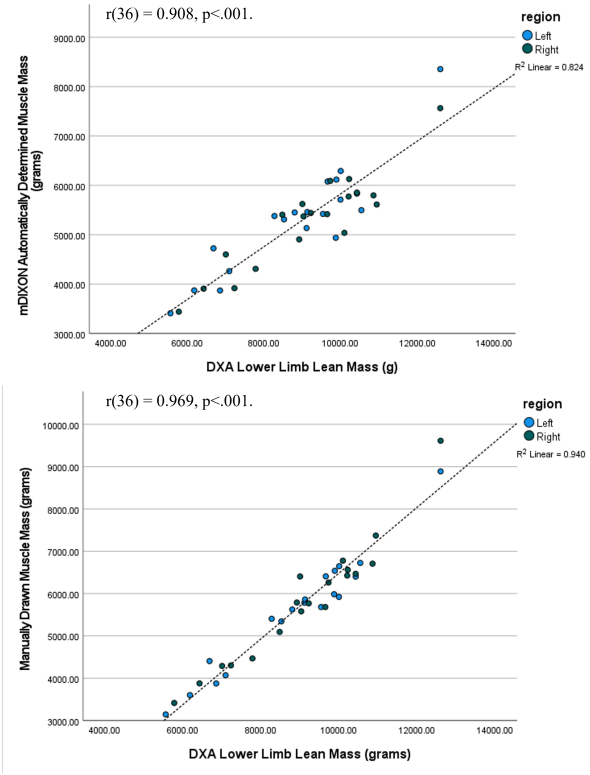

Figure 4.28: DEXA versus semi-automatic segmentation and manual segmentation showing only data present in both subsets

4.4.2 Application of semi-automatic segmentation estimated leg muscle mass across subject groups

mDIXON MRI scans were collected in healthy volunteers (HV), older trained (OT), older untrained (OU), Chronic Obstructive Pulmonary Disease (COPD) patients, Inflammatory Bowel Disease (IBD) patients, post-COVID-19 recovery patients and those deemed as Pre-Frail. The demographics for these groups are summarised in Figure 4.29. Body surface area (BSA) was used to correct for muscle volume before doing any group comparisons.

	n	M/F	Mean age (years)	BMI	BSA (m^2)
Healthy Volunteers (HV)	20	11/9	47 ± 20	26 ± 3	1.9 ± .2
Older Trained (OT)	9	9/0	72 ± 2	25 ± 3	1.8 ± .1
Older Untrained (OU)	7	7/0	74 ± 4	28 ± 4	1.9 ± .2
Chronic Obstructive Pulmonary Disease (COPD)	7	4/3	71 ± 4	26 ± 6	1.8 ± .2
Irritable Bowel Disease (IBD)	12	6/6	43 ± 15	24 ± 4	1.9 ± .2
Post-COVID-19 Fatigue	27	19/8	56 ± 10	32 ± 5	2.1 ± .2
Pre-Frail	3	0/3	70 ± 5	26 ± 5	1.8 ± .4
Total	85	56/29	57 ± 17	28 ± 5	1.9 ± .2

Figure 4.29: Participant demographics across patient groups

The semi-automatic segmentations were used to compute body-surface-area-normalised-leg-muscle-volume. These revealed significant differences between the volunteer groups, after covarying for age and sex, and Bonferroni correction, as shown in Figure 4.30. In the calf, there was a significant group effect of muscle volume, $F(6) = 6.304$, $p=0.001$, and effect of sex, $F(1) = 5.377$, $p=0.023$. The only within group effect of sex was in the COVID-19 patients, where women had smaller calf volumes than men ($p=0.022$). The COPD and IBD groups showed the most group differences, with the COPD patients having smaller calf volumes than COVID-19 recovery patients and healthy volunteers in both males ($p=0.001$ and $p=0.017$) and females ($p=0.014$ and $p=0.02$). For males, IBD patients had significantly smaller calf volumes than COVID-19 recovery patients ($p=0.005$) and healthy volunteers ($p=0.02$). Thigh volume also significantly differed across groups, $F(6) = 2.604$, $p=0.024$, and had an effect of sex, $F(1) = 13.123$, $p<0.001$. There were more significant sex differences within groups in the thigh, with women having smaller thigh volumes than men in the COVID-19 group ($p=0.002$) and in the healthy volunteers ($p=0.024$), and women had trend level smaller thighs in the IBD group ($p=0.052$). How-

ever, between group differences were not as apparent, and only occurred in the males, with the COPD group having significantly smaller thigh volumes than the COVID-19 group (p=0.32) and the older trained group (p=0.012).

Figure 4.31 shows the mean fat fractions within tissue differed significantly across groups, although only in the men, with the women exhibiting greater variability. In the calf, male groups differed significantly, $F(6)=5.747$, $p<0.001$, driven by higher fat fractions in the COVID-19 and COPD groups. The COVID-19 group had significantly higher fat fractions than the healthy volunteers (p=0.008), the older trained group ($p<0.001$) and the older untrained group ($p<.001$). The COPD patients had higher fat fractions than the older trained group (p=0.004). The thigh fat fractions also showed significant group differences, $F(6) = 5.627$, $p<0.001$, again driven by high COPD and COVID-19 fat fractions. COPD patients had higher amounts of fat compared to the healthy volunteers (p=0.008), the IBD patients (p=0.019), the older trained group ($p<0.001$) and the older untrained group ($p<0.001$). The COVID-19 group also differed significantly from the older trained group (p=0.004). The fat fraction group differences are driven by unusually high values in the COPD group that could be reflective of a pathological feature. However, the COPD group did show considerable variability in both thigh and calf fat fraction levels and have a small sample size (4), so conclusions should not be drawn from these results.

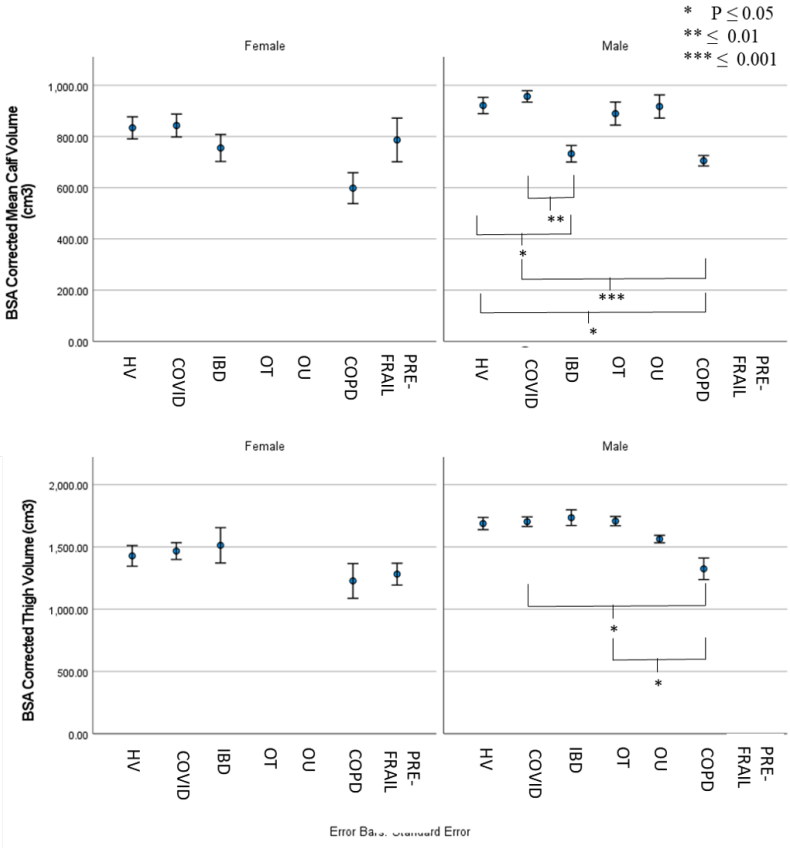

Figure 4.30: Calf and thigh BSA-corrected muscle volumes across older trained (OT) and older untrained (OU) from the EXAGE study, healthy volunteers (HV), Chronic Obstructive Pulmonary Disease (COPD) patients, Inflammatory Bowel Disease (IBD) patients, post-COVID-19 recovery patients (COVID-19) and those deemed as Pre-Frail (PRE-FRAIL).

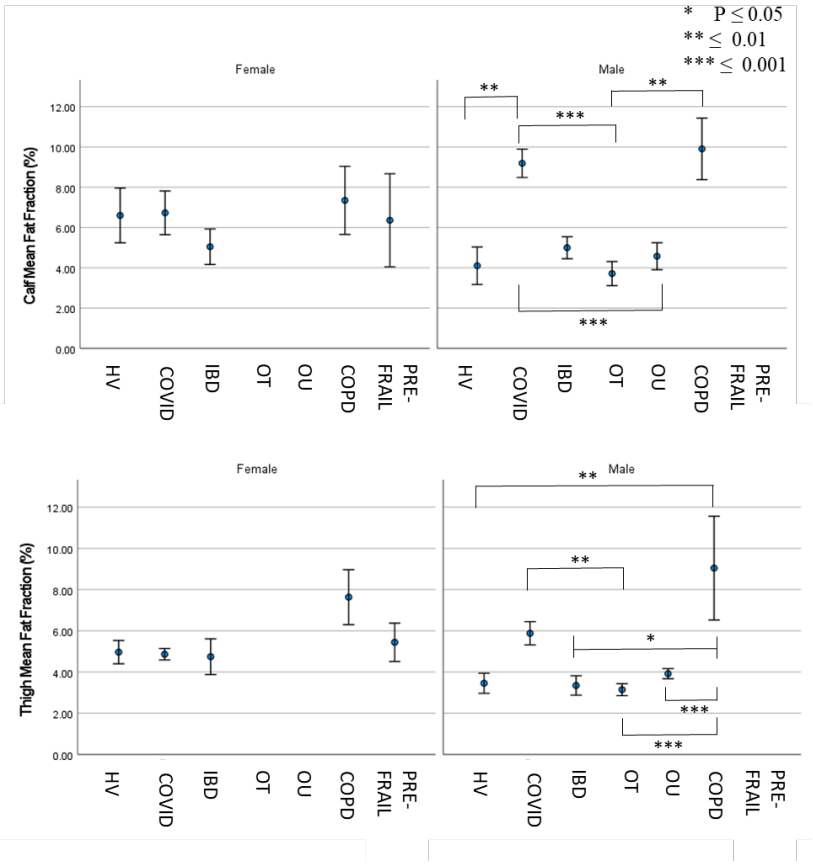

Figure 4.31: Calf and thigh muscle intramuscular fractions across older trained (OT) and older untrained (OU) from the EXAGE study, healthy volunteers (HV), Chronic Obstructive Pulmonary Disease (COPD) patients, Inflammatory Bowel Disease (IBD) patients, post-COVID-19 recovery patients (COVID-19) and those deemed as Pre-Frail (PRE-FRAIL). Significant differences between groups for $p<0.05$, $p<0.01$, $p<0.001$ are shown.

4.5 Discussion

Muscle volume and fat fractions are useful and physiologically important measures, both for cross sectional studies across groups and for use in longitudinal studies such as to study the response to a training intervention. These measures are most commonly assessed by DEXA indirectly by looking at lean tissue mass or manually drawing around mDIXON slices collected using MRI. However, DEXA has radiation exposure which must

be considered, and the method provides low spatial detail with body thickness, hydration status and water retention affecting the results. Whilst manual drawing on MRI whole body mDIXON scans is labour intensive and time consuming. The semi-automatic pipeline developed in this thesis chapter was built around FSL's FAST and thus provides an easy, accessible way of quickly analysing mDIXON data for estimating muscle volume and intramuscular fat fraction. Manually drawing around leg muscles in mDIXON MRI images can allow for greater specificity if a particular muscle is desired, but when investigating multiple muscle groups this will increase analytical variation due to deviations in human choice, and is not as robust at discarding the extramuscular lipid (fat) and connective tissue between different muscle groups. The bias in muscle volumes determined by the semi-automatic compared to the manual method can be attributed to the extramuscular fat and connective tissue which is assigned as muscle tissue by the manual raters but excluded in the semi-automatic method. This could be important to future studies aiming to investigate the relationship between muscle mass and body fat in ageing and disease and allow for greater investigation of fat infiltration in muscle in such conditions as sacropenic obesity. This was particularly evident in the thigh which had a bias of -540g, or -17% of the mean thigh volume over both methods. The semi-automatic pipeline is much faster and less labour intensive than manual drawing. It also removes the human element of choice, though this did not prove to be large in this small subset of data, but some variability is to be expected. The UNET had more variability that the semi-automatic method, especially for the thigh, as shown from the Bland Altman plot and higher standard deviation of DICE similarity scores. The UNET method was less able to cope with inhomogeneities remaining in the water images after bias-correction than the semi-automatic pipeline. This could be ameliorated by exploring other methods of correcting the water image, or

increased training of the UNET. Ideally, the UNET could be further trained to create the thigh and calf masks from the whole body image instead of a cropped version. Further training with the UNET on more thigh regions should improve its performance. This will require initial masks from which to train on, and the semi-automatic pipeline allows for the creation of such masks whilst also providing the benefit of training data that remove extra-muscular fat and connective tissue, at a much lower time cost than manual drawing and exclusion of these areas.

The semi-automatic method and manual methods were compared to DEXA, with results showing a consistent bias of MRI measures of muscle mass compared to DEXA, with DEXA yielding values of 3000g higher. This is likely due to DEXA including a wider volume coverage of DEXA which include up to the hip and includes all non-bone and non-fat tissue, and also the much coarser granularity than the MRI mDIXON images. However, a very good correlation was shown between the manual segmentations and DEXA at r=0.97, with a lower correlation of r=0.89 for semi-automatic segmentations. Note the better correlation for manual methods than semi-automatic likely as manual includes all connective tissue and extramuscular fat. Prior studies comparing lean soft tissue from thigh DEXA with cross sectionally determined MRI manual method have shown correlations in similar ranges (r^2=0.88, p<0.001 [13] and r^2=0.96, p<0.001 [14]). It should be also noted that DEXA will only give values in larger body regions, e.g. left leg and right leg, and once acquired cannot be further divided into smaller regions if desired. The semi-automatic pipeline groups the muscles into calf and thigh, from mDIXON images, and so can be revisited at any time if finer granularity is desired. The datasets studied in this chapter have been compiled from multiple studies that collected the same mDIXON whole body scans. Their use here is primarily to test the automatic segmentation

pipeline's effectiveness. While it is useful to look at the group differences as a method of examining the tool's sensitivity, the groups are not balanced or controlled to the healthy volunteer group, which were pooled from those collected for each study. When compared to the healthy volunteers, the significant results were smaller calf volumes for the COPD and IBD male groups, and larger intramuscular fat fractions in men in the COVID-19 calf and COPD thigh. Between the other groups, COVID-19 patients had significantly larger calf volumes than COPD patients and IBD patients (in males only) and larger thigh volumes the COPD group (in males only). The older trained group also had higher thigh volumes than the COPD group. Notably, the COVID-19 group had significantly higher intramuscular fat fractions than both the older trained and older untrained groups, and the COPD patients had higher fat fractions than the older trained group. COPD patients had higher amounts of fat compared to the IBD patients, the older trained and older untrained groups. The COVID-19 group also had higher intramuscular fat than the older trained group.

In future work, the mDIXON images could be used to compute subcutaneous adipose tissue (SAT) and extramuscular lipid (EMCL) from other PVE segmentations. Some attempt was made at developing this, but was complicated by the greater types of adipose tissue covered by one PVE component, including bone marrow adipose tissue as well as SAT and IMAT.

In conclusion, this semi-automatic pipeline can be used on multiple datasets for comparison of muscle volume and intramuscular fat fraction between groups. It allows for more rapid comparison of large datasets than manual drawing and does not require any retraining that a machine learning pipeline might need for new cohorts.

References

[1] Madoka Ogawa, Robert Lester, Hiroshi Akima, and Ashraf S Gorgey. Quantification of intermuscular and intramuscular adipose tissue using magnetic resonance imaging after neurodegenerative disorders. *Neural regeneration research*, 12(12):2100, 2017.

[2] Michael McLeod, Leigh Breen, D Lee Hamilton, and Andrew Philp. Live strong and prosper: the importance of skeletal muscle strength for healthy ageing. *Biogerontology*, 17:497–510, 2016.

[3] Ilvira M Khan, X-YD Perrard, Gerd Brunner, Hua Lui, Lauren M Sparks, Steven R Smith, Xukui Wang, Zheng-Zheng Shi, Dorothy E Lewis, Huaizhu Wu, et al. Intermuscular and perimuscular fat expansion in obesity correlates with skeletal muscle t cell and macrophage infiltration and insulin resistance. *International journal of obesity*, 39(11):1607–1618, 2015.

[4] Pablo Borrelli, Reza Kaboteh, Olof Enqvist, Johannes Ulén, Elin Trägårdh, Henrik Kjölhede, and Lars Edenbrandt. Artificial intelligence-aided ct segmentation for body composition analysis: a validation study. *European Radiology Experimental*, 5(1):1–6, 2021.

[5] Marianna S Thomas, David Newman, Olof Dahlqvist Leinhard, Bahman Kasmai, Richard Greenwood, Paul N Malcolm, Anette Karlsson,

Johannes Rosander, Magnus Borga, and Andoni P Toms. Test-retest reliability of automated whole body and compartmental muscle volume measurements on a wide bore 3t mr system. *European radiology*, 24(9):2279–2291, 2014.

[6] Anette Karlsson, Johannes Rosander, Thobias Romu, Joakim Tallberg, Anders Grönqvist, Magnus Borga, and Olof Dahlqvist Leinhard. Automatic and quantitative assessment of regional muscle volume by multi-atlas segmentation using whole-body water–fat mri. *Journal of Magnetic Resonance Imaging*, 41(6):1558–1569, 2015.

[7] Mirko Mandić, Eric Rullman, Per Widholm, Mats Lilja, Olof Dahlqvist Leinhard, Thomas Gustafsson, and Tommy R Lundberg. Automated assessment of regional muscle volume and hypertrophy using mri. *Scientific reports*, 10(1):1–8, 2020.

[8] Janne West, Thobias Romu, Sofia Thorell, Hanna Lindblom, Emilia Berin, Anna-Clara Spetz Holm, Lotta Lindh Åstrand, Anette Karlsson, Magnus Borga, Mats Hammar, et al. Precision of mri-based body composition measurements of postmenopausal women. *PloS one*, 13(2):e0192495, 2018.

[9] Yongyue Zhang, Michael Brady, and Stephen Smith. Segmentation of brain mr images through a hidden markov random field model and the expectation-maximization algorithm. *IEEE transactio26+ns on medical imaging*, 20(1):45–57, 2001.

[10] W Thomas Dixon. Simple proton spectroscopic imaging. *Radiology*, 153(1):189–194, 1984.

[11] Gary H Glover. Multipoint dixon technique for water and fat proton and susceptibility imaging. *Journal of Magnetic Resonance Imaging*, 1(5):521–530, 1991.

[12] Zhendi Gong, Rosemary Nicholas, Susan T. Francis, and Xin Chen. Thigh and calf muscles segmentation using ensemble of patch-based deep convolutional neural network on whole-body water-fat mri. In *Medical Image Understanding and Analysis: 26th Annual Conference, MIUA 2022, Cambridge, UK, July 27–29, 2022, Proceedings*, page 262–270, Berlin, Heidelberg, 2022. Springer-Verlag.

[13] Tom Maden-Wilkinson, H Degens, DA Jones, and JS McPhee. Comparison of mri and dxa to measure muscle size and age-related atrophy in thigh muscles. *Journal of Musculoskeletal and Neuronal Interactions*, 13(3):320–328, 2013.

[14] Jaehee Kim, ZiMian Wang, Steven B Heymsfield, Richard N Baumgartner, and Dympna Gallagher. Total-body skeletal muscle mass: estimation by a new dual-energy x-ray absorptiometry method. *The American journal of clinical nutrition*, 76(2):378–383, 2002.

Chapter 5

Muscle structure and effects of ageing and exercise

5.1 Introduction

With ageing there are noticeable declines in muscle strength, motor control, balance, and gait. These are largely driven by a reduction in muscle mass and neuromuscular function [1]. Muscle mass was been reported to decrease at a rate of 0.64-0.98% per year from the age of 65 years [2] with muscle mass loss twice as high in the lower body than the upper [3]. Loss of muscle mass is associated with increased fall rates and all-cause mortality [4] with sarcopenic participants being found to be over three times more likely to have a fall than non-sarcopenic controls [5]. Engelke et al. also found 37% lower thigh muscle volume between ages 40 to 70 years, but the relationship was quadratic and not linear, with muscle volume also greater by 8% from ages 20 to 40 years [6]. Hogrel et al. also compared a young and older group and found 22% lower thigh muscle volume in the older group [7].

The Engelke et al. study also investigated fat infiltration in sedentary men used MR images to measure the percentage of fat within the thigh muscle, and found 1.3% greater fat fraction per year [6]. Farrow et al. examined specific muscles within the thigh in three age groups, and found higher fat fractions in the hamstrings and quadriceps between the youngest (26 +/- 8 years) and oldest (79 +/- 5 years) [8]. The fat fraction within muscle correlated to gait speed, grip strength and muscle power measured by isokinetic knee extensions. In the Hogrel et al. study, fat fraction was found to be 87% higher in the older group than the young in the thigh [7]. A separate study by Schwenzer et al. using MR imaging of the calf showed greater fat fraction in an older group than a younger group [9].

An active lifestyle comprising exercise has been found to attenuate sarcopenia, body fat accumulation and inflammation [10], and intermuscular adipose tissue infiltration [11]. Bed rest studies that severely limit physical activity levels demonstrate the role of activity in retaining muscle mass, resulting in lower muscle volume and power to a greater degree in older participants than younger [12].

A large longitudinal study of older adults by Buchman et al. [13] (mean age 80 years) found higher rates of physical activity were associated with a slower rate of mobility decline, as measured by a timed-up-and-go task. For each additional weekly hour of activity, average decline in mobility was reduced by 3 percent. The population examined had levels of physical activity that were relatively low in intensity and duration (0-35 hours per week, mean, 3.0 h/wk; SD, 3.6 h; 10th percentile, 0 h/wk; 90th percentile, 7.0 h/wk).

The functional power of muscles has been shown to decrease to a greater degree than can be accounted for by mass loss alone. In a five year longi-

tudinal study by Delmonico et al. [14] a decline in strength, as measured by knee extensor torque, was found to be 2–5 times more than the loss of cross sectional area (CSA) of the thigh as measured by CT, and in other longitudinal studies a decline in strength was found to be 3 times greater than the muscle atrophy measured by DEXA [15, 16].

Changes of muscle function have been examined by investigating motorneurons in addition to muscle strength. Neuronal motor unit structural and functional differences have been observed in older populations. A difference in motor units in the vastus lateralis in the quadriceps has been found with age even in the absence of sarcopenia [17], as well as lower motor unit firing rates [18]. This difference in motor unit loss has been shown to be compensated for by motor units increasing in size and enervating more muscle fibres. However this does not occur if the individual is sarcopenic [19] and is more successful in highly active older people [20, 21]. Conversely, the Baltimore Longitudinal study of ageing found increases in motor unit firing with ageing [22], with the older groups using greater firing rates to achieve lower force levels. The stability of the stimulation of the muscle fibre can also be measured by investigating neuromuscular junction transmission, the synaptic transmission between the motorneuron and the muscle fibre that stimulates the action potential and muscle contraction. Previous studies have found greater instability with age [17, 18, 23], but this has been found to be modulated by high levels of physical activity [24].

The current chapter aims to investigate ageing in relation to muscle volume, strength and motor control in the EXAGE study, comprising of older male endurance cyclists, termed an older trained (OT) group, age-matched controls who are untrained (OU), and a younger untrained (YU) group. Because an maximal exercise task had to be completed with sufficient data

points to participate in this study, the task created a minimum required strength to participate and those who could not complete the task would be excluded. This created YU and OU groups that were not truly sedentary as found in other studies, and so differences in muscle strength are expected to be less pronounced. The recruitment to this study necessitated being able to maintain a medium intensity exercise, therefore the non-exercising control groups will not be expected to show as low motor performance as the Boyle study.

The hypothesis was that the YU group would have greater leg muscle volume, lower fat fraction, greater strength and greater motor function than both older groups (OT and OU), but the OT group having muscle volumes and motor control more closely matched to the YU group than the OU group. Full methods for each task described in this chapter are detailed in Chapter 3.

5.2 Effect of age and exercise level on muscle volume and fat fraction measured with MRI

The results shown in this section are those of the semi-automatic pipeline applied to the wholebody mDIXON images (as shown in Chapter 4, Figure 4.14) described in Chapter 4 in the groups of the EXAGE study. An example dataset with muscle volume and fat fraction masks for calf and thigh in shown in Figure 5.1.

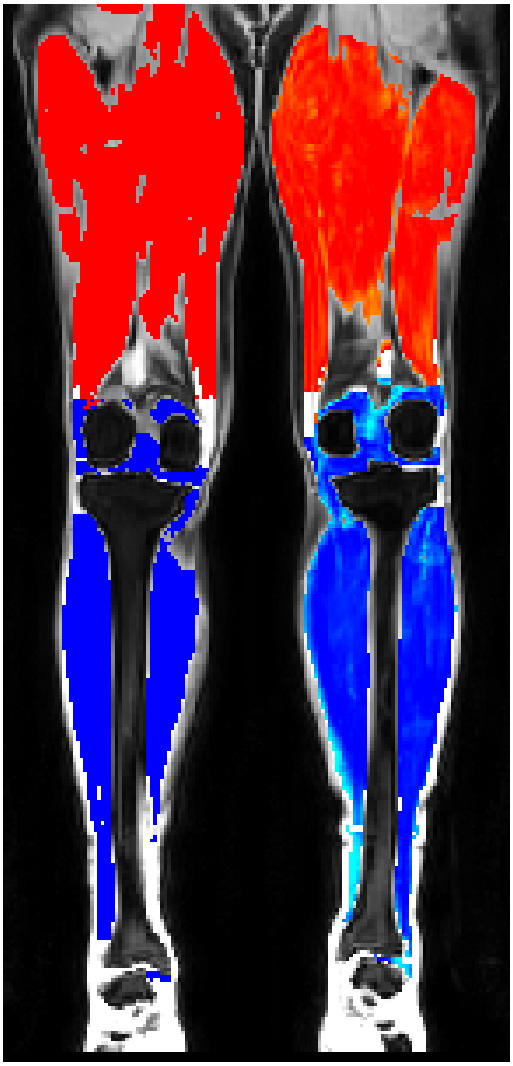

Figure 5.1: Example thigh (red) and calf (blue) masks created through the semi-automatic pipeline for muscle volume (right) and fat fraction (left, where lighter colours indicated higher fat fraction)

The demographics of these groups are shown in Figure 5.2. A t-test revealed no significant difference in age between the two older groups ($F(14) = 1.979$, $p=0.305$). In BMI, there was a significant difference when examining all three groups ($F(2,23) = 3.68$, $p=0.043$), with the YU group having a lower mean BMI than the OU group ($p=.047$) but not the OT ($p=.172$), and no difference between the two older groups ($p=1.00$). The BSA method of composition estimation did not show significant differences between groups ($F(2,23) = 2.742$, $p =.088$).

	n	Mean age (years)	BMI (kg/m^2)	BSA (m^2)
Older Trained	9	72 ± 2	25 ± 3	1.8 ± .1
Older Untrained	7	74 ± 4	28 ± 4	1.9 ± .2
Younger Untrained	8	24 ± 3	23 ± 3	1.9 ± .2

Figure 5.2: Demographics of participants included in the EXAGE study in the muscle composition analysis

5.2.1 Muscle Volume for the Leg

The leg calf and thigh muscle volume from the semi-automatic segmentations were normalised for body surface area (BSA) (see Chapter 4). The calf muscle volumes showed no significant differences between the EXAGE groups, as shown in Figure 5.3, both when adjusted for BSA (in the calf, $F(2,23) = 0.71$, $p=0.503$, and thigh $F(2,22) = 1.595$, $p=0.228$) and in absolute terms (in the calf, $F(2,23) = 2.26$, $p=0.13$, and thigh $F(2,22) = 1.05$, $p=0.369$). Although no significant differences were found for the thigh, it should be noted that thigh masses had low variability within groups for the OT (1701 g +/- 105) and OU (1564 g +/- 80), but were highly variable in the YU group (1841 g +/- 308).

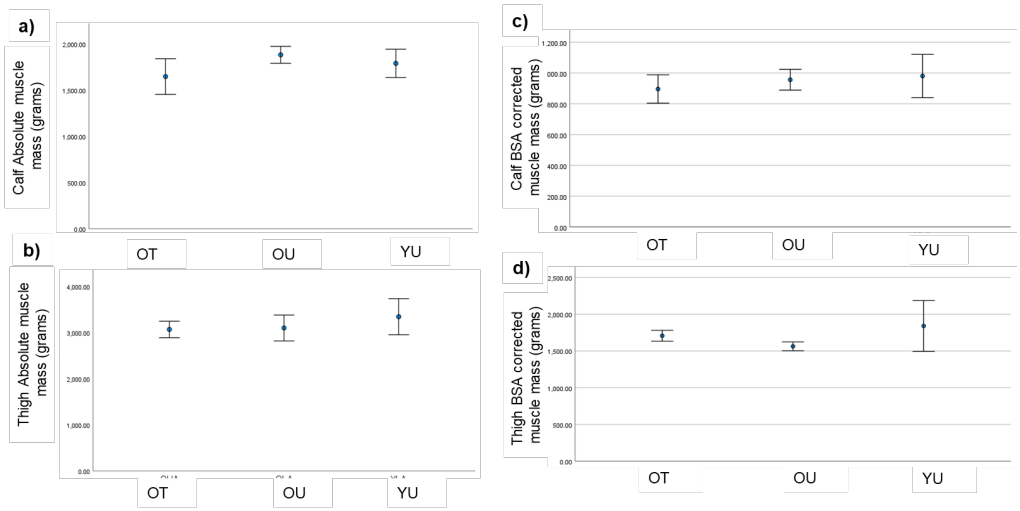

Figure 5.3: Absolute muscle mass of the (a) calf and (b) thigh and BSA corrected muscle mass for the calf (c) and thigh (d) for the Older Trained (OT), Older Untrained (OU) and Younger Untrained (YU) groups.

5.2.2 Intra-Muscular Fat Fraction

Fat fraction values are taken as the fat percentage in each voxel across the muscle mask, with means calculated using a Gaussian curve as describe in Chapter 4. When studying intramuscular fat fraction, there was a significant difference for the calf ($F(2,21) = 7.225$, $p=0.005$), see Figure 5.4. The YU group had lower calf fat fraction than the OT ($p=.043$) and OU ($p=.005$), but the two older groups did not differ significantly in calf muscle fat fraction ($p=0.828$). Muscle fat fraction did not differ in the thigh ($F(2,21) = 1.537$, $p=0.242$). The YU group had a large variance in fat fraction, particularly in the thigh, with one participant's data removed due to MR artifacts in the thigh.

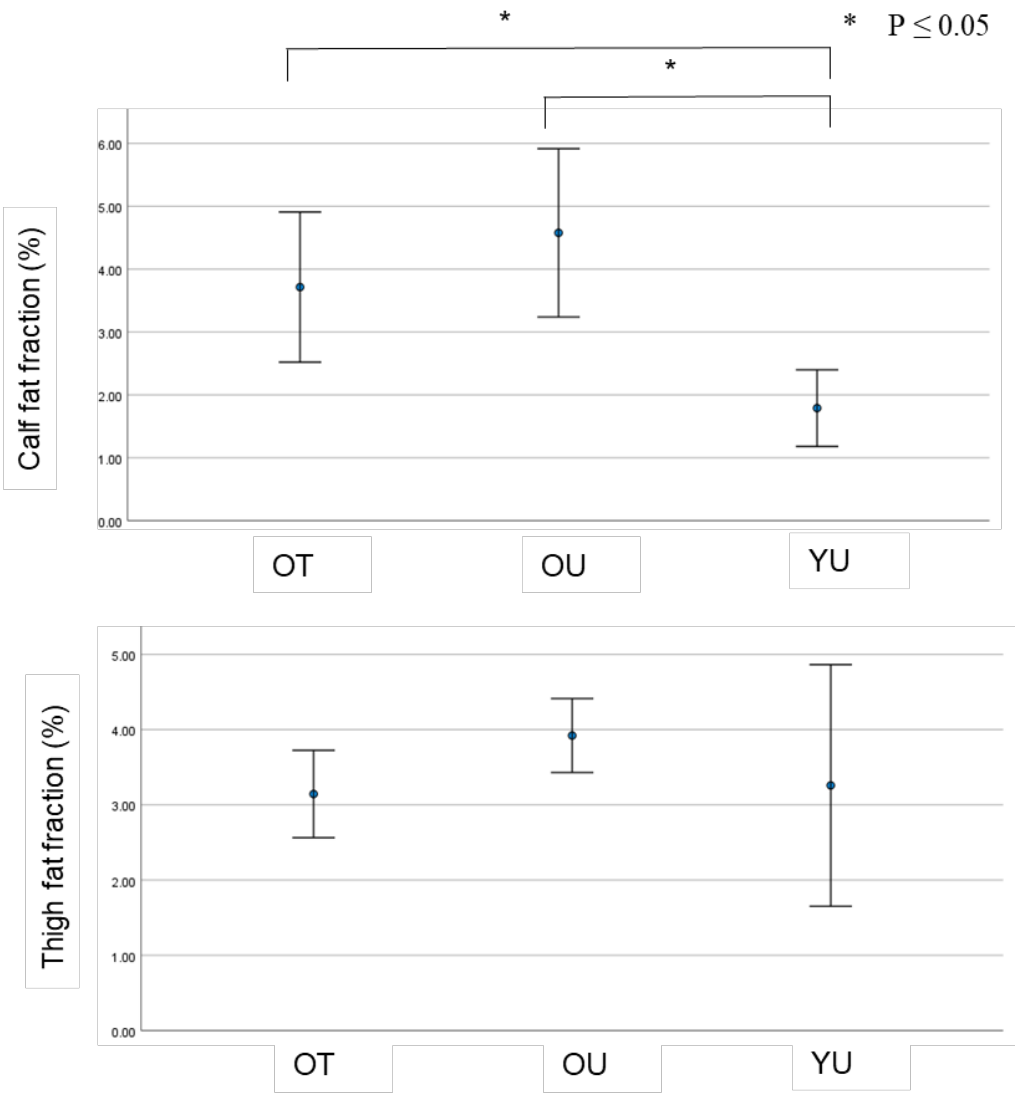

Figure 5.4: Leg muscle fat fraction in the a) calf and b) thigh for the OT, OU and YU groups.

5.3 Physical Function

This section outlines the results of the physical function tests performed in the EXAGE YU, OU and OT groups. For methods see Chapter 3.

In brief, a timed-up-and-go (TUG) test involving standing from a chair, walking 3 metres before returning to the chair and sitting, was administered and an accelerometer was used to indicate determine siting and standing

points. Additionally, the accelerometer measured jump height and power test was performed, and a Cybex isokinetic and isometric dynanometer was used to assess maximal voluntary isometric contraction (MVC) of the dominant leg as well and isokinetic work output, or fatigability. A balance board was used to measure standing and one-footed balance.

Logistical, scheduling and technical difficulties limited the acquisition of these measures in some participants. With the exception of the cybex isometric strength and isokinetic work done tests the measures discussed in the section will reflect the OT and OU groups only. The demographics of these groups can be seen in Figure 5.5, where it can also be seen that the OU group is underpowered in these measures.

Group n	TUG	Jump	Cybex	Balance	iEMG
Older Trained	9	9	7	8	8
Older Untrained	4	5	6	5	5
Young Untrained	n/a	n/a	6	n/a	n/a

Figure 5.5: Demographics of participants included in the EXAGE study for the TUG, jump, cybex isokinetic and isometric contractions, balance and iEMG measures.

5.3.1 Time-up-and-go (TUG) test

No significant differences were found in the TUG test in measures of a) the total time taken to complete the task, b) time taken to stand from a seated position, and c) time taken to sit in the chair from standing, as seen in Figure 5.6. All participants were classified as independent, none taking longer than the 12 seconds determined to indicate a fall risk.

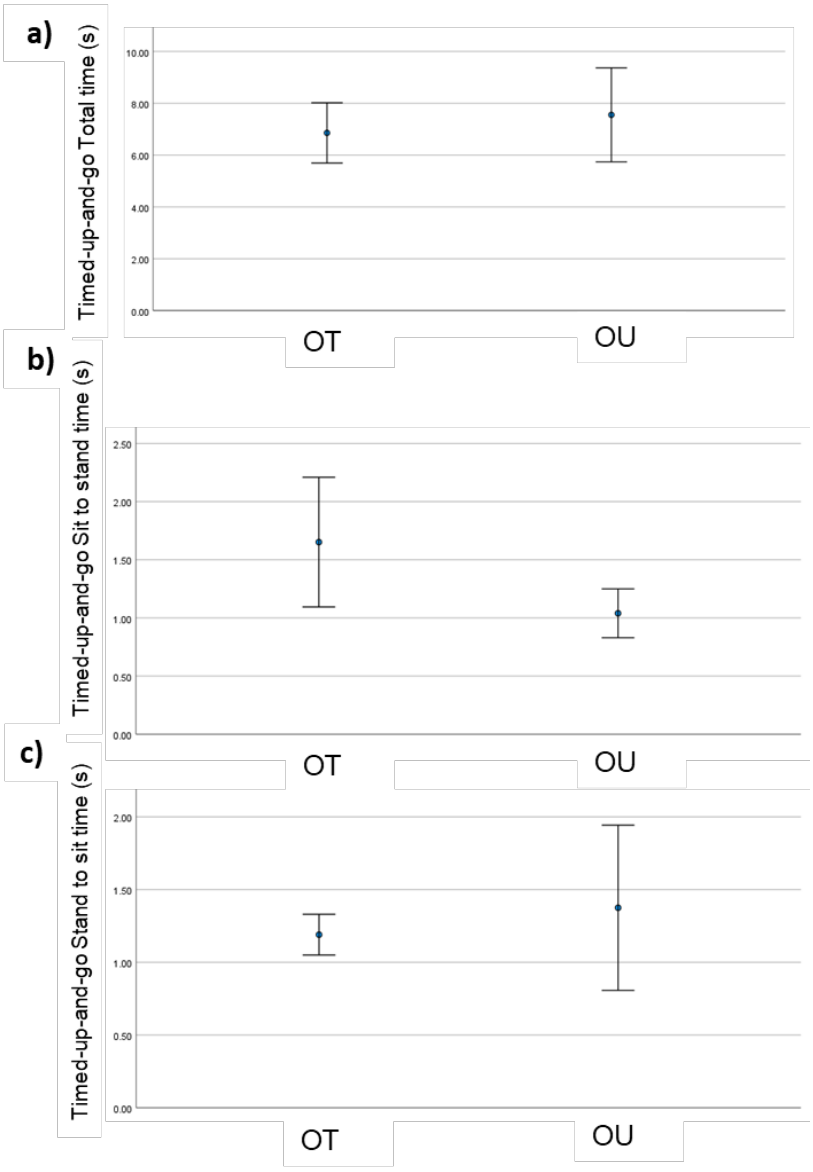

Figure 5.6: Timed-up-and-go test results. Note lower times indicate greater motor function and control. No differences were seen between the OT and OU groups for a) total time, b) sit to stand time, or c) stand to sit time

5.3.2 Jump Test

There were no differences in jump height or power between the older groups (Figure 5.7).

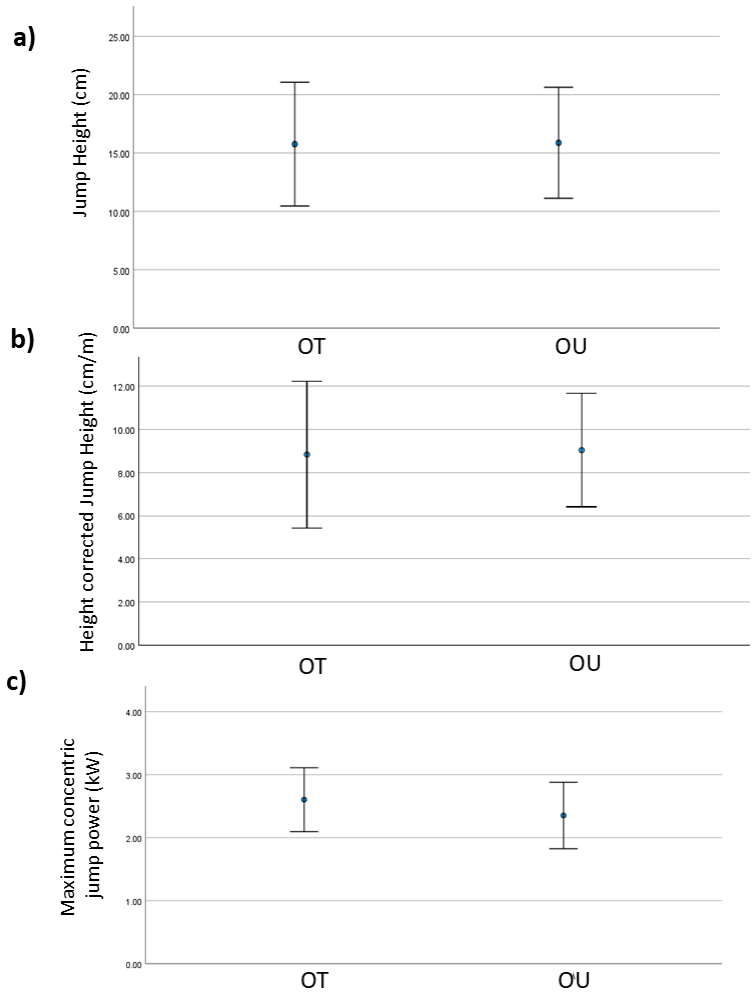

Figure 5.7: Jump Test results showing a) jump height, b) jump height corrected for participant height (centimeters height hump for meters height), and c) jump power in the OT and OU groups.

5.3.3 Isometric and isokinetic contractions

Isometric MVC force was greater in the YU group ($F(2,18)=5.31$, $p=0.017$, compared to the OT ($p=0.031$) and OU ($p=0.041$) groups, as shown in Figure 5.8a. Muscle quality can also be interrogated by calculating MVC per unit of thigh muscle volume (Figure 5.8b), where the YU group had better muscle quality ($F(2,18)=9.7$, $p=0.002$, compared to the OT ($p=0.006$) and OU ($p=0.004$) groups. These MVCs can also be seen to be significantly correlated ($p<.001$) with BSA-corrected thigh volume, shown in Figure 5.8c,

R^2=0.74, F(1,16)=29.58.

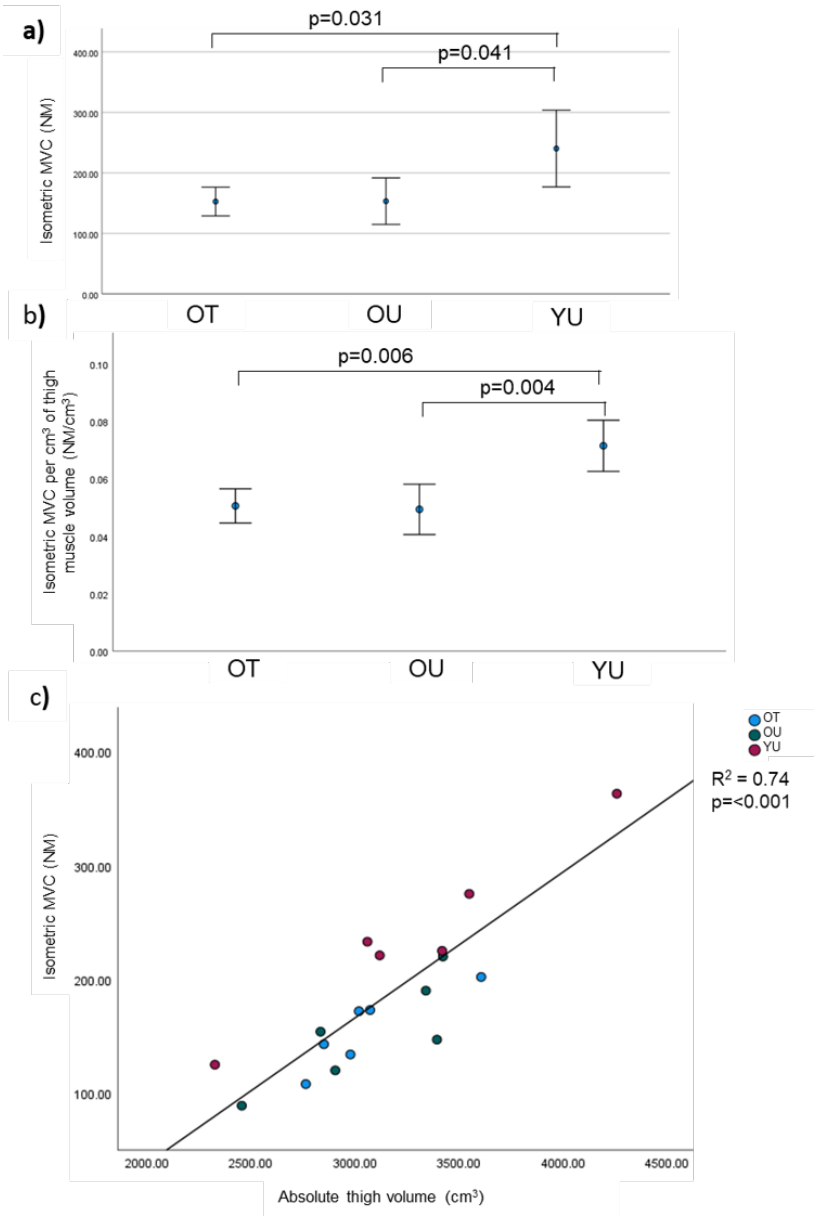

Figure 5.8: a) Isometric maximal voluntary contraction (MVC) of the quadriceps b) MVC per unit of thigh muscle volume across the OT, OU and YU groups and c) correlation of MVC with absolute thigh volume.

There were significant differences between groups in the total work performed over 20 repeated isokinetic contractions, F(2,16)=5.35,p=0.019. The OU group performed lower overall work than the YU (p=0.019). The difference between the OU and OT groups did not reach significance (p=0.074), however when taken into account with the similarity of work be-

tween the OT and YU (p=1), there is a suggestion that a larger sample size may support the OU lower work overall (Figure 5.9a). When muscle quality is assessed by examining total work done per unit of thigh muscle volume, the lower OU muscle quality becomes apparent (F(2,16)=9.68,p=0.003), as shown in Figure 5.9b. The OU group had significantly lower muscle quality than both the OT (p=0.009) and YU (p=0.003) groups, with no difference between the OT and YU groups (p=1.00).

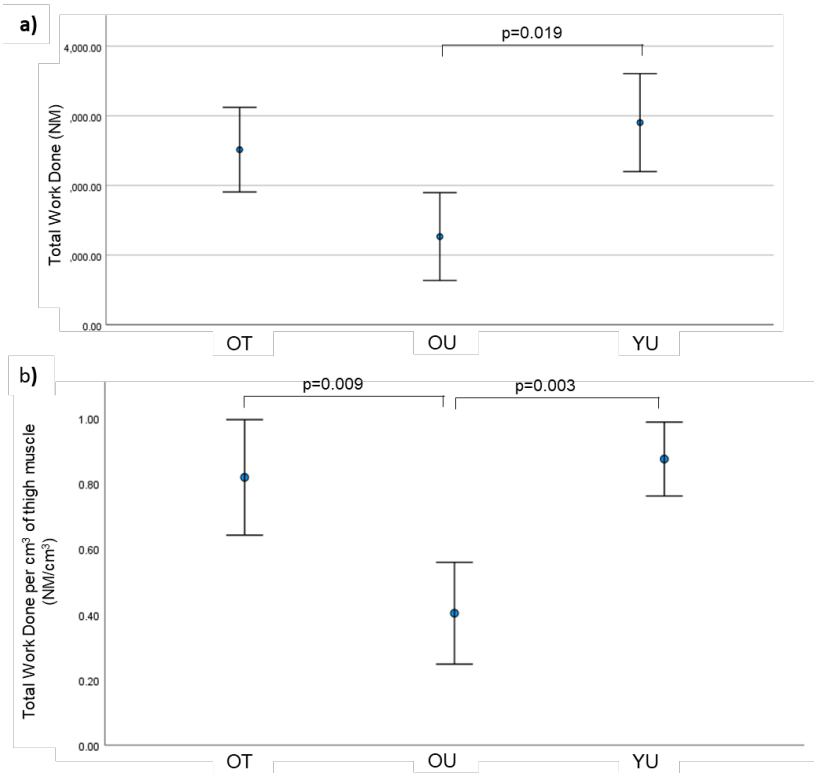

Figure 5.9: a) Total work over 20 isokinetic repetitions and b) total work done per unit of thigh muscle volume, shown for the OT, OU and YU groups

5.4 Motor Control

5.4.1 Balance

Bilateral and unilateral balance tests were conducted on an electronic force pressure plate (RS Footscan), as described in Chapter 3. Each trial was 30 seconds and participants were allowed to practice before the final recording. Measures to be recorded were the travel distance of the foot or feet on the balance board, and the total elliptical area of that travel distance, where lower values indicate better stability and motor control.

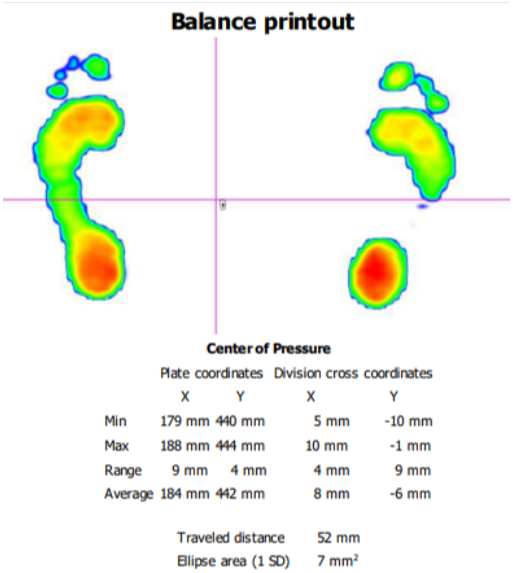

Figure 5.10: Balance board example output, where lower values reflect less distance travelled and better balance.

There were no differences between the groups in either the standing or one footed balance travel distances (Figure 5.11) or elliptical area (Figure 5.12), where lower values reflect less distance travelled and better balance. The elliptical area when stood on two feet was the closest to reaching significant difference at p=.116, with greater stability in the OT, but the variability in the underpowered OU group is too great to indicate

differences.

All but one older participant could not balance on one foot with their eyes closed for the full 30 seconds, therefore it was not possible to collect travel distance or area data and this measure has been excluded from the analysis. In some cases where balance was poor in the eyes open tests, eyes closed was not attempted at all.

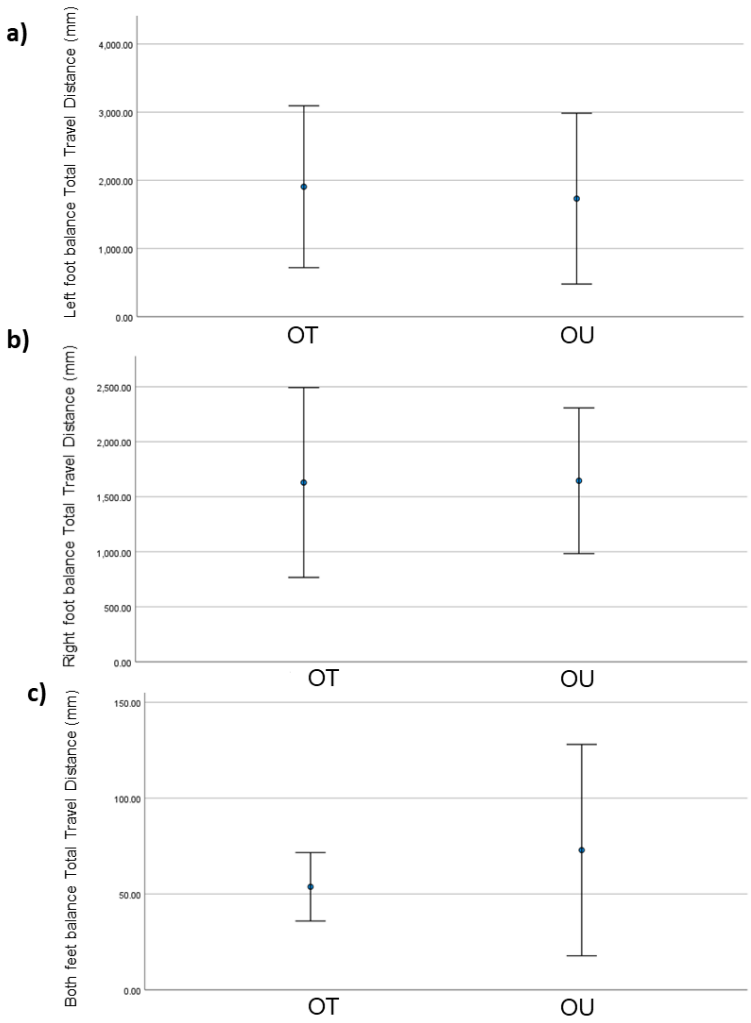

Figure 5.11: Balance travel distance for a) the left foot, b) the right foot, and c) both feet.

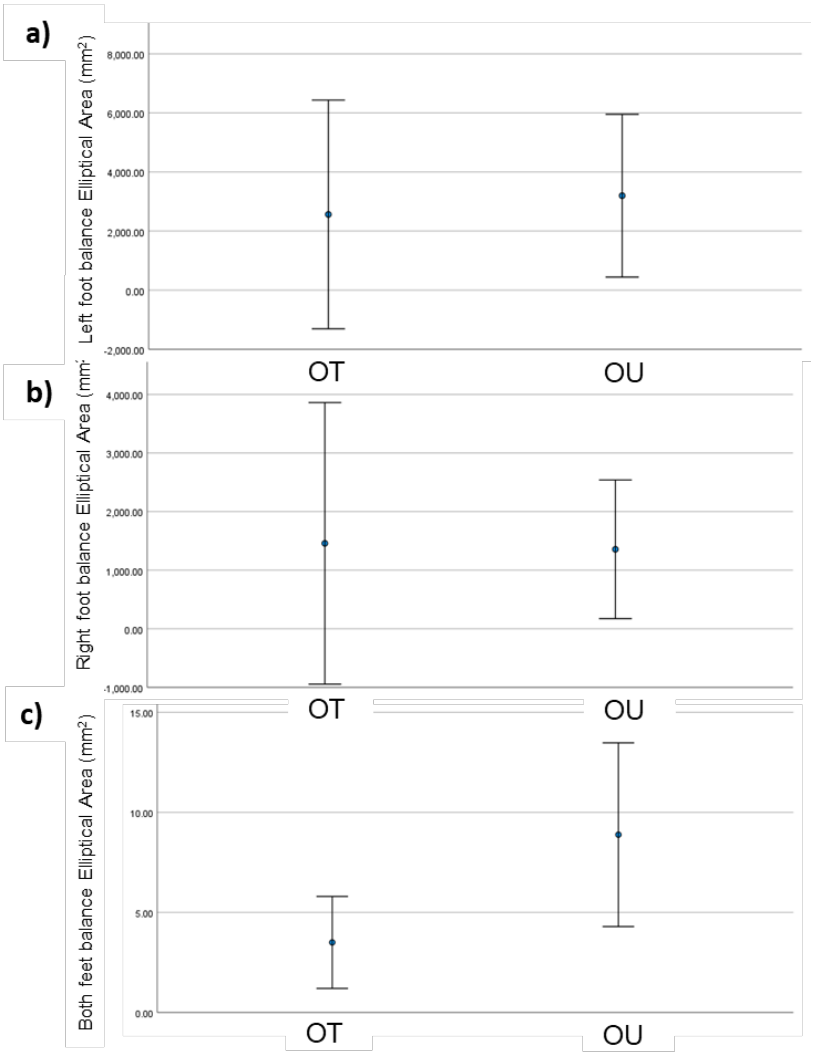

Figure 5.12: Balance elliptical area for a) the left foot, b) the right foot, and c) both feet.

5.4.2 Intramuscular Electromyography

Intramuscular electromyography (iEMG) using a single electrode measuring motor unit firing in the vastus lateralis (VL) was used to measure motor unit firing rate at isokinetic contractions with participants keeping as close as possible to a target set at 25% MVC with real-time visual feedback (see Chapter 3). Their ability to remain on target is measured as the covariance of the force trace and yields a force steadiness measure. Neuromuscular junction transmission instability can be measured from the variability in

consecutive near fibre motor unit potentials [25].

There was no significant difference in force steadiness between the groups, as seen in Figure 5.13a, where lower values indicate better control. There was also no significant difference in motor unit firing rates between groups, as seen in Figure 5.13b. The difference in motor unit firing rate variability did not reach significance, but there was a trend level difference between groups The OT group had lower variability than the OU (p=.062) as seen in Figure 5.13c.

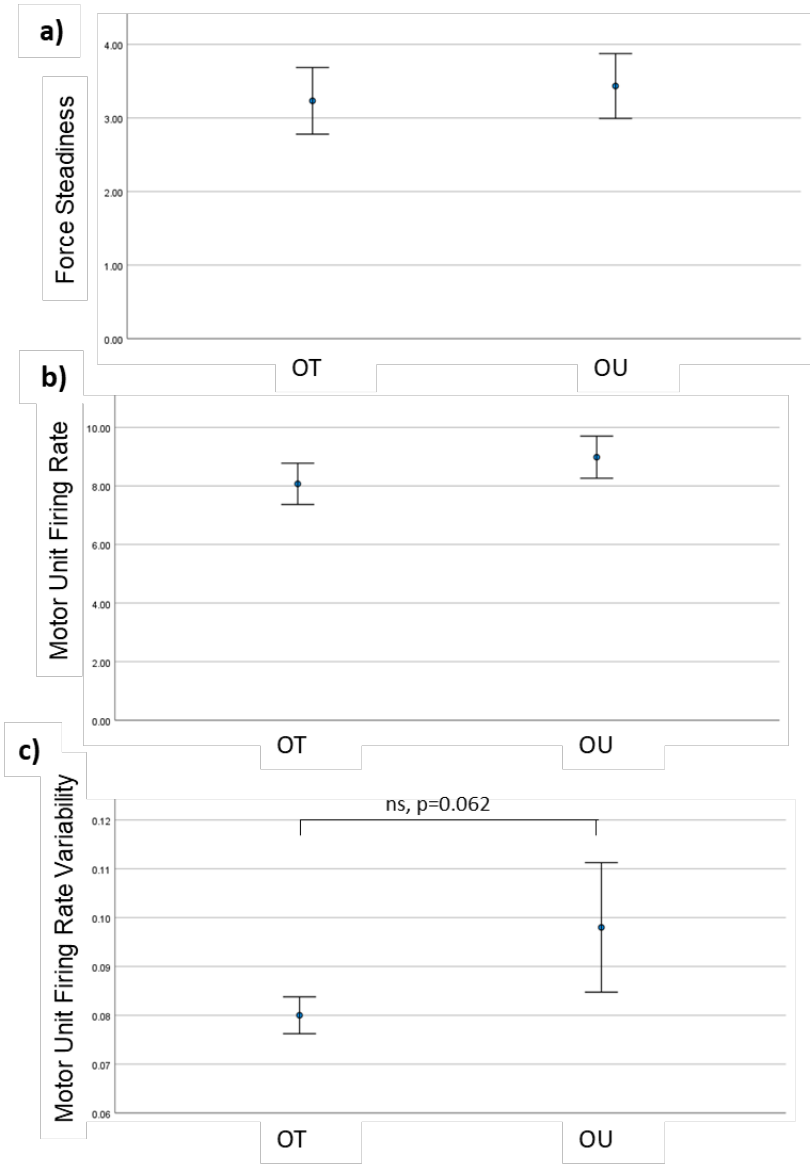

Figure 5.13: iEMG test results for a) Force Steadiness, b) motor unit firing rate, and c) motor unit firing rate variability

5.5 Discussion

This chapter explored the relationship between ageing and exercise on leg muscle volumes, fat fraction and whole body physical function. The impact of a highly active lifestyle on the OT group compared to the OU group was not apparent in most measures, but there were some indications that larger sample sizes that would reduce variability are worth pursuing in these measures in future studies, and are useful markers of the extent of the impact of a highly active lifestyle.

In the EXAGE groups, there were no muscle volume differences that are typically associated with ageing as typically some muscle atrophy is present in older individuals [2], suggesting both older groups had greater physical fitness and muscle health than might be found in the general population of their age group. There were also no difference between the older trained and untrained groups; the trained group were all long distance cyclists, which is an endurance sport and does not provide the resistance training more commonly associated with muscle volume building and strength training [26]. Another possibility is the quadratic relationship to muscle volume and age found by the Engelke et al study [6], where muscle volume had a positive relationship to age from ages 20 to 40 years. The younger group in this thesis was aged 24 +/- 3 years, and thus may not have shown as many differences to the older groups as a group in their thirties. However, other studies have found clear differences in thigh muscle volume in these age ranges [27], thus it is more likely that the study is simply underpowered.

In addition to this, the untrained group were required to be able to complete the exercise task and therefore had some muscle strength and physical fitness. The OU participants who came forward for the study were untrained and did not perform cardiovascular exercises, but lived otherwise

active lifestyles, including short daily walks and gardening, for example. In the general population more sarcopenia would be expected in an otherwise healthy age matched control group. A systematic review looking at sacropenia in community-dwelling older adults found, depending on the definition used, 9.9 to 40.4% prevalence rates [28].

To truly investigate this, measurements would need to be collected on another group that was not selected for their ability to do the exercise task, such as a pre-frail group. The data from the Pre-frail group (from the PHENOFRIM study) was included in Chapter 4. This group was shown to have the lowest calf volumes, but only female participants were enrolled to the PHENOFRIM study and so they cannot be compared to the male EXAGE OT and OU groups.

The YU group had lower calf fat fraction than both the older groups, showing greater age-related fat infiltration unrelated to fitness levels, aligning with Schwenzer et al.'s findings [9]. There was no significant difference in fat fractions between older groups or in the thigh, though the YU group had high variance driven by larger fat fractions in one participant. This participant had a z-score of 2.2, and thus did not meet the threshold to be considered an outlier, but with a larger sample size would likely become sufficiently distinct to be excluded, and yield a YU group with significantly lower fat fraction that the older groups. Other studies have found significant differences in fat fraction in the thigh, such as Engelke et al. [6], Farrow et al. [8] and Hogrel et al. [7] who all found greater fat fraction in an older group than a younger one. Comparing past studies introduces some difficulty in a lack of standardization in definition of muscular fat fraction. The Engelke et al. study separates muscular fat fraction and intermuscular adipose tissue (IMAT), and defines IMAT as the combination of extracellular adipose tissue between muscle groups and of larger adipocyte

agglomerations within muscle [6]. This seems to reflect best the fat fraction used in this study, excluding IMAT, where fat between muscle groups would be excluded in the semi-automatic segmentation, and areas within the muscle would be excluded if they were large enough and had sufficient fat content. However, the Interdisciplinary Workshop at the National Institute on Aging stated that myosteatosis included three components "(a) intermuscular adipose tissue (IMAT), the extra-myocellular adipose tissue found beneath the fascia and in-between muscle groups; (b) intramuscular adipose tissue, the extramyocellular adipose tissue found within an individual muscle; and (c) intramyocellular lipids (IMCL)" [29]. Under this definition, this thesis would have excluded areas of fat fraction that are deemed intramuscular adipose tissue. In a meta-analysis of the effects of exercise interventions, only a small effect of exercise intervention was found for intramuscular and intermuscular accumulation [30], however most of the interventional studies were resistance training.

As expected, there were no differences in the timed-up-and-go test as all participants were independently functional and reported no significant impacts of frailty on lifestyle or everyday tasks. Greater physical activity has been associated with reduced risk of developing impairments in activities of daily living [31], but all participants in this study did not exhibit impairments.

The YU had higher isometric maximal voluntary contractions (MVCs) of the quadriceps than the both older groups, and these MVCs significantly correlated with thigh muscle volume across groups, similar to results found by Farrow et al. [27] who showed correlations between muscle volume and MVC.

On the isokinetic work output test, the OU group performed lower overall

work than the YU, and at trend level also lower than the OT group, while there was no difference between the YU and OT. Extending the number of repetitions of the total work test could prove valuable in detecting the impact of endurance training on muscle function in ageing in future. Clear differences were however visible in the muscle quality in the isokinetic total work output, with the older trained showing similar muscle quality to the young untrained, while the older untrained were able to output significantly less work than both. While participating in high levels of endurance physical activity does not improve muscle mass, the quality of that muscle is preserved equal to a younger group, while the untrained show lower levels.

Postural sway increases with ageing and is associated with greater fall risk [32], and static balance can be used to measure sway. There were no differences in measured balance between groups, though the near significance in elliptical area between the OU and OT when standing on two feet in such underpowered groups suggests it would be a useful measure to collect in future studies with larger sample sizes. A systematic review found a moderate effect of physical activity on balance, though the age range was younger than this study at 40 to 65 years old [33]. The studies that measured balance were mostly studies whose exercise intervention included some form of balance training. As the older trained participants were cyclists, it would be interesting to examine whether the balance require to cycle translates to standing balance. A one-year interventional moderate intensity endurance training programme found improved standing balance in older participants [34].

Initial data collection also included a test on one foot with eyes closed. This proved too difficult for the older groups, with all but one unable to complete the 30 seconds, and so data is not available to compare. The young were able to complete the eyes-closed task, and so it can be stated that the older

groups had worse eyes-closed balance than the young, although the more detailed measures are not available. A measure to quantify this without having to complete the 30 seconds on the balance board could prove useful in the future. Decreases in motor unit firing rate with ageing seen in other studies [18] were not able to be investigated here, but the OT had better trend level better firing rate stability than the OU. With the inclusion of a younger dataset and further participants, the relationship between these strength and motor control measures could be better understood.

Endurance training in ageing did not reveal significant differences in most muscle structure and function measures compared to their not highly active, but not sedentary, peers in this small study, however trend level differences suggest further research could uncover substantial findings. The small sample sizes greatly limited the power of the chapter, particularly the measures such as the jump, balance and iEMG that were collected at the Royal Derby Hospital and necessitated travel to a third site, which was not possible in all cases.

References

[1] Rachael D Seidler, Jessica A Bernard, Taritonye B Burutolu, Brett W Fling, Mark T Gordon, Joseph T Gwin, Youngbin Kwak, and David B Lipps. Motor control and aging: links to age-related brain structural, functional, and biochemical effects. *Neuroscience & Biobehavioral Reviews*, 34(5):721–733, 2010.

[2] W Kyle Mitchell, John Williams, Philip Atherton, Mike Larvin, John Lund, and Marco Narici. Sarcopenia, dynapenia, and the impact of advancing age on human skeletal muscle size and strength; a quantitative review. *Frontiers in physiology*, 3:260, 2012.

[3] Ian Janssen, Steven B Heymsfield, ZiMian Wang, and Robert Ross. Skeletal muscle mass and distribution in 468 men and women aged 18–88 yr. *Journal of applied physiology*, 2000.

[4] Preethi Srikanthan and Arun S Karlamangla. Muscle mass index as a predictor of longevity in older adults. *The American journal of medicine*, 127(6):547–553, 2014.

[5] Francesco Landi, Rosa Liperoti, Andrea Russo, Silvia Giovannini, Matteo Tosato, Ettore Capoluongo, Roberto Bernabei, and Graziano Onder. Sarcopenia as a risk factor for falls in elderly individuals: results from the ilsirente study. *Clinical nutrition*, 31(5):652–658, 2012.

[6] Klaus Engelke, Mansour Ghasemikaram, Oliver Chaudry, Michael Uder, Armin M Nagel, Franz Jakob, and Wolfgang Kemmler. The effect of ageing on fat infiltration of thigh and paraspinal muscles in men. *Aging Clinical and Experimental Research*, 34(9):2089–2098, 2022.

[7] Jean-Yves Hogrel, Yoann Barnouin, Noura Azzabou, Gillian Butler-Browne, Thomas Voit, Amélie Moraux, Gaëlle Leroux, Anthony Behin, Jamie S McPhee, and Pierre G Carlier. Nmr imaging estimates of muscle volume and intramuscular fat infiltration in the thigh: variations with muscle, gender, and age. *Age*, 37:1–11, 2015.

[8] Matt Farrow, John Biglands, Steven F Tanner, A Clegg, L Brown, EMA Hensor, P O'Connor, P Emery, and AL Tan. The effect of ageing on skeletal muscle as assessed by quantitative mr imaging: an association with frailty and muscle strength. *Aging clinical and experimental research*, 33:291–301, 2021.

[9] Nina F Schwenzer, Petros Martirosian, Jürgen Machann, Christina Schraml, Günter Steidle, Claus D Claussen, and Fritz Schick. Aging effects on human calf muscle properties assessed by mri at 3 tesla. *Journal of Magnetic Resonance Imaging: An Official Journal of the International Society for Magnetic Resonance in Medicine*, 29(6):1346–1354, 2009.

[10] Adeel Safdar, Mazen J Hamadeh, Jan J Kaczor, Sandeep Raha, Justin Debeer, and Mark A Tarnopolsky. Aberrant mitochondrial homeostasis in the skeletal muscle of sedentary older adults. *PloS one*, 5(5):e10778, 2010.

[11] Bret H Goodpaster, Peter Chomentowski, Bryan K Ward, Andrea Rossi, Nancy W Glynn, Matthew J Delmonico, Stephen B

Kritchevsky, Marco Pahor, and Anne B Newman. Effects of physical activity on strength and skeletal muscle fat infiltration in older adults: a randomized controlled trial. *Journal of applied physiology*, 105(5):1498–1503, 2008.

[12] Rado Pišot, Uros Marusic, Gianni Biolo, Sara Mazzucco, Stefano Lazzer, Bruno Grassi, Carlo Reggiani, Luana Toniolo, Pietro Enrico Di Prampero, Angelina Passaro, et al. Greater loss in muscle mass and function but smaller metabolic alterations in older compared with younger men following 2 wk of bed rest and recovery. *Journal of Applied Physiology*, 120(8):922–929, 2016.

[13] Aron S Buchman, Robert S Wilson, Patricia A Boyle, Yuxiao Tang, Debra A Fleischman, and David A Bennett. Physical activity and leg strength predict decline in mobility performance in older persons. *Journal of the American Geriatrics Society*, 55(10):1618–1623, 2007.

[14] MJ Delmonico, TB Harris, M Visser, SW Park, MB Conroy, P Velasquez-Mieyer, R Boudreau, TM Manini, M Nevitt, AB Newman, et al. Health agingbody composition study. *Longitudinal study of muscle strength, quality, and adipose tissue infiltration. Am J Clin Nutr*, 90(6):1579–1585, 2009.

[15] Bret H Goodpaster, Seok Won Park, Tamara B Harris, Steven B Kritchevsky, Michael Nevitt, Ann V Schwartz, Eleanor M Simonsick, Frances A Tylavsky, Marjolein Visser, and Anne B Newman. The loss of skeletal muscle strength, mass, and quality in older adults: the health, aging and body composition study. *The Journals of Gerontology Series A: Biological Sciences and Medical Sciences*, 61(10):1059–1064, 2006.

[16] Annemarie Koster, Jingzhong Ding, Sari Stenholm, Paolo Caserotti, Denise K Houston, Barbara J Nicklas, Tongjian You, Jung Sun Lee, Marjolein Visser, Anne B Newman, et al. Does the amount of fat mass predict age-related loss of lean mass, muscle strength, and muscle quality in older adults? *Journals of Gerontology Series A: Biomedical Sciences and Medical Sciences*, 66(8):888–895, 2011.

[17] Mathew Piasecki, A Ireland, D Stashuk, A Hamilton-Wright, DA Jones, and JS McPhee. Age-related neuromuscular changes affecting human vastus lateralis. *The Journal of physiology*, 594(16):4525–4536, 2016.

[18] Jessica Piasecki, Thomas B Inns, Joseph J Bass, Reece Scott, Daniel W Stashuk, Bethan E Phillips, Philip J Atherton, and Mathew Piasecki. Influence of sex on the age-related adaptations of neuromuscular function and motor unit properties in elite masters athletes. *The Journal of Physiology*, 599(1):193–205, 2021.

[19] M Piasecki, A Ireland, J Piasecki, Dan W Stashuk, Agniezka Swiecicka, MK Rutter, DA Jones, and JS McPhee. Failure to expand the motor unit size to compensate for declining motor unit numbers distinguishes sarcopenic from non-sarcopenic older men. *The Journal of physiology*, 596(9):1627–1637, 2018.

[20] M Piasecki, A Ireland, J Piasecki, H Degens, DW Stashuk, A Swiecicka, MK Rutter, DA Jones, and JS McPhee. Long-term endurance and power training may facilitate motor unit size expansion to compensate for declining motor unit numbers in older age. *Frontiers in Physiology*, 10:449, 2019.

[21] Eleanor J Jones, Shin-Yi Chiou, Philip J Atherton, Bethan E Phillips, and Mathew Piasecki. Ageing and exercise-induced motor unit remodelling. *The Journal of Physiology*, 600(8):1839–1849, 2022.

[22] Shari M Ling, Robin A Conwit, Luigi Ferrucci, and E Jeffrey Metter. Age-associated changes in motor unit physiology: observations from the baltimore longitudinal study of aging. *Archives of physical medicine and rehabilitation*, 90(7):1237–1240, 2009.

[23] Maddison L Hourigan, Neal B McKinnon, Marjorie Johnson, Charles L Rice, Daniel W Stashuk, and Timothy J Doherty. Increased motor unit potential shape variability across consecutive motor unit discharges in the tibialis anterior and vastus medialis muscles of healthy older subjects. *Clinical Neurophysiology*, 126(12):2381–2389, 2015.

[24] Geoffrey A Power, Matti D Allen, Kevin J Gilmore, Daniel W Stashuk, Timothy J Doherty, Russell T Hepple, Tanja Taivassalo, and Charles L Rice. Motor unit number and transmission stability in octogenarian world class athletes: Can age-related deficits be outrun? *Journal of Applied Physiology*, 121(4):1013–1020, 2016.

[25] Mathew Piasecki, Oscar Garnés-Camarena, and Daniel W Stashuk. Near-fiber electromyography. *Clinical Neurophysiology*, 132(5):1089–1104, 2021.

[26] Gary R Hunter, John P McCarthy, and Marcas M Bamman. Effects of resistance training on older adults. *Sports medicine*, 34:329–348, 2004.

[27] TM Maden-Wilkinson, JS McPhee, Jörn Rittweger, David A Jones, and Hans Degens. Thigh muscle volume in relation to age, sex and femur volume. *Age*, 36:383–393, 2014.

[28] AJ Mayhew, K Amog, S Phillips, G Parise, PD McNicholas, RJ De Souza, L Thabane, and P Raina. The prevalence of sarcopenia in community-dwelling older adults, an exploration of differences between studies and within definitions: a systematic review and meta-analyses. *Age and ageing*, 48(1):48–56, 2019.

[29] Rosaly Correa-de Araujo, Odessa Addison, Iva Miljkovic, Bret H Goodpaster, Bryan C Bergman, Richard V Clark, Joanne W Elena, Karyn A Esser, Luigi Ferrucci, Michael O Harris-Love, et al. Myosteatosis in the context of skeletal muscle function deficit: an interdisciplinary workshop at the national institute on aging. *Frontiers in physiology*, 11:963, 2020.

[30] Régis Radaelli, Dennis R Taaffe, Robert U Newton, Daniel A Galvão, and Pedro Lopez. Exercise effects on muscle quality in older adults: A systematic review and meta-analysis. *Scientific Reports*, 11(1):21085, 2021.

[31] Patricia A Boyle, Aron S Buchman, Robert S Wilson, Julia L Bienias, and David A Bennett. Physical activity is associated with incident disability in community-based older persons. *Journal of the American geriatrics society*, 55(2):195–201, 2007.

[32] Danuta Roman-Liu. Age-related changes in the range and velocity of postural sway. *Archives of gerontology and geriatrics*, 77:68–80, 2018.

[33] Manuela L Ferreira, Catherine Sherrington, Kate Smith, Phil Carswell, Rebecca Bell, Morton Bell, Dafne P Nascimento, Leani Souza Máximo Pereira, and Paul Vardon. Physical activity improves strength, balance and endurance in adults aged 40–65 years: a systematic review. *Journal of physiotherapy*, 58(3):145–156, 2012.

[34] Marybeth Brown and John O Holloszy. Effects of walking, jogging and cycling on strength, flexibility, speed and balance in 60-to 72-year olds. *Aging clinical and experimental research*, 5:427–434, 1993.

Chapter 6

The impact of lifelong exercise and age on the cardiovascular responses to acute exercise and recovery in healthy volunteers

6.1 Introduction

Cardiorespiratory fitness (CRF) or maximum oxygen uptake (VO_2max) reflects the capacity of the cardiovascular, respiratory and skeletal muscle systems to collectively provide oxygen to tissues and extract and utilise it in response to steady state moderate or high intensity exercise. It is considered an objective indicator of habitual physical activity and is known to be one of the best predictors for all-cause mortality [1]. Intensities of exercise required to reach equivalent levels of cardiorespiratory stress vary dependent on sex, age, body mass and composition and muscle fibre composition and exercise modality [2]. Therefore, when setting exercise

intensities and/or training workloads this must be done relative to an individual's VO_{2max}, considered a gold standard of cardiorespiratory fitness [3].

The Fick equation defines maximal oxygen consumption (VO_{2max}) as:

$$VO_{2max} = Q \cdot (C_aO_2 - C_vO_2) \tag{6.1}$$

where C_aO_2 is the arterial (delivered) oxygen content, C_vO_2 is the venous (returned) oxygen content and Q is the cardiac output. From Equation 6.1 it can be seen that cardiac output is a major driver of VO_{2max} [4], and thus measured VO_{2max} is assumed to linearly relate to cardiac output. This has been confirmed in experiments demonstrating that if blood volume increases or decreased VO_2max increases or decreases accordingly.

VO_{2max} is measured during an incremental intensity exercise test, with an initial incremental test, followed by a second test to confirm VO_{2max} has been reached, as confirmation test, as described in Chapter 3. To achieve a true VO_{2max} oxygen consumption must plateau, i.e, the point where it no longer increases despite increased workload. If no plateau is observed at the point of volitional exhaustion this is defined as VO_{2peak}. This is often seen in untrained and older volunteers and patients with non-communicable disease. Here peripheral muscle fatigue often limits exercise tolerance before VO_{2max} is achieved. While cardiac output is very much assumed to be linearly associated with VO_2 during incremental intensity exercise, a study of n=72 found that in 35% of participants the cardiac output and VO_2 relationship displayed negative curvature rather than a linear relationship, and this was associated with higher fitness levels in normal, non-elite-athletic subjects [5].

Cross sectional studies of younger and older participants have shown lower VO_2max in older groups compared to their younger peers, in a population-based study [6]. Pollock et al studied a range of physiological functions in a group of highly active older individuals aged 55-79 and found declines in VO_2max with age even in this highly active cohort [7]. VO_2max was the best predictor of age in this cohort. A meta-analysis of longitudinal studies by Burtscher et al. on VO_2max of master athletes attributed 54% of variance in males to changes in training volume [8].

VO_{2peak} has been shown to decrease with age, as reviewed in Betik et al, [9]. A longitudinal study modelling all-cause mortality and cardiorespiratory fitness found that each increase increment of 1 mL/kg/min of VO_{2peak} was associated with a 45 day increase in life expectancy in a population of men over a 46 year period [10]. A large cross sectional study on participants aged 21-81 years found decreased cardiorespiratory fitness with age, associated with a smaller stroke volume and cardiac output as measured by cardiac MRI, but no association with ejection fraction [6].

Many studies have investigated cardiac function measures (such as stroke volume and structural measures) and how they relate to high levels of habitual physical activity. Studies have shown higher habitual levels of physical activity to be associated with greater cardiac stroke volume and cardiac size [11, 12, 13, 14]. A longitudinal study of cardiac MRI by Howden et al. was able to distinguish the effects of ageing and exercise using an interventional exercise training regime in otherwise sedentary participants aged 45 to 64 years. Two years of exercise training yielded increased stroke volume, end diastolic volume, VO_{2peak} and decreased resting heart rate [15], while a non-trained control group showed no changes. In Murias et al.'s interventional training study, maximal cardiac output and stroke volume were higher in the older group than the young after 3 weeks of endurance

training [16].

In this chapter the cardiorespiratory fitness (VO_{2peak}) is compared across participant groups of young untrained (YU), older untrained (OU) and older trained (OT) individuals in the EXAGE group. The 50% level of the VO_{2peak} is used to calculate the workload at which each participant exercises within the MR scanner. MRI measures of cardiac function are taken at rest, during exercise, and during a recovery period. These measures aim to untangle the differences due to ageing compared to training induced differences in cardiac response to exercise. As a highly active lifestyle has been shown to improve cardiorespiratory fitness and cardiac stroke volume in older individuals, the older trained group may exhibit cardiovascular measures closer to a younger group than an age-matched untrained group. The use of MR scanning during exercise provides further insight to cardiac function differences that have been less studied and allows for the mechanism underlying cardiac output differences to be explored.

6.2 Cardiorespiratory fitness

6.2.1 Methods

In the work in this thesis, a supine Cardio-Step VO_{2max} test was performed in the David Greenfield Human Physiology Unit (DGHPU) to ensure the relative exercise workload to be performed inside the MR scanner was matched for all volunteers. This yielded greater peripheral fatigue than central cardiorespiratory strain, which is not uncommon for supine exercise with all participants indicating they ended the protocol because of muscular rather than cardiorespiratory exhaustion, (this is discussed in

detail Chapter 3). This therefore yields a measure of VO_{2peak} rather than VO_{2max} to define cardiorespiratory fitness. VO_{2peak} is then used throughout this thesis to standardise exercise workloads across participants to allow comparison across the EXAGE groups.

Example VO_{2peak} data for one older trained (OT) participant of the EXAGE group is shown in Figure 6.1. In two of the older untrained (OU) participants VO_{2peak} values could not be collected during heightened COVID-19 restrictions. For these two participants in-scanner workload was calculated using heart rate, which should linearly correlate to VO_{2peak} [17], see Figure 6.5.

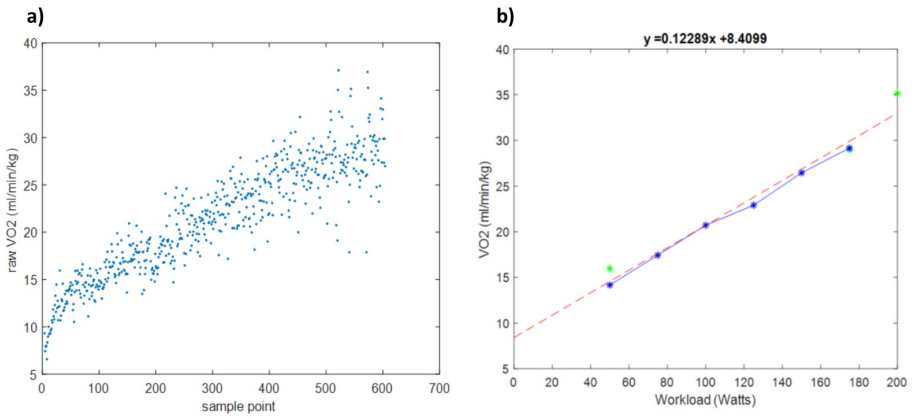

Figure 6.1: Example data from one participant from the OT group showing VO_2/kg data. a) Depicts every sampled data point during the incremental test and b) shows the mean VO_2/kg for the last 30 seconds of each workload. The initial incremental test data points are shown in blue and the confirmation points in green. This participant had a VO_{2peak} of 35 ml/kg/min, giving a 50% workload of 80 W.

6.2.2 Results

Figure 6.2 shows VO_2 values across workload during the supine exercise protocol for each participant separated into young untrained (YU), older trained (OT) and older untrained (OU) groups. The plots clearly suggests that the OU group were not able to reach as high workloads as the OT or

YU groups. The OU group reached a workload no higher than 190 Watts. The heart rate responses of each group across workload can be seen in Figure 6.3.

Figure 6.4a shows the VO_2 peak in the OT, the OU and the YU groups. VO_2 peak was significantly different between groups, f(2,21)=4.16, p=0.032, with a post-hoc Bonferoni corrected test indicating the Older Trained (OT) group had significantly higher VO_{2peak} values than the Older Untrained group (OU), p=0.033. The difference between the OU and Young Untrained (YU) groups did not reach significance (p=0.106), due to the higher variance in the OU and YU groups than the OT group, suggesting that a greater sample size could yield a significant results. Together with the VO_{2peak} p=1 result between the YU and OT groups, this suggests that the OT group resembles the YU group more-so than their age-matched OU peers.

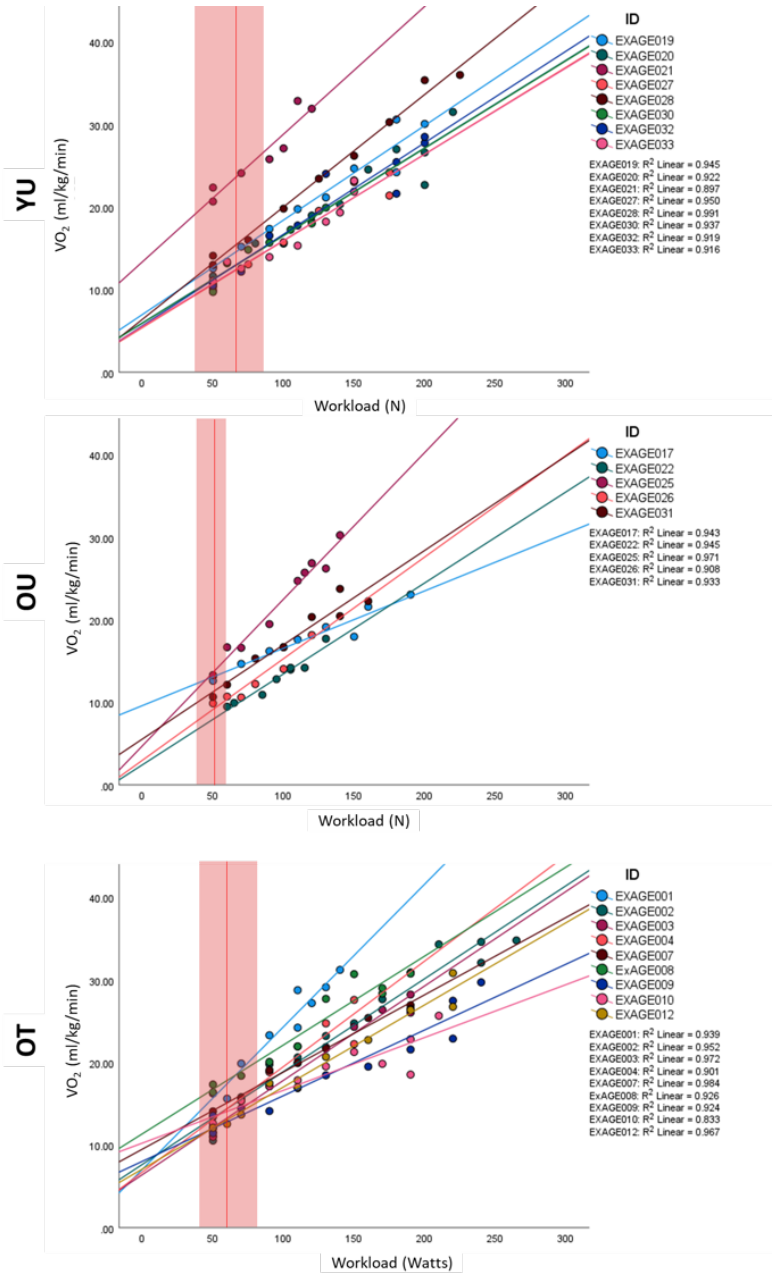

Figure 6.2: VO_2 of each participant across workload shown for the Young Untrained (YU), Older Trained (OT), and Older Untrained (OU) groups. Vertical red line represents the mean workload used in the scanner for each group, and transparent overlay indicates the range.

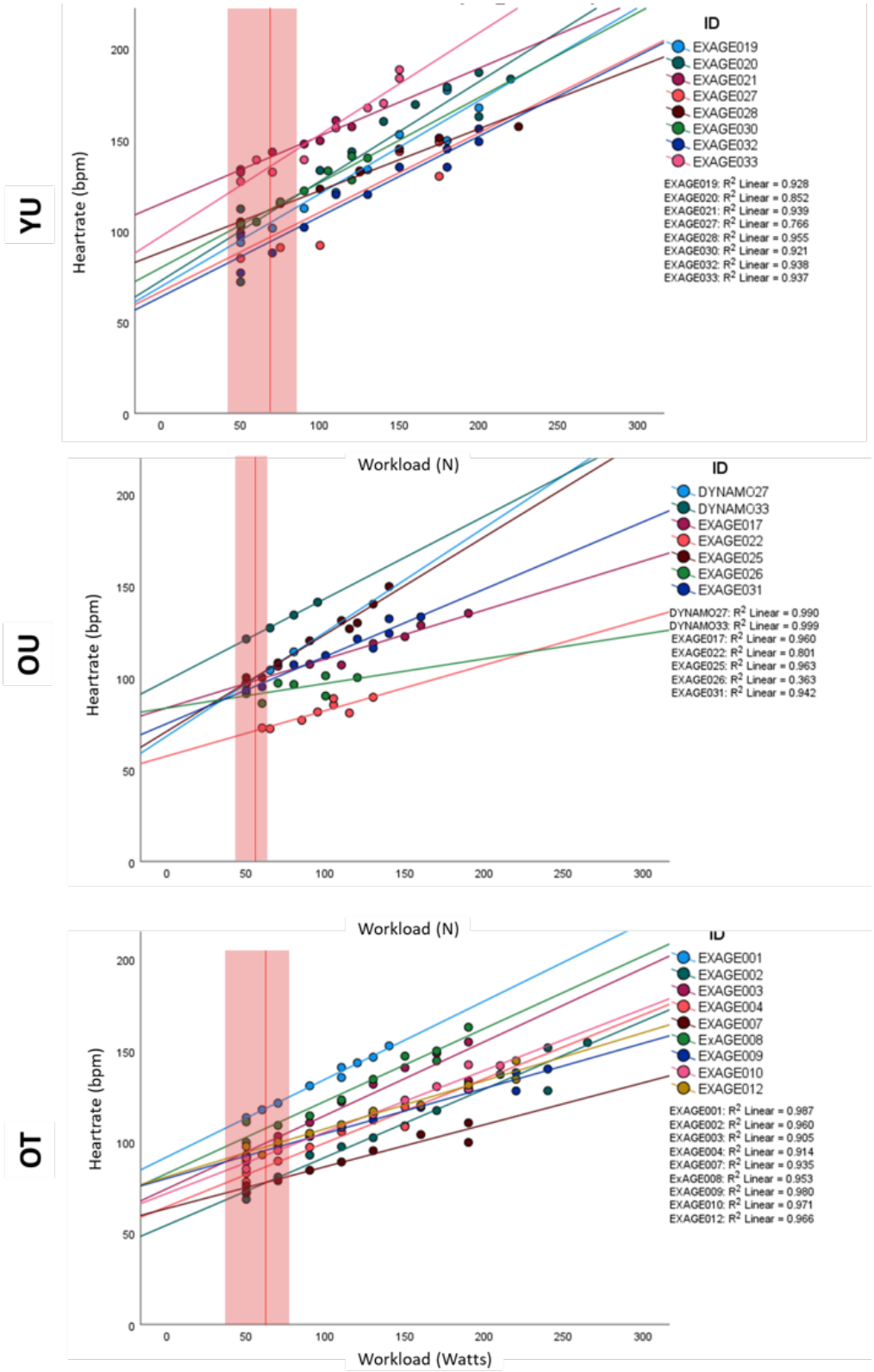

Figure 6.3: Heart rate across workloads for each participant, divided into groups. Vertical red line represents the mean workload used in the scanner for each group, and transparent overlay indicates the range.

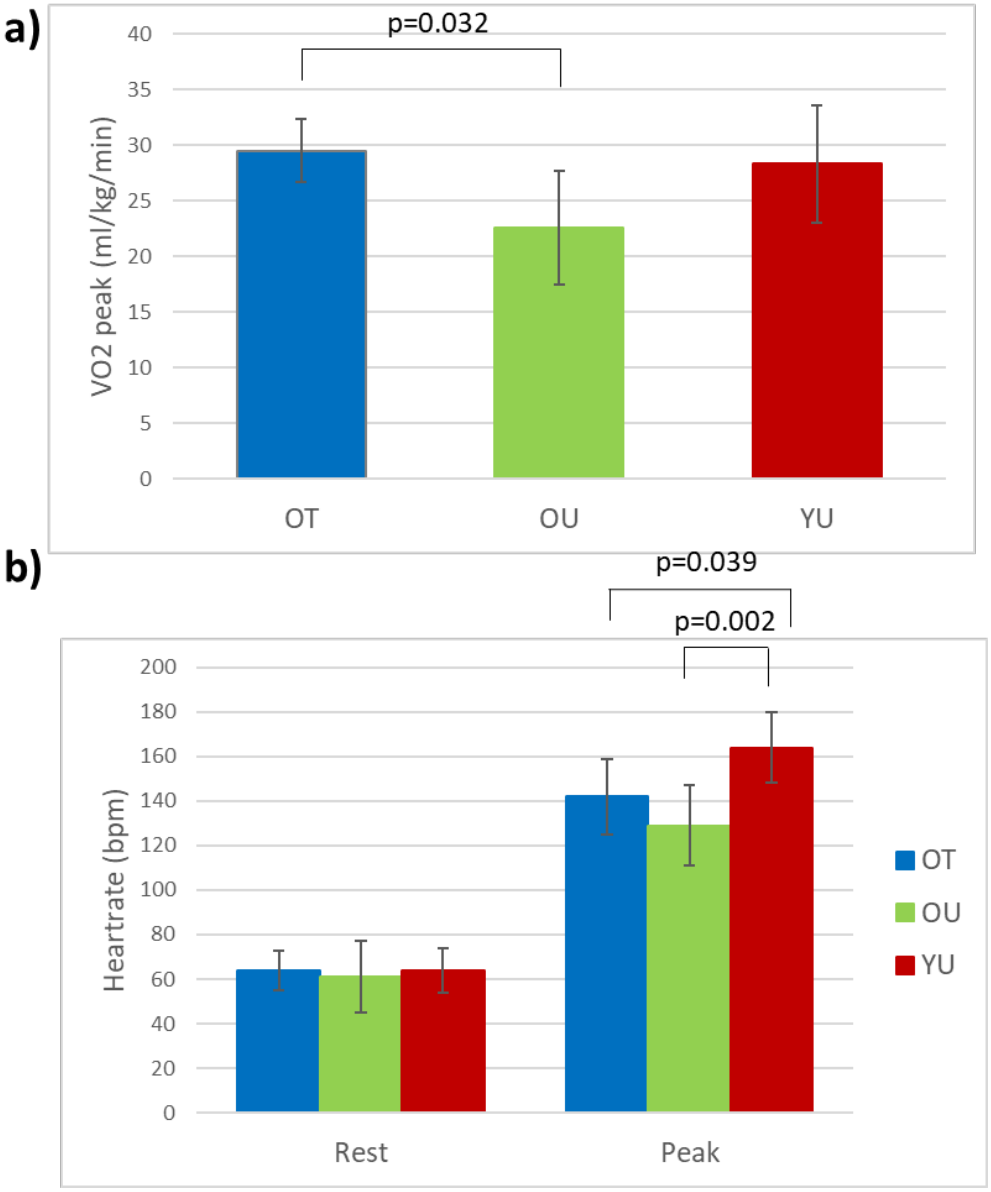

Figure 6.4: Cardiorespiratory fitness across groups. a) VO_2 measured at peak and b) heart rate at rest and at peak in the OT, the OU and the YU groups.

Figure 6.4b shows heart rate at rest and at peak VO_2 peak in the OT, OU and YU groups. There were no significant differences between the groups in heart rate at rest (p=0.866). However, there was a significant difference in peak heart rate between groups on supine exercise, F(2,23)=8.18,p=0.002. The YU group showed higher peak heart rate than both older groups (OU:p=0.002, OT:0.039), but peak heart rate of the older groups did not

differ significantly from each other (p=0.468).

Figure 6.5 shows the relationship between heart rate and VO_2 for the young untrained (YU), older trained (OT) and older untrained group (OU). For each participant the linear regression is plotted and it can be seen that in general R^2 values are > 0.8, with a mean R^2 of 0.91 in the YU, 0.82 in the OU and 0.93 in the OT group. The lower OU R^2 is driven by a single participant (EXAGE026). This data supports the use of heart rate measures in the two OT participants who did not have VO_2 data. While heart rate and VO_2 values are linearly related (see Figure 6.5), peak values were highest in OT for VO_2, but highest in YU for heart rate. The YU group show greater increase in heart rate relative to VO_2.

Figure 6.6 shows the ventilation (VE) versus workload for each participant in each of the groups. The YU group was the only group to have some participants who displayed plateauing of their VO_2 response at higher workloads. The peripheral fatigue induced by the supine exercise likely prevented other participants from reaching this threshold.

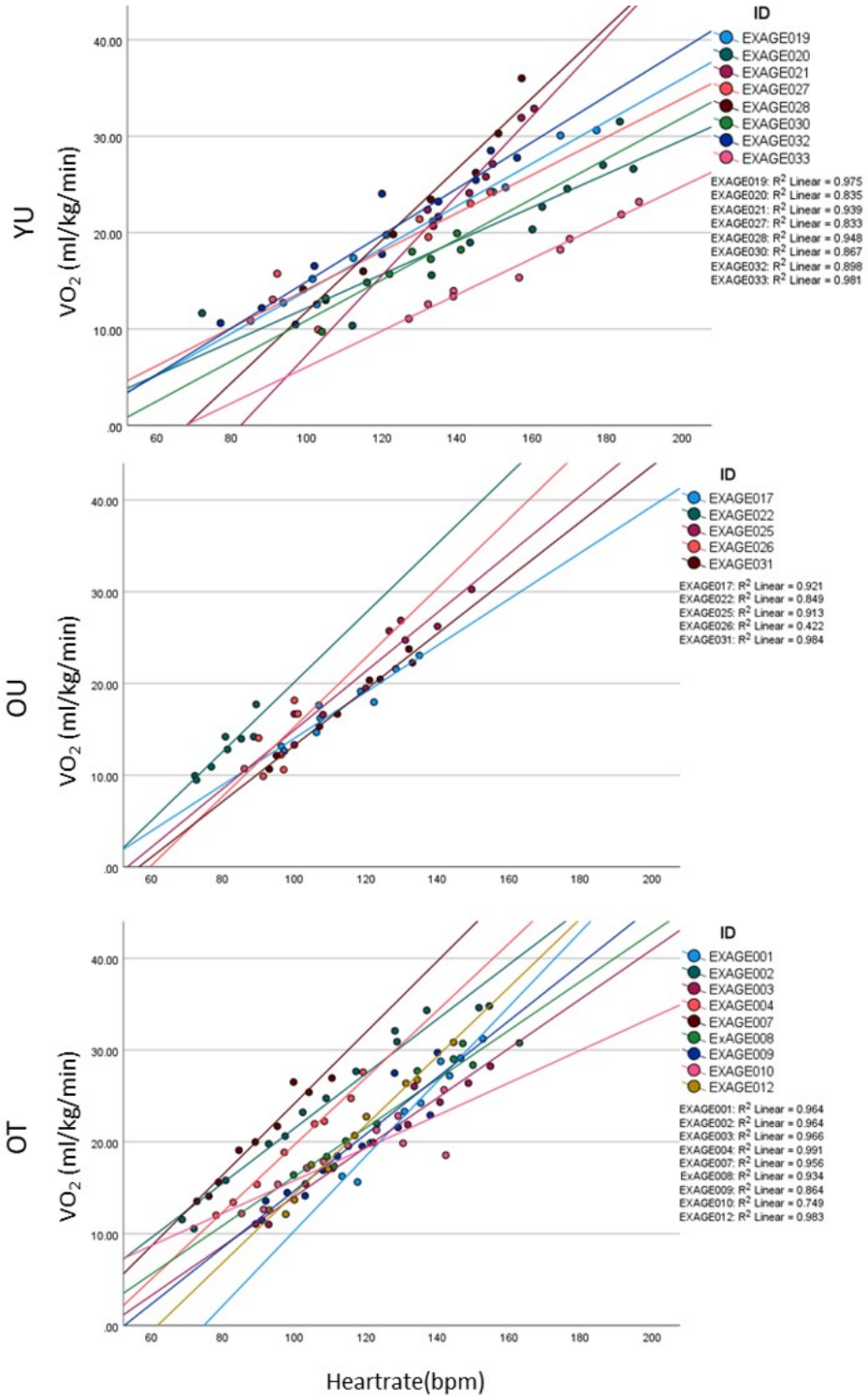

Figure 6.5: Relationship between VO_2 and heart rate during the supine exercise protocol separated by group for the young untrained (YU), the older trained (OT), and the older untrained (OU) groups. For each participant the linear regression and associated R^2 is provided.

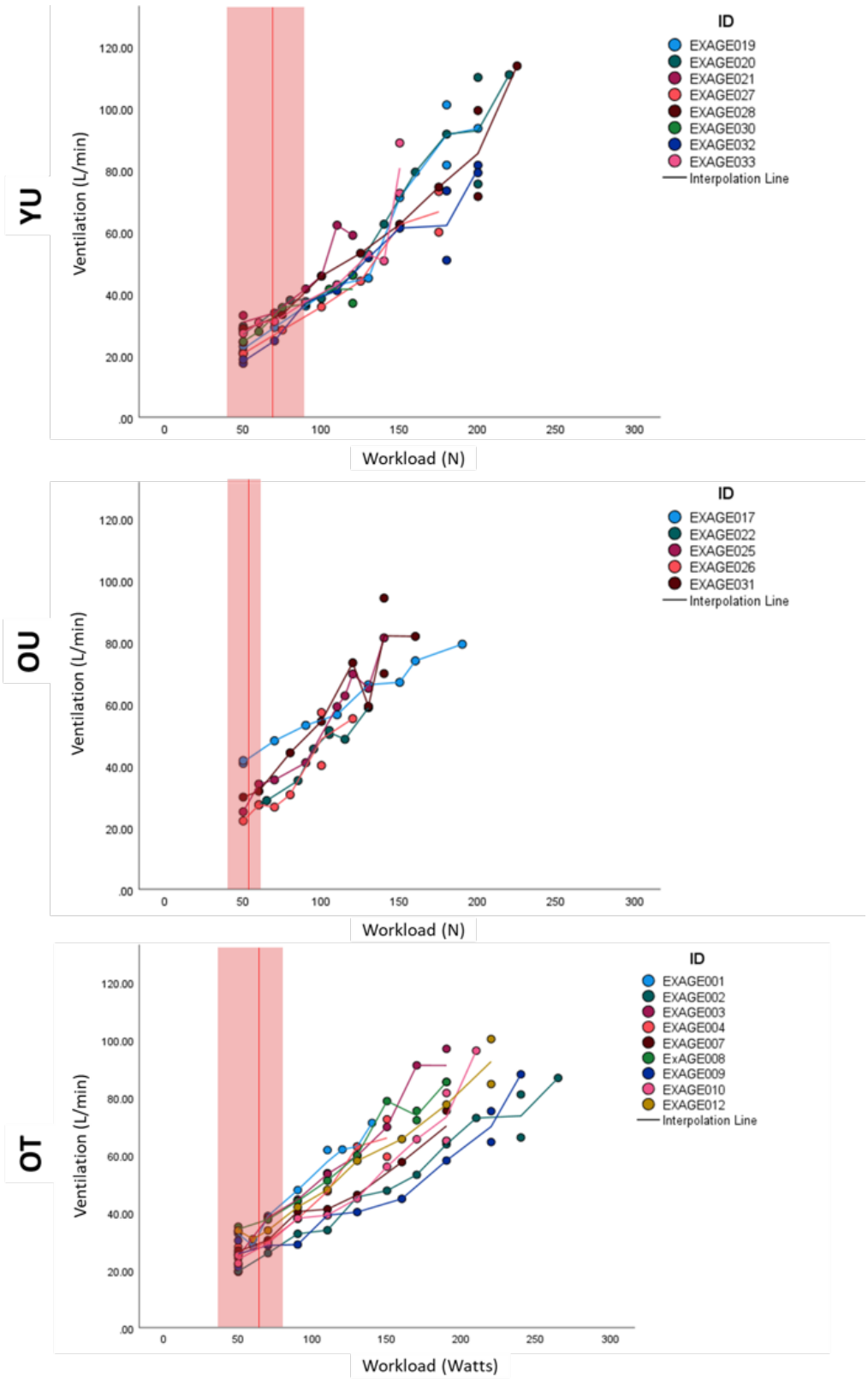

Figure 6.6: Ventilation across workloads shown for each participant in each group. Vertical red line represents the mean workload used in the scanner for each group, and transparent overlay indicates the range.

6.3 Blood gas and lactate measurements during incremental intensity supine exercise

Steady-state venous blood gas measurements (pH, BEecf, PCO_2, HCO_3-, TCO_2, sO_2) and lactate were acquired during the cardiorespiratory protocol collected in the DGHPU at the end of each workload via a retrograde cannula. Cannulas were inserted in the back of the hand into dorsal vein by a medically trained individual, however retrograde cannulas are more difficult to put in place in older individuals. For each participant the cannula was attempted a minimum of two times, but for patient comfort was not repeated more than this and was not successful in all cases. Across the groups, measures of blood gases were collected in n=5 of the YU group, n=8 of the OT group and n=3 of the OU group. The cannula was left in place only for the initial incremental task and not for the confirmation test.

Figure 6.7 shows the results of the blood measures related to metabolic acidosis as indicated by base excess of extracellular fluid (BEecf) values of less than -4 mEq/L. Brain level vasoreactivity occurs when PCO_2 levels change, triggered by respiratory compensated metabolic acidosis. Respiratory compensated metabolic acidosis which is exercise induced metabolic acidosis from blood lactic acid production, which is buffered by bicarbonate (HCO_3-), and instigates a respiratory compensation resulting in increased minute ventilation and thereby increased CO_2 removal. The decrease in PCO_2 with greater exercise workload is seen in Figure 6.8). Critically, it can be seen that at 50% workload, shown by the red bar which corresponds to the level at which participants performed exercise in the scanner, PCO_2 did not show decreases from baseline and there can be expected to

not induce cerebral vessel vasoreactivity. While some participants show decreased PCO_2 at the highest workloads, these changes occur well outside the workloads used when acquiring the MR exercise data.

Oxygen saturation (sO_2) and partial pressure of oxygen (PO_2) did not differ significantly from baseline at the 50% workload, as shown in Figure 6.9. Interestingly, the OT group showed lower PO_2 changes at the higher workloads than the OU and YU groups, with the OT group never reaching higher than 10 kPA.

Figure 6.10 shows lactate concentration, most participants saw large increases at the higher workloads, but only a small increase was seen at the 50% workload, with the YU group showing the largest and fastest increases in lactate. Figure 6.11 shows the relationship between the blood latate concentration and minute ventilation. This can be seen to be largely linear in the YU group which reaches the highest values, but non-linear in the OT group where lactate increases slowly until the higher ventilation points.

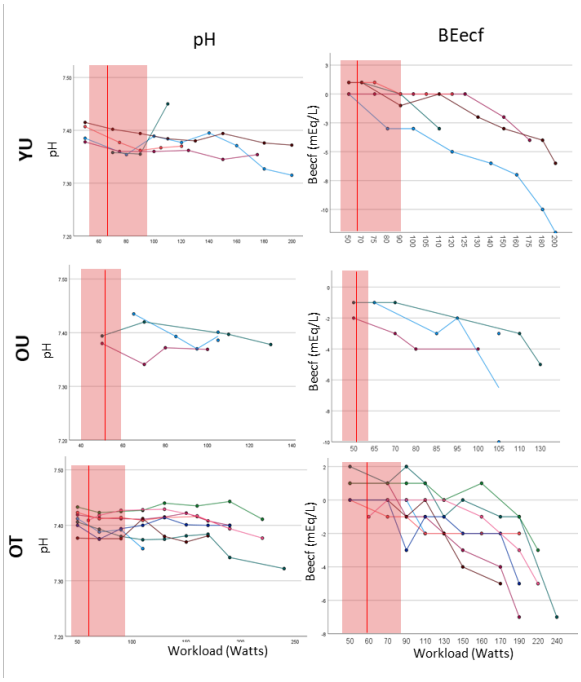

Figure 6.7: pH and BEecf blood gas measurements across workloads for participants in each of the groups. Vertical red line represents the mean 50% workload which is used in the MR scanner for each group. The transparent overlay indicates the range.

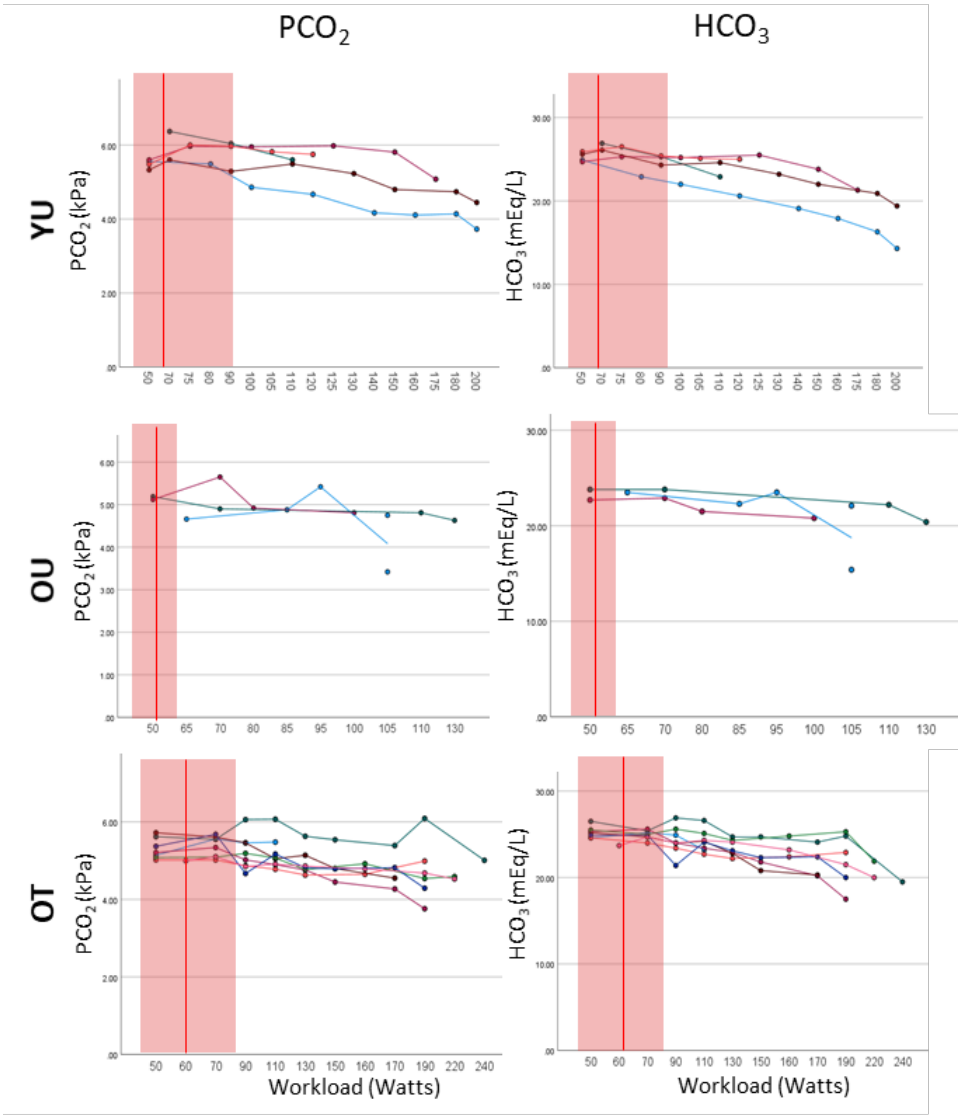

Figure 6.8: Blood gas measurements across workloads for participants in each of the groups for PCO_2 and HCO_3. Vertical red line represents the mean 50% workload which is used in the MR scanner for each group. The transparent overlay indicates the range.

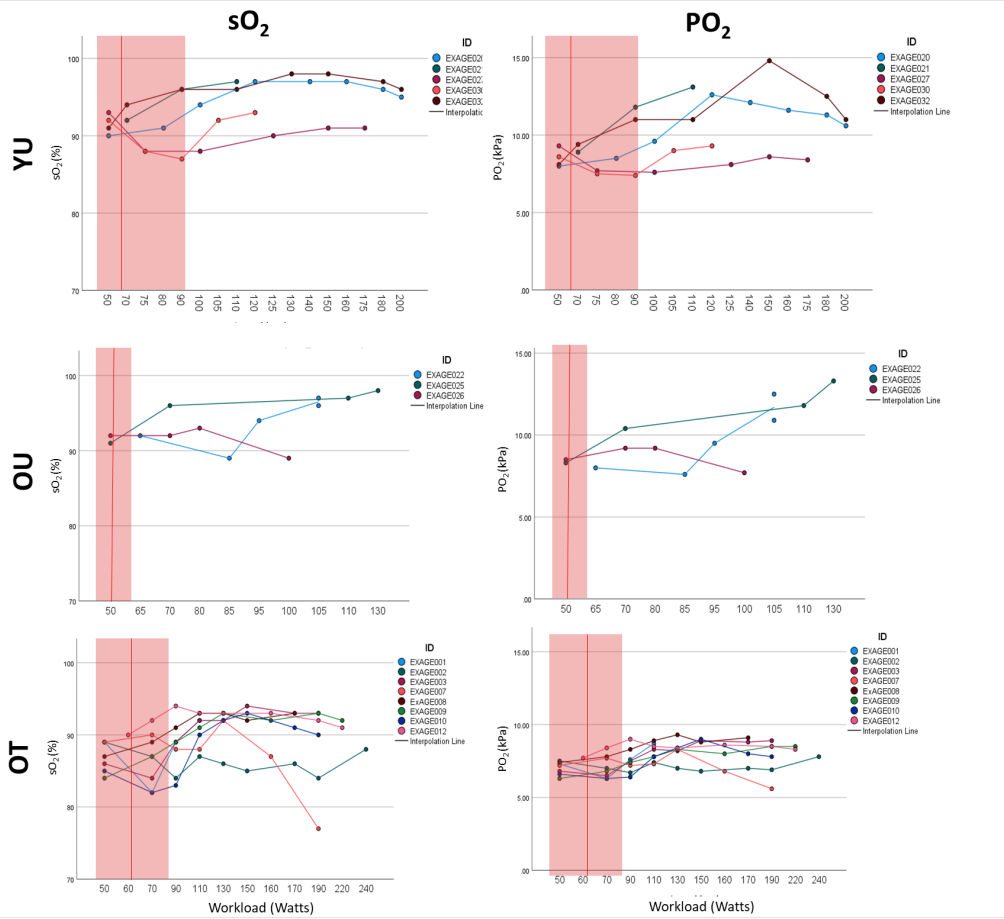

Figure 6.9: Oxygen saturation and partial pressure across workloads for the YU, OT and OU groups. Vertical red line represents the mean workload used in the scanner for each group, and transparent overlay indicates the range.

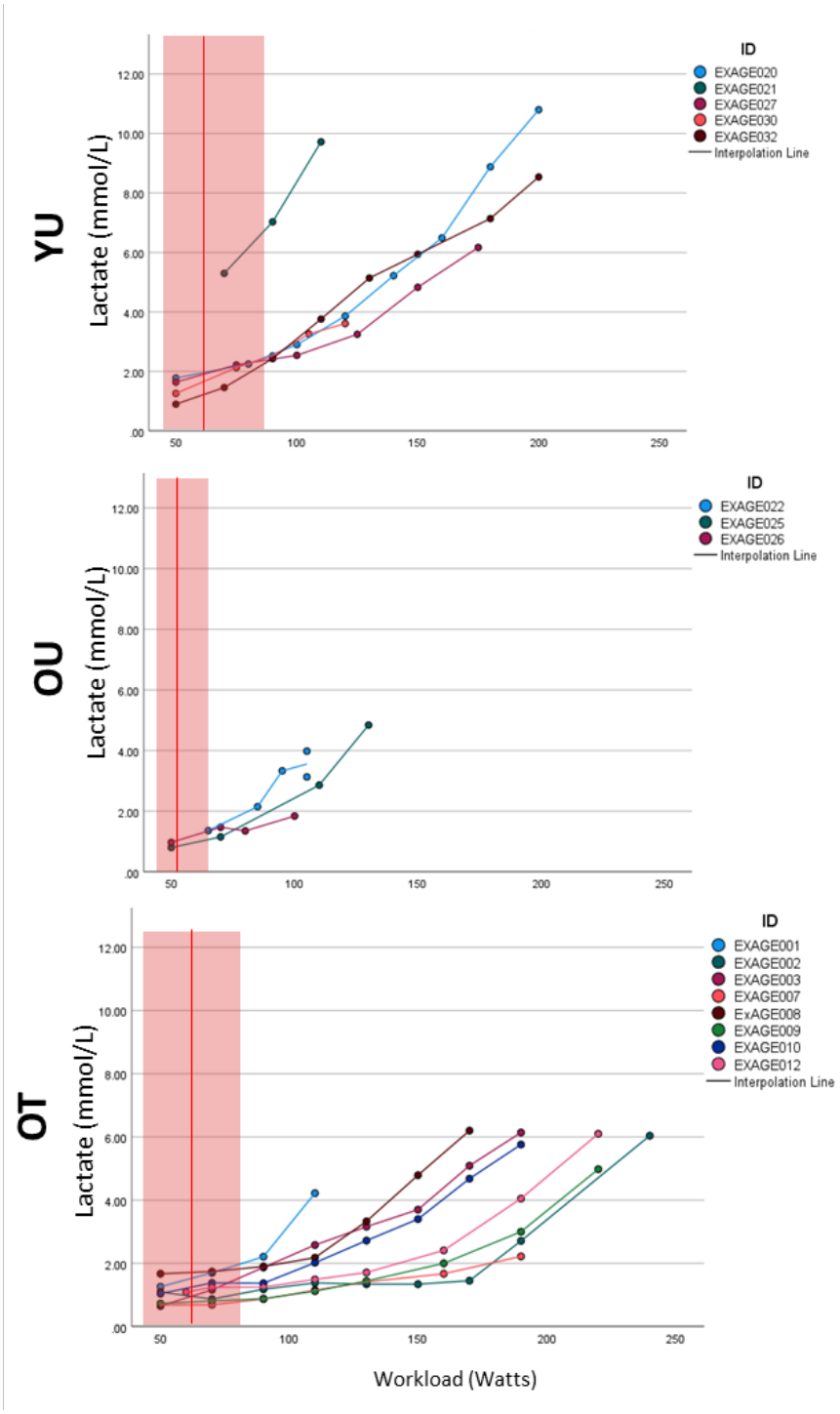

Figure 6.10: Lactate buildup across workloads for the YU, OT and OU groups. Vertical red line represents the mean workload used in the scanner for each group, and transparent overlay indicates the range.

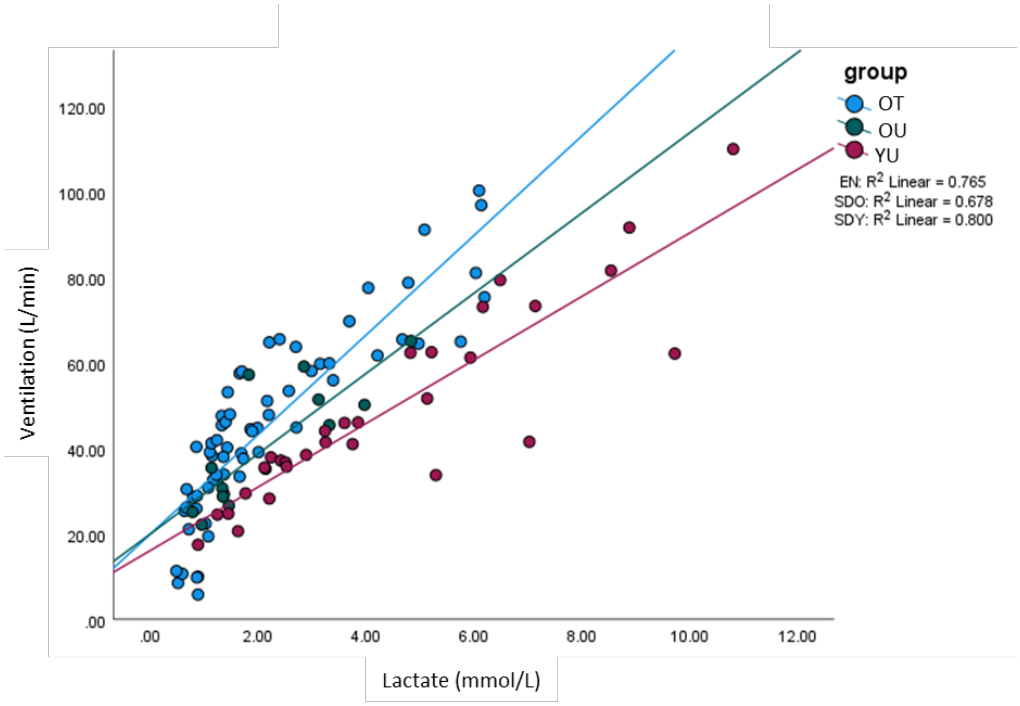

Figure 6.11: Ventilation versus blood lactate for all points collected during VO_2 incremental test for each of the YU, OT and OU groups.

6.4 Cardiac Function during supine submaximal exercise and recovery assessed with MRI

6.4.1 Methods

Cardiac MRI measures were collected in the participants to assess cardiac function at baseline, during moderate supine exercise at a workload of 50% VO_2 peak and in a recovery period. Cardiac MRI measures were acquired using both aortic Phase Contrast MRI, and two chamber (2CH) and four chamber (4CH) long axis cine and short axis cine scans. For full scan acquisition protocol see Chapter 3. Using both of the scans cardiac output can be calculated from the stroke volume multiplied by heart rate, with

cardiac index (CI) computed by correcting cardiac output (CO) for body surface area (BSA).

6.4.1.1 Aortic Flow from Phase Contrast MRI

The aortic Phase Contrast MRI (PC-MRI) scans were taken using a slice placed across the ascending aorta (as shown in Figure 3.21) which was collected across cardiac phases under free breathing. Data was analysed using Philip's Viewforum software, where an ROI was drawn around the aorta in one phase, and this was then propagated to all cardiac phases using an automated contouring function, then checked and edited for accuracy. The output measures from the aortic PC-MRI included stroke distance, stroke volume, velocity, cardiac index, flux, forward and backward flow, regurgitation factor, distensibility, and strain.

Figure 6.12 shows a typical ROI used to assess aortic flow measures over cardiac cycle and an example dataset across the cardiac cycle of a OT participant. This shows the shorter cardiac cycle (higher heart rate) and increased velocity and flow during exercise relative to baseline and recovery.

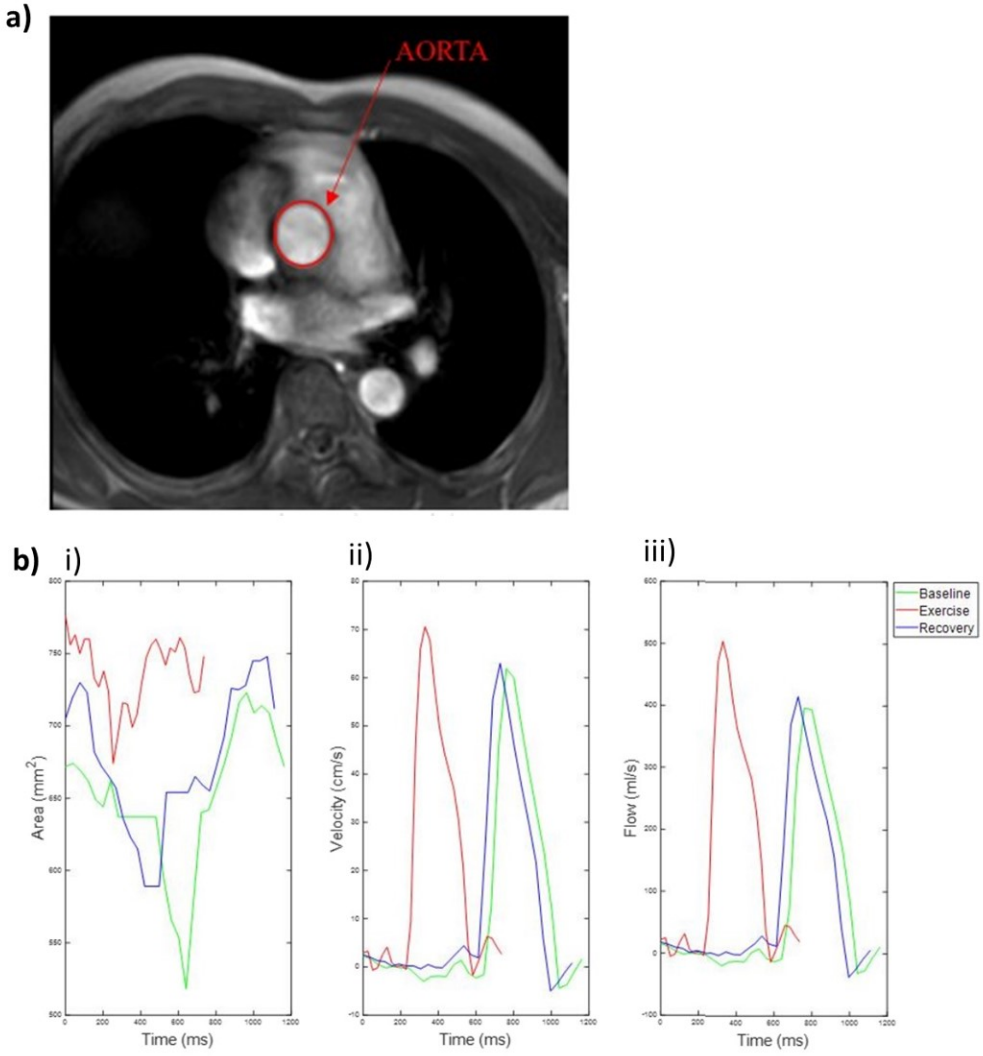

Figure 6.12: a) Example ROI used to determine aortic flow measures and b) examples plots of i) aortic area, ii) velocity and iii) flow an OT dataset at baseline (green), exercise (red) and recovery (blue) across time. On exercise (red) the peak is seen to be shifted due to the shorter cardiac cycle and higher heart rate.

6.4.1.2 Two Chamber (2CH) and four Chamber (4CH) Long Axis Cardiac Cine Measures

Figure 6.13 shows example long axis cine scans collected in a two chamber (2CH) and four chamber (4CH) view of the heart. These were analysed together to yield biplane results using the Cardiovascular Imaging software (CVI, Circle). This software provides automatic drawing of ROIs on the

single slice around the left ventricle and end systole and end diastole, this is then propagated between cardiac phases, and manually inspected and corrected for any ROI irregularities.

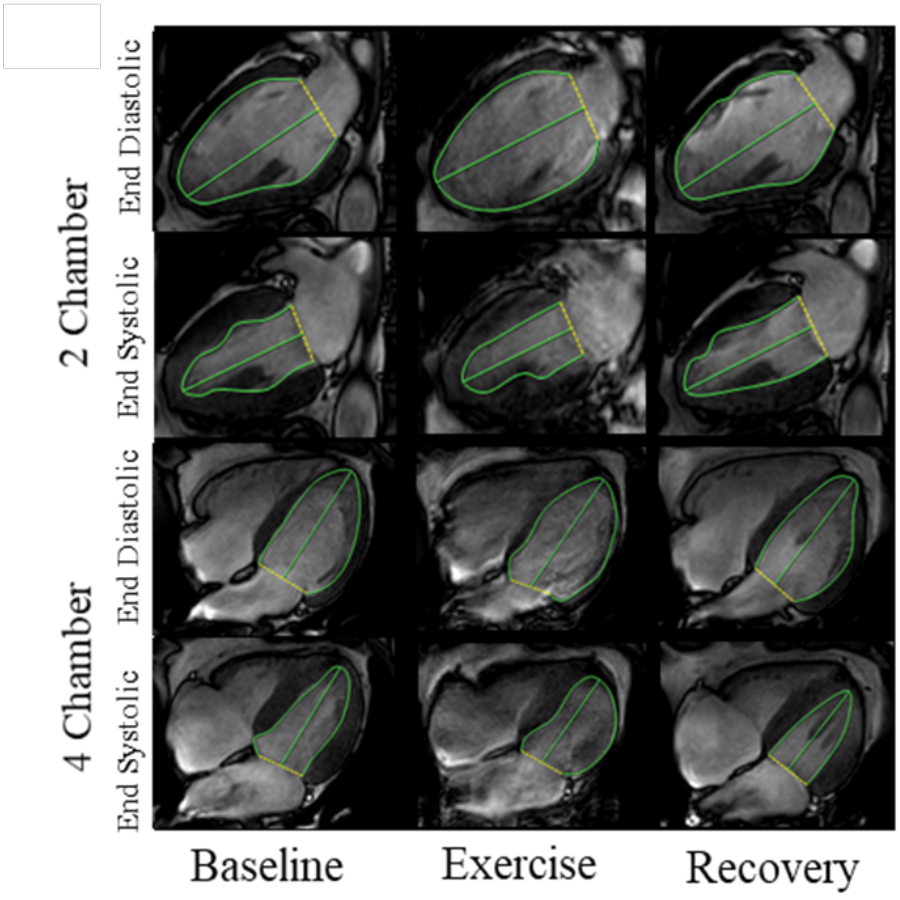

Figure 6.13: Two and four chamber long axis cardiac cine at end systole and end diastole at rest, during supine exercise, and in recovery.

The long axis scans collected of the left ventricle allows the examination of stroke volume (SV), ejection fraction (EF), end diastole volume (EDV), end systole volume (ESV), cardiac output (CO) and cardiac index (CI), which is CO corrected for BSA.

6.4.1.3 Short Axis Cardiac Measures and Strain

Figure 6.14 shows an example of a short axis (SA) scan taken across the left ventricle of the heart at rest. To collect full coverage of the heart this requires 6 breath holds. This scan time and number of breath holds to acquire this data made it unfeasible to collect during exercise. These SA scans were also analysed in CVI Circle to estimate end systolic volume, end diastolic volume, stroke volume, ejection fraction, cardiac output, and cardiac index, as measured using the long axis scans. In addition, the short axis scan also provides measures of left ventricular myocardium mass, global circumferential strain and global longitudinal strain. Automatic drawing of ROIs around the epicardium and endocardium at end systole and end diastole across on each slice, encompassing the whole heart was performed as shown by the contours in Figure 6.14.

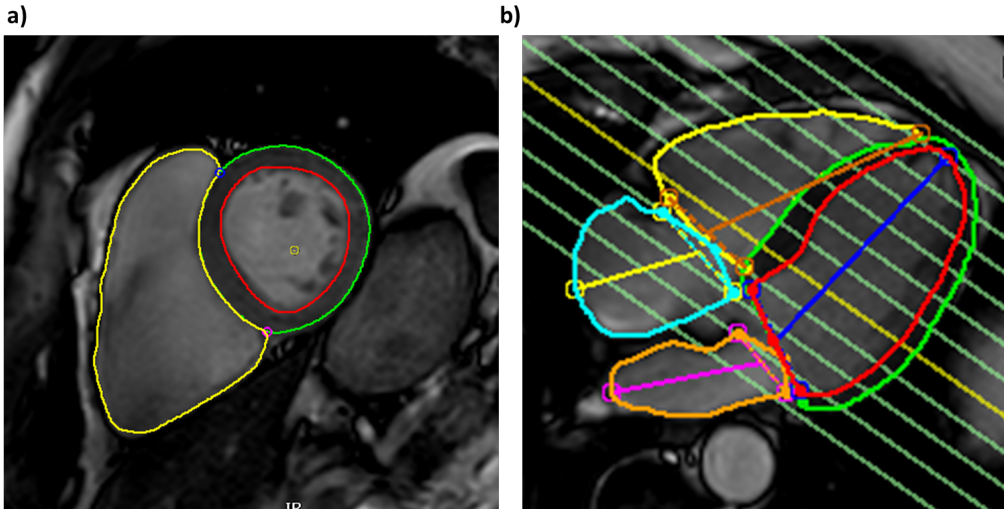

Figure 6.14: a) Example Short Axis cine slice with eipcardium and endocardium contours drawn in the left ventricle and b) Four chamber long axis cine showing positioning of the short axis slices. Contours are taken from CVI Circle software.

6.4.2 Results

6.4.2.1 Aortic Flow from Phase Contrast MRI

Figure 6.15 shows the results of aortic Phase Contrast. Aortic stroke volume (Figure 6.15a) did not differ significantly between groups at baseline, $F(2,23)=2.143$, $p=0.142$, but differences were evident on exercise; stroke volume did not change in the YU group, which was significantly different to the increase observed in the OT ($p=0.016$) and OU ($p=0.004$) groups. The lack of increase in stroke volume during exercise in the YU is compensated by a greater increase in heart rate ($F(2,18)=6.074$, $p=0.009$, Bonferroni-corrected post-hoc, YU>OT, $p=.008$; Figure 6.15b). There was no significant difference between groups or conditions at recovery.

Figure 6.15c shows the aortic cardiac index (CI). Baseline differences were significant ($F(2,23)=5.952$,$p=0.009$), with greater CI in the YU than the OU ($p=0.008$) but not the OT ($p=0.266$). An increase in cardiac index was shown for all groups on supine exercise, but no difference in response to exercise across groups, as expected and indicating they are achieving equivalent stress levels as dictated by using their VO_2peak workload. While cardiac index during exercise did not differ, the mechanism used to increase cardiac index with exercise changes with age. The older groups exhibited lower increases in heart rate than the YU, which were paralleled by greater increases in stroke volume, as can be seen in Figure 6.15d.

Figure 6.16 shows aortic velocity, flux and stroke distance at baseline, during supine exercise at 50% workload, and on recovery. The YU group had a higher aortic velocity (Figure 6.16a) in all conditions ($F(2,65)=35.928)<0.001$), and a greater absolute increase in velocity from baseline to exercise than the older groups ($p=0.03$). Velocities returned to baseline levels in the re-

covery phase. Aortic flux (Figure 6.16b) increased for all groups on supine exercise ($F(1,43)=89.424$, $p<0.001$) but did not show any significant differences between the groups, again indicating equivalent exercise induced cardiac stress levels between participants. The young group had higher stroke distances than the older groups in all three conditions ($F(2,65) = 60.099$, $p<0.001$), but no group had changes in stroke distance were detected during exercise compared to baseline or recovery (Figure 6.16c).

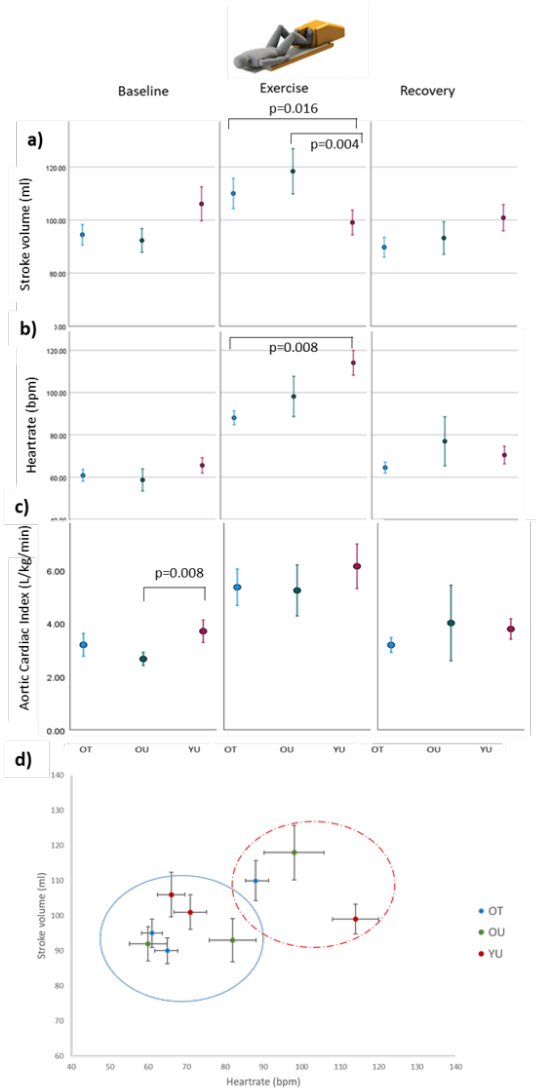

Figure 6.15: a) Aortic Stroke Volume, b) Heart rate and c) Cardiac Index of each of the OT, OU and YU groups and d) Mean heart rate and mean aortic stroke volume for OT, OU and YU groups. Baseline and recovery are circled in blue and the red dashed circle indicates the exercise condition.

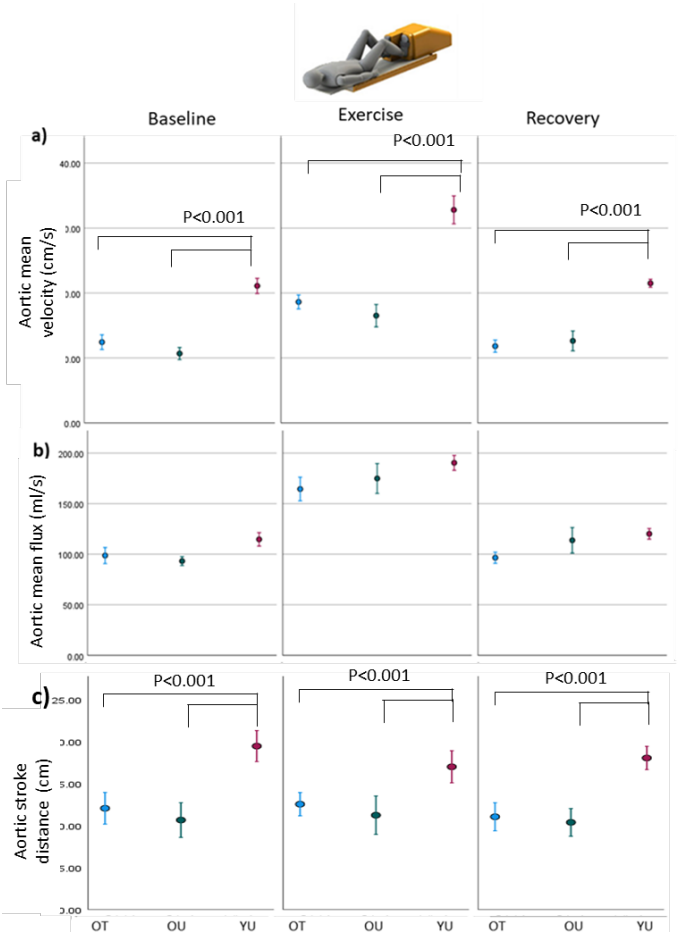

Figure 6.16: a) Aortic Velocity, b) Aortic Flux, and c) Stroke Distance of the OT, OU and YT groups

While aortic forward flow was largely consistent, backward flow was significantly lower in the YU compared to the OU and OT ($F(2,67)=9.09, p<0.001$, post-hoc OU:$p<0.001$, OT:$p=0.008$), driven by baseline and recovery levels, shown in Figure 6.17. It was hypothesised this could be due to increased stiffening with age, however, aortic distensibility, as measured by the change in aortic area divided by maximum aortic area, did not reveal any differences.

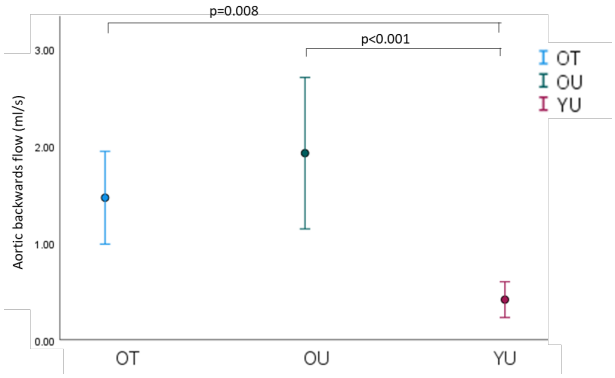

Figure 6.17: Aortic backwards flow meaned across conditions for the OT, OU and YU groups.

6.4.2.2 Two Chamber (2CH) and four Chamber (4CH) Cardiac Cine Measures

Here results of 2CH and 4CH cine are shown which can be compared with the aortic PC-MRI. The longer acquisition time and need for a single breathhold make the two and four chamber cardiac images more difficult to obtain during exercise, and some data had to be excluded (Baseline, OT:n=9, OU:n=6, YU:n=7, Exercise, OT:n=9, OU:n=3, YU:n=7, Recovery, OT:n=9, OU:n=4, YU:n=7), significantly impacting the ability to interpret these results, as in the OU group, only three participants' data was usable in the exercise condition. Results in this section therefore primarily detail differences in the YU. End Diastole Volume (EDV) (Figure 6.18b) and Stroke volume (Figure 6.18d) were not significantly different between the groups or conditions. However, there was an effect of exercise on End systole Volume (ESV) in the YU group (Figure 6.18c). The YU group had a significant decrease in ESV during exercise compared to baseline, $F(2,21) = 5.28$, $p=0.016$, Bonferoni-corrected post-hoc $p=0.013$. This may be in part driven by higher ESV at baseline, though this had high variance in the YU group and therefore it was not significantly higher in YU than OT or OU. There was no significant difference in ejection fraction (EF) between

groups at baseline. Only the YU group had a significant increase in EF on exercise relative to baseline, $F(2,21) = 4.74$, $p=0.022$, Bonferoni-corrected post-hoc $p=0.021$, though the OU group cannot be interpreted due to low N (Figure 6.18e). All groups increase cardiac index during exercise, but there were no significant differences between groups (Figure 6.18f).

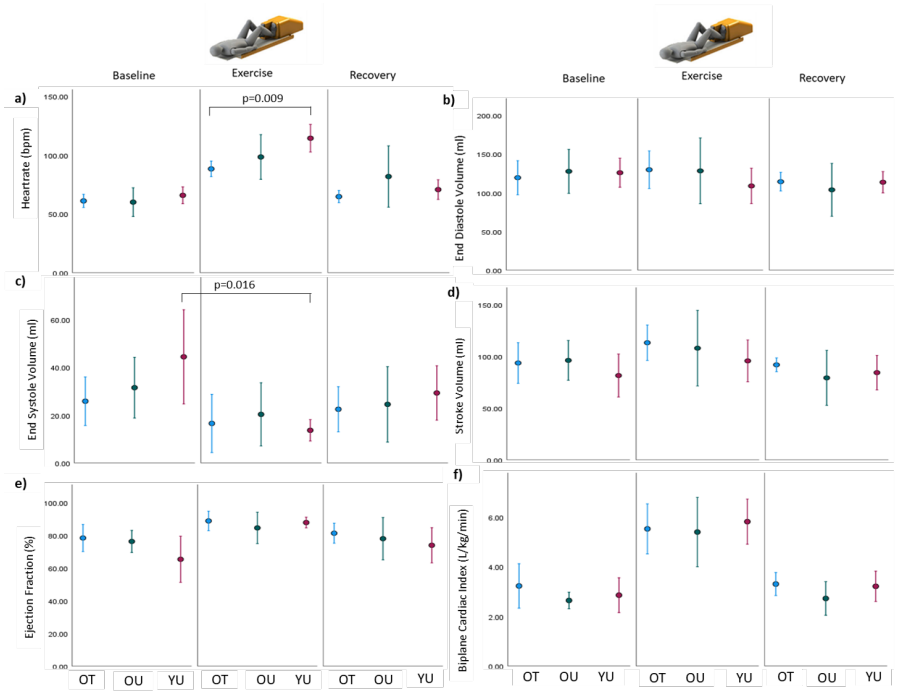

Figure 6.18: Long Axis a) heart rate b) End Diastole Volume (EDV), c) End Systole Volume (ESV), d) Stroke Volume (SV), e) Ejection Fraction (EF) and f) Cardiac Index (CI) for each of the OT, OU and YU groups.

Figure 6.19 shows cardiac index as measured by biplane cardiac index taken from the 2CH and 4CH long axis cines compared to the aortic phase contrast MRI scan. The correlation between the two measures is present but not robust, at $R^2=0.544$,$p<.001$. Greater variation occurred during exercise, as might be expected, with motion effecting quality of the 2CH and 4CH images. However, the biplane images also yielded lower cardiac index values for some participants at rest and recovery. Due to the effects of motion aortic cardiac index is thought to be the more reliable measure.

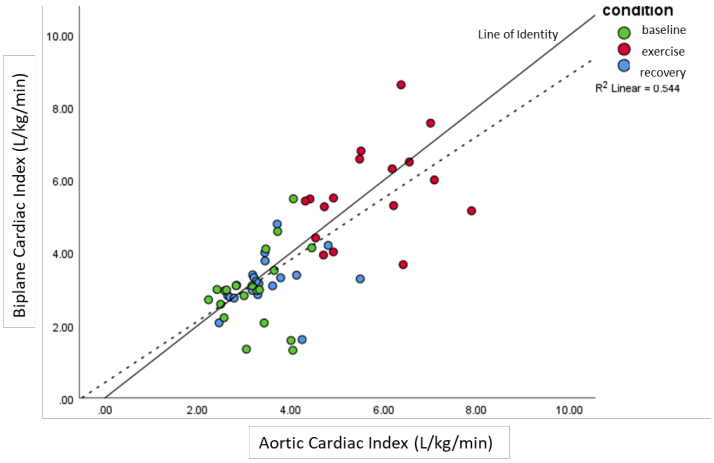

Figure 6.19: Cardiac Index measured from the phase contrast on the aorta and the biplane measures from two and four chamber scans.

6.4.2.3 Short Axis Cardiac Measures and Strain at Baseline

Left ventricle myocardium mass (LV mass) was measured at baseline using the short axis scans, no difference in LV mass was found between EXAGE groups, as shown in Figure 6.20. Similar results were found for long axis LV mass measures.

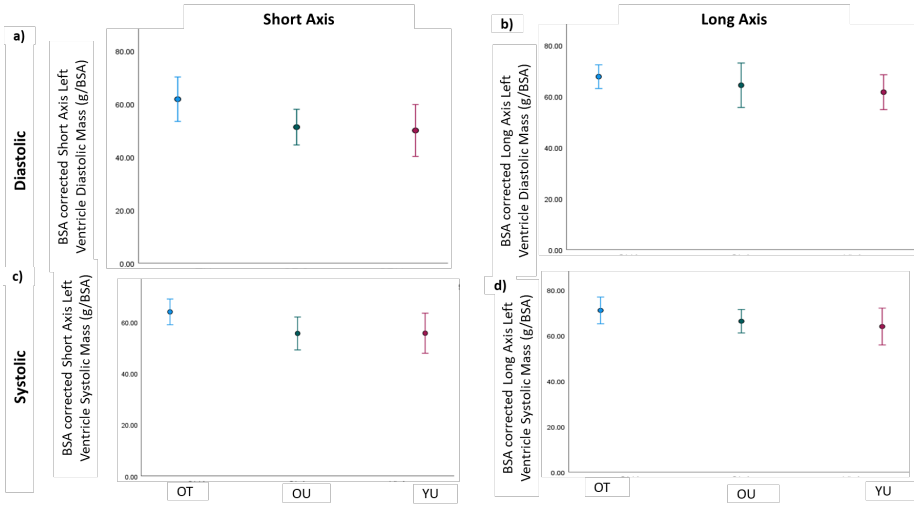

Figure 6.20: Left ventricular mass (LV mass) measured at diastole (a,b) and systole (c,d) in both the short (a,c) and long (b,d) axis cine data. No significant differences were seen across groups.

Short axis baseline measures of end diastolic volume, end systolic volume,

stroke volume, ejection fraction, and cardiac index showed no significant differences between groups at baseline (Figure 6.21.

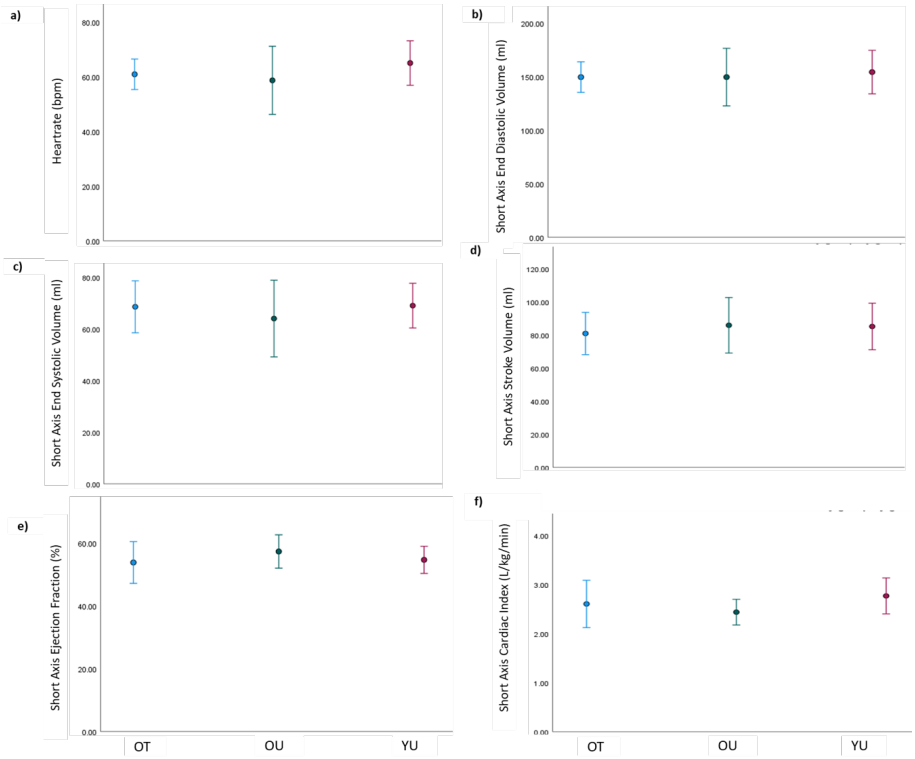

Figure 6.21: Short Axis left ventricular a) heart rate, b) end diastolic volume (EDV), c) end systolic volume (ESV), d) stroke volume (SV), e) ejection fraction (EF), and f) cardiac index (CI) for older trained (OT), older untrained (OU) and younger untrained (YU) groups.

There was no difference in global circumferential or global longitudinal strain between groups as measured from the short axis cine scans (Figure 6.22), in agreement with the strain as measured from the aortic PC-MRI.

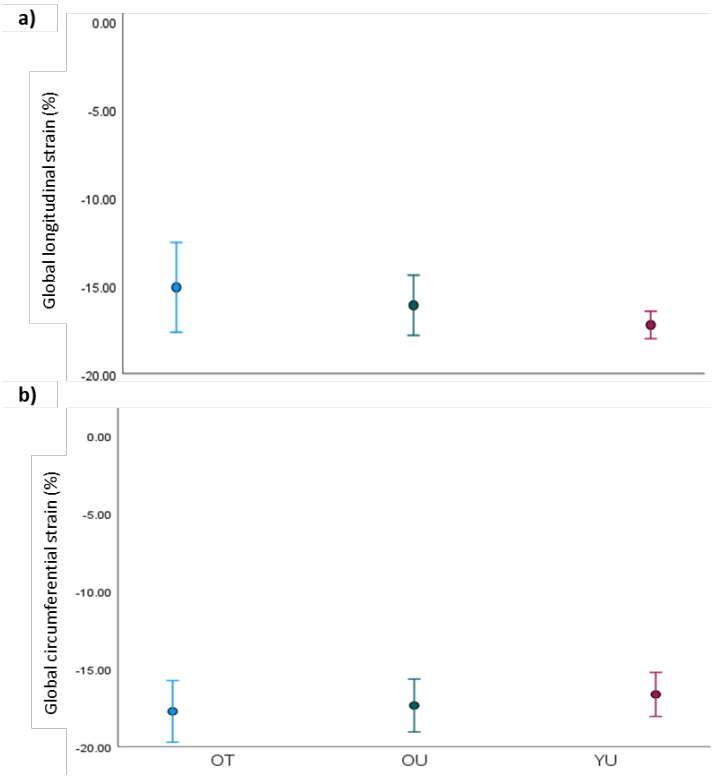

Figure 6.22: a) Global longitudinal strain, b) global circumferential strain measured at baseline across the OT, OU and YU groups.

6.5 Discussion

This chapter studied the impact of lifelong exercise and age on the cardiovascular responses to acute submaximal exercise and recovery in healthy participants. When exercising to exhaustion, the older trained group had a cardiorespiratory response more similar to that of the younger untrained group than the older untrained group, as reflected by the higher VO_2peak value. Although greater sample sizes are needed, this suggests that participants who have a high exercise lifestyle maintain cardiovascular fitness levels which otherwise deteriorates with ageing, as found in other studies [7, 6].

Lower resting cardiorespiratory fitness is often associated with higher phys-

ical fitness levels [18]. In this study, we did not see any significant differences in heart rate at rest between the groups, however, training regimes in older participants have failed to decrease resting cardiac measures despite improving maximum exercise induced cardiac output in at least one study [19]. There was a significant difference in peak heart rate on supine exercise between the groups, with the YU group showing a higher peak heart rate than both the OT and OU groups. This data aligns with the 30% reduction in peak exercise heart rate between 20 and 85 years of age found in the Baltimore Longitudinal Study of Aging [20]. This was seen both in peak measures collected in the DGHPU (6.4) and in 50% of VO_2 from the cardiac MRI session (Figure 6.15. At 50% of VO_2 the older untrained had higher heart rates than the older trained. This differed from the peak heart rate, where training appears to increase the maximum heart rate reached. Instead, the OT have the lowest heart rate response to the workload at 50% of VO_2. Importantly, the YU group show greater increase in heart rate per unit increase of VO_2, which is reflected in the greater increase in heart rate seen at 50% VO_2 in the MR scanner. The OU and OT supplement their slower increases in heart rate with increased stroke volume to maintain the same cardiac output needed with increasing VO_2 and exercise workloads.

The ventilation rates of workloads used for the MRI exercise task did not exceed 40 L/min or drop below 15 L/min, this is within the range expected for light to moderate exercise (15 - 50 L/min) [21]. Some participants did reach hyperventilation and hypocapnia (defined as less than 4.67 kPa of PCO_2) during the end workloads on the VO_2 peak test collected at the DGHPU, but all participants had PCO_2 values above this in the MRI exercise workload ranges. Respiratory alkalosis indicated by a pH greater than 7.45 did not occur in any of the participants, even at peak workloads. While metabolic acidosis (indicated by a BEecf of less than -4 mEq/L) did

occur at the highest workloads, importantly this range was much higher than those used in the MRI exercise task. CO_2 measures (PCO_2, TCO_2) showed decreases at maximal exercise in the VO_2 exercise test, but remained stable in the workload range used in the MRI exercise task.

There were increases in blood lactate accumulation with increasing workload in all participants, but the inflection points at which the rate of blood lactate accumulation increased occurred well outside the range used for the MRI exercise task, with the increases in blood lactate during the MRI task expected to be small. The OT group shows a slower accumulation of blood lactate than the YU, as would be expected as a result of lifelong endurance training [22].

At baseline, aortic cardiac measures were greater in the YU than older untrained and trained in stroke distance, stroke volume and stroke velocity, but greater than only the older untrained in cardiac index (CI). The OU and OT had greater aortic backflow than YU at rest, but this was not explained by aortic stiffening as aortic distensibility was not different. This suggests that age-related backflow in healthy participants is instead driven by peripheral vascular resistance preventing onward blood flow. Further analysis could be done on this by investigating blood pressure differences.

During supine exercise, the YU saw a decrease in ESV. There were no significant differences in MRI measures of cardiac function between the older trained and untrained groups, but the younger untrained group had a lower stroke volume driven by higher heart rate and ejection fraction. Beaudry et al. conducted a study using a very similar protocol using VO_2 testing and cardiac imaging using the Ergospect Cardio-Step in healthy young adults [23]. They collected 2CH and 4CH long axis cardiac images similar to the ones used in this thesis, and increases in heart rate and

cardiac index during exercise reflect this thesis' results, with only a modest stroke volume increase, exhibited in the lack of significant difference in this study's long axis stroke volume measurement. In measures where the YU group saw exercise induced differences while the OT and OU did not, results follow a similar pattern to the Beaudry et al.'s, the YU exhibiting the same decrease in End Systole Volume and increase in ejection fraction during exercise, although OU results do not have sufficient quality samples to be interpretable.

This increase in stroke volume to compensate for lower heart rates is key to understanding the ageing response to exercise. It was seen previously in a study by Rodeheffer et al as a part of the Baltimore Longitudinal Study of Aging [24], where no changes in function were found between age groups at rest, but during an upright cycling task blood pool scans collected with a collimator detected an increase in age-related stroke volume and decrease in heart rate. These were driven by a greater increase in EDV in the older group and an association of decreased heart rate with increased filling time. It is suggested that some factors in the ageing act to compromise the ejection of blood. Other studies also found an older group to have greater stroke volume with lower heart rate at peak exercise [25], older participants had reduced cardiac output and stroke volume under resting conditions in another study [2], although another exercise study in older males found no increases in stroke volume with lowered heart rate [26]. This thesis expands on these results using update MR capabilities that provide more analysis possibilities, and has the additional advantage of VO_2 data ensuring equal exercise stress on each participant.

This ability to increase or maintain stroke volume during exercise is a result of the age associated cardiac changes in end diastolic volume through the Frank Starling law [20]. The Frank-Starling law states that the stroke

volume of the heart increases in response to an increase in end diastolic volume. In this thesis, differences in stroke volume were only seen in the aortic measures, and so these differences in end diastolic volume measured by 2CH and 4CH scanning were not seen, as would be expected when no stroke differences were found in the 2CH and 4CH scans.

A cross-sectional training study on young and old groups using radionuclide ventriculography found, before training, that the old group had a lesser increase in heart rate, a greater increase in mean blood pressure, lesser increases in ejection fraction and peak ejection rate, a greater increase in end-diastolic volume index, a lesser fall in end-systolic volume index, and a lesser increase in cardiac index, but unlike other studies found no difference in stroke volume response to exercise in ageing [27]. After 6 months of exercise training, reduced heartrate and increased stroke volumes were found in all groups at rest, with a higher cardiac index response to exercise driven by stroke volume with no change in heartrate response from pre-training levels. Another study using radionuclide ventriculography compared endurance trained older men and age-matched untrained men. Larger peak cardiac index was found in the endurance trained group, mediated entirely by greater stroke volume and no difference in peak heart rate. The greater stroke volume in the endurance trained groups was achieved through larger end-diastolic volume and higher ejection fraction [28].

In this chapter, cardiac MRI measures on exercise were assessed using both PC-MRI and long axis cine measures. An increase in cardiac output, as measured by aortic flux, was shown for all groups on supine exercise, but age impacted this mechanism. The older groups exhibited lower increases in heart rate which was paralleled by greater increases in stroke volume. While the long axis (LA) scans are a more direct measure of cardiac output, showing the change in size and blood pool of the heart, the aortic PC-

MRI proved to be more reliable at higher heart rates, likely as PC-MRI is collected freebreathing whilst long axis cine scans are each collected on a breathhold.

In agreement to our work, cardiac output differences at rest were not found in a larger study comparing older active and sedentary participants [29]. Their study had a lower threshold for defining physically active, which included a daily brisk walk of 30 minutes. Both their study and this thesis's study may suffer from groups that are not sufficiently divergent in physical activity. In the future work, the study could benefit from a further cohort that is truly sedentary and only takes part in the non-exercise parts of the study, allowing for greater baseline comparison.

Other considerations include the inherent restrictions of the design of VO_2 peak tasks, which may be effected in terms of reliability by variations in familiarity, motivation and tolerance of discomfort [30], making it difficult to assess if self-determined exhaustion has been reached. The confirmation test goes some way to mitigate this in establishing consistency between rounds, but cannot account for participant reluctance to continue if uncomfortable.

In conclusion, while greater sample sizes and further cohorts are needed to provide further insight, initial results show age related decreases in heart rates at peak. Cardiac output during supine MR exercise is equal between groups, as expected by using their 50% VO_2 peak workload, but the mechanism used to increase cardiac output from baseline differs. The younger group rely on large heartrate increases while the older groups increase both stroke volume and heart rate. There is some evidence of improved cardiovascular function in the VO_2 data of the older trained compared to the untrained. The older trained have a slower lactate accumulation than even

the young. Blood gas data confirm that the MRI exercise task occurred in a range that should not induce hypocapnia, respiratory alkalosis or metabolic acidosis.

References

[1] Taryn Davidson, Baruch Vainshelboim, Peter Kokkinos, Jonathan Myers, and Robert Ross. Cardiorespiratory fitness versus physical activity as predictors of all-cause mortality in men. *American heart journal*, 196:156–162, 2018.

[2] Takeshi Ogawa, Robert J Spina, WH Martin 3rd, Wendy M Kohrt, Kenneth B Schechtman, John O Holloszy, and Ali A Ehsani. Effects of aging, sex, and physical training on cardiovascular responses to exercise. *Circulation*, 86(2):494–503, 1992.

[3] Robert Ross, Steven N Blair, Ross Arena, Timothy S Church, Jean-Pierre Després, Barry A Franklin, William L Haskell, Leonard A Kaminsky, Benjamin D Levine, Carl J Lavie, et al. Importance of assessing cardiorespiratory fitness in clinical practice: a case for fitness as a clinical vital sign: a scientific statement from the american heart association. *Circulation*, 134(24):e653–e699, 2016.

[4] Allyson R. Zazulia, Joanne Markham, and William J. Powers. 4 - cerebral blood flow and metabolism in human cerebrovascular disease. In J.P. Mohr, Philip A. Wolf, James C. Grotta, Michael A. Moskowitz, Marc R. Mayberg, and Rüdiger von Kummer, editors, *Stroke (Fifth Edition)*, pages 44–67. W.B. Saunders, Saint Louis, fifth edition edition, 2011.

[5] Kenneth C Beck, Lakesha N Randolph, Kent R Bailey, Christina M Wood, Eric M Snyder, and Bruce D Johnson. Relationship between cardiac output and oxygen consumption during upright cycle exercise in healthy humans. *Journal of applied physiology*, 101(5):1474–1480, 2006.

[6] Marcello Ricardo Paulista Markus, Till Ittermann, Christine Julia Drzyzga, Martin Bahls, Sabine Schipf, Ulrike Siewert-Markus, Sebastian Edgar Baumeister, Paul Schumacher, Ralf Ewert, Henry Völzke, et al. Cardiac mri shows an association of lower cardiorespiratory fitness with decreased myocardial mass and higher cardiac stiffness in the general population–the sedentary's heart. *Progress in Cardiovascular Diseases*, 68:25–35, 2021.

[7] Ross D Pollock, Scott Carter, Cristiana P Velloso, Niharika A Duggal, Janet M Lord, Norman R Lazarus, and Stephen DR Harridge. An investigation into the relationship between age and physiological function in highly active older adults. *The Journal of physiology*, 593(3):657–680, 2015.

[8] Johannes Burtscher, Barbara Strasser, Martin Burtscher, and Gregoire P Millet. The impact of training on the loss of cardiorespiratory fitness in aging masters endurance athletes. *International Journal of Environmental Research and Public Health*, 19(17):11050, 2022.

[9] Andrew C Betik and Russell T Hepple. Determinants of v˙ o2 max decline with aging: an integrated perspective. *Applied physiology, nutrition, and metabolism*, 33(1):130–140, 2008.

[10] Johan SR Clausen, Jacob L Marott, Andreas Holtermann, Finn Gyntelberg, and Magnus T Jensen. Midlife cardiorespiratory fitness and

the long-term risk of mortality: 46 years of follow-up. *Journal of the American College of Cardiology*, 72(9):987–995, 2018.

[11] Evrim B Turkbey, Neal W Jorgensen, WC Johnson, Alain G Bertoni, Joseph F Polak, AV Diez Roux, Russell P Tracy, Joao AC Lima, and David A Bluemke. Physical activity and physiological cardiac remodelling in a community setting: the multi-ethnic study of atherosclerosis (mesa). *Heart*, 96(1):42–48, 2010.

[12] Carrie P Aaron, Harikrishna Tandri, R Graham Barr, W Craig Johnson, Emilia Bagiella, Harjit Chahal, Aditya Jain, Jorge R Kizer, Alain G Bertoni, João AC Lima, et al. Physical activity and right ventricular structure and function: the mesa-right ventricle study. *American journal of respiratory and critical care medicine*, 183(3):396–404, 2011.

[13] Babette M Pluim, Aeilko H Zwinderman, Arnoud van der Laarse, and Ernst E van der Wall. The athlete's heart: a meta-analysis of cardiac structure and function. *Circulation*, 101(3):336–344, 2000.

[14] Mehmet Yildiz, Ahmet Afşin Oktay, Merrill H Stewart, Richard V Milani, Hector O Ventura, and Carl J Lavie. Left ventricular hypertrophy and hypertension. *Progress in cardiovascular diseases*, 63(1):10–21, 2020.

[15] Erin J Howden, Satyam Sarma, Justin S Lawley, Mildred Opondo, William Cornwell, Douglas Stoller, Marcus A Urey, Beverley Adams-Huet, and Benjamin D Levine. Reversing the cardiac effects of sedentary aging in middle age—a randomized controlled trial: implications for heart failure prevention. *Circulation*, 137(15):1549–1560, 2018.

[16] Juan M Murias, John M Kowalchuk, and Donald H Paterson. Time course and mechanisms of adaptations in cardiorespiratory fitness with

endurance training in older and young men. *Journal of applied physiology*, 108(3):621–627, 2010.

[17] Scott J Strath, Ann M Swartz, DAVID R Bassett Jr, WILLIAM L O'Brien, George A King, and Barbara E Ainsworth. Evaluation of heart rate as a method for assessing moderate intensity physical activity. *Medicine and science in sports and exercise*, 32(9 Suppl):S465–70, 2000.

[18] Magnus Thorsten Jensen, Poul Suadicani, Hans Ole Hein, and Finn Gyntelberg. Elevated resting heart rate, physical fitness and all-cause mortality: a 16-year follow-up in the copenhagen male study. *Heart*, 99(12):882–887, 2013.

[19] Ali A Ehsani, Takeshi Ogawa, Tom R Miller, Robert J Spina, and Sarah M Jilka. Exercise training improves left ventricular systolic function in older men. *Circulation*, 83(1):96–103, 1991.

[20] Jerome L Fleg, F O'connor, G Gerstenblith, LC Becker, J Clulow, SP Schulman, and EG Lakatta. Impact of age on the cardiovascular response to dynamic upright exercise in healthy men and women. *Journal of applied physiology*, 78(3):890–900, 1995.

[21] JVGA Durnin and RG Edwards. Pulmonary ventilation as an index of energy expenditure. *Quarterly Journal of Experimental Physiology and Cognate Medical Sciences: Translation and Integration*, 40(4):370–377, 1955.

[22] Mikel Izquierdo, Keijo Häkkinen, Alazne Antón, Miriam Garrues, Javier Ibañez, Maite Ruesta, and Esteban M Gorostiaga. Maximal strength and power, endurance performance, and serum hormones in middle-aged and elderly men. *Medicine & Science in Sports & Exercise*, 33(9):1577–1587, 2001.

[23] Rhys I Beaudry, T Jake Samuel, Jing Wang, Wesley J Tucker, Mark J Haykowsky, and Michael D Nelson. Exercise cardiac magnetic resonance imaging: a feasibility study and meta-analysis. *American Journal of Physiology-Regulatory, Integrative and Comparative Physiology*, 315(4):R638–R645, 2018.

[24] Richard J Rodeheffer, Gary Gerstenblith, LC Becker, JL Fleg, ML Weisfeldt, and EG Lakatta. Exercise cardiac output is maintained with advancing age in healthy human subjects: cardiac dilatation and increased stroke volume compensate for a diminished heart rate. *Circulation*, 69(2):203–213, 1984.

[25] David Houghton, Thomas W Jones, Sophie Cassidy, Mario Siervo, Guy A MacGowan, Michael I Trenell, and Djordje G Jakovljevic. The effect of age on the relationship between cardiac and vascular function. *Mechanisms of ageing and development*, 153:1–6, 2016.

[26] Polly A Beere, Stuart D Russell, Miriam C Morey, Dalane W Kitzman, and Michael B Higginbotham. Aerobic exercise training can reverse age-related peripheral circulatory changes in healthy older men. *Circulation*, 100(10):1085–1094, 1999.

[27] John R Stratton, Wayne C Levy, Manuel D Cerqueira, Robert S Schwartz, and Itamar B Abrass. Cardiovascular responses to exercise. effects of aging and exercise training in healthy men. *Circulation*, 89(4):1648–1655, 1994.

[28] Jerome L Fleg, Steven P Schulman, FC O'Connor, Gary Gerstenblith, Lewis C Becker, Suzanne Fortney, Andrew P Goldberg, and Edward G Lakatta. Cardiovascular responses to exhaustive upright cycle exercise in highly trained older men. *Journal of applied physiology*, 77(3):1500–1506, 1994.

[29] Hayley Guiney, Samuel JE Lucas, James D Cotter, and Liana Machado. Investigating links between habitual physical activity, cerebrovascular function, and cognitive control in healthy older adults. *Neuropsychologia*, 125:62–69, 2019.

[30] David C Poole and Andrew M Jones. Measurement of the maximum oxygen uptake vo2max: Vo2peak is no longer acceptable. *Journal of applied physiology*, 122(4):997–1002, 2017.

Chapter 7

The impact of lifelong exercise and age on brain structure and functional responses to acute exercise and recovery in healthy volunteers

7.1 Introduction

Declining cerebral blood flow (CBF) with healthy ageing has long been documented [1, 2], but greater aerobic fitness has been suggested to modulate this decline [3], protect against cognitive decline [4], and reduce the risk of cardiovascular and neurodegenerative diseases [5].

Previous work conducted at the University of Nottingham has shown that older adults show deficits in CBF during an exercise task, with the expected

increase in CBF on exercise being blunted in older adults [6]. Further, this CBF deficit during exercise was mirrored by a reduction in global brain perfusion. A possible mechanism underpinning this observation could be a reduction in cardiac output that accompanies ageing, possibly reflected by a difference in aortic cardiac index between OU and YU at baseline in this study, but not reflected in the other cardiac measures made. In addition, greater oxygen extraction was found in the older group than the younger group during rest, exercise and recovery periods [6]. It was suggested that this arose from a compensatory mechanism developed in ageing to mediate the drop in CBF, although no differences in cerebral metabolic rate of oxygen ($CMRO_2$) which measures the rate of oxygen consumption by the brain, were found, suggesting decreased metabolic efficiency. A study on CBF and metabolic rate of the brain in ageing by Pen et al [7] showed an expected age-related decline in CBF, but that $CMRO_2$ after correction for grey matter volume increased with age, revealing a greater expenditure of energy in the older brain.

Arterial partial pressure of carbon dioxide (PCO_2) is a major regulator of CBF, with increases in arterial PCO_2 inducing increased CBF. Arterialised-venous blood samples can serve as an accurate indicator of arterial PCO_2 [8], as can end-tidal PCO_2 and minute ventilation. These can therefore be measured to distinguish CBF changes due to arterial PCO_2 changes as compared to other factors, such as changes in cardiac output. The CBF deficit during exercise in older adults may also be due to reduced cardiac output, brain atrophy or induced vasoconstriction relative to younger participants. Lower cardiac output has been found to be associated with lower CBF during exercise, where both CBF and cardiac output had a reduced response to exercise after the administration of a cardio-selective beta blocker [9]. Additionally, Meng et al's review shows CBF changes associated with cardiac

output driven by lower body negative pressure, standing up, leg tensing, albumin infusion and normal saline infusion, as well as chronic reduction in CBF in those with heart failure [10]. Cardiac output and VO_2 are linearly related, and both decrease in ageing. This age-related reduction in cardiac output, coupled with an increased need of blood flow to skeletal muscle when subjected to exercise, may blunt increases in brain blood perfusion during exercise [9]. It is reasonable to suggest therefore that if cardiac output at baseline can be maintained with age, this blunting in CBF on exercise may be minimised.

Structural differences have also been found when investigating the impact of physical activity on ageing, with studies showing greater white matter volume [11, 12] and grey matter volume [13] in those who are more physically active. In regional analysis of the brain, hippocampal volume differences are found with ageing, and have increasingly been investigated with physical activity, with associations found between cardiorespiratory fitness and hippocampal volume and spatial memory [14, 15]. These differences extended beyond cross sectional studies to an exercise intervention study of older adults, where hippocampus volume increased after aerobic exercise training [16]. The structural connectivity and integrity of white matter tracts has also been found to be mediated by physical activity in ageing, with greater fractional anisotropy (representing greater white matter tract integrity) associated with greater levels of physical activity [17].

In this chapter, the effects of sub-maximal steady-state exercise on CBF and oxygen extraction fraction response is studied for the EXAGE group of older trained (OT), older untrained (OU) and young untrained (YU). In addition structural changes across the groups associated with brain tissue volumes, white matter hyperintensities and structural connectivity are studied.

7.2 Functional Brain Measures collected during exercise and recovery

MRI measures were collected on a 3T Philips Ingenia wide-bore scanner using the Cardio-Step ergometer described in Chapter 3. Functional brain measures were taken at rest, during 10 minutes of steady-state exercise at 50% VO_2peak, and during 10 minutes of recovery immediately following exercise. Chapter 3 details how the workload was determined for a 50% VO_2peak for each individual, the full exercise protocol, and the MRI scan protocol. The following section provides a summary of the functional brain measures at baseline and during exercise and recovery.

7.2.1 Methods

7.2.1.1 Cerebral Blood Flow

Cerebral blood flow (CBF) was measured using Phase Contrast (PC-MRI) of left and right cerebral arteries and the basilar artery. The data were analysed using Philips' Viewforum Q-Flow to calculate velocity, stroke volume (the volume of blood passing through the vessel per heart beat) and flux through each vessel. The flow from all three vessels was then summed and corrected for grey-matter (GM) volume estimated from the MPRAGE data (see Section 7.3) to obtain a GM corrected cerebral blood flow (gmCBF).

7.2.1.2 Oxygen Extraction Fraction

T_2-relaxation-under-spin-tagging (TRUST) scans were acquired to determine brain venous oxygenation (Yv) in the sagittal sinus from which to

compute oxygen extraction fraction (OEF). Using an in-house MATLAB script, the TRUST data were processed following the methods of Lu et al [18]. The venous blood signal was calculated from the pairwise subtraction of the FAIR arterial spin labelling (ASL) label and control images to obtain difference images for each effective TE. An ROI of four voxels was drawn around the sagittal sinus signal in the difference image, and from this the blood T_2 relaxation time (in ms) was calculated by fitting the signal across echo times to a monoexponential. Then, a calibration plot was used to determine oxygenation as described by Lu et al [18]. Figure 7.1 outlines this method. OEF was calculated as the difference between arterial (Ya) and venous (Yv) oxygenation where Ya was assumed to be 100%.

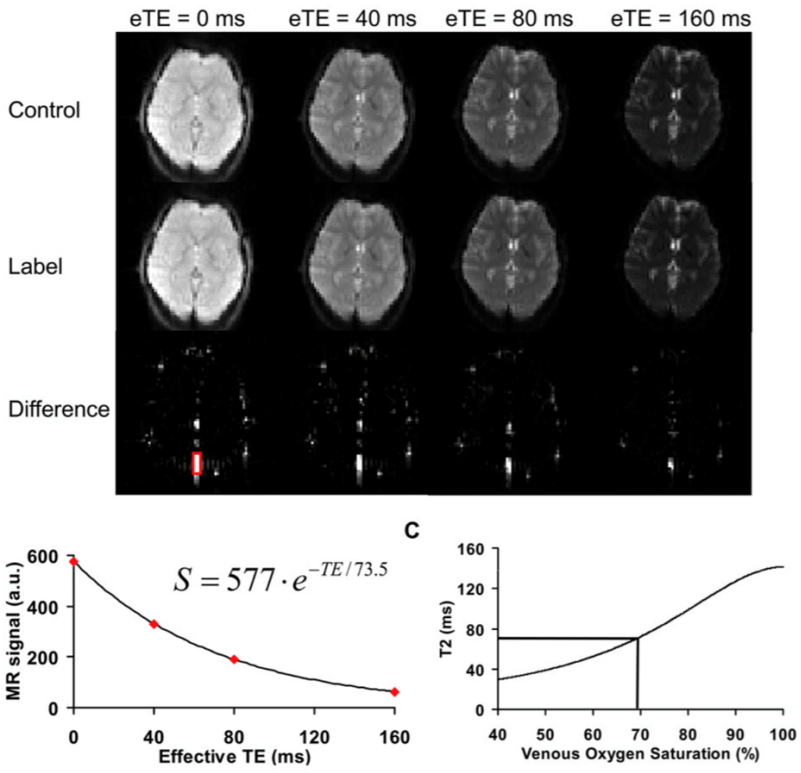

Figure 7.1: TRUST analysis showing computation of the difference image through pairwise subtraction of the FAIR ASL label and control images at each TE. The T_2 decay of venous blood in the superior sagittal sinus is then fit to computer T_2, and the calibration plot is used to determine the venous oxygenation (Yv).

7.2.2 Results

7.2.2.1 Cerebral Blood Flow (CBF)

Head motion was a problem for some participants, particularly during supine exercise. A good quality scan versus one where head motion was problematic is shown in Figure 7.2, with an example data output from the participant with low head motion. Data were collected in OT (n=9), OU (n=7) and YU (n=8), and the data for three participants, one from each group, had to be excluded due to motion effects. Attempts were made to mitigate this, with head padding and handles to grip on during exercise, but these were not sufficient in some cases, and some participants expressed discomfort at the head padding which had to be removed.

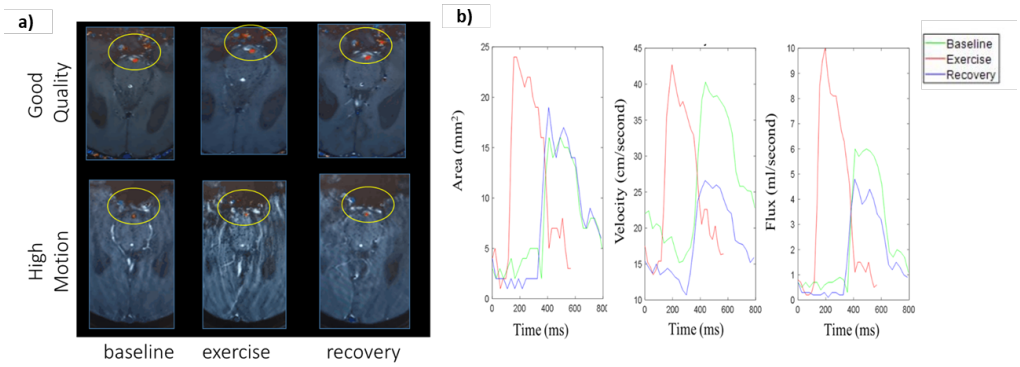

Figure 7.2: a) Cerebral blood vessel contours drawn in ViewForum and b) area, velocity and flow results from one participant in all three conditions. Baseline is green, exercise is red and recovery is blue.

The mean flux values captured across the cerebral arteries are shown in Figure 7.3a for each group of older trained (OT), older untrained (OU) and young untrained (YU). A breakdown by participant and vessel is provided in Figure 7.3b. The variability in response to exercise between participants can be seen, some participants show large increases in blood flow, whilst others instead show decreases. Exercise values are missing from some ves-

sels if there was a high degree of motion during acquisition, resulting in image quality that was insufficient or the participant had moved out of plane and the vessel was no longer visible. Note this is more apparent in the YU group who exercised at higher absolute workloads for their 50% VO_2peak.

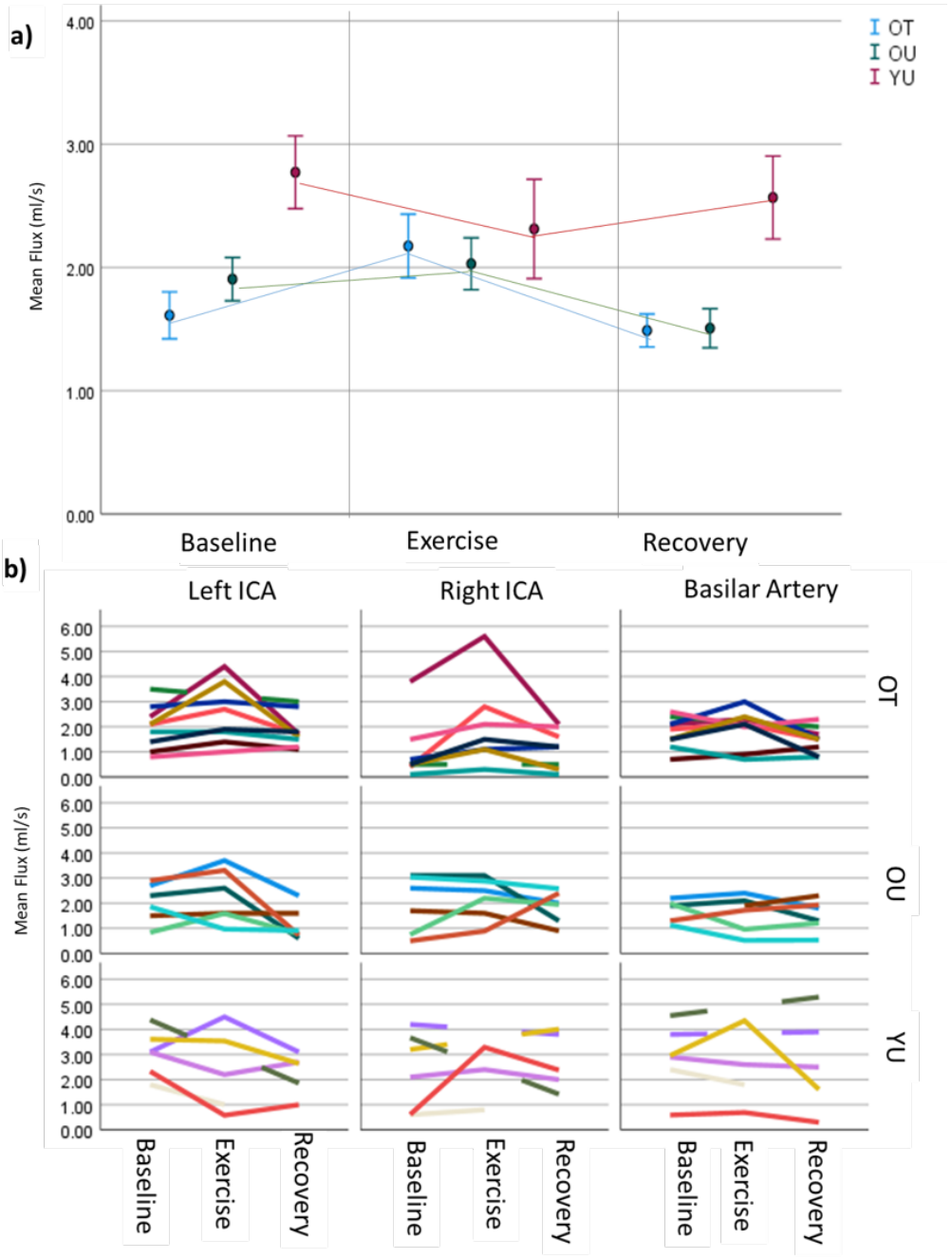

Figure 7.3: a) Mean flux across CBF vessels for condition per OT, OU and YU group and b) CBF flux values for each participant, for each vessel, under each condition, separated by group.

Figure 7.4 shows the mean stroke volume of the vessels (Figure 7.4a), and each vessel individually (Figure 7.4b).

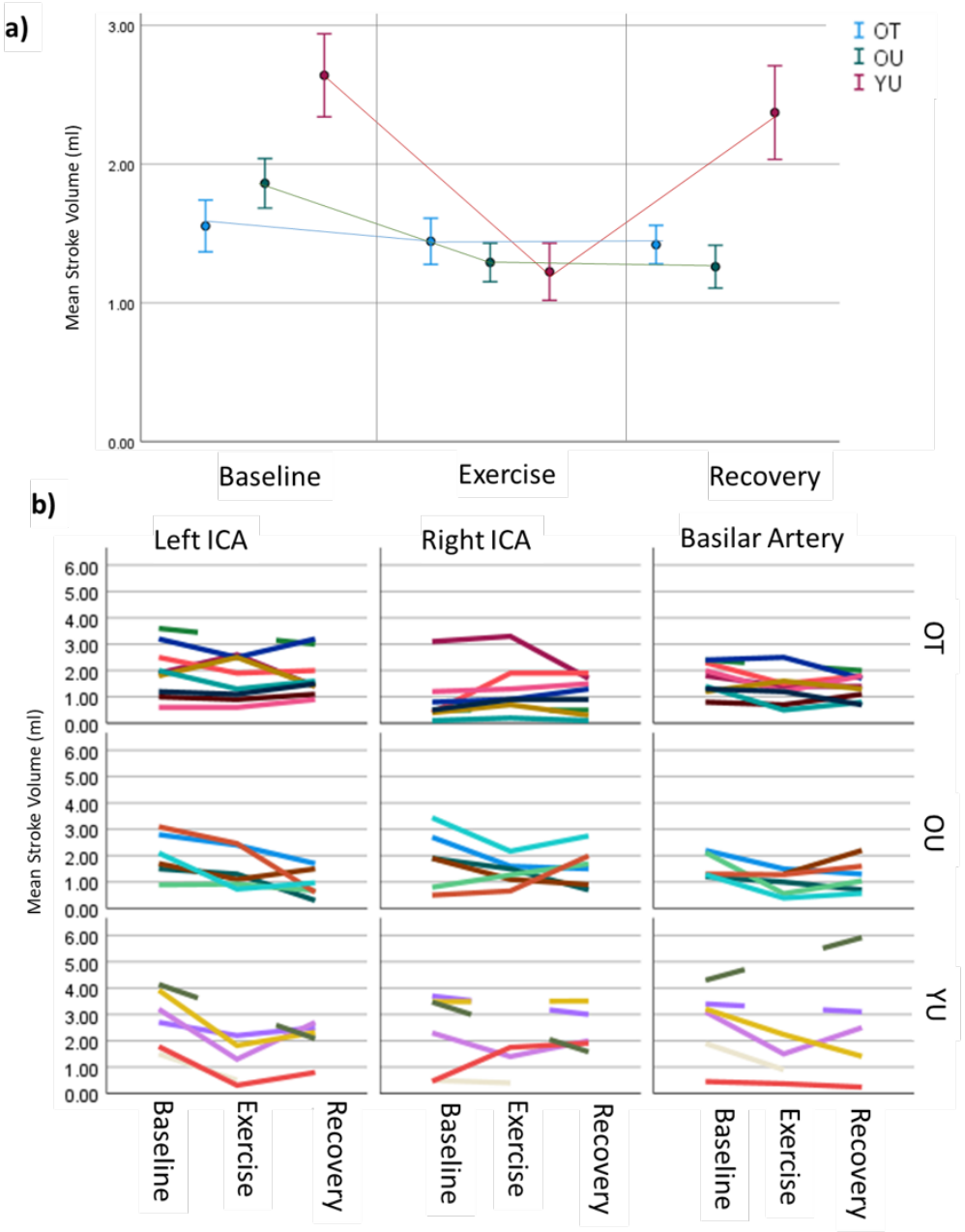

Figure 7.4: a) Mean stroke volume across CBF vessels for each condition per group and b) CBF stroke volume values for each participant, for each vessel, under each condition, separated by group.

Since accurate estimates of the diameter of the vessel can be compromised during exercise, the velocity within the cerebral vessels were assessed as an alternative that is less reliant on ROI placement, The mean across all three

vessels was taken and can be see in Figure 7.5. For cerebral velocity, there was a significant difference between groups ($F(8,57) = 3.577$, $p=.002$), the YU group had higher velocities than both older groups (OT , $p=0.036$ and OU, $p<0.001$), and the OT had higher velocities than the OU group ($p=0.019$). There was not a significant effect of condition, ($F(2,16) = 3.49$, $p=0.055$), however the OU group did have a trend level difference in velocity, with lower velocity in recovery as compared to baseline ($p=0.053$).

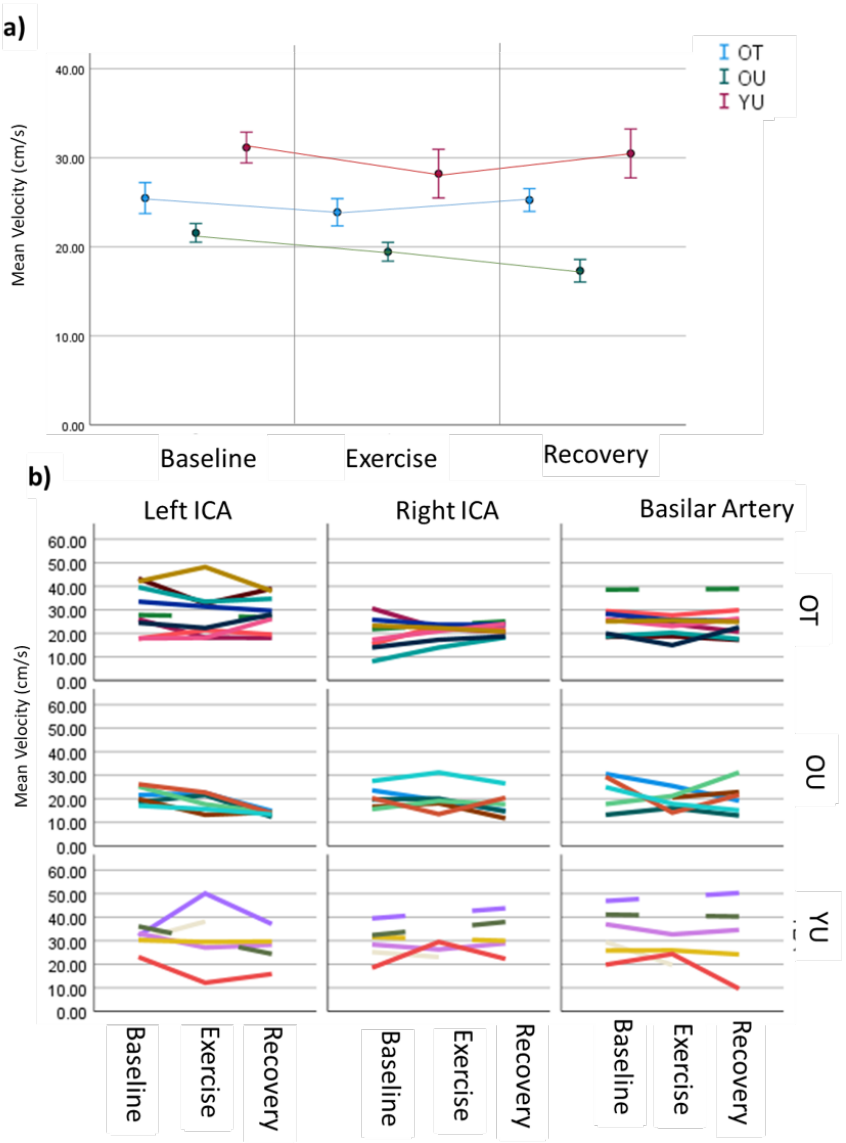

Figure 7.5: a) Mean velocity across CBF vessels for each condition per OT, OU and YU group and b) CBF velocity values for each participant, for each vessel, under each condition, separated by group.

Mean gmCBF differences existed across groups ($F(8,53) = 3.105$, $p=0.006$), but not across conditions, as seen in Figure 7.6a. The YU group had significantly higher gmCBF than the OT group ($p<0.001$) and OU ($p=0.006$) groups across all conditions, with differences diminishing during exercise.

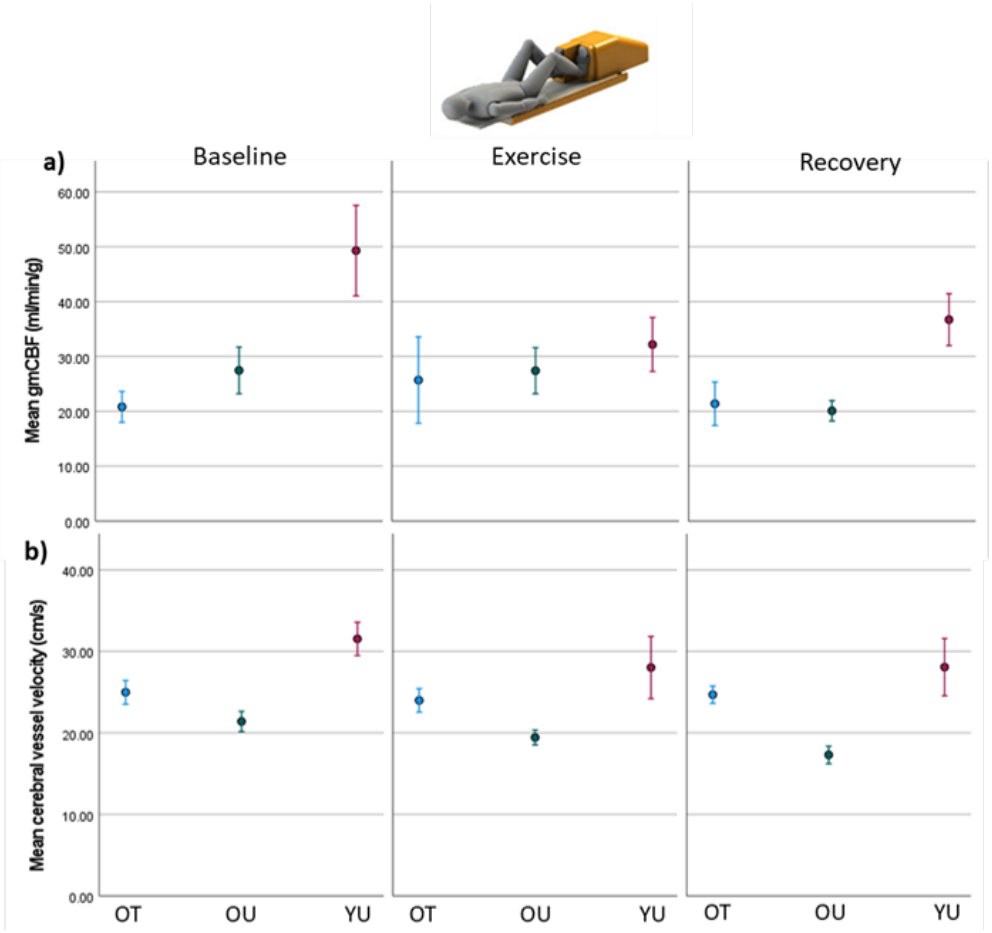

Figure 7.6: Mean gmCBF (a) and mean cerebral vessel velocity (b) across conditions for OT, OU and YU.

7.2.2.2 Oxygen Extraction Fraction (OEF)

There was a significant overall group effect of OEF ($F(8,49)=3.247$, $p=0.005$), with the OU group having greater OEF than YU ($p<.001$), but not than the OT ($p=0.095$). There was no significant difference in OEF at baseline, but on exercise ($F2,18)=4.751$, $p=0.022$) and recovery ($F(2,18)=6.054$, $p=0.009$), OEF in the OU group was significantly greater than for the YU

group (p=0.02, and p=0.008) but not for the OT group (p=0.117 and p=0.172).

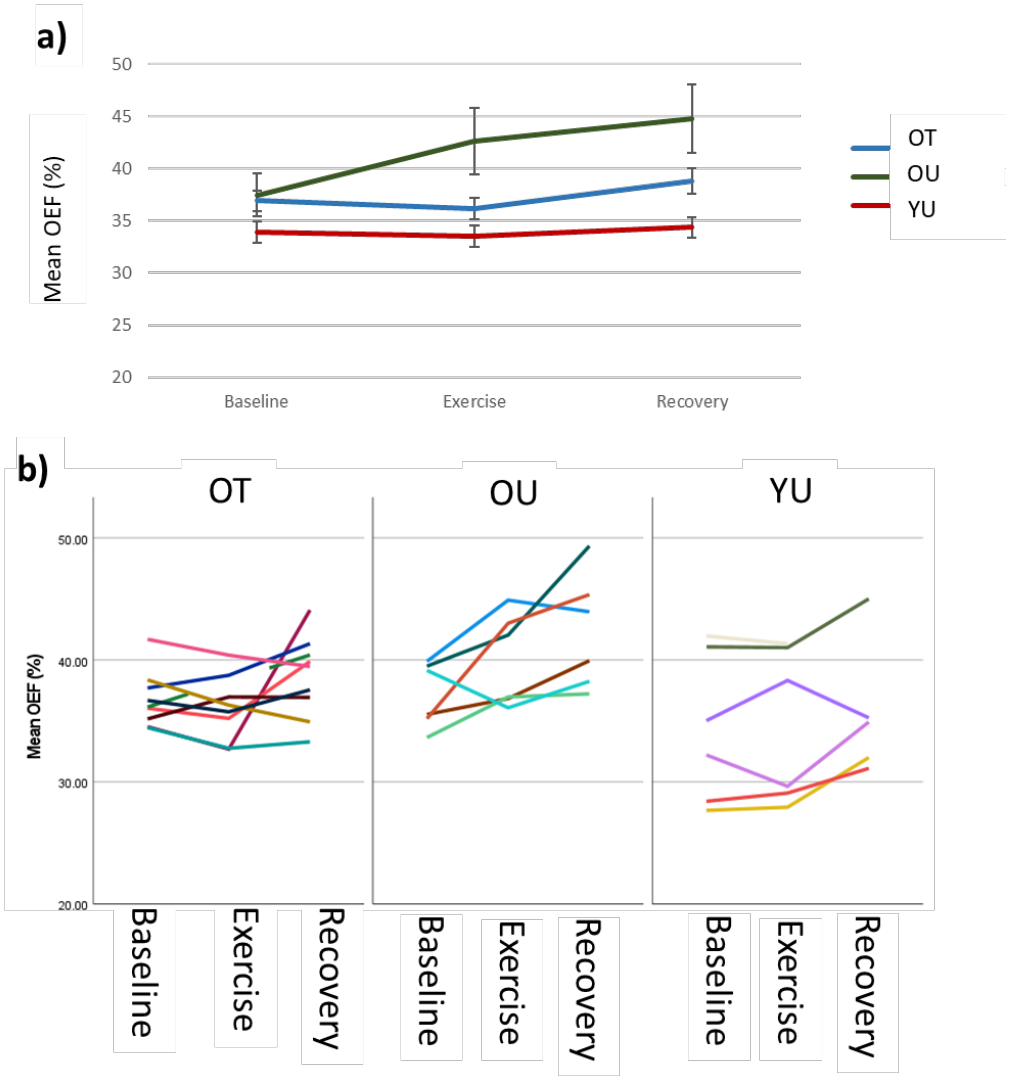

Figure 7.7: a) Mean OEF for the OT, OU and YU group and b) OEF per participant across conditions for each group.

7.2.2.3 Relationship between CBF and OEF

Figure 7.8 shows that OEF is weakly inversely related to gmCBF (R^2 = 0.127, F(1,56) = 8.001, p=0.007) when plotted across participants using all three conditions. This relationship is primarily driven by the high gmCBF values with lower OEF values in the younger group and higher OEF value

with lower gmCBF values in the older groups.

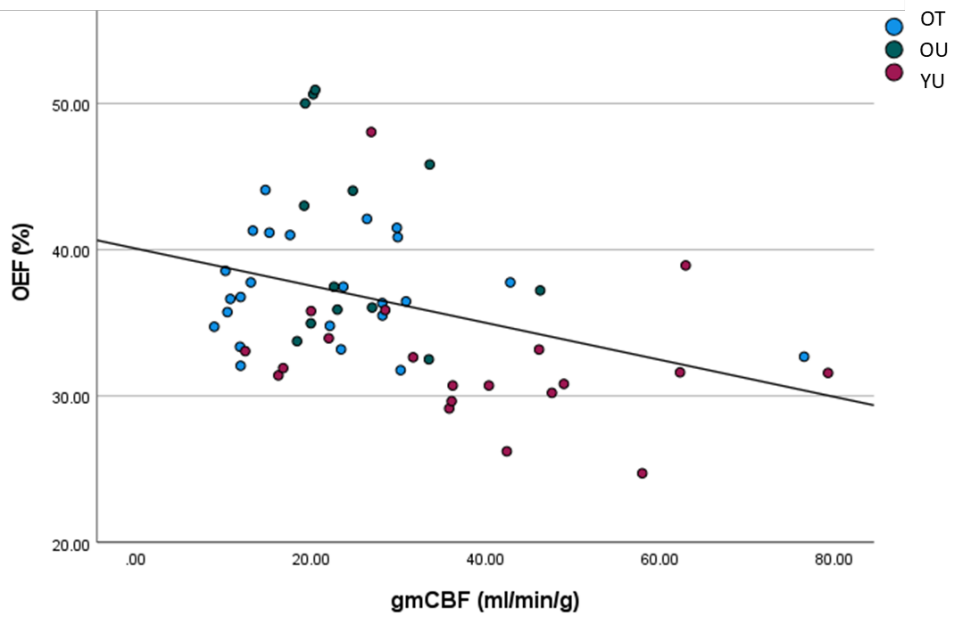

Figure 7.8: Relationship between OEF and gmCBF in all groups.

7.3 Brain Structure

The following section outlines structural measures in the EXAGE groups. Measures are collected of grey matter (GM), white matter (WM) and cerebrospinal fluid (CSF), cortical thickness, surface and volume based morphometry, the number of hyperintensities and structural connectivity.

7.3.1 Methods

7.3.1.1 Volumes and Surface and Voxel Based Morphology

An MPRAGE scan was collected to assess brain structure. This included GM, WM, CSF metrics and regional volumes of the hippocampus and amygdala. These were calculated from the MPRAGE using Freesurfer [19]

for total volumes and SPM CAT [20] to calculate surface and voxel based morphologies. Volumes were corrected for estimated total intracranial volume (eTIV).

7.3.1.2 White Matter Hyperintensities

A T_2-weighted-Fluid-Attenduated Inversion Recovery (T_2-FLAIR) was used to assess white matter hyperintensities or lesions. White matter hyperintensities were isolated from the image using FSL's Brain Intensity AbNormality Classification Algorithm (BIANCA) [21].

The identified hyperintensities were divided into clusters using a MATLAB connectivity function and separated into size categories defined as 'puncate' if less than 14 mm^3, 'focal' if 14 to 900 mm^3 and 'large' if over 900 mm^3, as defined in Wen et al. [22]. In addition, a category of 'extra-large' was also included for any lesions that were greater than 2000 mm^3.

Structural Connectivity

Diffusion tensor imaging (DTI) data was collected using 64 directions at a b value of 1000 ms. Voxelwise statistical analysis of the data was carried out using TBSS (Tract-Based Spatial Statistics, [23], a function of FSL [24]. TBSS projects all the participants' fractional anisotropy (FA) and mean diffusivity (MD) data onto a mean tract skeleton, before applying voxelwise cross-subject statistics. MD indicates the mobility of water molecules in each measured direction and can be indicative of white matter integrity and FA shows the primary direction of diffusion and is an indicator of myelination, fibre density and axonal diameter.

7.3.2 Results

7.3.2.1 Tissue volumes, and surface and voxel based morphology

Tissue volumes, and surface and voxel based morphology differences were examined in the OT (n=9), OU (n=7) and YU (n=8). There were significant differences in global cortical thickness between the groups ($F(2,23) = 18.58$, $p<0.001$), with a thicker cortex for the YU group than both the OU and OT groups ($p<0.001$), as seen in Figure 7.10. The variations in cortical thickness across the brain in each group is shown in Figure 7.9, note the thinner cortex in the sensorimotor strip.

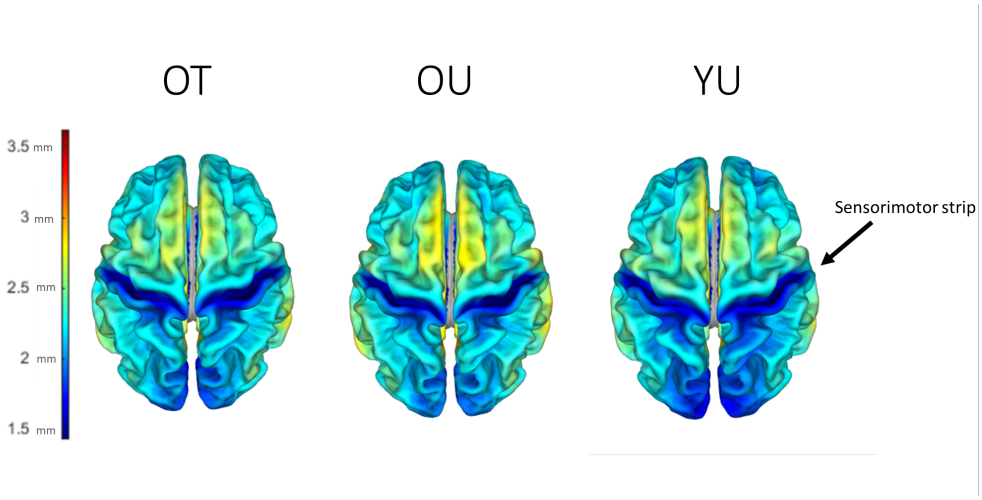

Figure 7.9: Cortical thickness across brain regions for the OT, OU and YU groups.

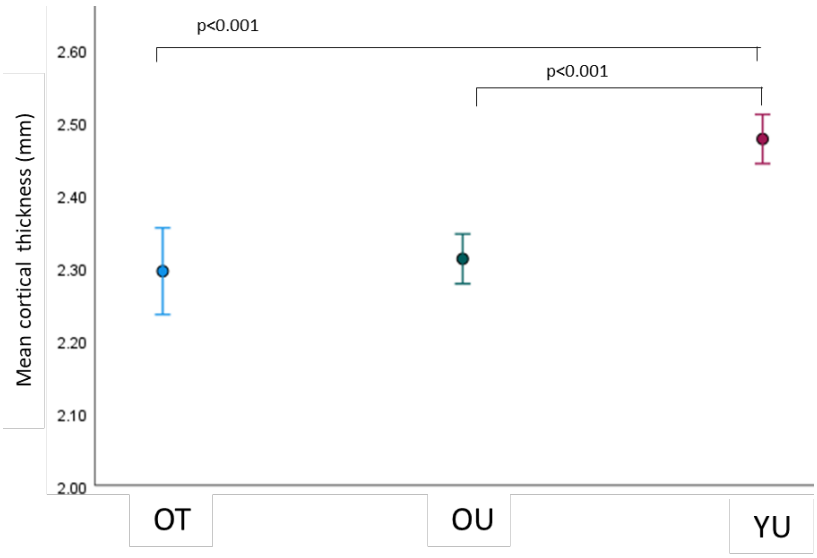

Figure 7.10: Mean cortical thickness for the OT, OU and YU groups.

Using surface-based morphometry (FWE-corrected at $p<0.05$), the location of the differences in cortical thickness were assessed. Local differences were seen between the YU and older (OT and OU) groups, but not between the OT and OU groups (Figure 7.11). These differences were primarily located in the pre-central and post-central gyrus.

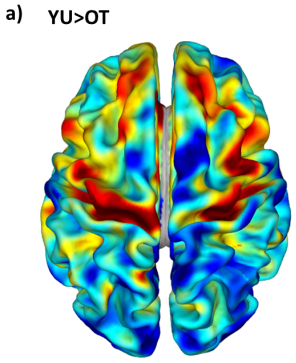

Cluster level pfdr corrected p values	YU>OT
.004	Intracalcarine Cortex
.010	Paracingulate Gyrus
.005	Intracalcarine Cortex
.022	Postcentral Gyrus
.013	Postcentral Gyrus
.035	Heschl's Gyrus
.035	Paracingulate Gyrus

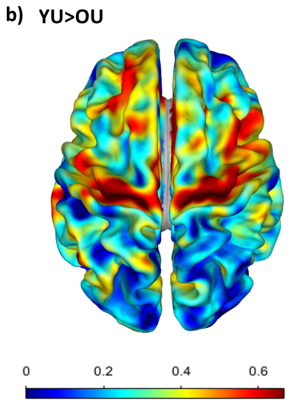

Cluster level pfdr corrected p values	YU>OU
.000	Precentral Gyrus
.005	Heschl's Gyrus
<.001	Planum Temporale/Heschl's Gyrus
.011	Postcentral Gyrus
.046	Paracingulate Gyrus
<.001	Postcentral Gyrus(low)/
.016	Right alns interior insula
.008	Right cerebral white matter

Figure 7.11: Cortical thickness differences between a) the YU and OT group (YU>OT) and b) the YU and OU group (YU>OU).

On studying the volume of each tissue type, the YU group had greater volume in white matter ($F(2,23) = 10.024$, $p<0.001$, OT: $p=0.001$, OU: $p=0.006$) and grey matter ($F(2,23) = 27.513$, $p<0.001$, OT:$p<0.001$, OU: $p<.001$), but there were no differences in CSF volume between groups (Figure 7.12). Once divided into cortical and subcortical grey matter (as seen in Figure 7.13) the YU group had greater volumes in both the cortical ($F(2,23) = 21.916$, $p<0.001$, OT:$p<0.001$, OU: $p<0.001$) and subcortical ($F(2,23) = 33.801$, $p<0.001$, OT:$p<0.001$, OU: $p<0.001$) regions. Voxel-based morphometry (FWE-corrected at $p>0.05$) localised regions can be seen for white matter in Figure 7.14 and for grey matter in Figure 7.15.

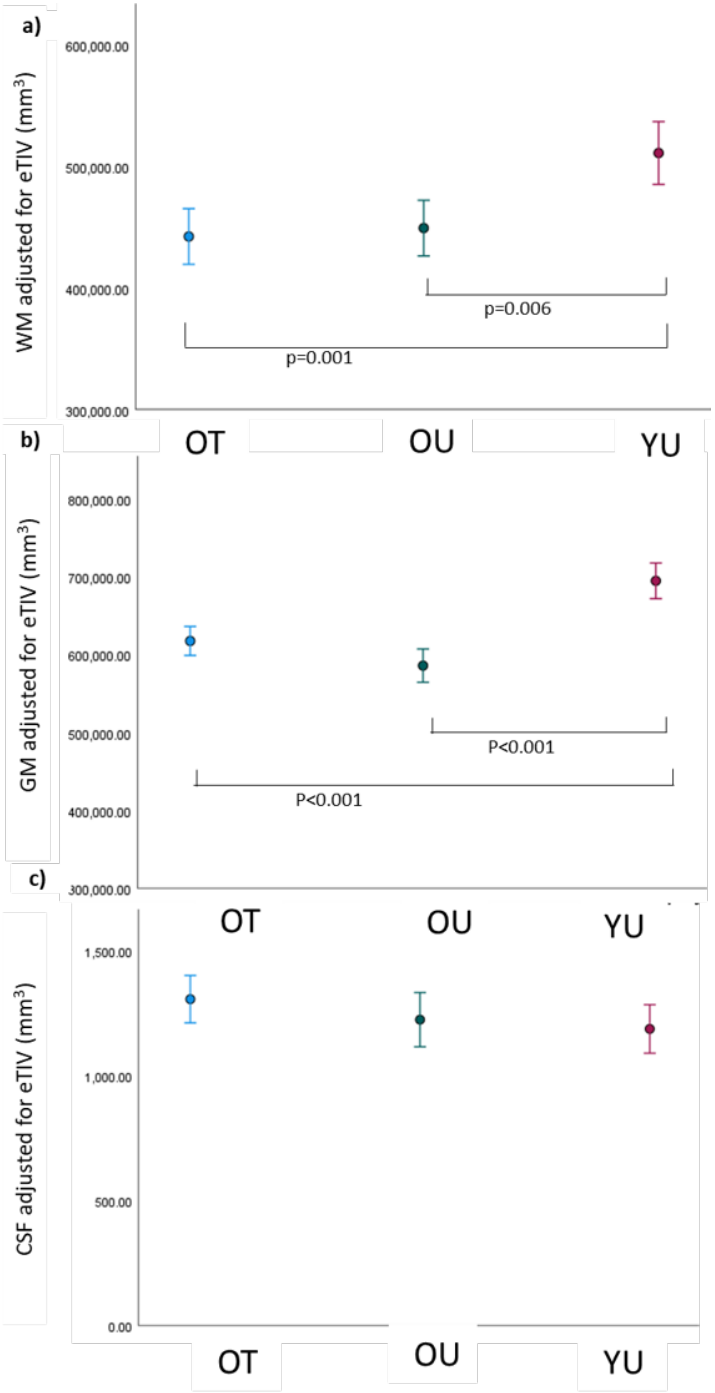

Figure 7.12: a) White matter (WM), b) grey matter (GM) and c) CSF volume for the OT, OU and YU groups.

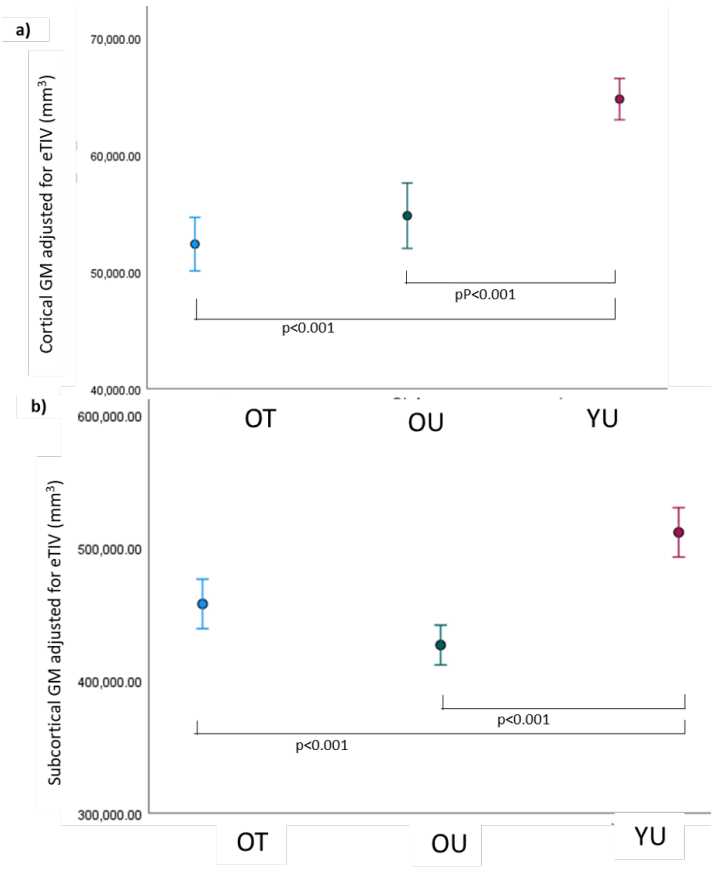

Figure 7.13: a) Cortical and b) sub-cortical grey matter (GM) volumes for the OT, OU and YU groups.

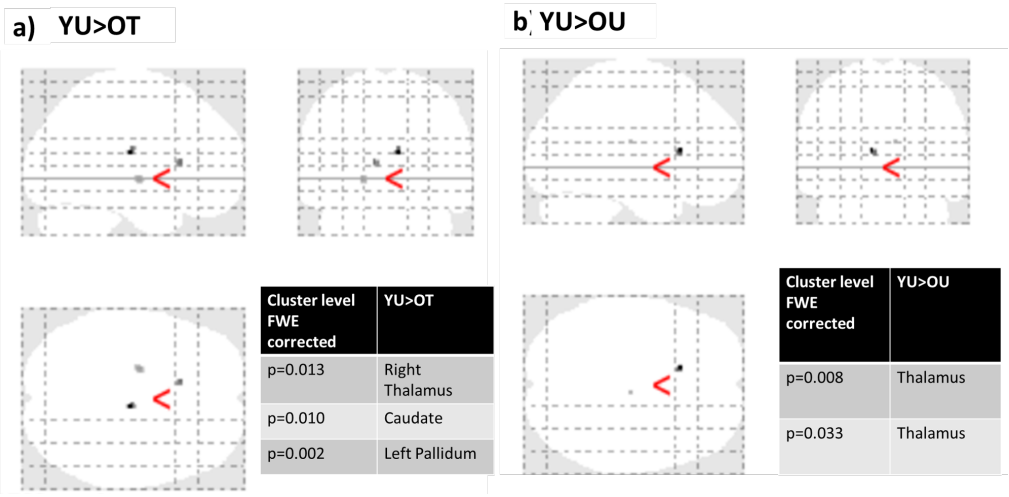

Figure 7.14: White matter differences found through voxel-based morphometry, showing areas for which a) YU>OT and b) YU>OU.

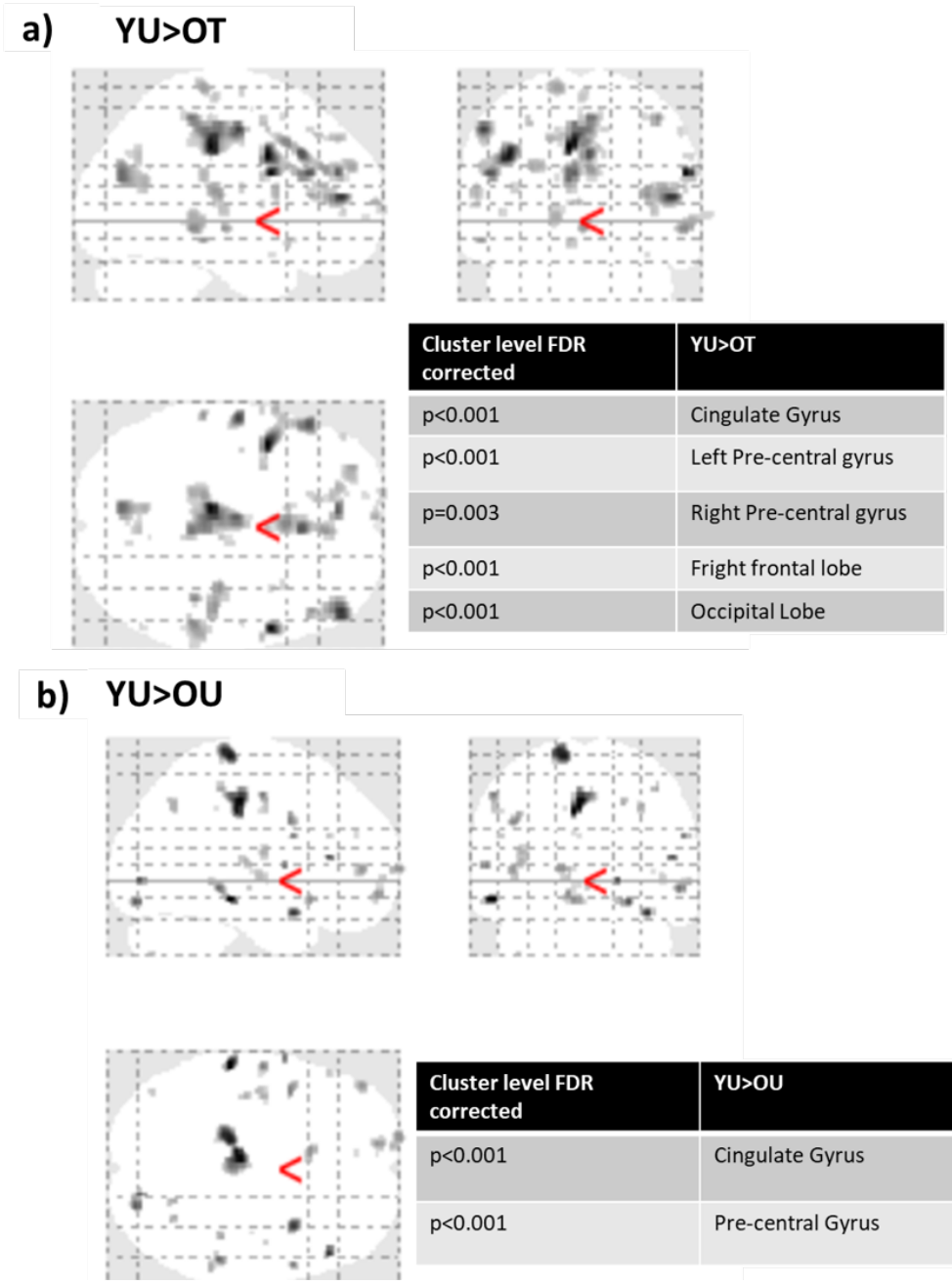

Cluster level FDR corrected	YU>OT
p<0.001	Cingulate Gyrus
p<0.001	Left Pre-central gyrus
p=0.003	Right Pre-central gyrus
p<0.001	Fright frontal lobe
p<0.001	Occipital Lobe

Cluster level FDR corrected	YU>OU
p<0.001	Cingulate Gyrus
p<0.001	Pre-central Gyrus

Figure 7.15: Grey matter differences found through voxel-based morphometry, showing areas for which a) YU>OT and b) YU>OU.

The amygdala ($F(2,23) = 17.242$, $p<0.001$) and hippocampus ($F(2,23) = 22.41$, $p<0.001$) also had larger volumes in the YU group than the OT ($p<0.001$ in both groups) and OU ($p=0.002$ in both), as shown in Figure 7.16.

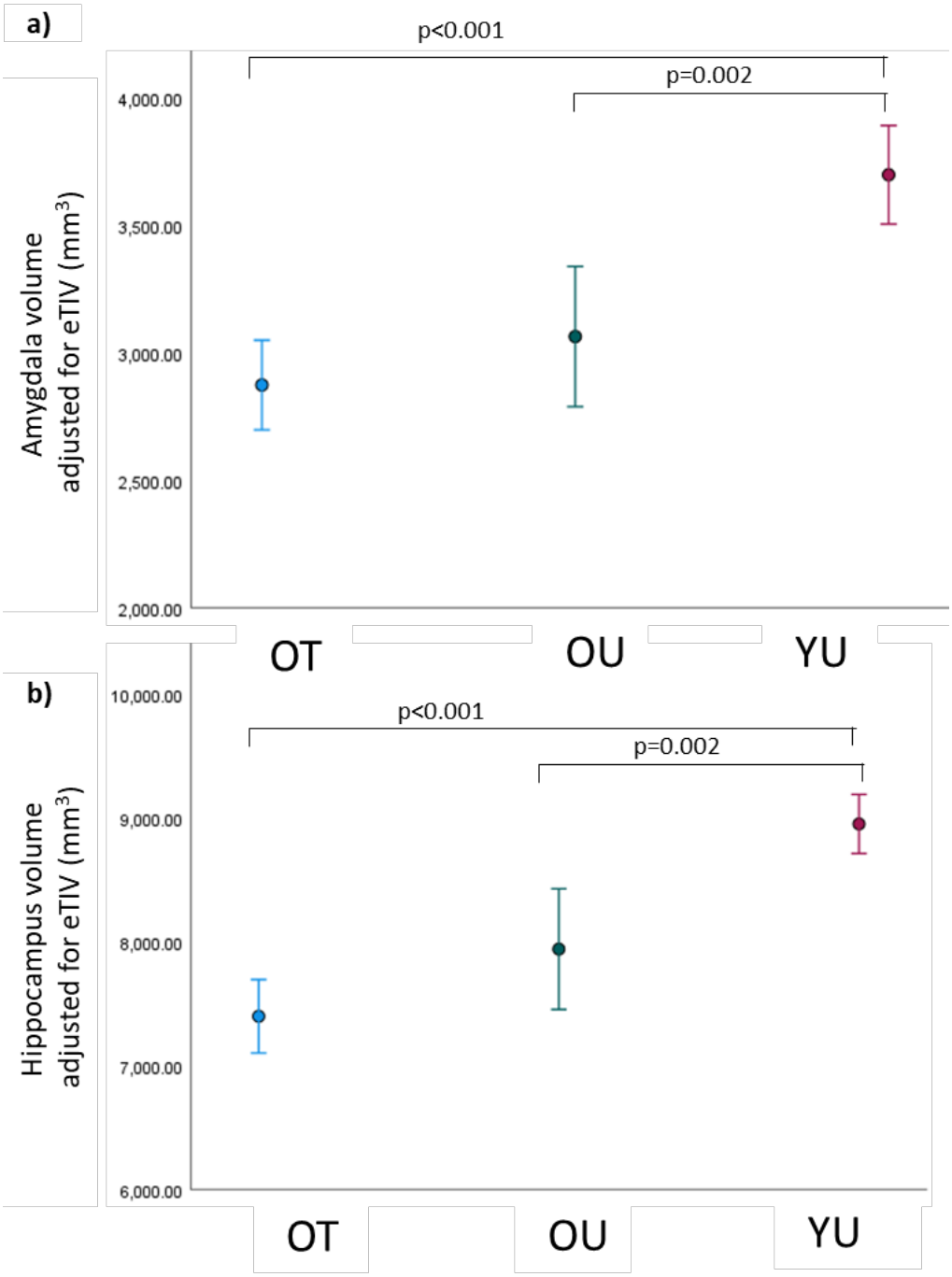

Figure 7.16: a) Amygdala and b) hippocampus volumes for the OT, OU and YU groups.

7.3.2.2 White matter hyperintensities

White matter hyperintensities differed between the EXAGE groups, as shown in Figure 7.17, which depicts the total lesion volume ($F(2,23) =$

7.254, p=0.004) and the lesion volume as a percentage of eTIV (F(2,23) = 7.577, p=0.003). As expected, only the YU differed significantly from the older groups (total volume, OT: p=0.025, OU: p=0.005, and percent of eTIV, OT: p=0.028, OU: p=.004).

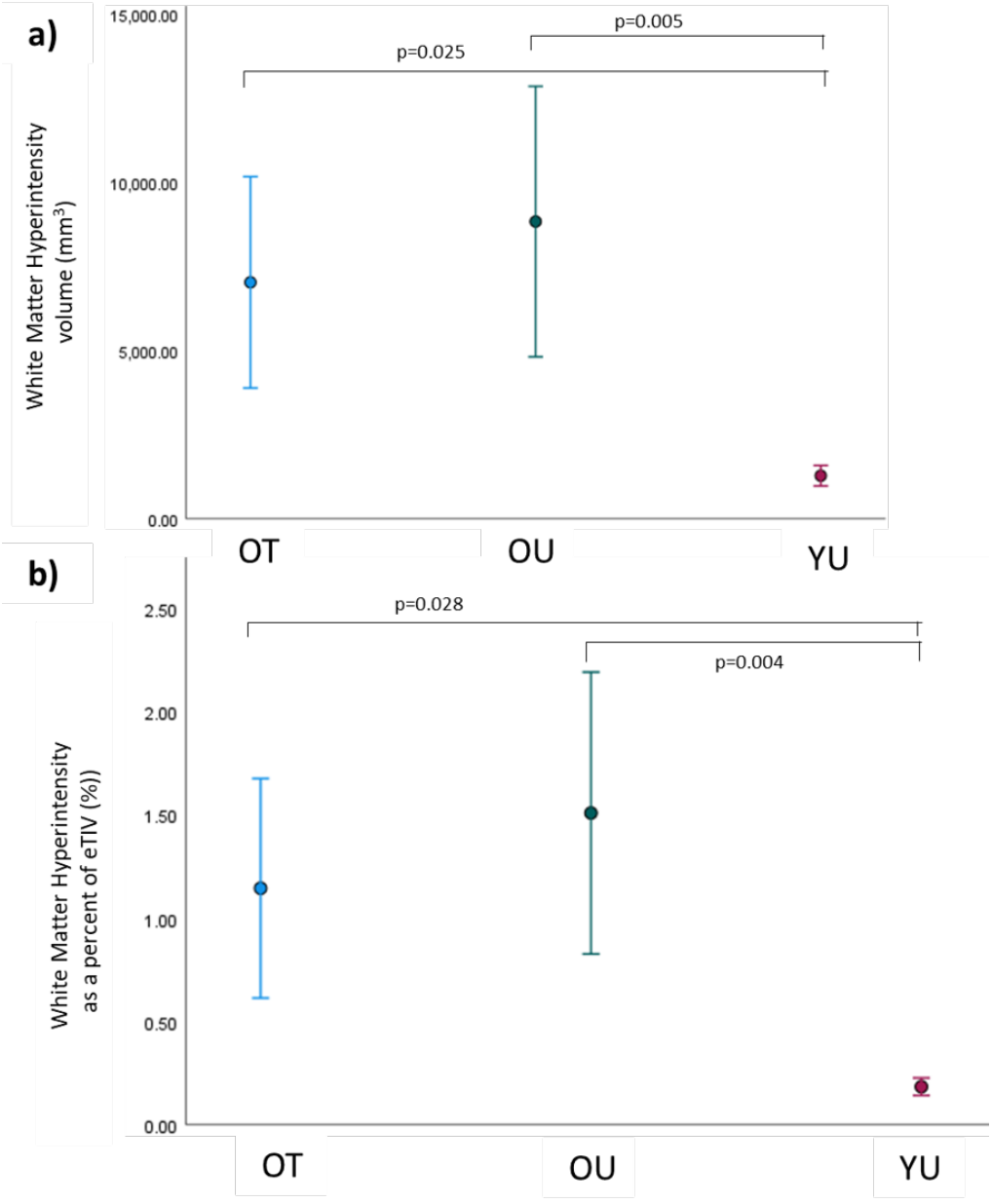

Figure 7.17: Mean white matter hyperintensity as a) Total Volume and b) as percentage of estimated total intercranial volume (eTIV) for the OT, OU and YU groups.

There was no significant difference in total number of white matter hyper-

intensity clusters between groups (F(2,23) =3.123,p=.065), Figure 7.18a. The mean size of the clusters differed between groups, (F(2,23)= 7.021 p=.005), with the OU group having larger clusters than the YU (OU:p=.004), with no significant difference between the other groups (Figure 7.18b).

A linear regression in Figure 7.19 further shows that the differences in total white matter hyperintensity volume is driven by the size of the clusters (R_2 = .69, p<0.001) rather than the number of clusters present (R_2 =.231, p=0.023).

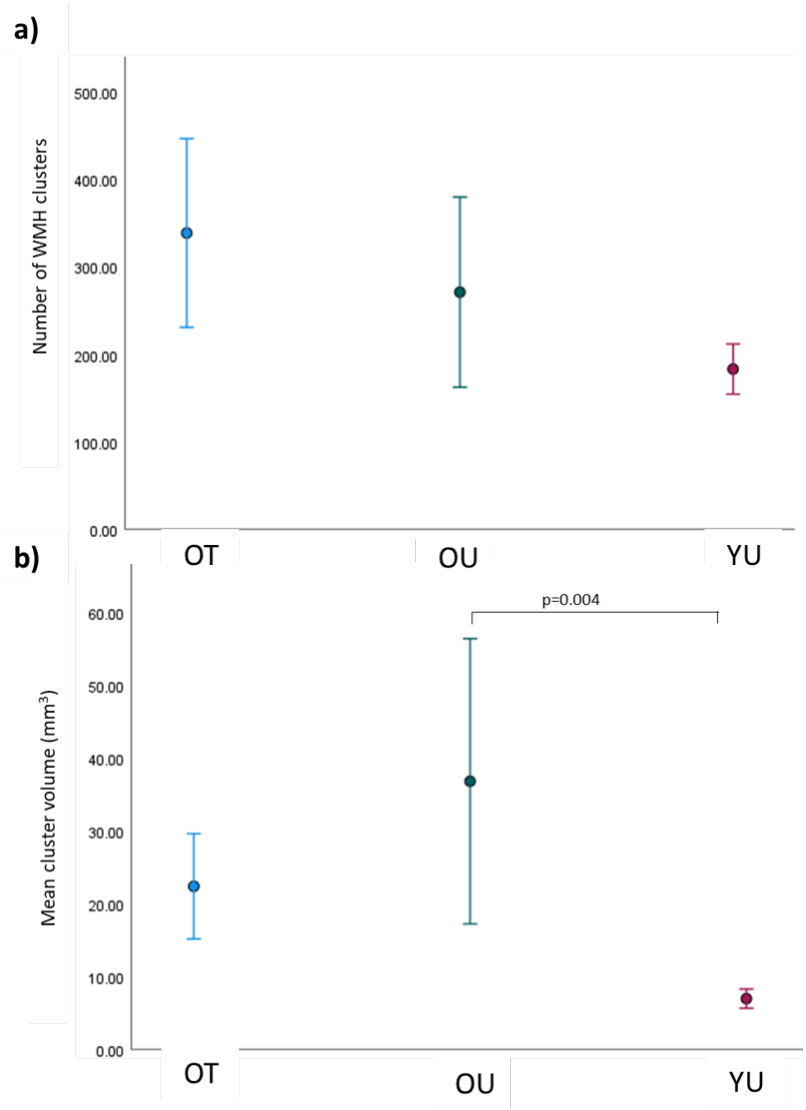

Figure 7.18: a) Mean number of white matter hyperintensity clusters and b) mean cluster volume for the OT, OU and YU groups.

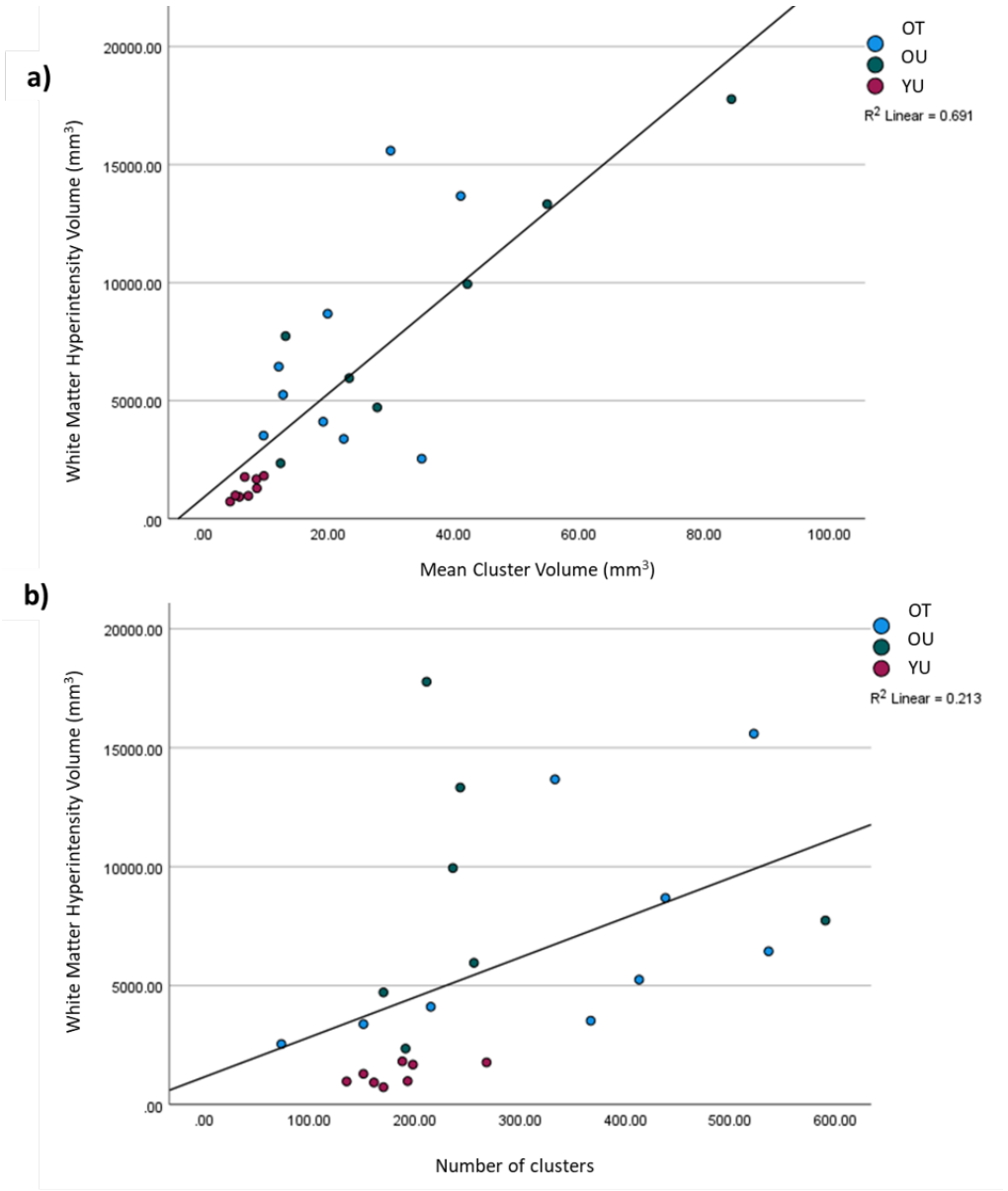

Figure 7.19: Linear regression of white matter hyperintensity volume against a) mean cluster size and b) mean number of clusters in OT, OU and Yu groups.

When separated by cluster size, group differences between number of 'punctate' and 'focal' clusters were not significant, but there were group differences in the number of 'large' and 'extra-large' clusters, as shown in Figure 7.20. YU had no large or extra-large clusters, significantly different to the number of 'large' in both older groups, ($F(2,23) = 6.310$, $p=0.007$, OT:$p=0.008$, OU:$p=0.05$), but only significantly different to the

number of 'extra large' clusters in the OU group (F(2,23)=3.517,p=0.048, OU:0.047), where the OT group did not differ significantly from the YU group (p=0.353).

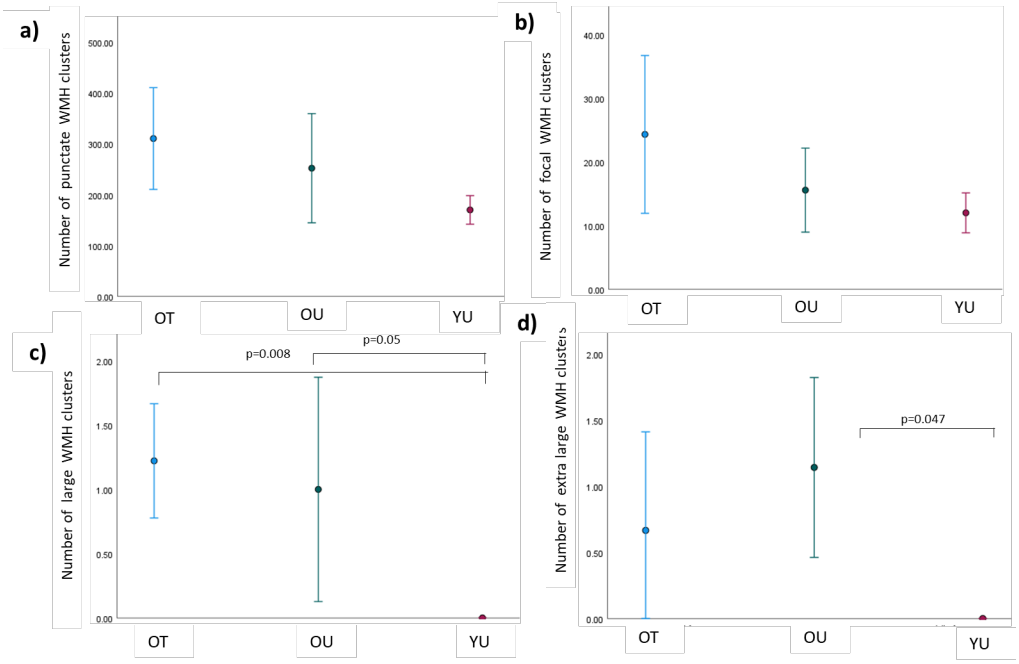

Figure 7.20: Number of white matter hyperintensity clusters by size for a) punctate, b) focal, c) large and d) extra-large clusters for the OT, OU and YU groups.

7.3.3 Structural connectivity

Structural connectivity was assessed form the DTI data in the OT (n=9), OU (n=7) and YU (n=8). Fractional aniosotropy (FA) and mean diffusivity (MD) differed significantly between the groups, as shown in Figure 7.21. The FA was significantly different between groups (F(2,23) = 14.010, p<.001), with greater FA in the YU group than the OT (p<.001) and OU (p<.001). MD was also significantly different across groups (F(2,23) = 20.858, p<.001). The OT group had significantly higher MD than the OU group (p<.001) and YU group (p=.006), while the YU group had higher MD than the OU group (p=0.025). Regional comparisons of mean FA

values showed greater FA in the YU than the OT and OU in multiple regions as shown in Figure 7.22. Voxelwise statistics did not yield significant results.

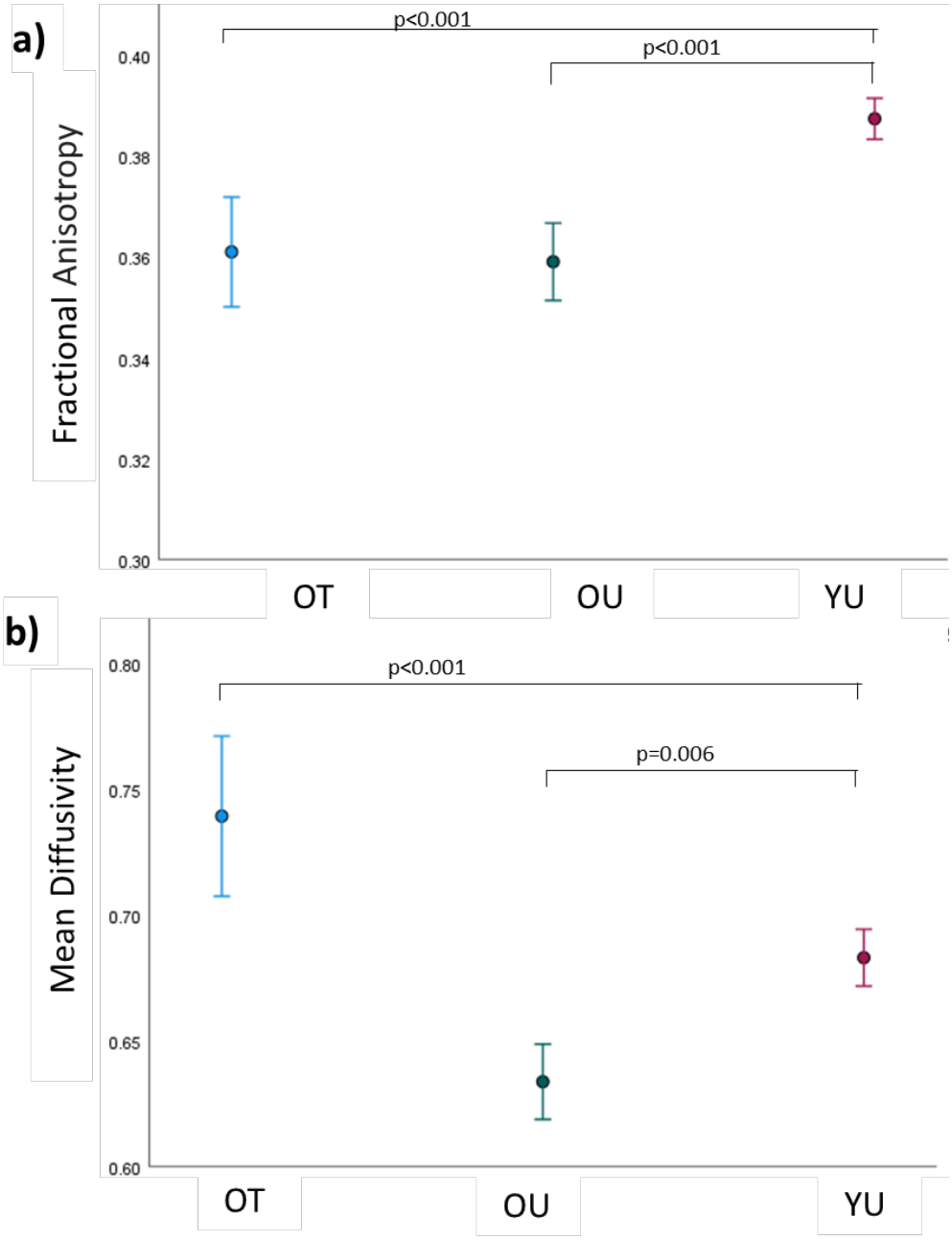

Figure 7.21: a) Fractional aniosotropy (FA) and b) mean diffusivity (MD) in the OT, OU and YU groups.

JHU White Matter Atlas region	p-value	Post-hoc YU>OT	Post-hoc YU>OU
Anterior thalamic radiation L	0.071		
Anterior thalamic radiation R	0.086		
Corticospinal tract L	0.023*	0.02*	
Corticospinal tract R	0.004**	0.003**	
Cingulum (cingulate gyrus) L	0.02*	0.046*	0.04*
Cingulum (cingulate gyrus) R	0.007**	0.009**	0.039*
Cingulum (hippocampus) L	0.247		
Cingulum (hippocampus) R	0.024*	0.022*	
Forceps major	0.013*	0.026*	0.034*
Forceps minor	0.003**	0.008**	0.007**
Inferior fronto-occipital fasciculus L	0.005**	0.045*	0.005**
Inferior fronto-occipital fasciculus R	0.003**	0.016*	0.005**
Inferior longitudinal fasciculus L	0.009**	0.055	0.011*
Inferior longitudinal fasciculus R	<.001***	0.005**	<.001***
Superior longitudinal fasciculus L	0.114		
Superior longitudinal fasciculus R	0.053	0.051	
Uncinate fasciculus L	0.484		
Uncinate fasciculus R	0.5		
Superior longitudinal fasciculus (temporal part) L	0.096		
Superior longitudinal fasciculus (temporal part) R	0.234		

Figure 7.22: Table showing Johns Hopkins University (JHU) white matter atlas regions where mean FA differed between groups. *Indicates p-values <.05, **p<.01 and ***p<.001 and Bonferoni corrected post-hoc results are shown where significant. There were no significant differences between the OT and OU groups.

FA and MD are considered inversely related, to confirm this relationship in the EXAGE data this data is plotted in Figure 7.23. The OT and YU groups share a linear relationship of FA and MD (R^2=0.844), whereas the OU group is offset with lower MD values for each FA value (R^2=0.407).

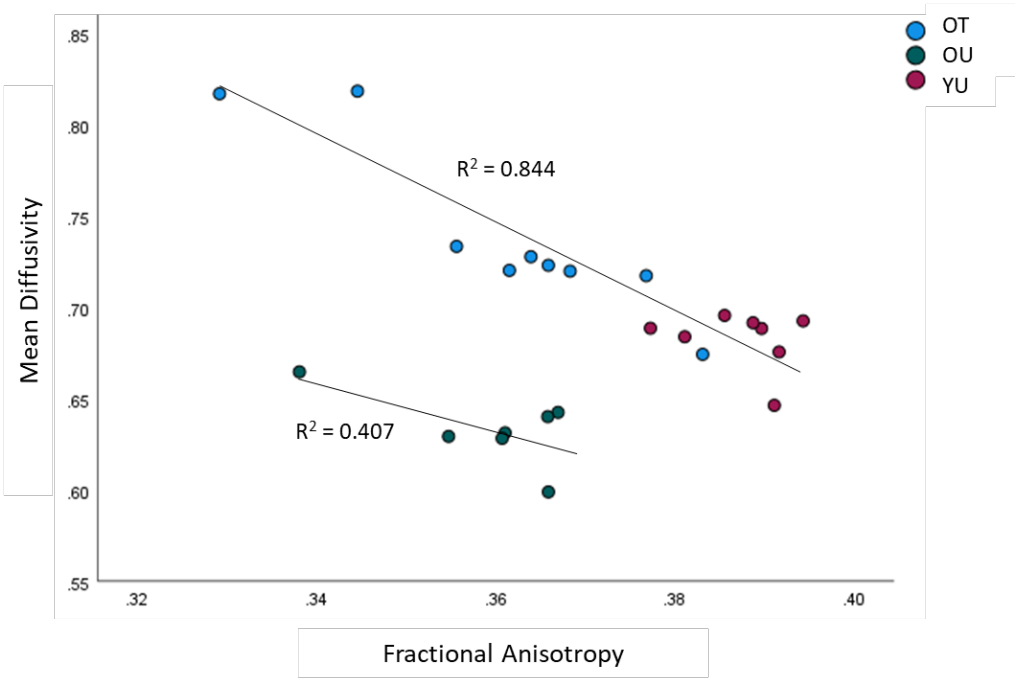

Figure 7.23: Fractional aniosotropy (FA) plotted against mean diffusivity (MD) in the OT, OU and YU groups.

7.4 Cognitive Measures

7.4.1 Montreal Cognitive Assessment (MOCA)

The Montreal Cognitive Assessment (MOCA) is a brief cognitive screening tool for detecting mild cognitive impairment (MCI) [25]. A score below 26 indicates mild cognitive impairment. There was a significant difference in MOCA score between groups ($F(2,23) = 7.081$, $p=0.004$), as shown in Figure 7.24, with the YU group having higher scores than the OT ($p=0.031$) and OU ($p=0.006$) groups. There was no difference between the two older groups, though the mean difference from the YU was greater for the OU (2.78) than the OT (2.00) group.

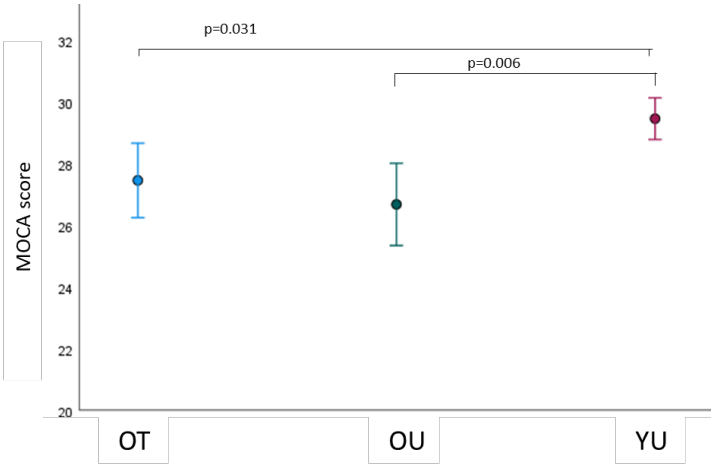

Figure 7.24: MOCA values for the OT, OU and YU groups.

7.4.2 Trail Making Test

The Iowa Trail Making Test consists of two parts, both consisting of 25 circles distributed over a sheet of paper. In Trail A, the circles are numbered 1 through 25, and the participant must draw lines to connect the numbers in ascending order. In Trail B, the circles are made up of numbers (1 – 13) and letters (A – L) and the participant draws lines to connect the circles in an ascending pattern, alternating between letters and numbers.

For Trail A, the reported average time is 29 seconds, with deficiency determined at greater than 78 seconds. For Trail B, the reported average time is 75 seconds, with deficiency at greater than 273 seconds. No participants were deficient in either Trail task. There were significant differences between groups for Trail A, ($F(2,23) = 7.577$, $p=0.003$), as seen in Figure 7.25a, with the YU group having faster scores than the OT ($p=0.005$) and OU ($p=0.021$) groups. There were also significant differences between groups for Trail B, ($F(2,23) = 3.786$, $p=0.039$), as seen in Figure 7.25b, but differences did not survive post-hoc Bonferoni corrections.

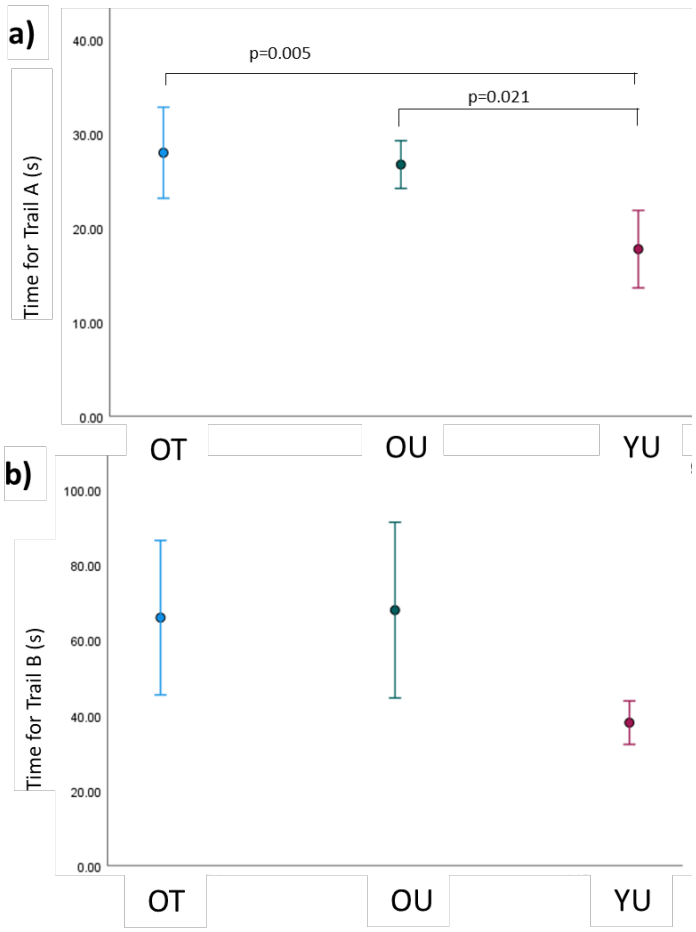

Figure 7.25: Mean time taken for the ascending numbers in a) Trail A Test and b) for the alternating letters and numbers in the Trail B Test for the OT, OU and YU groups.

7.5 Relationship between cardiovascular fitness measures and cognitive measures

Relationships were explored amongst many facets of both the cardiovascular and cognitive measures. Regressions were applied to structural and functional measures of the heart and brain and VO_2peak with no significant associations emerging. Peak heartrate and cerebral vessel blood velocity during exercise yielded the strongest relationships to cerebral and cognitive measures.

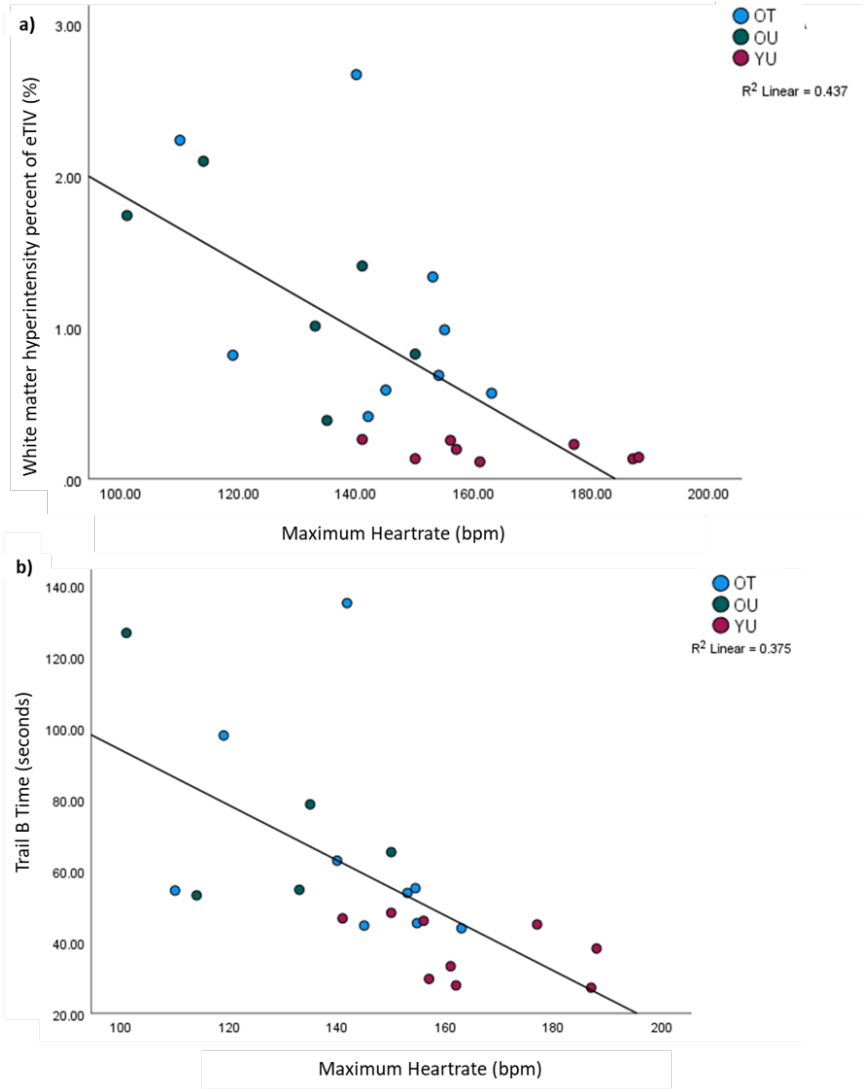

Figure 7.26: Peak Heartrate versus a) white matter hyperintensity volumes and b) the Trail B timed test.

Peak heartrate correlated with both white matter hyperintensities (higher heartrate yielding lower lesion volumes, $F(1,21)=16.3, p<0.001$, $R^2=.437$) and Trail B times (higher heartrates yielding shorter (better) times, $F(1,21)=12.6$, $p=0.002$, $R^2=.375$)), as seen in Figure 7.26.

Cerebral vessel blood velocity during exercise predicted both grey and white matter volumes and cortical thickness. The correlations were significant in all regions for which volumes were obtained except the hippocampus and their R^2 values were between 0.313 and 0.476. All p-values and R^2 values

are shown in Figure 7.27.

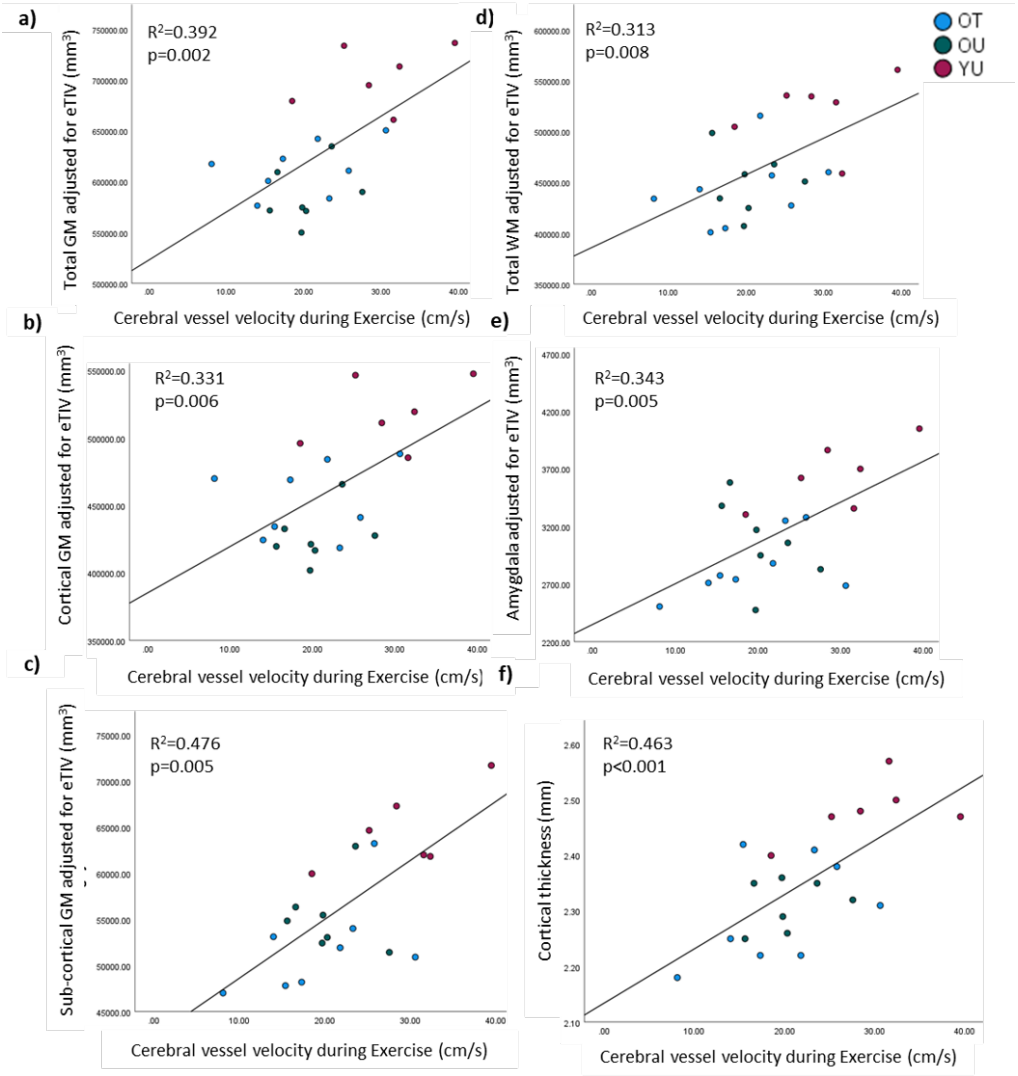

Figure 7.27: Cerebral blood velocity versus eTIV adjusted volumes for a) Total GM, b) Cortical GM, c) Sub-cortical GM, d) Total WM, e) Amygdala and f) cortical thickness.

7.6 Discussion

The impact of ageing was apparent in the cerebral measures collected. The stability of blood gas changes during the workloads used for MRI, provided in Chapter 6, indicate that changes in cerebral blood flow (CBF) during exercise were not driven by changes in PCO_2 and that group responses to

exercise are not driven by differing changes in PCO_2.

The older groups had lower gmCBF than the younger group, as expected [6]. This lowering of gmCBF was accompanied by a decreased cerebral volume seen in the white matter, cortical and sub-cortical grey matter, the hippocampus and amygdala, as well as the increased white matter hyperintensities and decreased connectivity as measured by fractional anisotropy. Greater cortical thickness was also found in the YU group compared to both the OU and OT groups. The deterioration of the structure of the brain aligns with the lower cognitive scores seen in the MOCA and the Trail making tests, which were less in the both older groups than the young group.

The possible impacts of exercise on ageing were seen in the greater velocity of CBF in the OT group than the OU group, with the OT group closer to the YU CBF velocities and with significantly higher CBF velocities in the OT group than the OU group. Cerebral velocities during exercise correlated to cerebral volumes of grey and white matter, and suggest a possible mechanism of cerebral atrophy. White matter hyperintensity cluster sizes where greater in the OU group than YU group, but there were no significant differences between the OT and either OU or OT group. A greater sample size would be needed to examine which group the OT resembled more. The mean diffusivity was highest in the YU, followed by the OT, with the OU having the lowest mean diffusivity.

During exercise, when peripheral oxygen demand is markedly increased, the OU group did not show an increase in CBF, instead compensating by increasing OEF. This effect is even more apparent during recovery, where cardiac output has returned to normal and CBF has decreased to or below baseline levels. The higher CBF velocities of the OT group (compared

to the OU) may explain the lack of change in OEF in this group during exercise, as they are able to achieve sufficient oxygen levels in the brain from greater blood flow.

In context of the literature, a reduction in BOLD cerebrovascular reactivity measurements has been observed in masters athletes relative to age matched sedentary controls. This has been hypothesised to be an adaptive response to high levels of CO_2 exposure across the lifespan of these athletes, dampening the cerebral vasodilation response to CO_2 [26], though current evidence for this mechanism is limited. While the present study did not find lower gmCBF in the OT group than the OU, we also do not expect CO_2 driven vasodilation to be a major driver of gmCBF levels, as CO_2 levels remained stable during this mid-level exercise, as confirmed by blood gases. Another study found middle aged endurance trained participants had greater cerebrovascular reactivity relative to sedentary healthy controls [27], therefore the impact of exercise is not yet conclusive.

Exercise may not only slow brain atrophy, but induce the formation for new blood vessels and neurons, though evidence of this is primarily in rodent work. Angiogenesis has been proposed as an intermediary for exercise-induced increases in cerebral blood volume (CBV) and neurogenesis [28]. In a rodent aerobic exercise intervention, Pereira et al. found increased neurogenesis and CBV in the dentate gyrus (DG) of the hippocampus that correlated with increases in VO_2max after the intervention, as well as with verbal recall. As cerebral angiogenesis has been associated with CBV [29], Pereira et al. propose this as a possible mechanism. This is also supported by other rodent work, which shows exercise inducing angiogenesis in the rat frontoparietal cortex and striatum, motor cortex, [30, 31], cerebellum [32] and the mouse hippocampus [33] (as reviewed in Stimpson, Davison, & Javadi, 2018 [34]). Investigation of the cerebral angiogram and perfusion

data acquired but not yet analysed in this study may provide further insight into exercise induced angiogenesis and cerebral blood volume, though the association of cerebral blood velocity to brain volumes is an early indicator that an association may be found. In a training intervention study of older adults (aerobic or toning and stretching exercises), no group differences were found after the intervention in cortical thickness [35]. However, at baseline aerobic fitness was associated with cortical thickness in the dorsolateral prefrontal cortex (dfPFC). This lab's previous study found cortical thickness associated with cardiorespiratory fitness in older adults [6], which was not apparent in this study, though cortical thickness was associated with cerebral vessel velocity during exercise.

Higher levels of physical activity were associated with greater global white matter volumes in two larger studies (n = 331 and n = 673) [11, 12], although three smaller studies did not report a significant association (n = 52, n = 64 and n – 20) [36, 37, 38]. A meta-analysis of grey matter volume shows a network of brain areas accounting for 82% of grey matter is associated with physical activity [13]. Another review found the grey matter regions associated with cardiorespiratory fitness to be relatively consistent across studies of healthy older adults, and include prefrontal, anterior cingulate, lateral parietal, and lateral temporal cortex [39]. In this lab's previous study, greater grey matter volume was associated with cardiorespiratory fitness across the adult age range [6]. While grey matter and white matter volume in this thesis' study was only found to be significantly different as a factor of age, the increased white matter lesion volume associated with lower maximum heart rate during exercise indicates an association of cardiorespiratory fitness to cerebral volume quality.

As with other brain volume measures, the hippocampus was larger in the young than older groups in this study, but not impacted by training. There

has been considerable work investigating hippocampal volume in past studies. In rodent physical activity studies, the hippocampus is a region that often comes into focus [40, 41], and is often explored as a large factor in human neurodegeneration and cognitive decline [42, 43]. Several studies have looked at associations of hippocampal volume and structure with cardiorespiratory fitness. Two studies show mediation of the relationship between aerobic fitness and spatial memory [14, 15], with one also showing an association with reductions in frequency of everyday forgetfulness. Another study looked at tissue density in the hippocampus, and found increased fitness was associated with increased density, which may bring about the changes in volume [44]. In a training intervention study of older adults hippocampus volume increases were associated with aerobic fitness increases over time [16]. In the EXAGE study, a correlation between hippocampal volume and cerebral vessel velocity in exercise was not found, contrary to the other brain regions investigated. The strong evidence in the literature suggest that further investigation could be done into this data. The hippocampal volume could be segmented into its sub-regions to examine possible differences in the distribution of volume.

In normal ageing, after reaching adulthood, FA decreases and MD increases [45] with neuronal death inducing decreases in size of axonal tracts, and loss of white matter integrity. In a study by Smith et al, greater levels of physical activity were found to be associated with fractional anisotropy (FA) in healthy older adults who did not possess the APOE-ϵ4 allele associated with greater Alzheimer's disease (AD) risk [17]. Fitness appears to be positively associated with white matter integrity across the literature, but studies do not agree on the regions effected. Marks et al indicated that cardiorespiratory fitness was positively associated with fractional anisotropy in the middle and posterior segments of the cingulum bundle [46], which

is an important tract connecting to the hippocampus and therefore crucial in memory formation, and whose structural integrity has been found to be associated with mild cognitive impairment in ageing [47]. Another study showed correlation with fractional anisotropy measures in the body and genu of the corpus callosum [35]. While the EXAGE study did not find fitness related associations, the strongest associations of FA to age were found in the cingulum, as found in Marks et al, and the inferior longitudinal fasciculus (associated with visual processing and language comprehension).

An fMRI task based study on cardiovascular fitness found increased fitness can affect improvements in the plasticity of the ageing human brain and therefore cognitive function [48], and another shows that moderate levels of exercise in mid- and late-life are associated with decreased risk of developing Mild Cognitive Impairment (MCI) [49]. However, a meta-regression review of the effects of physical activity on cognition did not find a significant relationship [50]. They propose that aerobic fitness may not be sensitive enough predictor of cognitive ability, but a precursor to more direct functions. While the cognitive measures in the EXAGE study did not differentiate the OT from the OU, a faster Trail B Trail-Making score (the more cognitively challenging of the two Trail-Making tests) was associated with higher maximum heart rate during exercise.

While limited sample sizes of this study may have resulted in a lack of significant differences in many measures, differences in cerebral blood velocity indicate an impact of exercise that should be explored further. This study controlled for age-related chronic diseases, and therefore the OU group was healthier than many of their more sedentary peers. A further study could investigate the imapact of age-related diseases on these same physiological traits.

References

[1] KL Leenders, D Perani, AA Lammertsma, JD Heather, P Buckingham, T Jones, MJR Healy, JM Gibbs, RJS Wise, J Hatazawa, et al. Cerebral blood flow, blood volume and oxygen utilization: normal values and effect of age. *Brain*, 113(1):27–47, 1990.

[2] Terry G Shaw, Karl F Mortel, John Stirling Meyer, Robert L Rogers, Jeffery Hardenberg, and Michael M Cutaia. Cerebral blood flow changes in benign aging and cerebrovascular disease. *Neurology*, 34(7):855–855, 1984.

[3] Philip N Ainslie, James D Cotter, Keith P George, Sam Lucas, Carissa Murrell, Rob Shave, Kate N Thomas, Michael JA Williams, and Greg Atkinson. Elevation in cerebral blood flow velocity with aerobic fitness throughout healthy human ageing. *The Journal of physiology*, 586(16):4005–4010, 2008.

[4] Arthur F Kramer, Sowon Hahn, Neal J Cohen, Marie T Banich, Edward McAuley, Catherine R Harrison, Julie Chason, Eli Vakil, Lynn Bardell, Richard A Boileau, et al. Ageing, fitness and neurocognitive function. *Nature*, 400(6743):418–419, 1999.

[5] Stanley J Colcombe, Kirk I Erickson, Paige E Scalf, Jenny S Kim, Ruchika Prakash, Edward McAuley, Steriani Elavsky, David X Mar-

quez, Liang Hu, and Arthur F Kramer. Aerobic exercise training increases brain volume in aging humans. *The Journals of Gerontology Series A: Biological Sciences and Medical Sciences*, 61(11):1166–1170, 2006.

[6] Andrew P. Hale. *Application of MR to Identify Metabolic and Physiological Correlates of Human Ageing and Inactivity*. PhD thesis, 2017.

[7] Shin-Lei Peng, Julie A Dumas, Denise C Park, Peiying Liu, Francesca M Filbey, Carrie J McAdams, Amy E Pinkham, Bryon Adinoff, Rong Zhang, and Hanzhang Lu. Age-related increase of resting metabolic rate in the human brain. *Neuroimage*, 98:176–183, 2014.

[8] IW Gallen and IA Macdonald. Effect of two methods of hand heating on body temperature, forearm blood flow, and deep venous oxygen saturation. *American Journal of Physiology-Endocrinology and Metabolism*, 259(5):E639–E643, 1990.

[9] JJ VAN LIESHOUT. Middle cerebral artery blood velocity depends on cardiac output during exercise with a large muscle mass. *Acta physiologica Scandinavica*, 162(1):13–20, 1998.

[10] Lingzhong Meng, Wugang Hou, Jason Chui, Ruquan Han, and Adrian W Gelb. Cardiac output and cerebral blood flow: the integrated regulation of brain perfusion in adult humans. *Anesthesiology*, 123(5):1198–1208, 2015.

[11] Christian Benedict, Samantha J Brooks, Joel Kullberg, Richard Nordenskjöld, Jonathan Burgos, Madeleine Le Grevès, Lena Kilander, Elna-Marie Larsson, Lars Johansson, Håkan Ahlström, et al. Association between physical activity and brain health in older adults. *Neurobiology of aging*, 34(1):83–90, 2013.

[12] Alan J Gow, Mark E Bastin, Susana Muñoz Maniega, Maria C Valdés Hernández, Zoe Morris, Catherine Murray, Natalie A Royle, John M Starr, Ian J Deary, and Joanna M Wardlaw. Neuroprotective lifestyles and the aging brain: activity, atrophy, and white matter integrity. *Neurology*, 79(17):1802–1808, 2012.

[13] Seyed Amir Hossein Batouli and Valiallah Saba. At least eighty percent of brain grey matter is modifiable by physical activity: A review study. *Behavioural brain research*, 332:204–217, 2017.

[14] Kirk I Erickson, Ruchika S Prakash, Michelle W Voss, Laura Chaddock, Liang Hu, Katherine S Morris, Siobhan M White, Thomas R Wójcicki, Edward McAuley, and Arthur F Kramer. Aerobic fitness is associated with hippocampal volume in elderly humans. *Hippocampus*, 19(10):1030–1039, 2009.

[15] Amanda N Szabo, Edward McAuley, Kirk I Erickson, Michelle Voss, Ruchika S Prakash, Emily L Mailey, Thomas R Wójcicki, Siobhan M White, Neha Gothe, Erin A Olson, et al. Cardiorespiratory fitness, hippocampal volume, and frequency of forgetting in older adults. *Neuropsychology*, 25(5):545, 2011.

[16] Lars S Jonasson, Lars Nyberg, Arthur F Kramer, Anders Lundquist, Katrine Riklund, and Carl-Johan Boraxbekk. Aerobic exercise intervention, cognitive performance, and brain structure: results from the physical influences on brain in aging (phibra) study. *Frontiers in aging neuroscience*, 8:336, 2017.

[17] J Carson Smith, Kristy A Nielson, John L Woodard, Michael Seidenberg, Sally Durgerian, Piero Antuono, Alissa M Butts, Nathan C Hantke, Melissa A Lancaster, and Stephen M Rao. Interactive effects

of physical activity and apoe-ε4 on bold semantic memory activation in healthy elders. *Neuroimage*, 54(1):635–644, 2011.

[18] Hanzhang Lu and Yulin Ge. Quantitative evaluation of oxygenation in venous vessels using t2-relaxation-under-spin-tagging mri. *Magnetic Resonance in Medicine: An Official Journal of the International Society for Magnetic Resonance in Medicine*, 60(2):357–363, 2008.

[19] Bruce Fischl. Freesurfer. *Neuroimage*, 62(2):774–781, 2012.

[20] Christian Gaser, Robert Dahnke, Paul M Thompson, Florian Kurth, and Eileen Luders. Cat-a computational anatomy toolbox for the analysis of structural mri data. *BioRxiv*, pages 2022–06, 2022.

[21] Ludovica Griffanti, Giovanna Zamboni, Aamira Khan, Linxin Li, Guendalina Bonifacio, Vaanathi Sundaresan, Ursula G. Schulz, Wilhelm Kuker, Marco Battaglini, Peter M. Rothwell, and Mark Jenkinson. Bianca (brain intensity abnormality classification algorithm): A new tool for automated segmentation of white matter hyperintensities. *NeuroImage*, 141:191–205, 2016.

[22] Wei Wen, Perminder S Sachdev, Jason J Li, Xiaohua Chen, and Kaarin J Anstey. White matter hyperintensities in the forties: their prevalence and topography in an epidemiological sample aged 44–48. *Human brain mapping*, 30(4):1155–1167, 2009.

[23] Stephen M Smith, Mark Jenkinson, Heidi Johansen-Berg, Daniel Rueckert, Thomas E Nichols, Clare E Mackay, Kate E Watkins, Olga Ciccarelli, M Zaheer Cader, Paul M Matthews, et al. Tract-based spatial statistics: voxelwise analysis of multi-subject diffusion data. *Neuroimage*, 31(4):1487–1505, 2006.

[24] Stephen M Smith, Mark Jenkinson, Mark W Woolrich, Christian F Beckmann, Timothy EJ Behrens, Heidi Johansen-Berg, Peter R Bannister, Marilena De Luca, Ivana Drobnjak, David E Flitney, et al. Advances in functional and structural mr image analysis and implementation as fsl. *Neuroimage*, 23:S208–S219, 2004.

[25] Ziad S Nasreddine, Natalie A Phillips, Valérie Bédirian, Simon Charbonneau, Victor Whitehead, Isabelle Collin, Jeffrey L Cummings, and Howard Chertkow. The montreal cognitive assessment, moca: a brief screening tool for mild cognitive impairment. *Journal of the American Geriatrics Society*, 53(4):695–699, 2005.

[26] Binu P Thomas, Uma S Yezhuvath, Benjamin Y Tseng, Peiying Liu, Benjamin D Levine, Rong Zhang, and Hanzhang Lu. Life-long aerobic exercise preserved baseline cerebral blood flow but reduced vascular reactivity to co2. *Journal of Magnetic Resonance Imaging*, 38(5):1177–1183, 2013.

[27] Takashi Tarumi, Mitzi M Gonzales, Bennett Fallow, Nantinee Nualnim, Jeongseok Lee, Martha Pyron, Hirofumi Tanaka, and Andreana P Haley. Cerebral/peripheral vascular reactivity and neurocognition in middle-age athletes. *Medicine and science in sports and exercise*, 47(12):2595, 2015.

[28] Ana C Pereira, Dan E Huddleston, Adam M Brickman, Alexander A Sosunov, Rene Hen, Guy M McKhann, Richard Sloan, Fred H Gage, Truman R Brown, and Scott A Small. An in vivo correlate of exercise-induced neurogenesis in the adult dentate gyrus. *Proceedings of the National Academy of Sciences*, 104(13):5638–5643, 2007.

[29] Antonio CM Maia, Suzana MF Malheiros, Antonio J da Rocha, Carlos J da Silva, Alberto A Gabbai, Fernando AP Ferraz, and Joao N

Stávale. Mr cerebral blood volume maps correlated with vascular endothelial growth factor expression and tumor grade in nonenhancing gliomas. *American Journal of Neuroradiology*, 26(4):777–783, 2005.

[30] Quiuping Ding, S Vaynman, M Akhavan, Z Ying, and F Gomez-Pinilla. Insulin-like growth factor i interfaces with brain-derived neurotrophic factor-mediated synaptic plasticity to modulate aspects of exercise-induced cognitive function. *Neuroscience*, 140(3):823–833, 2006.

[31] Yun-Hong Ding, Jie Li, Yandong Zhou, Jose A Rafols, Justin C Clark, and Yuchuan Ding. Cerebral angiogenesis and expression of angiogenic factors in aging rats after exercise. *Current neurovascular research*, 3(1):15–23, 2006.

[32] Krystyna R Isaacs, Brenda J Anderson, Adriana A Alcantara, James E Black, and William T Greenough. Exercise and the brain: angiogenesis in the adult rat cerebellum after vigorous physical activity and motor skill learning. *Journal of Cerebral Blood Flow & Metabolism*, 12(1):110–119, 1992.

[33] Cecilie Morland, Krister A Andersson, Øyvind P Haugen, Alena Hadzic, Liv Kleppa, Andreas Gille, Johanne E Rinholm, Vuk Palibrk, Elisabeth H Diget, Lauritz H Kennedy, et al. Exercise induces cerebral vegf and angiogenesis via the lactate receptor hcar1. *Nature communications*, 8(1):15557, 2017.

[34] Nikolas J Stimpson, Glen Davison, and Amir-Homayoun Javadi. Joggin'the noggin: towards a physiological understanding of exercise-induced cognitive benefits. *Neuroscience & Biobehavioral Reviews*, 88:177–186, 2018.

[35] Nathan F Johnson, Chobok Kim, Jody L Clasey, Alison Bailey, and Brian T Gold. Cardiorespiratory fitness is positively correlated with cerebral white matter integrity in healthy seniors. *Neuroimage*, 59(2):1514–1523, 2012.

[36] Julie M Bugg and Denise Head. Exercise moderates age-related atrophy of the medial temporal lobe. *Neurobiology of aging*, 32(3):506–514, 2011.

[37] Jeffrey M Burns, Benjamin B Cronk, Heather S Anderson, Joseph E Donnelly, George P Thomas, Amith Harsha, William M Brooks, and Russell H Swerdlow. Cardiorespiratory fitness and brain atrophy in early alzheimer disease. *Neurology*, 71(3):210–216, 2008.

[38] Benjamin Y Tseng, Jinsoo Uh, Heidi C Rossetti, C Munro Cullum, Ramon F Diaz-Arrastia, Benjamin D Levine, Hanzhang Lu, and Rong Zhang. Masters athletes exhibit larger regional brain volume and better cognitive performance than sedentary older adults. *Journal of Magnetic Resonance Imaging*, 38(5):1169–1176, 2013.

[39] Scott M Hayes, Jasmeet P Hayes, Margaret Cadden, and Mieke Verfaellie. A review of cardiorespiratory fitness-related neuroplasticity in the aging brain. *Frontiers in aging neuroscience*, 5:31, 2013.

[40] Carl W Cotman and Nicole C Berchtold. Exercise: a behavioral intervention to enhance brain health and plasticity. *Trends in neurosciences*, 25(6):295–301, 2002.

[41] Henriette Van Praag. Neurogenesis and exercise: past and future directions. *Neuromolecular medicine*, 10:128–140, 2008.

[42] Heiko Braak and Eva Braak. Neuropathological stageing of alzheimer-related changes. *Acta neuropathologica*, 82(4):239–259, 1991.

[43] CR Jack, DW Dickson, JE Parisi, YC Xu, RH Cha, PC O'brien, SD Edland, GE Smith, BF Boeve, EG Tangalos, et al. Antemortem mri findings correlate with hippocampal neuropathology in typical aging and dementia. *Neurology*, 58(5):750–757, 2002.

[44] Maike Margarethe Kleemeyer, Simone Kühn, John Prindle, Nils Christian Bodammer, Lars Brechtel, Alexander Garthe, Gerd Kempermann, Sabine Schaefer, and Ulman Lindenberger. Changes in fitness are associated with changes in hippocampal microstructure and hippocampal volume among older adults. *Neuroimage*, 131:155–161, 2016.

[45] Lars T Westlye, Kristine B Walhovd, Anders M Dale, Atle Bjørnerud, Paulina Due-Tønnessen, Andreas Engvig, Håkon Grydeland, Christian K Tamnes, Ylva Østby, and Anders M Fjell. Life-span changes of the human brain white matter: diffusion tensor imaging (dti) and volumetry. *Cerebral cortex*, 20(9):2055–2068, 2010.

[46] BL Marks, LM Katz, M Styner, and JK Smith. Aerobic fitness and obesity: relationship to cerebral white matter integrity in the brain of active and sedentary older adults. *British journal of sports medicine*, 45(15):1208–1215, 2011.

[47] Claudia Metzler-Baddeley, Derek K Jones, Jessica Steventon, Laura Westacott, John P Aggleton, and Michael J O'Sullivan. Cingulum microstructure predicts cognitive control in older age and mild cognitive impairment. *Journal of Neuroscience*, 32(49):17612–17619, 2012.

[48] Arthur F Kramer and Stanley Colcombe. Fitness effects on the cognitive function of older adults: a meta-analytic study—revisited. *Perspectives on Psychological Science*, 13(2):213–217, 2018.

[49] Yonas E Geda, Rosebud O Roberts, David S Knopman, Teresa JH Christianson, V Shane Pankratz, Robert J Ivnik, Bradley F Boeve,

Eric G Tangalos, Ronald C Petersen, and Walter A Rocca. Physical exercise, aging, and mild cognitive impairment: a population-based study. *Archives of neurology*, 67(1):80–86, 2010.

[50] Jennifer L Etnier, Priscilla M Nowell, Daniel M Landers, and Benjamin A Sibley. A meta-regression to examine the relationship between aerobic fitness and cognitive performance. *Brain research reviews*, 52(1):119–130, 2006.

Chapter 8

Conclusion

8.1 Summary of main findings

The work presented in this thesis applies a broad scope of modalities to study the impact of lifelong high levels of physical activity in the context of physiological ageing. This aimed to contribute to a greater understanding of human physiological ageing using MRI methods that can be applied non-invasively to an ageing population, and more uniquely, to quantify physiological responses to supine exercise collected both outside and within an MR scanner.

8.1.1 Methodological Developments

The work in this thesis established that the Ergospect Cardio-Step equipment is tolerated in an older population of healthy, non-sedentary individuals, who were able to complete VO_2peak testing using the Cardio-Step. It was possible to collect both cardiac and brain MR data during supine exercise as described in Chapters 6 and 7. Blood gas results confirmed

this supine exercise protocol did not induce changes in arterialised-venous blood PCO_2 at 50% VO_2peak that in itself would alter cerebral blood flow.

The semi-automatic muscle segmentation method described in Chapter 4 was shown to be a useful tool to extract measures of muscle volumes from wholebody mDIXON datasets without time consuming manual measures, and within-muscle fat fraction of the calf and thigh was also measured. Muscle volume measures from the semi-automatic method were shown to provide good reliability compared to manual drawing of ROIs. They yielded lower values compared to DEXA as the field of view examined was larger in the DEXA (including the glutes) and lower compared to manual drawing because of the removal of intermuscular fat, see Chapter 4 discussion.

8.1.2 Age related differences

Most of the end-point measurements presented in this thesis are age-driven, with differences found between the young untrained (YU) and both the older untrained (OU) and older trained (OT) groups. These age-related differences are summarised in Figure 8.1, for both baseline measures and measures collected during supine exercise. These results agree with existing understanding of age-related changes in muscle, cardiac and cerebral measures. In the muscle, lower muscle strength with increasing age was found, although in this group no difference in muscle volume was found. Intra and extramuscular fat within the muscle volume contributes to the overall muscle volume in the MRI derived volumes, therefore fat included within the muscle with age could disguise the expected smaller muscle voxel in older groups in the data. Alternatively, all of the older volunteers in this thesis were non-frail, non-sedentary and healthy so it is possible age related sarcopenia had not fully manifested in the OT and OU populations.

In support of this, older frail and chronic disease patients did present with lower muscle volumes than the healthy volunteers studied in this thesis using the same imaging methodologies to determine muscle volume. Future work should focus on mapping both subcutaneous and extramuscular adipose tissues and subtracting these from the muscle mask to provide a more accurate measure of true muscle volume.

For cardiac measures, peak heartrate during the VO_2 test, aortic stroke volume and stroke distance were all lower in the older trained and older untrained groups. Aortic stroke volume however was higher in the older OT and OU groups than the YU group during supine exercise, reflecting differing mechanisms of increasing cardiac index in response to supine exercise in older participants. The heartrate of all participants increased during exercise, but for the YU group this was the primary driver of their increase in cardiac output with no increase in stroke volume, whereas the older OT and OU groups compensated for lower increases in heartrate with concurrent increases in stroke volume. Aortic backflow was also greater in older groups at rest, without increased aortic stiffening, suggesting greater peripheral vasculature resistance in the older groups compared to the younger group, which will be confirmed with the available blood pressure data.

In the brain measures, gmCBF at baseline and cerebral vessel velocity at both baseline and during supine exercise were lower with age. As expected, white matter, cortical and subcortical grey matter, amygdala and hippocampus volume, as well as cortical thickness were all lower in the older groups than the young group. Modest correlations exist between cerebral velocity during supine exercise and cortical and sub-cortical grey matter, white matter and amygdala volume and cortical thickness, though any correlation with hippocampus volume was weak and not significant. This presents the possibility that cerebral vessel velocity is a predictor of

brain volumes, as a mechanism by which exercise induces greater blood flow to the brain and therefore greater oxygen, slowing cerebral atrophy by slowing the neuronal death associated with restricted oxygen supply promoting reactive oxygen species formation and calcium dyshomeostasis [1]. However, as no differences in overall gmCBF were found during exercise, more work needs to be done in this area to address this phenomena with larger participant groups and better cerebral PC-MRI data quality and also the study of sedentary individuals. Structural connectivity measured by fractional anisotropy was greater in the young than older groups, along with the cognitive scores from the MOCA and Trail A tests. The cognitive tests may have been impacted by post-exercise effects, and in future study design should account for this an aim to conduct cognitive test before exercise tasks.

Effect of Age	Baseline	Exercise
Muscle strength and Muscle strength for muscle volume		YU > OT & OU
Peak Heartrate		YU > OT & OU
Aortic Stroke Volume		OT & OU > YU
Aortic Stroke Velocity and Distance	YU > OT & OU	YU > OT & OU
Aortic backwards flow	OT & OU > YU	
End Systolic Volume		Decrease with exercise only seen in YU
gmCBF	YU > OT & OU	
Cerebral vessel velocity	YU > OT > OU	YU > OU
WM, GM, amygdala and hippocampus volume	YU > OT & OU	
Cortical Thickness	YU > OT & OU	
White matter hyperintensities	OT & OU > YU	
Fractional Anisotropy	YU > OT & OU	
MOCA and Trail A	YU > OT & OU	

Figure 8.1: Main findings driven by age related differences between the young untrained (YU) and both the older trained (OT) and older untrained (OU) groups.

8.1.3 Training related differences

Some effects of a long term lifestyle of high physical activity were seen, as summarised in Figure 8.2, where the OT group were more similar to the YU group than the OU group. This lifestyle effect was exhibited in maintained muscle quality during isokinetic contractions, higher VO_2peaks, and greater velocity of cerebral blood flow at rest. While not significant, balance and motor unit firing rate variability would be important measures to collect

in the future to explore the OT trend of better balance and greater motor unit firing stability.

Effect of Training	Baseline	Exercise
Work done for muscle volume		YU & OT > OU
VO_2 peak		OT > OU
Cerebral vessel velocity	YU > OT > OU	YU > OU
Balance	OT > OU *trend level	
Motor Unit Firing Variability		OU > OT *trend level

Figure 8.2: Main findings driven by training related differences comparing the OU group with the OT group, and with the OT and YU groups.

8.1.4 Other group differences

Other findings of note that are not attributed to the effect of ageing (YU vs OU and OT) or training (OT and YU vs OU) are provided in Figure 8.3. The older untrained (OU) had greater fat percentages within their calf muscles than the young untrained (YU), but the older trained (OT) were not different from either group. Aortic cardiac index was lower and OEF was higher in the OU group than YU group. Increased brain OEF appears to be a compensatory mechanism for reduced cerebral velocity in the OU during exercise, and maintained during recovery despite cerebral velocity returning to baseline. A greater sample size is needed to determine if these effects are driven by age or training. The OT group also had lower heartrates than the YU at 50% of VO_2 peak while in the MR scanner, driving their increase in cardiac index primarily from increase in stroke volume. Mean diffusivity values were highest in the OT group, with values for the YU group also higher than the OU group. This does not agree with the literature understanding of increased mean diffusivity with age [2] and

requires further investigation.

Other	Baseline	Exercise	Recovery
Calf Fat Fraction	OU > YU		
Aortic Cardiac Index	YU > OU		
50% VO_2 peak heartrate		YU > OT	
OEF		OU > YU	OU > YU
MD	OT > YU > OU		

Figure 8.3: Findings driven by differences not primarily explained by age or training.

8.2 Future work

Participant recruitment was impacted by COVID-19 restrictions, as highlighted at the start of this thesis. Increasing the number of participants in the same OT, OU and YU groups explored in this thesis would allow for greater understanding of the results presented in this thesis, particularly in measures where data was excluded for poor quality due to within magnet movement artifacts.

The semi-automatic leg muscle segmentation pipeline outlined in Chapter 4 will be expanded to generate masks of the subcutaneous adipose tissue (SAT) and the extramuscular fat (EMAT). These measures are predicted to increase with inactivity and age [3]. In addition the wholebody mDIXON will be used to segment additional SAT and visceral adipose tissue (VAT). Machine learning methods will be explored, improving the current methods for skeletal muscle and using these semi-automatic and new SAT, EMAT and VAT masks for high input of datasets in machine learning training datasets to create a faster tool and more accurate assessments of adipose tissue and muscle volumes. MRS measures of within muscle fibre could

also be investigated.

The Cardio-Step equipment and protocols described in this thesis have been adapted and employed in other concurrent studies including work in IBD fatigue and individuals effected by acute COVID-19, and collaborative work with Ergospect has contributed to further development of the Cardio-Step for improved use in human volunteer exercise studies. This will be continued to be used in future studies investigating exercise induced changes in healthy and patient populations.

In future for cardiac scan acquisitions during supine exercise, aortic Phase Contrast MRI scans would be recommended over 2CH and 4CH long axis cines that require breath holding during exercise which is difficult to achieve. The cerebral Phase Contrast MRI scan can then be acquired multiple times during exercise to allow robustness to be estimated, and data could also be reacquired should the participant move out of the FOV during exercise. The use of compressed sensing to shorten the PC-MRI acquisition time and therefore image quality was tested in a subset of participants. Further development of this scan could prove useful to provide more reliable data capture.

The group has two Cardio-Step devices and their interchangeability needs to be improved. Ergospect will service the Cardio-Step devices together and test for interchangeability measures between the two systems. At this time, the possibility of using the Cardio-Step to begin at lower workloads should also be investigated by Ergospect. For this thesis work, the lowest workload setting was 50 W. When no air resistance is applied the force output reads at an average of 50 W at 70 bpm, with only slightly lower workloads achievable by changing step frequency. Starting at a lower workload would expand the utility of the Cardio-Step to populations that would

otherwise not be able to complete a VO_2peak test where strong resistances are quickly reached. Developmental work could also consider the impacts of hyperventilation within a COSMED mask compared to within the scanner. A decommissioned scanner is currently available and VO_2peak testing could be carried out within the scanner and be compared to outside the scanner to investigate the impact of the semi-enclosed nature of the MRI scanner on hyperventilation and VO_2. The MR scans could then be taken while wearing the COSMED mask (without any gas data collected) and compared to without the mask, to see if the enclosed nature of the mask also has an impact. A 50% test in the decommissioned scanner could also be collected, to compared gas data to the incremental peak test, as well as collecting a recovery period of gas data.

Some data collected in the EXAGE protocol was not analysed in the scope of this thesis but will be analysed in the future. This includes measures of thymus volume and fat fraction, which has been shown to have little total volume change with age but greater fat infiltration, which results in decreased functional (non-fat) volume and therefore lower immune function [4]. The association of thymic function with physical activity was investigated by Duggal et al. using the immune cell phenotypes of highly active older adults, age-matched sedentary adults and young not highly active adults [5]. The highly active group showed higher native T cells, recent thymic emigrants and thymoprotective cytokines, and lower levels of the cytokines that induce thymus atrophy. These results lead to the hypothesis that high levels of physical activity could prevent this accumulation of fat and preserve function.

A cerebral time-of-flight angiogram was collected at baseline, and brain perfusion arterial spin labelling scans were collected at baseline, during supine exercise and recovery. These will be analysed in future work to

assess vascular integrity across groups, and regional perfusion changes during supine exercise. In future, other measures could be explored such as a cerebrovascular reactivity, consisting of a CO_2 challenge where cerebrovascular reactivity could be measured with ASL and blood oxygen level dependent (BOLD) response during blocks of breathing normal air compared to breathing air at greater CO_2 partial pressure. Additionally, area of interest could be expanded to include other organs, such as the liver, which plays an essential role in maintaining blood glucose homeostasis and is negatively impacted by the hepatic lipid accumulation associated with poor cardiometabolic health, obesity and diabetes, which are in turn associated with ageing.

Other studies that would provide additional insight include pharmacological intervention and interventional studies. A pharmacological intervention could include administering a non-selective beta-blocker in healthy young participants to reduced cardiac output during exercise and investigate its impact of cardiac function and blood flow and oxygenation in the brain. Alternatively, a simple infusion of saline to increase the blood volume could be used to investigate the impact of reduced blood volume in ageing on cardiac output. Interventional studies, including exercise training over an extended period, could also be considered, with measures taken pre and post training intervention.

References

[1] Chris Peers, Mark L Dallas, Hannah E Boycott, Jason L Scragg, Hugh A Pearson, and John P Boyle. Hypoxia and neurodegeneration. *Annals of the New York Academy of Sciences*, 1177(1):169–177, 2009.

[2] Grégory Beaudet, Ami Tsuchida, Laurent Petit, Christophe Tzourio, Svenja Caspers, Jan Schreiber, Zdenka Pausova, Yash Patel, Tomas Paus, Reinhold Schmidt, et al. Age-related changes of peak width skeletonized mean diffusivity (psmd) across the adult lifespan: a multi-cohort study. *Frontiers in psychiatry*, 11:342, 2020.

[3] Adeel Safdar, Mazen J Hamadeh, Jan J Kaczor, Sandeep Raha, Justin Debeer, and Mark A Tarnopolsky. Aberrant mitochondrial homeostasis in the skeletal muscle of sedentary older adults. *PloS one*, 5(5):e10778, 2010.

[4] Kenneth W Fishbein, Sokratis K Makrogiannis, Vanessa A Lukas, Marilyn Okine, Ramona Ramachandran, Luigi Ferrucci, Josephine M Egan, Chee W Chia, and Richard G Spencer. Measurement of fat fraction in the human thymus by localized nmr and three-point dixon mri techniques. *Magnetic resonance imaging*, 50:110–118, 2018.

[5] Niharika Arora Duggal, Ross D Pollock, Norman R Lazarus, Stephen Harridge, and Janet M Lord. Major features of immunesenescence, in-

cluding reduced thymic output, are ameliorated by high levels of physical activity in adulthood. *Aging cell*, 17(2):e12750, 2018.